SERDP

FINAL REPORT

Relating the Phase, Flow, and Coalescence Behavior of Complex Shipboard Emulsions to the Physical and Chemical Properties of Model Surfactant-Oil-Water Systems

John Howarter
Kendra Erk
Carlos Martinez
Purdue University

April 2023

SERDP Project WP18-1215

DISTRIBUTION STATEMENT A
This document has been cleared for public release.

This report was prepared under contract to the Department of Defense Strategic Environmental Research and Development Program (SERDP). The publication of this report does not indicate endorsement by the Department of Defense, nor should the contents be construed as reflecting the official policy or position of the Department of Defense. Reference herein to any specific commercial product, process, or service by trade name, trademark, manufacturer, or otherwise, does not necessarily constitute or imply its endorsement, recommendation, or favoring by the Department of Defense.

REPORT DOCUMENTATION PAGE

Form Approved
OMB No. 0704-0188

The public reporting burden for this collection of information is estimated to average 1 hour per response, including the time for reviewing instructions, searching existing data sources, gathering and maintaining the data needed, and completing and reviewing the collection of information. Send comments regarding this burden estimate or any other aspect of this collection of information, including suggestions for reducing the burden, to Department of Defense, Washington Headquarters Services, Directorate for Information Operations and Reports (0704-0188), 1215 Jefferson Davis Highway, Suite 1204, Arlington, VA 22202-4302. Respondents should be aware that notwithstanding any other provision of law, no person shall be subject to any penalty for failing to comply with a collection of information if it does not display a currently valid OMB control number.
PLEASE DO NOT RETURN YOUR FORM TO THE ABOVE ADDRESS.

1. REPORT DATE *(DD-MM-YYYY)*	**2. REPORT TYPE**	**3. DATES COVERED** *(From - To)*
17/04/2023	SERDP Final Report	5/17/2018 - 5/18/2022

4. TITLE AND SUBTITLE

Relating the Phase, Flow, and Coalescence Behavior of Complex Shipboard Emulsions to the Physical and Chemical Properties of Model Surfactant-Oil-Water Systems

5a. CONTRACT NUMBER
18-C-0021

5b. GRANT NUMBER

5c. PROGRAM ELEMENT NUMBER

6. AUTHOR(S)
John Howarter
Kendra Erk
Carlos Martinez

5d. PROJECT NUMBER
WP18-1215

5e. TASK NUMBER

5f. WORK UNIT NUMBER

7. PERFORMING ORGANIZATION NAME(S) AND ADDRESS(ES)
Purdue University
701 W. Stadium Avenue
West Lafayette, IN 47907

8. PERFORMING ORGANIZATION REPORT NUMBER
WP18-1215

9. SPONSORING/MONITORING AGENCY NAME(S) AND ADDRESS(ES)
Office of the Deputy Assistant Secretary of Defense (Energy Resilience & Optimization)
3500 Defense Pentagon, RM 5C646
Washington, DC 20301-3500

10. SPONSOR/MONITOR'S ACRONYM(S)
SERDP

11. SPONSOR/MONITOR'S REPORT NUMBER(S)
WP18-1215

12. DISTRIBUTION/AVAILABILITY STATEMENT
DISTRIBUTION STATEMENT A. Approved for public release: distribution unlimited.

13. SUPPLEMENTARY NOTES

14. ABSTRACT

The bilgewater of Armed Forces vessels is often contaminated with complex oil-in-water (OW) shipboard emulsions that result from on-board cleaning and mechanical operations. These emulsions are strongly stabilized against phase separation by a complex mixture of surfactants and particulates, which increases the time and energy inputs that are required to break the emulsions and separate the organic and inorganic components prior to bilgewater discharge. To address the need for a better understanding of the formation and stability of shipboard emulsions, the following three objectives were investigated in the research project: (1) understand emulsion composition and generation including the timeline and processing route for emulsion formation and the components/contaminants within on-board bilgewater; (2) measure and identify the surfactant-oilwater (SOW) chemical and physical parameters that influence the emulsion formation, phase behavior, and stability; and (3) construct binary and ternary phase diagrams relevant for real-world shipboard emulsions using model emulsion formulations as a starting point.

15. SUBJECT TERMS
Shipboard Emulsions, Model Surfactant-Oil-Water Systems, emissions and waste reduction, bilgewater

16. SECURITY CLASSIFICATION OF:			**17. LIMITATION OF ABSTRACT**	**18. NUMBER OF PAGES**	**19a. NAME OF RESPONSIBLE PERSON**
a. REPORT	**b. ABSTRACT**	**c. THIS PAGE**			John Howarter
UNCLASS	UNCLASS	UNCLASS	UNCLASS	151	**19b. TELEPHONE NUMBER** *(Include area code)* 765-496-3103

Table of Contents

Abstract *15*

Executive Summary *16*

Background *28*

Materials & Methods *33*

Spontaneous Emulsion Characterization **33**

Interfacial Tension **34**

Emulsion Imaging **34**

Dynamic Light Scattering **34**

Emulsion Characterization For Dynamic Ageing Tests **35**

Emulsification Process For Accelerated Ageing And High Energy Mixing **36**

Accelerated Creaming Tests **37**

Measurement Of Clarification Rate, Instability Index, And Creaming Velocity **39**

Measurement Of Droplet Size And Droplet Size Distribution **40**

Measurement Of Remnant Oil **41**

Results and Discussion *42*

Surfactant Composition and Emulsion Stability **42**

Effect of Mixed Surfactant Ratio on Interfacial Surfactant Packing **43**

Effect of Mixed Surfactant Ratio on Emulsion Drop Size Distribution and Stability against Coalescence **46**

Effect of Mixed Surfactant Ratio on Emulsion Stability against Flocculation and Creaming Dynamics **47**

Effect of mixed surfactant ratio on remnant oil content **48**

Spontaneous Emulsion **50**

Visual Observations of Spontaneous Emulsification **50**

Emulsion Stability **52**

Spontaneity via Micelle Swelling **56**

Impact of Oil Concentration on Micelle Size **60**

Dynamic Interfacial Tension **62**

Mechanism of Spontaneous Emulsification **63**

Predicting Spontaneous Emulsification using HLD Model **64**

Spontaneous Emulsification in NPE-Saltwater Environments **66**

Spontaneous Emulsification in SDBS-Saltwater Environments **68**
Spontaneous Emulsification in Mixed NPE-SDBS Systems **71**
HLD Analysis of Spontaneous Emulsification **74**
Dynamic Aging and Low Energy Emulsification **86**
Effect of interfacial tension on O/W emulsion stability **88**
Oil drop size after static ageing in salt **90**
Oil drop size after dynamic ageing at 12 rpm **94**
Oil drop size after dynamic ageing at 30 rpm **98**
Emulsion ageing conditions and characterization **103**
Energy density for dynamic ageing **103**
Effect of dynamic ageing with 50% and 0% air inside the ageing vial **104**
Effect of dynamic ageing on the dispersion of oil into surfactant and salt solutions **109**
Scenario 1: Dynamically ageing non-pre-mixed emulsions with 0% air **110**
Scenario 2: Dynamically ageing non-pre-mixed emulsions with 70% air **111**
Surfactant-to-oil ratios that produce narrow drop size distributions **114**
Impact of processing routes on droplet size **116**
Droplet Size as a function of Energy Density **116**
Droplet size as a function of the emulsification process **117**
Droplet size as a function of oil concentration **119**
Droplet size as a function of surfactant chemistry **122**
Droplet Size as a Function of Ageing Time **125**
Impact of processing routes on creaming dynamics **126**
Creaming as a function of droplet size distribution **126**
Creaming behavior as a function of oil and surfactant concentration **128**
Remnant Oil measurement **130**
Conclusions and Implications for Future Research ***133***
Future Perspectives ..... Error! Bookmark not defined.
4.4: Conclusions ..... Error! Bookmark not defined.
Literature Cited ***136***
Appendices ***147***

LIST of TABLES

Table 1:[1] Surface excess concentration (Γ), surfactant head group area (A_0), critical micelle concentration (CMC), packing parameter (P), and the mole fraction of surfactant in the mixed micelle ($\boldsymbol{x}$) for NPE, SDBS, and an equal molar NPE-SDBS mixture at different salt concentrations. Errors represent the propagated standard error of the fitted curve(s) from which the calculation originated. SDBS solutions began salting out (phase separating) at concentrations between 0.27 and 0.31 M NaCl and therefore were not tested above 0.21 M NaCl. 17
Table 2**:** [3] Values of CMC, surface excess concentration, and surfactant head group area for SLES and Triton X-100 in the presence of salt. 18
Table 3: [5] Estimated HLD values with different oils. The same surfactant composition (Span-80:SLES = 5:1, wt./wt.) and the salinity of seawater (0.42 M NaCl) was used. 21
Table 4: [6] Elastic, viscous, and dilatational moduli for salt concentrations of 0, 0,42 M NaCl and 0.42 M $MgCl_2$ at oscillation frequencies of 0.01, 0.05 and 0.10 s^{-1}. Error represents one standard deviation from the mean. 23
Table 5**.** Zeta potential of oil drops with 0.42 M NaCl and 500 ppm surfactant at different ratios. 45
Table 6: Initial micelle diameter (d_0), swelling start time (t_0), micelle growth rate (k_m), micelle diameter at 60 minutes (d_{60}), and solubility in water at 25 °C (S_o) for toluene, xylenes, cyclohexane, and mineral oil. Errors represent one standard deviation. 59
Table 7: Calculated diffusion coefficient for each oil in a 500 ppm NPE solution ($D_{oil\text{-}NPE}$), diffusion coefficient for each oil in water ($D_{oil\text{-}water}$), and the ratio of $D_{oil\text{-}NPE}$ to $D_{oil\text{-}water}$. 60
Table 8: Surface excess concentration (Γ), surfactant head group area ($\boldsymbol{A0}$), critical micelle concentration (CMC), packing parameter (P), and the mole fraction of surfactant in the mixed micelle ($\boldsymbol{x}$) for NPE, SDBS, and an equal molar NPE-SDBS mixture at different salt concentrations. Errors represent the propagated standard error of the fitted curve(s) from which the calculation originated. 65
Table 9: NPE micelle swelling rates at 0, 0.21, and 0.42 M NaCl calculated from the slope of the micelle size over time. Error represents the standard error from the corresponding fitted curve. 68
Table 10. Estimated HLD values with different oils. The same surfactant composition (Span-80:SLES = 5:1, wt./wt.) and the salinity of seawater (0.42 M NaCl) was used. 85
Table 11**:**Values of CMC, surface excess concentration, and surfactant head group area for SLES and Triton X-100 in the presence of salt. 90
Table *12***:** Emulsion compositions used to investigate unimodal drop distributions after dynamic ageing. 115
Table *13***:** Light and heavy mineral oil density and viscosity at 40°C 115
Table 14. Summary of the harmonic mean droplet size for emulsions in Figure 53 123

LIST of FIGURES

Figure 1**:** [2] (a) Equilibrium interfacial tension between mineral oil and the aqueous solution with 0.42M NaCl and 500 ppm surfactant at different SLES : Triton X-100 ratios (b) Critical micelle concentration (CMC) of surfactant mixtures with different SLES : Triton X-100 ratios. The values of CMC in ppm are shown above / below each data point. 18
Figure 2: [4] Mechanism of spontaneous emulsification: diffusion-driven micelle swelling. 19
Figure 3**:** [4] Spontaneous emulsification of 5000-ppm toluene, xylenes, and cyclohexane with a 500-ppm of NPE solution after 40 min of contact. The scale bar applies to all images. 20
Figure 4**:** [5] Photographs of spontaneous emulsification. The images were taken 20 minutes, 1 hour and 24 hours after the oil and aqueous phase were brought in contact. The oil phase (upper phase) is hexadecane with 100, 300, 500, 800, 5000 ppm Span-80 (from left to right). The aqueous phase (bottom phase) is DI water with 100 ppm SLES and 0.1 M NaCl. 21
Figure 5: [5] HLD_{mix} calculated for systems with 0.1 M NaCl. The solid curves indicates where $HLD_{mix} = \pm 1$. The dashed curves indicates where $HLD_{mix} = \pm 2$. The region between the solid line is where spontaneous emulsification is more likely to occur. The solid, red data points represent spontaneous emulsification in both oil and aqueous phases. The hollow triangles pointing up represent spontaneous emulsification observed only in the oil phase. The hollow triangles pointing down represent spontaneous emulsification observed only in the aqueous phase. The black cross indicates no spontaneous emulsification observed. 22
Figure 6: [5] HLD_{mix} calculated for systems with hexadecane (EACN = 16). The solid curves indicates where $HLD_{mix} = -1$. The dashed curves indicates where $HLD_{mix} = -2$. The region above the solid line is where spontaneous emulsification is more likely to occur. 22
Figure 7: [6] (A) IFT decay for the first 60 seconds after drop formation normalized by the IFT at 300 seconds (γ_{300}). (B) Adsorption time to reach 95% of γ_{300} for SLES at the mineral oil-water interface for different ionic strengths. Error bars represent one standard deviation from the mean. 23
Figure 8: [2] Optical images of (a) emulsion flocculation and creaming in saline environment with 500 ppm mixed surfactant composed of 40 wt. % SLES + 60 wt. % Triton X-100, (c) 50 wt. % SLES + 50 wt. % Triton X-100. (The red arrows are pointing at non-flocculated oil droplets or small flocs) (b) the bottom of the creamed layer with 500 ppm mixed surfactant composed of 40 wt. % SLES + 60 wt. % Triton X-100, (d) 50 wt. % SLES + 50 wt. % Triton X-100 after aging for 5 days. The red rectangle is highlighting the layer of small oil droplets with diameter < 10 μm. 24
Figure 9: [2] Estimated remnant oil content in the emulsion subnatant at different surfactant ratios. The estimation was based on the turbidity values at 450 nm and calibration curves in Fig. 7 (a). The values in ppm were shown above/below each data point. 25
Figure 10: [3] The evolution of average oil drop size distribution over 20 days for dynamically aged emulsions at 12 rpm with a) SLES and b) Triton X-100 from 10 to 1000 ppm surfactant. The darkening of the distribution curves is proportional to time. 26
Figure 11: Temperature as a function of ethoxylate surfactant concentration fish diagram. The emulsion system contains TEP lubricating oil and the salinity is 3.5 mg/100 ml. Plot created from data obtained from fish diagram app developed by Prof. Steven Abbott[21,28]. 31
Figure 12: Generation of single and double emulsion droplets using microfluidic devices fabricated by Martinez and coworkers.[175,176] 33

Figure 13: Photograph of a) the Benchmark BenchRocker 3D Nutating Shaker with tilt angle θ, and b) emulsification container with falling height h. 36
Figure 14: Orifice Mixer Schematics..... 37
Figure 15. Rotor-Stator schematics 37
Figure 16: LUMiSizer working principle. The Transmission (%) over Position (mm) fingerprints represent the vial position and concentration of droplets within the bulk of the emulsion under centrifugation. Low transmission values indicate droplet-concentrated areas. High transmission values indicate droplet-depleted areas. 38
Figure 17: Representation of the clarification rate, instability index, and creaming velocity calculation 40
Figure 18. Photographs of the emulsion creaming layer with different surfactant concentrations: 100, 200, 300, 400 ppm SLES or Triton X-100 after 24 hours. The emulsions were collected in sealed capillaries and stored, photographed vertically. The darker gray regions are the creaming layer, and the lighter region below is the subnatant. The circled 42
Figure 19. Drop size distribution of emulsions with different surfactant concentrations: (a) 200 ~ 1000 ppm SLES, (b) 300 ~ 1000 ppm Triton X-100. Measurements were taken 1 hour after emulsification. 43
Figure 20: Drop size distribution of emulsions with different surfactant concentrations: (a) 200 ~ 1000 ppm SLES, (b) 300 ~ 1000 ppm Triton X-100. Measurements were taken 1 hour after emulsification. 44
Figure 21: Drop size distribution of emulsions with different surfactant ratios: pure Triton X-100, SLES : Triton X-100 = 2:8, 3:7, 4:6, 5:5, 6:4, 8:2, pure SLES. Measurements were taken (a) 1 hour, (b) 5 days and (c) 20 days after emulsification. (d) Photographs of the emulsion creaming layer with different surfactant ratios: SLES : Triton X-100 = 2:8, 4:6, 5:5, 6:4, 8:2, after 0 day, 2 days, 5 days, and 20 days. 46
Figure 22. Optical images of (a) emulsion flocculation and creaming in saline environment with 500 ppm mixed surfactant composed of 40 wt. % SLES + 60 wt. % Triton X-100, (c) 50 wt. % SLES + 50 wt. % Triton X-100. (The red arrows are pointing at unflocculated oil drops or small flocs) (b) the bottom of the creamed layer with 500 ppm mixed surfactant composed of 40 wt. % SLES + 60 wt. % Triton X-100, (d) 50 wt. % SLES + 50 wt. % Triton X-100 after aging for 5 days. (The red rectangle is highlighting the layer of small oil drops with diameter less than 10 μm.) 48
Figure 23: Typical drop size distribution of remanent mineral oil after ultrasonication at 10% power for 20 minutes. The solid line was measured directly after ultrasonication and the dash line was measured with 25 vol% dilution (0.25 ml ultrasonicated emulsion + 0.75 ml DI water) 49
Figure 24.(a) Turbidity of calibration emulsion samples with 0.03125 wt. %, 0.04688 wt. %, 0.0625 wt. %, 0.09375 wt. %, 0.125 wt. % mineral oil and different surfactant ratios (pure SLES, SLES : Triton X-100 = 8:2, 5:5, 2:8, pure Triton X-100). Measurements were conducted at 450 nm wavelength. (b) Turbidity of the bottom layer of aged emulsion samples. Each sample had a volume of 15 ml and was ultrasonicated at 10% power for 20 minutes then diluted with 75 vol% DI water (1 ml ultrasonicated emulsion + 3 ml DI water). The oil concentrations of the calibration samples were calculated after dilution..... 50
Figure 25: Spontaneous emulsification of 5000 ppm toluene in a 500 ppm NPE solution after 0, 30, and 90 minutes of contact. The toluene-water interface is marked by the red dotted line at 0 minutes. The toluene droplet size distribution at 90 minutes is also reported. Note that toluene

was used in such a small quantity that it did not completely cover the air-water interface. The two white asterisks labelled on the far-left image indicate optical artifacts (light reflections) and are not to be mistaken for features of emulsification. These reflections appear in each image.... 51
Figure 26: Images depicting (A) convective flow due to interfacial tension gradients along the interface forming streams of toluene droplets from a larger, bulk toluene droplet in an aqueous phase which contained 500 ppm NPE and (B) a roll cell (dark regions surrounding the outside of the roll cell arrows) formed during spontaneous emulsification of the same toluene droplet located in image A. 51
Figure 27: Spontaneous emulsification of 5000-ppm toluene, xylenes, and cyclohexane with a 500-ppm NPE solution after 40 minutes of contact. The scale bar applies to all images..... 52
Figure 28: Photographs of toluene, xylene, and cyclohexane emulsions aged for 90 min, 17 days, and 30 days. After 30 days, all emulsions were transparent. The scale bar applies to all images. 53
Figure 29: Evolution of swollen micelle and droplet size distributions from 90 minutes to 40 days of ageing for toluene (left), xylenes (middle), and cyclohexane (right). For all 40-day size distributions, the NPE micelle size distribution is overlaid for comparison (dashed line). All peaks are labeled with their corresponding average size ($\boldsymbol{D50}$). 54
Figure 30: Z-average swollen NPE micelle and droplet diameters for toluene, xylenes, and cyclohexane between 90 minutes and 40 days. Error bars represent one standard deviation. Dotted line represents the NPE micelle diameter. The y-axis is plotted on a logarithmic scale... 54
Figure 31**:** Z-Average swollen NPE micelle and droplet diameters for an emulsion containing 5000 ppm toluene (solid symbols) and excess toluene (open symbols) between 90 minutes to 40 days. Error bars represent one standard deviation. The y-axis is plotted on a logarithmic scale. To the right of the plot are images of the spontaneous emulsion with excess toluene at 0, 2, 11, and 32 days. Light reflections can be seen in the bottom corners of each vial and should not be mistaken for features of emulsification..... 56
Figure 32: Swollen NPE micelle size distribution before (0 min) and after contact with toluene for 30 and 60 minutes. Intensity was normalized to the size distribution at 0 min. Z-average diameters are reported above each size distribution. 57
Figure 33: NPE micelle swelling response in the presence of excess oil for (A) 60 minutes and (B) magnification of data in the early stages of swelling. Plot B illustrates the intersection of each data series with the initial micelle size (d_0 horizontal line) to determine approximate values of t_0 (reported in Table 5). Error bars represent one standard deviation in both micelle diameter and time. 58
Figure 34: Measured (red squares) and predicted (open circles) equilibrium NPE micelle diameter for different concentrations of toluene. Error bars represent one standard deviation. ... 61
Figure 35: Dynamic interfacial tension of toluene, xylenes, cyclohexane, and mineral oil with an aqueous solution containing 500 ppm NPE. In these experiments, the pendant drop contained the aqueous phase and was surrounded by a continuous phase of oil. 63
Figure 36: Diagram displaying the governing mechanism for spontaneous emulsification of toluene, xylenes, and cyclohexane in an NPE surfactant solution during DLS experiments. The initial micelle size (d_0) is smaller than the micelle size after swelling with oil (d). Image not to scale. Times *t* correspond to relevant times in micelle swelling experiments (Error! Reference source not found. and Table 7). 64
Figure 37: Gibbs adsorption isotherms for (A) NPE, (B) SDBS, and (C) an equal molar NPE-SDBS mixture at different concentrations of NaCl. Dotted and solid lines represent a best curve

fit before and after the CMC, respectively. Error bars represent one standard deviation from the mean of three equilibrium surface tension measurements. 65
Figure 38: Images of spontaneous emulsification for toluene with NPE aqueous solutions containing (top row) 0 M NaCl and (bottom row) 0.42 M NaCl using 10, 50, 100, and 500 ppm of NPE. The top layer of the vial is toluene, and the bottom layer is the aqueous solution. Each image was taken four hours after toluene was pipetted onto the surface of the aqueous solution. The scale bar is 5 mm and applies to all images. 67
Figure 39: Spontaneity measurements via dynamic light scattering over time for 500 ppm NPE solutions containing 0, 0.21, and 0.42 M NaCl. Solid lines represent the fitted curves for the swelling region of each system. Error bars represent one standard deviation from the mean of three measurements..... 68
Figure 40: Images of spontaneous emulsification for toluene with 5000 ppm SDBS aqueous solutions containing 0, 0.06, 0.07, 0.10, and 0.21 M NaCl. The top layer of the vial is toluene, and the bottom layer is the aqueous solution. The dotted white line in the 0.07 M NaCl image represents the oil-water interface and the solid blue line represents the top of the emulsified oil layer in the aqueous phase. Each image was taken four hours after toluene was pipetted onto the surface of the aqueous solution. The scale bar is 5 mm and applies to all images..... 69
Figure 41: Images of spontaneous emulsification for toluene with SDBS aqueous solutions containing (first row) 0.08 M NaCl, (second row) 0.10 M NaCl, and (third row) 0.21 M NaCl using 50, 100, 300, 1000, and 5000 ppm of SDBS. The top layer of the vial is toluene, and the bottom layer is the aqueous solution. Each image was taken four hours after toluene was pipetted onto the surface of the aqueous solution. The scale bar is 5 mm and applies to all images. 70
Figure 42: Spontaneity measurements via dynamic light scattering for aqueous solutions containing 5000 ppm SDBS with (A) 0.10, (B) 0.15, and (C) 0.21 M NaCl. The time label for each curve represents the elapsed time after toluene was pipetted onto the surface of the aqueous solution. The first curve (light grey) in each plot is similar to the initial micelle size. The next two curves (medium grey and black) represent the first detection of droplets and droplet growth, respectively. Labels for each peak represent the mean droplet diameter of that peak. 71
Figure 43: Images of spontaneous emulsification for toluene with a 5000 ppm, equal molar NPE-SDBS solution containing 0, 0.01, 0.02, 0.10, and 0.21 M NaCl. The top layer of the vial is toluene, and the bottom layer is the aqueous solution. Each image was taken four hours after toluene was pipetted onto the surface of the aqueous solution. The scale bar is 5 mm and applies to all images..... 72
Figure 44: Images of toluene on top of a 5000 ppm, equal molar NPE-SDBS solution containing 0 and 0.01 M NaCl. These images were taken six days after toluene was pipetted onto the surface of the aqueous solution. Red circles locate larger droplets that can be seen at the surface of the aqueous solution. The scale bar represents 5 mm and applies to both images..... 72
Figure 45: Spontaneity measurements via dynamic light scattering over time for 5000 ppm, equal molar NPE-SDBS solutions containing 0.10 M NaCl. The solid line represents the fitted curve for the swelling region. Error bars represent one standard deviation from the mean of three measurements. The micelle swelling rate (i.e., the slope of the fitted curve) was 0.296 ± 0.004 nm/min. 73
Figure 46: Spontaneity measurements via DLS for aqueous solutions containing 5000 ppm, equal molar NPE-SDBS with (A) 0.15 and (B) 0.21 M NaCl. The time label for each curve represents the elapsed time after toluene was pipetted onto the surface of the aqueous solution. Labels for each major peak represent the mean droplet diameter of that peak..... 74

Figure 47: Calculated HLD values as a function of salt (NaCl) concentration for different surfactant-oil systems. Green symbols represent samples that showed spontaneous emulsification while red symbols represent samples that were not spontaneous. The symbol for cyclohexane is yellow because there was very little emulsification that could only be detected via DLS. Xylenes, cyclohexane, and mineral oil systems were observed in a previous study.[114] 75
Figure 48: Calculated HLD values for samples with different turbidities (i.e., total emulsified toluene). Turbidity was taken as the absorbance at 400 nm and was measured after two days of contact with toluene. Error bars represent one standard deviation from the mean of three measurements. 76
Figure 49. Photographs of spontaneous emulsification at 20 minutes, 1 hour and 24 hours. The oil phase (upper phase) is hexadecane with 100, 300, 500, 800, 5000 ppm Span-80 (from left to right). The aqueous phase (bottom phase) is DI water with 100 ppm SLES and 0.1 M NaCl. The C_c* values were estimated based on molar mixing rule. 78
Figure 50. Photographs of spontaneous emulsification at 20 minutes, 1 hour and 24 hours. The oil phase (upper phase) is hexadecane with 500 ppm Span-80. The aqueous phase (bottom phase) is DI water with 10, 50, 100, 150, 500 ppm SLES (from left to right) and 0.1 M NaCl. The C_c* values were estimated based on molar mixing rule. 79
Figure 51. Photographs of spontaneous emulsification at 20 minutes, 1 hour and 24 hours. The oil phase (upper phase) was hexadecane with 500 ppm Span-80. The aqueous phase (bottom phase) was DI water with 100 ppm SLES and 0, 0.1, 0.2, 0.3, 0.42 M NaCl (from left to right). 81
Figure 52. Oil drop size evolution in the aqueous phase with (a) 0 M, (b) 0.1 M, (c) 0.2 M, (d) 0.3 M NaCl. The measurements were made at 2 mm below the oil-water interface. The mean drop diameter (D_{50}) at equilibrium were noted in each figure. 82
Figure 53: Water drop size evolution in the oil phase with (a) 0 M, (b) 0.1 M, (c) 0.2 M, (d) 0.3 M NaCl. The measurements were made at 2 mm above the oil-water interface. The mean drop diameter (D_{50}) of the peaks were noted in each figure. 83
Figure 54. Photographs of spontaneous emulsification at 20 minutes, 1 hour and 24 hours with different oils. The oil phase (upper phase) was paraffin oil, hexadecane, dodecane, decane and heptane (from left to right) with 500 ppm Span-80. The EACN values were noted below the figure.[123] The aqueous phase (bottom phase) was DI water with 100 ppm SLES and 0.1 M NaCl. 84
Figure 55**:** Zeta potential of emulsions with 5000 ppm mineral oil, 0.42 M NaCl, and 10 ppm - 2500 ppm SLES (black) and Triton X-100 (gray) after 3 hours of static ageing. 87
Figure 56: Optical microscopy of emulsions made with 5000 ppm Mineral Oil, 0.42 M NaCl, and 500 ppm of a) Triton X-100 and b) SLES after 3 hours of static ageing. 88
Figure 57**:**Equilibrium interfacial tension of SLES + 0.42 M NaCl (black) and Triton X-100 + 0.42 M NaCl (gray) in mineral oil as a function of surfactant concentration. Equilibrium IFT was obtained via the Pendant Drop Method. 89
Figure 58:The evolution of average oil drop size distribution over 20 days for statically aged emulsions with a) SLES and b) Triton X-100 from 10 to 1000 ppm surfactant. The darkening of the distribution curves is proportional to time. 91
Figure 59**:**Average oil drop diameter, D(4,3) during static ageing with increasing concentrations of SLES (left) and Triton X-100 (right). Lines were added between data points as visual guides. Dashed lines represent unstable emulsions that result from increased over time. Error bars represent the standard deviation. 92

Figure 60**:** Photograph of the top view of a statically aged emulsion (20 days) with 0.42M NaCl, 10 ppm Triton X-100, and 5000 ppm mineral oil in a 50 mL centrifuge tube. 93
Figure 61**:**Photographs of (a) 500 ppm SLES, 0.42 M sodium chloride, and 5000 ppm mineral oil in a 50 mL centrifuge tube. The figure shows brightfield optical images of 500 ppm SLES, 0.42 M sodium chloride, and 5000 ppm mineral oil 20 days after emulsification. 93
Figure 62**:**The evolution of average oil drop size distribution over 20 days for dynamically aged emulsions with 70% air at 12 rpm with a) SLES and b) Triton X-100 from 10 to 1000 ppm surfactant. The darkening of the distribution curves is proportional to time. 96
Figure 63**:**Brightfield optical image of 1000 ppm SLES aged for 20 days at 12 rpm. 96
Figure 64**:** Average oil drop diameter, D(4,3) during dynamic ageing at 12rpm with 70% air and increasing surfactant concentration for SLES (left) and Triton X-100 (right). Dashed lines represent unstable emulsions that result from increased oil drop size over time. The darkening of the distribution curve is proportional to time. 97
Figure 65**:**The evolution of average oil drop size distribution over 20 days for dynamically aged emulsions with 70% air at 30 rpm with a) SLES and b) Triton X-100 from 100 to 1000 ppm surfactant. The darkening of the distribution curves is proportional to time. 99
Figure 66**:** Brightfield optical image of an emulsion (0.42M NaCl, 1000ppm SLES, 5000ppm mineral oil) dynamically aged at 30rpm for 20 days and with 70% air within the ageing vial. ... 99
Figure 67**:** Average oil drop diameter, D(4,3) during dynamic ageing with 70% air at 30 rpm and increasing surfactant concentration for SLES (left) and Triton X-100 (right). Dashed lines represent unstable emulsions that result from increased oil drop size over time. The darkening of the lines is proportional to increased surfactant concentration. 100
Figure 68**:** Average oil drop size distribution after 20 days for 100 ppm SLES and 500 ppm Triton X-100 aged statically, dynamically at 12 rpm, and dynamically at 30 rpm. 102
Figure 69**:** Photographs of a 15 mL emulsion inside a) a 50 mL centrifuge tube with 70% air, b) a syringe with 50% air and c) a syringe with all air removed (0% air). 103
Figure 70**:** The evolution of average oil drop distribution over 20 days for dynamically aged emulsions with 50% air and concentrations from 10 – 1000 ppm of SLES. The darkening of the distribution curves is proportional to time. 105
Figure 71: Photograph of an emulsion dynamically aged for 5 days with 100 ppm SLES, 0.42 M sodium chloride, 5000 ppm mineral oil, and 0% air. 106
Figure 72**:** The evolution of average oil drop distribution over 20 days for dynamically aged emulsions with 0% air and concentrations from 10 – 1000 ppm of SLES. The darkening of the distribution curves is proportional to time. 107
Figure 73**:**Top view photograph of coalesced mineral oil drops in an emulsion with 10 ppm SLES, 0.42 M sodium chloride, and 5000 ppm mineral oil after 20 days of ageing with 0% air inside the syringe. 108
Figure 74: Brightfield optical images of a) 10 ppm b) 100 ppm c) 500 ppm and d) 1000 ppm SLES after 20 days of dynamic ageing with 0% air inside the syringe. 108
Figure 75**:** Photograph of the top view of a SLES and salt solution with 5000 ppm mineral oil added to the surface (0 days aged). 110
Figure 76: Photographs of the top view of emulsions with a) 10 ppm SLES and b) 1000 ppm SLES, 0.42 M sodium chloride, and 5000 ppm mineral oil that were not pre-emulsified and dynamically aged with 0% air for 10 days. 110

Figure 77**:**The average oil drop distribution for 10 – 1000 ppm of a) SLES and b) Triton X-100 after 10 days of dynamic ageing with 70% air. Mineral oil (5000 ppm) was dispensed, and the liquids were not pre-emulsified prior to ageing. 112
Figure 78**:** Brightfield optical images of a) 10 ppm and b) 1000 ppm SLES, 0.42 M sodium chloride, and 5000 ppm mineral oil after 10 days of dynamic ageing with 70% air and no pre-mixing. 112
Figure 79**:**Top view photographs of an emulsion with 1000 ppm SLES, 0.42 M sodium chloride, 5000 ppm Mineral oil after a) 0 days, b) 5 hours, and c) 2 days of dynamic ageing with 70% air and no pre-mixing. 113
Figure 80**:** Photograph of the top view of an emulsion with 100 ppm SLES, 0.42 M sodium chloride, and 5000 ppm mineral oil after 10 days of dynamic ageing with 70% air and no pre-mixing. 113
Figure 81**:** Optical Images of emulsions a) 2, b) 3, and c) 4 that were dynamically aged for 10 days at 30 rpm with 70% air within the ageing vial. The emulsions were made with heavy mineral oil and were not pre-mixed prior to ageing. 116
Figure 82**:**Optical Images of emulsions a) 5, b) 6, and c) 7 dynamically aged for 10 days at 30 rpm with 70% air within the ageing vial. The emulsions were made with light mineral oil and were not pre-mixed prior to ageing. 116
Figure 83 Droplet size and size distribution of mineral oil (5 wt%), SLE_1S (1 wt%) in water emulsions fabricated with variable energy density. (a) Median droplet size as a function of energy density. (b) Volume distribution density as a function of droplet size. 117
Figure 84 Mean droplet size as a function of the emulsification process and energy density. Mineral oil-waterer emulsions stabilized with SLE_1S and mixed with orifice mixer and rotor-stator. (a) Volume harmonic mean (b) Droplet size distribution. 118
Figure 85 (a) Representation of the reduction in channel size of the orifice mixer. (b) Representation of the energy dissipation in the radial direction of the rotor-stator mixer 119
Figure 86 Droplet size and size distribution of emulsions with variable oil concentration. Emulsions: mineral oil ranging between 0.5 wt% to 20 wt%, SLE_1S at 1 wt%, and energy density of 3.45 MPa. (a) Median droplet size as a function of mineral oil concentratio. (b) Volume distribution density as a function of droplet size 119
Figure 87 Light transmission profiles of emulsions stabilized with 1 and 10 ppm SLE_1S. Mineral oil concentration 1, 10 and 20 vol% 120
Figure 88 Mineral oil-water-SLE_1S emulsions at variable surfactant/oil concentrations. The picture was taken after the centrifugation cycle in LUMiSizer® (time=1.03 h. Centrifugation at RCA= 265 g) 121
Figure 89. Droplet size characterization of mineral oil-water emulsions stabilized with SLE_1S. (a) Harmonic mean droplet size (b) DSD for emulsions with 1 ppm SLE_1S (c) DSD for emulsions with 10 ppm SLE_1S 122
Figure 90. Mean droplet size as a function of energy density using the orifice mixer. Mineral oil–water emulsions fabricated with orifice mixer (a) Volume harmonic mean of emulsions stabilized with SLE_1S and Surfonic. (b) DSD for emulsions stabilized with SLE_1S at two different concentrations 123
Figure 91. Size distribution as a function of two levels of energy density using a rotor stator. Mineral oil (5wt%) emulsions stabilized with 1 wt% SLE_1S or Surfonic (a) Rotor-stator at low shear (9500 rpm 1 min) (b) Rotor-stator at high shear (13500 rpm 5 min) 124

Figure 92 Size distribution as a function of two levels of energy density using a rotor stator. Mineral oil (5wt%) emulsions stabilized with 1 wt% Sugamulse or Suganate (a) Rotor-stator at low shear (9500 rpm 1 min) (b) Rotor-stator at high shear (13500 rpm 5 min) 125
Figure 93 Droplet size and size distribution of model emulsions with variable dispersed phase concentration at 0 and 90 days of aging. Model emulsions: mineral oil ranging between 0.5 wt% to 20 wt%, SLE_1S at 1 wt%, and energy density of 3.45 MPa. (a) Median droplet size as a function of mineral oil concentration at 0 and 90 days. (b) Volume distribution density as a function of droplet size for day 0. (c) Volume distribution density as a function of droplet size for day 90. 126
Figure 94 Canola oil - water emulsion stabilized with SLE_1S or Surfonic at 1wt%. Rotor-stator at 19 and 226 MPa. (a) Resulting harmonic mean droplet size and DSD (b) Clarification rate (slope of the initial linear part of curve) 127
Figure 95: Creaming dynamics characterization of Mineral oil - water emulsions stabilized with SLE_1S (a) Instability index of emulsions with 1 ppm SLE_1S (b) Creaming velocity of emulsions with 1 ppm SLE_1S (c) Instability index of emulsions with 10 ppm SLE_1S (d) Creaming velocity of emulsions with 10 ppm SLE_1S 129
Figure 96 Calibration curve data. (a) droplet size distribution after homogenization. (b) characteristic peak for mineral oil solutions in isooctane. O% represent pure isooctane and 100% represents pure mineral oil. 130
Figure 97*:* Absorbance of calibration emulsions 131
Figure 98. Remnant oil of aged emulsions mixed with an orifice mixer. (a) emulsions mixed with variable energy density and constant oil concentration (5 wt% oil - 1 wt% SLE1S) (b) emulsions with variable oil concentration mixed under a constant energy density (3.45 MPa – 1 wt% SLE1S) 132

List of Acronyms

A	Area
ADSA	Axisymmetric Drop Shape Analysis
Cc	characteristic curvature of the surfactant
DLS	dynamic light scattering
DoD	Department of Defense
E’	Elastic Modulus or Storage Modulus
E’’	Viscous Modulus or Loss Modulus
E*	Viscoelastic Modulus
EACN	effective alkane carbon number of the oil
EO	ethoxylated
EOR	enhanced oil recovery
HLB	hydrophilic-lipophilic balance
HLD	hydrophilic-lipophilic difference
N	Number of Droplets
NAC	net average curvature
O	oil
OW	oil-in-water
P&G	The Procter & Gamble Company
PPM	Parts Per Million
S	surfactant
SOW	surfactant-oil-water
W	water
γ	Interfacial Tension
δ	Phase Angle
ω	Frequency

Acknowledgements

Purdue Principle Investigators:

Dr. John A. Howarter [a, b]
Dr. Kendra A Erk [a]
Dr. Carlos Martinez [a]

Purdue Research Associates:

Dr. Yue Zheng [a]
Dr. Cole Davis [a,c]
Rina Sabatello [a]
Dr. Eduard Caicedo [a]

P&G Partners:

Seth Lindberg
Dr. Patrick Stenger

[a] School of Materials Engineering, Purdue University, West Lafayette, IN, 47907 USA
[b] Environmental and Ecological Engineering, Purdue University, West Lafayette, IN, 47907 USA
[c] Naval Surface Warfare Center, Crane Division, 300 Highway 361, Crane, IN, 47522 USA

Abstract

Introduction and Objectives

The bilgewater of Armed Forces vessels is often contaminated with complex oil-in-water (OW) shipboard emulsions that result from on-board cleaning and mechanical operations. These emulsions are strongly stabilized against phase separation by a complex mixture of surfactants and particulates, which increases the time and energy inputs that are required to break the emulsions and separate the organic and inorganic components prior to bilgewater discharge. To address the need for a better understanding of the formation and stability of shipboard emulsions, the following three objectives were investigated in the research project: (1) understand emulsion composition and generation including the timeline and processing route for emulsion formation and the components/contaminants within on-board bilgewater; (2) measure and identify the surfactant-oil-water (SOW) chemical and physical parameters that influence the emulsion formation, phase behavior, and stability; and (3) construct binary and ternary phase diagrams relevant for real-world shipboard emulsions using model emulsion formulations as a starting point.

Technical Approach

This work was based on fundamental principles of surfactant and emulsion science to provide a detailed picture of the bilgewater SOW phase space. We draw inspiration from the enhanced oil recovery (EOR) field where the models of hydrophilic-lipophilic difference (HLD) and net average curvature (NAC) have revolutionize the selection of surfactants to maximize oil extraction. The HLD and NAC are semi-empirical models firmly based on thermodynamic principles and together they offer a practical approach to surfactant selection as well as the effects of water salinity, oil type, and temperature on the SOW phase space. The proposed work aims to utilize the HLD and NAC principles to determine the region of the SOW phase space relevant to shipboard bilgewater.

Results

We successfully identified and measured fundamental parameters that control the formation and stability of surfactant-oil-water emulsions that are generated aboard marine vessels with a specific focus on the evolution of fine emulsion droplets (diameter less than < 20 microns) which are difficult to separate from bilge water using traditional water treatment methods. Our experiments probed the spontaneous emulsification of components common in bilgewater. We demonstrated and measured stability of SOW emulsions across a range of compositions and energy inputs to simulate the impact of process formation on emulsion stability in order to provide insights on how to prevent or efficiently destabilize SOW emulsions.

Benefits

Overall project outcomes can be used in the future to develop strategies to avoid the formation of fine stable emulsions, including those that are generated spontaneously, as well as to develop new methods to minimize and remove emulsified oils from bilge water. The outcomes of this work can be used by Department of Defense (DoD) operators to rapidly assess the physicochemical nature of specific shipboard emulsions within a vessel's bilgewater as well as provide guidance on the best practices to destabilize the emulsions. Additionally, the outcomes of this work will provide improved guidance to DoD operations managers for optimizing their detergent formulations and/or cleaning procedures in order to facilitate end-of-use OW separations prior to bilgewater discharge that are effective but less time and energy intensive.

Executive Summary

Executive Summary: Introduction

The bilgewater of Armed Forces vessels is often contaminated with complex oil-in-water (OW) shipboard emulsions that result from on-board cleaning and mechanical operations. These emulsions are strongly stabilized against phase separation by a complex mixture of surfactants and particulates, which increases the time and energy inputs that are required to break the emulsions and separate the organic and inorganic components prior to bilgewater discharge. This project is responsive to the objectives articulated in the SERDP Statement of Need, WPSON-18-C1: "Advancing Emulsion Science for Application in Armed Forces Vessels": to build a fundamental knowledge base concerning the occurrence and behaviors of shipboard OW emulsions. Specifically, this project applied advanced measurement tools to experimentally characterize the fundamental physicochemical processes which drive the formation and (de)stabilization of SOW shipboard emulsions that are known to contaminate the bilgewater of Armed Forces vessels.

Executive Summary: Objectives

While it is largely understood how simple oil-in-water emulsions are stabilized, there are fundamental knowledge gaps with respect to the formation and long-term stability of complex oil-in-water emulsions that arise from shipboard operations. These complex emulsions, which contain a range of oil-based moieties, are stabilized by a mixture of common industrial and natural surfactants. As a result, the breaking and separation of these emulsions is difficult and costly. Advancing the knowledge of physicochemical factors that impact emulsion stability will enable new technology to be developed for advanced water treatment of stable oil-in-water emulsions. To address the need for a better understanding of the formation and stability of shipboard emulsions, the following three objectives were investigated in the research project: (1) understand emulsion composition and generation including the timeline and processing route for emulsion formation and the components/contaminants within on-board bilgewater; (2) measure and identify the surfactant-oil-water (SOW) chemical and physical parameters that influence the emulsion formation, phase behavior, and stability; and (3) construct binary and ternary phase diagrams relevant for real-world shipboard emulsions using model emulsion formulations as a starting point.

Executive Summary: Technical Approach

Emulsions with or without external energy input were investigated. We investigated the effects of salinity, surfactant composition, oils chemistry, and aging conditions. Sodium laureth sulfate (SLES), Triton X-100, nonylphenol polyethoxylated (NPE), sodium dodecylbenzenesulfonate (SDBS) and polysorbate 80 (Span-80) were selected as surfactants likely present in bilge water emulsions.

Spontaneous emulsification is historically difficult to predict and could be influenced by many variables including salinity, temperature, and chemical composition of the oil and surfactant. In our work, the mechanisms of spontaneous emulsification were investigated in detail. Different surfactant systems, including NPE, SDBS, NPE-SDBS, SLES-Span-80 were tested. We found the hydrophilic-lipophilic difference (HLD) framework could serve as a guide to predict the

spontaneous emulsion behavior. Overall, as HLD approached zero, conditions became more favorable for spontaneous emulsification. These results provide a practical method to suggest what aqueous and oil compositions could promote - or eliminate - the formation of spontaneous emulsions in saltwater environments.

For emulsions with external energy inputs, we investigated the effect of salinity, surfactant ratio, and dynamic aging on emulsion properties in the context of bilge water. These results aid in minimizing the impact of emulsified oils on natural water systems. Overall, an increase in emulsion stability against coalescence and flocculation was observed with increasing salinity and proportion of SLES. Shipboard rocking can promote coalescence or emulsification depending on rocking speed, surfactant concentration, and surfactant type. To avoid further emulsification during ship rocking, either the surfactant concentration must be relatively low or the amount of air within the emulsification chamber needs to be reduced.

Executive Summary: Results and Discussion

1. Surfactant and Micelle Characterization

In this project, interfacial tension isotherms were collected for some commonly used surfactants nonylphenol polyethoxylated (NPE), Sodium dodecyl benzene sulfonate (SDBS), sodium lauryl ether sulfate (SLE_1S), Triton X-100 and their mixtures to understand their surface adsorption and micellar properties. The major results are shown in Table 1. This part of data also serves as a base for our results on emulsion behavior.

Table 1:[1] Surface excess concentration (Γ), surfactant head group area (A_0), critical micelle concentration (CMC), packing parameter (P), and the mole fraction of surfactant in the mixed micelle ($\boldsymbol{x}$) for NPE, SDBS, and an equal molar NPE-SDBS mixture at different salt concentrations. Errors represent the propagated standard error of the fitted curve(s) from which the calculation originated. SDBS solutions began salting out (phase separating) at concentrations between 0.27 and 0.31 M NaCl and therefore were not tested above 0.21 M NaCl.

Surfactant	NPE		SDBS				NPE-SDBS	
[NaCl] (M)	0	0.42	0	0.08	0.10	0.21	0	0.21
$\Gamma / 10^{-6}$ (mol/m^2)	2.88 ± 0.32	2.47 ± 0.46	2.07 ± 0.052	3.68 ± 0.32	3.47 ± 0.74	3.38 ± 0.48	-	-
A_0 ($Å^2$)	57.6 ± 6.4	67.3 ± 13	80.1 ± 2.0	45.2 ± 3.9	47.8 ± 10	49.1 ± 7.0	-	-
CMC (ppm)	39.9 ± 9.0	30.4 ± 11	573 ± 150	57.9 ± 13	45.2 ± 21	33.8 ± 9.4	35.7 ± 9.8	15.2 ± 3.3
CMC (mM)	0.060 ± 0.014	0.046 ± 0.017	1.64 ± 0.43	0.166 ± 0.037	0.129 ± 0.060	0.097 ± 0.027	0.071 ± 0.019	0.030 ± 0.0065
P	0.46	0.39	0.32	0.57	0.53	0.52	-	-
$\boldsymbol{x}$	-	-	-	-	-	-	0.76 for NPE	0.55 for NPE

As seen here, nonionic surfactants like NPE are relatively insensitive to changes in salt concentration. Contrarily, anionic surfactants like SDBS are sensitive to salt. For the equal molar NPE-SDBS mixed surfactant system, the CMC at 0 M NaCl was like that of pure NPE. However,

due to the presence of SDBS, this mixed system was also sensitive to salt. This CMC was the lowest value measured across all systems which suggests that the NPE and SDBS interact synergistically.

From the calculated head group area, the packing parameter (P) was also calculated to determine the micelle structure under different salt concentrations. From these calculations, NPE is predicted to form oblong-spherical to cylindrical micelles independent of salt concentration. SDBS is predicted to form spherical micelles ($P \leq 0.33$) in salt-free environments (i.e., no additional salt added) and cylindrical micelles ($0.33 \leq P \leq 0.5$) at salt concentrations between 0.08 and 0.21 M NaCl.

Isotherms for SLES and Triton X-100 were also collected[2] with related parameters shown in Table 2. According to the interfacial tension data in Figure 1, the addition of SLES to Triton X-100 can effectively lower the interfacial tension between mineral oil and surfactant solutions in saline environment. The average head area (A_0) was calculated to be approximately 33 Å^2 for SLES and 81 Å^2 for Triton X-100. The estimated Debye length ($\frac{1}{\kappa}$) was less than 0.5 nm due to high salt concentration. As a result, SLES could pack more densely than Triton X-100 at the interface without electrostatic repulsion, causing the reduction in IFT.

Table 2**:** [3] Values of CMC, surface excess concentration, and surfactant head group area for SLES and Triton X-100 in the presence of salt.

Surfactant Type	**CMC with 0.42M NaCl [ppm]**	**Surface Excess Concentration, Γ_s $[10^{-6}\ mol/m^2]$**	**C_a Needed to form 1 µm monodisperse drops [ppm]**	**Surfactant Head Group Area, A $[Å^2/molecule]$**
SLES	33	6.38	74	26.0
Triton X-100	312	2.51	55	66.2

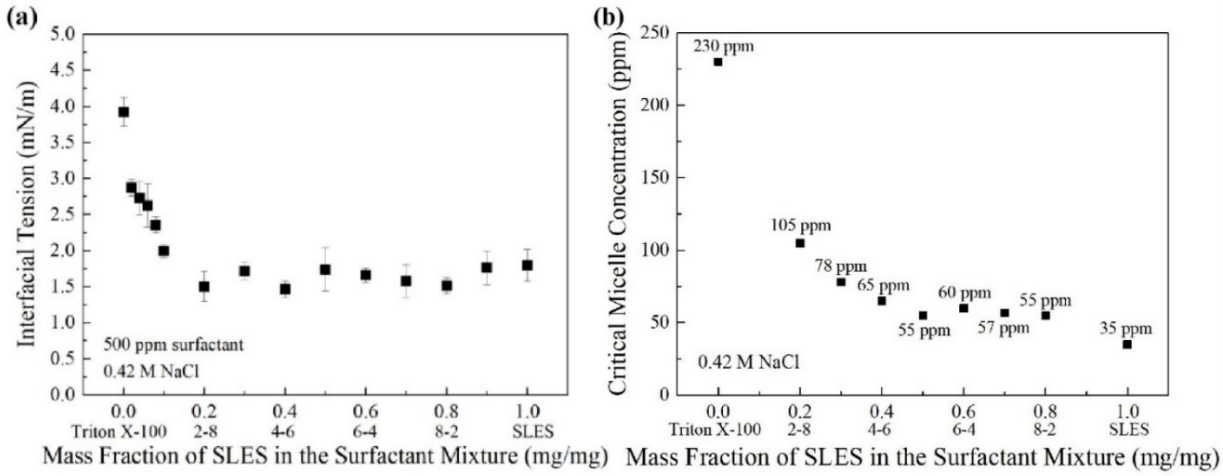

Figure 1**:** [2] (a) Equilibrium interfacial tension between mineral oil and the aqueous solution with 0.42M NaCl and 500 ppm surfactant at different SLES : Triton X-100 ratios (b) Critical micelle concentration (CMC) of surfactant mixtures with different SLES : Triton X-100 ratios. The values of CMC in ppm are shown above / below each data point.

2. Results on Spontaneous Emulsification

2.1 Systems with Single Surfactants

Spontaneous emulsification was observed in many systems with different oil, surfactant type and salinity. In this project, spontaneous emulsification in NPE and SDBS systems were investigated.[1,4] The effect of different surfactant concentrations (0 – 5000 ppm), salinity (0-0.42 M NaCl) and oil type (toluene, xylenes and cyclohexane) were tested.

We first tested systems that are not fully covered by an oil phase (toluene, xylenes or cyclohexane).[4] The mechanism of spontaneous emulsification under this condition is summarized in Figure 2. Typical images of these emulsions are shown in Figure 3. Next, we investigated systems that are fully covered by an oil phase.[1] In this case Marangoni effect should be reduced but the systems still spontaneously emulsify.

The main conclusions are:

- For water-soluble oils, nanoscale emulsions formed spontaneously by diffusion of oil molecules into the aqueous surfactant solutions and subsequent swelling of surfactant micelles with oil.
- Micelle swelling rates were quantified to assess system spontaneity, revealing that oil solubility in water was directly correlated to the spontaneity of the emulsion (toluene > xylenes > cyclohexane).
- When experiments were intentionally designed to create surfactant concentration gradients, Marangoni flows were found to enhance spontaneity.
- Toluene spontaneously emulsified with nonionic NPE at salt concentrations from 0 to 0.42 M NaCl. As salt concentration increased, there was a slight increase in the spontaneity. The mechanism for emulsification was oil diffusion and micelle swelling.
- Toluene spontaneously emulsified with anionic SDBS but only at salt concentrations between 0.07 and 0.27 M NaCl. As salt concentration increased, spontaneity increased significantly compared to the NPE system. Spontaneous emulsification for this system occurred via diffusion and stranding.

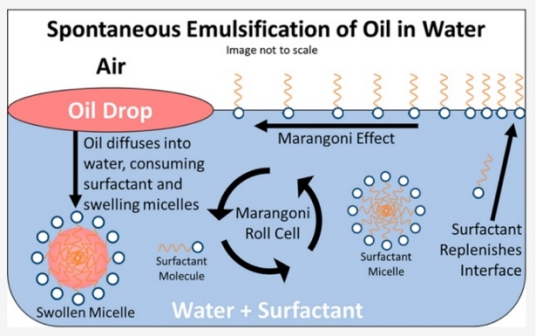

Figure 2: [4] Mechanism of spontaneous emulsification: diffusion-driven micelle swelling.

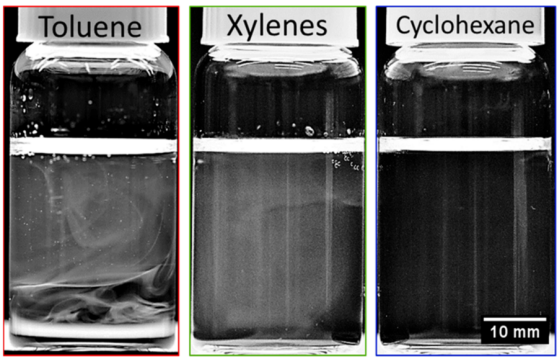

Figure 3**:** [4] Spontaneous emulsification of 5000-ppm toluene, xylenes, and cyclohexane with a 500-ppm of NPE solution after 40 min of contact. The scale bar applies to all images.

2.2 Systems with Mixed Surfactants

In this part, we went further and investigated the spontaneous emulsion systems with mixed surfactants. Both NPE-SDBS systems[1] and SLES-Span-80 systems[5] were investigated. The effect of salinity (0-0.42 M NaCl), surfactant ratio and oil type (toluene, paraffin oil, hexadecane, dodecane, decane and heptane) was tested in detail. Figure 4 shows the spontaneous emulsification of hexadecane with SLES-Span-80 systems with different surfactant ratios.

The main conclusions are:

- Toluene spontaneously emulsified with an equal molar NPE-SDBS mixture but only at salt concentrations above 0.02 M NaCl. Similar to pure SDBS, as salt increased, spontaneity increased. Both micelle swelling and diffusion and stranding were observed in this system.
- Spontaneous emulsification in the Span-80-SLES system resulted from a combined effect of ultra-low interfacial tension, Span-80 micelle swelling, and interfacial turbulence.
- Span-80 micelle swelling was observed and resulted in a gradual size increase over time of water droplets in oil. This effect was eliminated when salt concentration was higher than 0.2 M, possibly because the water transport in reverse micelles was retarded at higher salinity.
- Spontaneous emulsification was observed in many different oils, even the non-aromatic one (e.g., paraffin oil). This result indicates many oils collected in bilge water could spontaneously emulsify when an appropriate HLD_{mix} was reached.

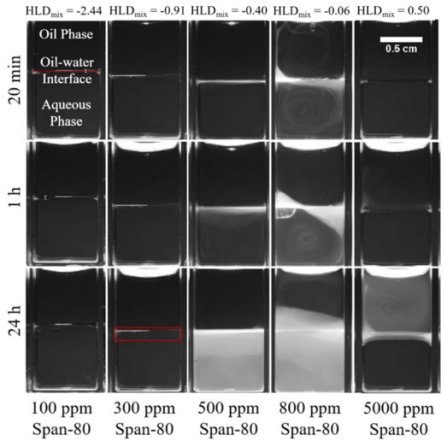

Figure 4**:** [5] Photographs of spontaneous emulsification. The images were taken 20 minutes, 1 hour and 24 hours after the oil and aqueous phase were brought in contact. The oil phase (upper phase) is hexadecane with 100, 300, 500, 800, 5000 ppm Span-80 (from left to right). The aqueous phase (bottom phase) is DI water with 100 ppm SLES and 0.1 M NaCl.

2.3 Predicting Spontaneous Emulsion Behavior with HLD Model

Overall, we found the HLD model can serve as a guide to indicate the spontaneity and spontaneous emulsification behavior with different oils, which is valuable in bilge water emulsion prevention and treatment processes. For instance, Table 3 shows the estimated HLD_{mix} values with the Span-80-SLES system and some common oils. The salinity of seawater was used due to its connection with bilge water. According to the calculation, those oils leading to an HLD_{mix} close to 0 (EACN = 12 ~ 16) could be the most problematic in bilge water with the surfactant composition we investigated. The other oils with lower EACN values would most likely lead to the formation of w/o emulsions, which would be less concerning for bilge water. However, HLD_{mix} would decrease with decreasing salinity. In that case, those oils with EACN values under 12 could be problematic. This model could potentially suggest oils that are creating conditions favorable to produce nanometer-sized spontaneous emulsion. The bilge water collecting process could also be optimized to avoid the formation of nano-sized droplets. For the Span-80-SLES systems, two phase diagrams (Figure 5 and Figure 6) have been made to better summarize the relation between HLD model and spontaneous emulsion behavior.
The main conclusions are:

- HLD analysis showed that the occurrence of spontaneous emulsification can be modeled. As the HLD of a system approached zero, spontaneous emulsification was more likely to occur.
- For the NPE-SDBS-Toluene system, a transition region in HLD between -2.4 and -2.05 existed where emulsification changed from non-spontaneous to spontaneous. Turbidity measurements showed that HLD can also model the spontaneity of a system.
- For the SLES-Span-80 system with a negative HLD_{mix}, the spontaneity in the aqueous phase (forming o/w emulsion) was always greater than that in the oil phase (forming w/o emulsion), and vice versa. When the HLD_{mix} was in the transition range (-0.22 to 0.56 in our systems), significant spontaneous emulsification could be observed within 20 minutes in both oil and aqueous phases and these systems displayed the largest spontaneity. This result was confirmed by estimating the dispersed phase content through turbidity measurements.

Table 3: [5] Estimated HLD values with different oils. The same surfactant composition (Span-80:SLES = 5:1, wt./wt.) and the salinity of seawater (0.42 M NaCl) was used.

EACN	**Oil**	**HLD_{mix}**
7 ~ 10	Heptane, Octane, Ethyl oleate	1 ~ 1.48
10 ~ 12	Decane	0.66 ~ 1
12 ~ 16	Dodecane, Isohexadecane, Sunflower Oil	-0.02 ~ 0.66
16 ~ 20	Corn Oil, Hexadecane, Paraffin Oil, Canola, Soy, etc.	-0.66 ~ -0.02

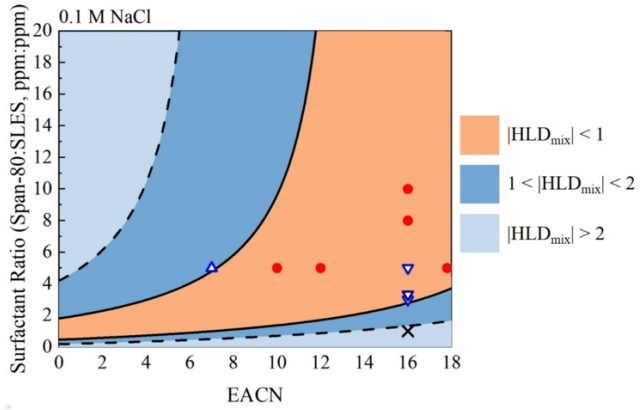

Figure 5: [5] HLD_{mix} calculated for systems with 0.1 M NaCl. The solid curves indicates where $HLD_{mix} = \pm 1$. The dashed curves indicates where $HLD_{mix} = \pm 2$. The region between the solid line is where spontaneous emulsification is more likely to occur. The solid, red data points represent spontaneous emulsification in both oil and aqueous phases. The hollow triangles pointing up represent spontaneous emulsification observed only in the oil phase. The hollow triangles pointing down represent spontaneous emulsification observed only in the aqueous phase. The black cross indicates no spontaneous emulsification observed.

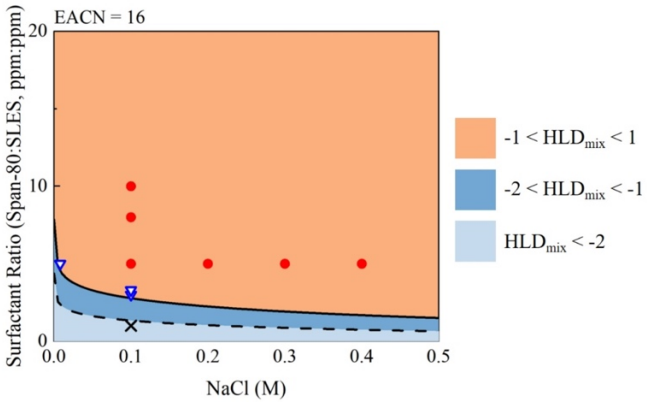

Figure 6: [5] HLD_{mix} calculated for systems with hexadecane (EACN = 16). The solid curves indicates where $HLD_{mix} = -1$. The dashed curves indicates where $HLD_{mix} = -2$. The region above the solid line is where spontaneous emulsification is more likely to occur.

3. Results on Emulsion with External Energy Input

3.1 Impact of Salinity on Emulsion Stability

In this part of the project, the impact of salts on the stability of oil-in-water emulsions to coalescence was studied to aid in minimizing the impact of emulsified oils on natural water systems. Here, oil-in-water emulsions were fabricated from mineral oil, deionized water, and SLES with a high-speed mixer. Overall, an increase in emulsion stability to coalescence was observed over an aging period of 56 days. This is probably due to a decreased electrostatic repulsion of the anionic surfactant, allowing the surfactant to pack more densely at the oil–water interface. Dynamic interfacial tension measurements (Figure 7) showed that surfactant adsorption rates increased with salt. As a result of faster adsorption kinetics, oscillating droplet tensiometry showed a decrease in the dilatational modulus when salt was present (Table 4).

The main conclusions are:

- Salt reduced the electrostatic repulsion between SLES head groups, allowing surfactant molecules to pack more densely at the interface. This decreased the probability of a vacancy appearing at the oil water interface and thus, prevented coalescence.
- A decrease in the dilatational modulus with salt was observed due to an increased rate of surfactant adsorption at the interface. This created a less rigid interface that could deform and flatten when two droplets approached each other.
- Dynamic interfacial tension measurements showed that salt increased the surfactant adsorption rate up until 0.42 M NaCl. At salt concentrations higher than 0.5 M NaCl, the apparent adsorption rate decreased due to salting out and desorption of the surfactant from the interface into the oil phase. An increase in adsorption rate allowed the interface to restore IFT gradients more quickly and prevent coalescence.

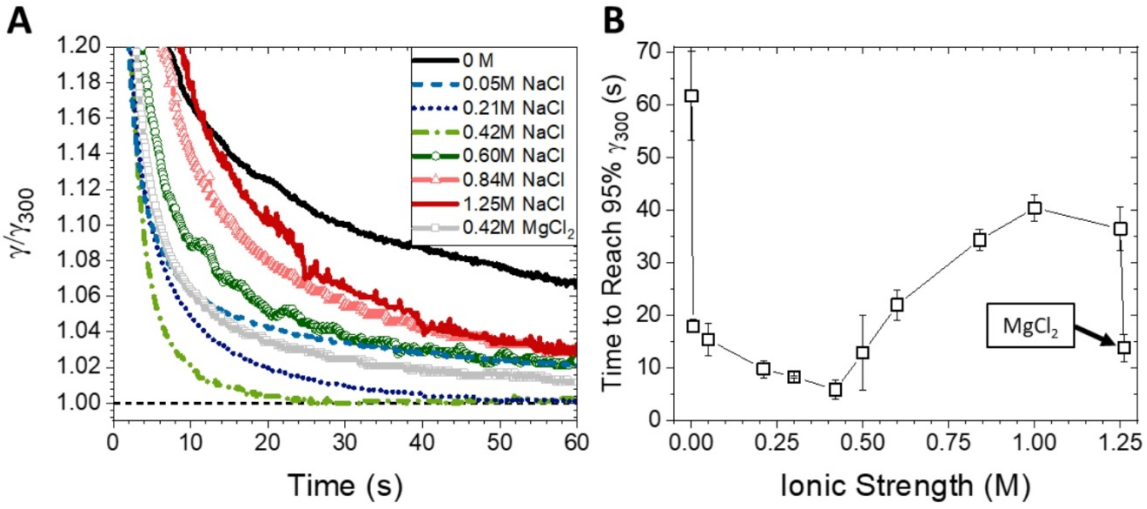

Figure 7: [6] (A) IFT decay for the first 60 seconds after drop formation normalized by the IFT at 300 seconds (γ_{300}). (B) Adsorption time to reach 95% of γ_{300} for SLES at the mineral oil-water interface for different ionic strengths. Error bars represent one standard deviation from the mean.

Table 4: [6] Elastic, viscous, and dilatational moduli for salt concentrations of 0, 0,42 M NaCl and 0.42 M $MgCl_2$ at oscillation frequencies of 0.01, 0.05 and 0.10 s^{-1}. Error represents one standard deviation from the mean.

Oscillation Frequency (s^{-1})	0.01			0.05			0.10		
Salt (M)	0	0.42 NaCl	0.42 $MgCl_2$	0	0.42 NaCl	0.42 $MgCl_2$	0	0.42 NaCl	0.42 $MgCl_2$
Elastic Modulus (mN/m)	1.35 ± 0.28	0.18 ± 0.08	0.29 ± 0.03	3.35 ± 0.27	0.85 ± 0.07	0.80 ± 0.06	5.17 ± 0.19	1.60 ± 0.12	1.36 ± 0.11
Viscous Modulus (mN/m)	1.63 ± 0.01	0.53 ± 0.01	0.47 ± 0.04	4.58 ± 0.17	1.75 ± 0.05	1.46 ± 0.05	6.68 ± 0.22	2.72 ± 0.05	2.34 ± 0.05
Dilatational Modulus (mN/m)	2.13 ± 0.19	0.55 ± 0.03	0.56 ± 0.04	5.80 ± 0.21	1.95 ± 0.05	1.71 ± 0.06	8.69 ± 0.21	3.16 ± 0.07	2.77 ± 0.07

3.2 Impact of Surfactant Ratio on Emulsion Drop Size Distribution

The influence of anionic and nonionic surfactant ratios on emulsion stability in saline environments was investigated in the context of bilge water. SLES and Triton X-100 were selected as surfactants likely present in bilge water emulsions. Our size distribution results showed emulsions with 500 ppm surfactants at different surfactant ratios had long-term (more than 20 days) stability against coalescence. However, according to Figure 8, SLES-rich emulsions had smaller oil droplets (< 8 μm) generated with the same energy input and were more stable against flocculation when compared to Triton X-100-rich emulsions. Turbidity measurements (Figure 9) showed that SLES-rich emulsions had higher remnant oil content in the supernatant than Triton X-100-rich emulsions, which is undesirable for phase separation and bilge water treatment.

The main conclusions are:

- Although no obvious difference in emulsion stability against coalescence or coarsening was observed, emulsion stability against flocculation and creaming was influenced by different surfactant ratios. For SLES-rich systems, more small oil droplets or flocs under 10 μm were not attached to the large aggregates and creamed at a slower rate. This is significant to bilge water because these oil droplets are hard to remove and could pose a severe environment threat when discarded in the ocean.
- The stronger stability against flocculation and creaming in SLES-rich emulsions could be attributed to the increasing number of small oil droplets, but more importantly, the strong electrostatic repulsion between oil droplets. According to the DLVO calculation and stability ratios, oil droplets flocculation would be limited by the interaction energy barrier in SLES-rich systems.
- Turbidity has been used to measure the remnant oil content in the modelled bilge water emulsion subnatant. Based on the results, SELS-rich systems led to a higher remnant oil content than Triton X-100 rich systems after aging for 5 hours. These oil droplets are difficult to separate through gravitational separation and thus undesirable for oily wastewater treatment.

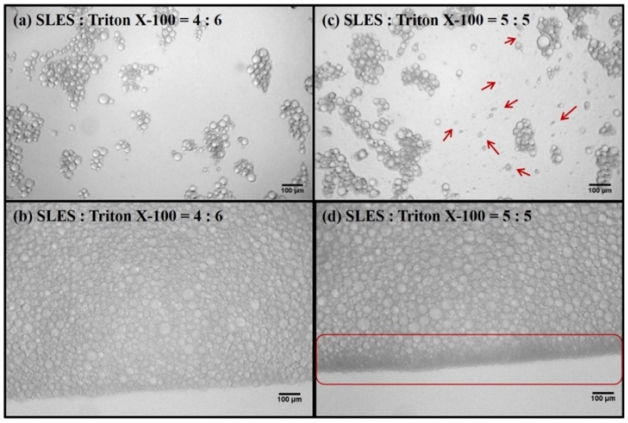

Figure 8: [2] Optical images of (a) emulsion flocculation and creaming in saline environment with 500 ppm mixed surfactant composed of 40 wt. % SLES + 60 wt. % Triton X-100, (c) 50 wt. % SLES + 50 wt. % Triton X-100. (The red arrows are pointing at non-flocculated oil droplets or small flocs) (b) the bottom of the creamed layer with 500 ppm mixed surfactant composed of 40 wt. % SLES + 60 wt. % Triton X-100, (d) 50 wt. % SLES + 50 wt. % Triton X-100 after aging for 5 days. The red rectangle is highlighting the layer of small oil droplets with diameter < 10 μm.

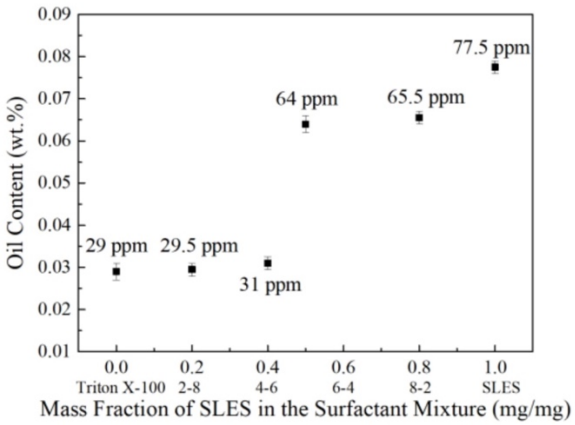

Figure 9: [2] Estimated remnant oil content in the emulsion subnatant at different surfactant ratios. The estimation was based on the turbidity values at 450 nm and calibration curves in Fig. 7 (a). The values in ppm were shown above/below each data point.

3.3 Impact of Dynamic Aging on Emulsion Stability

A ship's motion can promote emulsification or coalescence, depending on the surfactant type and concentration. Effects of motion on model bilge water O/W emulsions were investigated. The emulsions were firstly generated with mineral oil, 0.42 M NaCl, DI-water and either SLES or Triton X-100 with a high-speed mixer. The emulsion stability was then characterized by under static and dynamic conditions. The ship's motion was modeled with a 3-dimensional rocker. During dynamic aging at 12 rpm (Figure 10), the surfactant concentration to promote emulsification was 500 ppm for SLES and 1000 ppm for Triton X-100.

The main conclusions are:

- When compared to static ageing, dynamic ageing provided more energy to the system and increased the amount of surfactant needed to resist coalescence for 20 days. During dynamic ageing, an interplay exists between emulsification and coalescence. However, if the S/O ratio was greater than 0.2 for either surfactant, coalescence was not observed, and further emulsification was observed.
- Ship motion can promote coalescence at surfactant concentrations up to 100 ppm and emulsification at surfactant concentrations of 1000 ppm.
- To avoid further emulsification during dynamic ageing of bilge water, one must keep the surfactant concentration low. However, this is difficult to achieve. Therefore, one could investigate the behavior of O/W emulsions when the amount of air within the emulsification chamber is reduced during dynamic ageing. At 70% air inside the ageing vial, sloshing is responsible for drop formation and coalescence. Therefore, reducing the amount of air within the emulsification chamber will limit the sloshing and inhibit further emulsion formation and possibly promote coalescence.

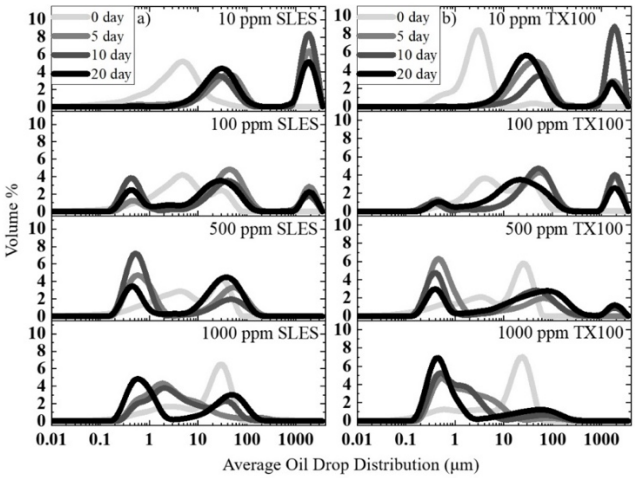

Figure 10: [3] The evolution of average oil drop size distribution over 20 days for dynamically aged emulsions at 12 rpm with a) SLES and b) Triton X-100 from 10 to 1000 ppm surfactant. The darkening of the distribution curves is proportional to time.

Executive Summary: Implications for Future Research and Benefits

This work provides experimental results on how anionic and nonionic surfactant ratio influence emulsion properties in saltwater environments which is valuable in eliminating the formation of undesired bilge water emulsions, and can help predict emulsion stability and remnant oil content in oily wastewaters. The physical and chemical properties which determine the stability of oil-in-water emulsions which can provide fundamental insight into effective water treatment operations designed to destabilize the emulsions and separate trace contaminates.

The research team has created a fully characterized dataset and predictive stability model for assessing contaminated bilgewater and shipboard emulsions in real-world marine environments. The outcomes of this work can be used by Department of Defense (DoD) operators to rapidly assess the physicochemical nature of specific shipboard emulsions within a vessel's bilgewater as well as provide guidance on the best practices to destabilize the emulsions. From this work, we provide recommendations to the DoD on how a given formulation of bilgewater can be amended to enhance coalescence and the speed up the associated time scales for oil-water separation. It is additionally possible that the outcomes from this work could inform cleaning and other shipboard operations which could prevent or mitigate the formation of stable bilgewater emulsions. Specifically, the outcomes of this work will provide improved guidance to DoD operations managers for optimizing their detergent formulations and/or cleaning procedures in order to facilitate end-of-use OW separations prior to bilgewater discharge that are effective but less time and energy intensive.

Objective

Our objective is to determine the influence of water chemistry (i.e. pH, salt concentration), temperature, and particulate and polymeric additives on the stability of model oil-in-water emulsions. We will achieve this object through a combination of interfacial rheometry, zeta-potential and dynamic light scattering measurements, and in situ flow visualization microscopy. While it is largely understood how simple oil-in-water emulsions are stabilized, there are fundamental knowledge gaps with respect to the formation and long-term stability of complex oil-in-water emulsions that arise from shipboard operations. These complex emulsions, which contain a range of oil-based moieties, are stabilized by a mixture of common industrial and natural surfactants. As a result, the breaking and separation of these emulsions is difficult and costly. Advancing the knowledge of physicochemical factors that impact emulsion stability will enable new technology to be developed for advanced water treatment of stable oil-in-water emulsions. This project is responsive to the objectives articulated in the Statement of Need; specifically we intend to apply advanced measurement tools to characterize the physicochemical processes which drive the formation and breaking of surfactant stabilized oil-in-water emulsions.

The long-term goal of the proposed research project is to characterize the droplet-droplet interactions and coalescence for complex oil-in-water emulsions. Specifically, we intend to quantify the fundamental structure-property relationships between the viscoelasticity of surfactant-laden immiscible fluid interfaces and the coalescence behavior observed between concentrated oil-in-water droplets As a step towards this goal, our objective is to understand how the physical and chemical attributes of surfactants and emulsions directly impact the kinetic stability at the droplet level. Our central hypothesis is that some polymer or surfactant additives are able to dynamically disrupt the chemical stabilizing shell surrounding small oil droplets and specifically, the coalescence of emulsion oil droplets in aqueous solution will strongly depend on the viscoelastic properties exhibited by the surfactant-stabilized oil-water interface under controlled system and environmental conditions. By measuring the rheological response of the surfactant-laden interface as a function of chemical composition of the interface and surrounding media, fundamental structure-property relationships can be developed to describe emulsion stability. To test this hypothesis through deliberate experimentation, the following specific aims will be pursued:

(1) Quantify the effect of water pH, salinity, and temperature on the rheology (dilatational viscoelasticity) of model oil-water interfaces for nanoscale and microscale droplets containing adsorbed surfactant molecules with known physical and chemical structures and controlled intermolecular associations.
(2) Correlate the measured interfacial viscoelasticity of surfactant-stabilized, oil-water interfaces with the observed rate of droplet coalescence between close-packed oil droplets in model two- and three-dimensional, concentrated emulsions.
(3) Develop predictive models to relate the rheology and physicochemical properties of oil-water interfaces with the kinetic stability of dispersed oil-in-water emulsion droplets across a range of droplet diameters.

Background

Bilgewater is a complex emulsion system that can be generated at a rate of 500 to 50,000 liters/day where the volume scales with the size of the vessel.[7] The cost of treating oily wastewater is significant, especially for complex wastewater compositions laden with mixed surfactants and other suspended or dissolved contaminates. The emulsion is comprised of a "coarse" dispersion with oil droplets diameters above 50 μm and a "fine" dispersion of < 50 μm diameter droplets.[8] While at sea, the vessel movement imparts energy into the bilgewater resulting in constant re-dispersion of the largest emulsion drops. Once at harbor, the emulsions phase separate into approximately a 20% oily top region, followed by a 70% fine emulsion with oil content ranging from 100 to 500 mg/L, and a 10% sedimentation layer composed of particulates and oily sludge.[7] The top and bottom regions can be easily extracted while the fine emulsion cannot be easily separated due to their small droplet size and use of highly effective detergents. Methods such as coalescence[9], coagulation[9], filtration[10] and electric fields[11] have been studied/developed to aid in the oil separation considering that the International Convention for the Prevention of Pollution from Ships (also known as MARPOL) regulation requires that oil discharge does not exceeds 15 mg/L.[7] These processes are generally effective; however, they are also expensive in terms of infrastructure, material consumption (e.g., contaminated adsorption media) and operational labor. And while a significant number of studies have investigated novel technologies for recovery of oil from contaminated waters, these studies tend to focus on relatively simple two- or three-component model systems.[12–17] Other investigations have focused on key performance metrics of value recovery from the waste stream or merely achieving separation sufficient to comply with existing regulations.[9,10,18,19] Thus, there is a clear lack of fundamental studies on the physicochemical factors that influence emulsion destabilization, especially when considering the complexity of produced oily wastewater.

Inducing droplet coalescence or coagulation by the careful selection of additives or changes in temperature can provide a simple and cost effective approach. However, surfactants in common commercial detergents such as Tide Ultra are exceptionally good at stabilizing OW droplets and preventing coalescence or coagulation. Additionally, the lack of knowledge of the SOW phase space makes it difficult to select additives or emulsion parameters such as changes in salinity and/or temperature that could be effective at destabilizing the adhered surfactants. The proposed work aims to utilize fundamental principles of surfactant and emulsion science to provide a detailed picture of the bilgewater SOW phase space. We draw inspiration from the enhanced oil recovery (EOR) field where the models of hydrophilic-lipophilic difference (HLD) and net average curvature (NAC) have revolutionize the selection of surfactants to maximize oil extraction. The HLD and NAC are semi-empirical models firmly based on thermodynamic principles and share similarities to the widely known hydrophilic lipophilic balance (HLB) as well as the Winsor R and packing parameters. However, the HLD and NAC offers a practical approach to surfactant selection as well as the effects of water salinity, oil type, and temperature

on the SOW phase space. The proposed work aims to utilize the HLD and NAC principles to determine the region of the SOW phase space relevant to shipboard bilgewater.

Hydrophilic-Lipophilic Difference (HLD) Model

The balance of hydrophilic-lipophilic components is of critical importance to emulsion formulations. The traditional hydrophilic-lipophilic balance (HLB) was born after the development of ethoxylated (EO) surfactants in which both the hydrophilic head (EO chains) and the long hydrophobic tails could be tailored methodically.[20,21] This provided the basis for a surfactant classification based on a neutral value of 7 where values > 7 corresponded to surfactants suitable for OW emulsions while < 7 to water-in-oil (WO) surfactants. The problem with the HLB system for emulsion formulation is that the number applies to the surfactant but not the hydrophilic-lipophilic balance of the emulsion system. The HLD was born of similar concepts but aims to "balance" the emulsion system based not only on the characteristics of the surfactant but also the oil, temperature, and water salinity as given by the following expression:

$$\mathrm{HLD} = \mathrm{C_c} - \mathrm{k} \times \mathrm{EACN} + \mathrm{f(S)} - \mathrm{c_T(\Delta T)} \ ,$$

where Cc is the characteristic curvature (or value) of the surfactant, EACN is the effective alkane carbon number of the oil, k is a scaling factor usually taken to be 0.17, c_T is a scaling factor that depends on the type of surfactant used, ΔT is the temperature difference with respect to 25°C, f(S) is the salinity term is usually 0.13S for nonionic and ln(S) for ionic surfactants where the S is given in g NaCl/100 mL.[21–23] Knowing the Cc value for a surfactant and the EACN value for the oil, it is straight-forward to find S and T values that will lead to a HLD = 0 where the average curvature of the emulsion is zero and the interfacial tension is at a minimum. When the interfacial tension is at a minimum, there is no energetic penalty for increasing surface area so droplets are made easily but also coalesce readily – a feature that is used by the enhanced oil recovery field to increase oil extraction. At first glance it will appear that HLD only applies to the formation of thermodynamically stable microemulsions, but HLD = 0 serves as a starting point for emulsion optimization and/or to understand where an emulsion is in the SOW phase space. Emulsion stability can be tailored by adding surfactants or changing water salinity and temperature.

Surfactant Characteristic Curvature (Cc) and Oil Effective Alkane Carbon Number (EACN)

One of the virtues of the HLD model is that its Cc and EACN parameters can be found easily. For example, the Cc can be measured following the methodology developed by Zarate-Muñoz et al.[24] In this method, the surfactant of interest is blended with a reference surfactant with a known characteristic curvature ($\mathrm{C_{c_{ref}}}$) for which the HLB constants b, K, c_T as well as the optimal salinity (S^*) and the EACN for a reference oil are known. The optimal salinity of the surfactant mixture (S^*_{mix}) is used to calculate the characteristic curvature of the test surfactant ($\mathrm{C_{c_{test}}}$). The constant b considers the salting out effect of the surfactant from the aqueous phase when the

ionic strength increases. The $C_{c_{ref}}$ is can be also measured and compared with literature values. S* is found at the minimum interfacial tension when the HLD = 0 given by:

$$HLD = 0 = b(S^*) - k \times EACN + C_c - c_T(T - T_{ref}) \ ,$$

while the optimal salinity for the reference surfactant is:

$$S^*_{rs} = \frac{K_{rs} \times EACN - C_{c_{rs}} - c_T(T - T_{ref})}{b_{rs}} \ .$$

The optimal salinity of the mixture is:

$$S^*_{mix} = \frac{K_{mix} \times EACN - C_{c_{mix}} - c_T(T - T_{ref})}{b_{mix}} \ .$$

The values of K and b for the surfactant mixture are assumed to be the same to those of the reference surfactant. Using a linear mixing rule for the surfactants given by the Y_{test} which is the ratio between the moles of the reference and test surfactant yields the following:

$$S^*_{mix} = S^*_{rs} + \left(\frac{C_{c_{rs}} - C_{c_{test}}}{b}\right) Y_{test}$$

and

$$C_{c_{test}} = C_{c_{ref}} - \left(\frac{S^*_{mix} - S^*_{ref}}{Y_{test}}\right) \times b \ .$$

The S^*_{rs} and S^*_{mix} can be found via several methods including measuring the solubility parameter (S_p) by finding the mL of oil and water soluble per mL of surfactant or the coalescence time (t_c) as a function of salinity usually given in g of NaCl/100 mL of water. Additionally, interfacial tension measurements via the spinning drop tensiometry method can be used to corroborate the optimal salinity values. In a typical measurement, a series of vials are filled with 1:1 ratio of water and oil, and the surfactant concentration is fixed to 2-5% while the salinity is increased. The Sp is found by measuring the volume of the water, oil phases. S^*_{mix} is simply the concentration(s) where the Winsor Type III emulsion is present, indicating the lowest interfacial tension and a HLD = 0. A similar approach can be used to find the EACN for the oils in the model suspension using two reference surfactants at different concentrations while the salt concentration is fixed.

Net Average Curvature (NAC)

The power of the HLD model is enhanced by the addition of the NAC model[25] which aims to provide a better understanding of the water, oil, and surfactant interaction by considering parameters such as the surfactant head area (A), tail length (l) and characteristics length ξ.[21] The net curvature is defined as $H = \frac{1}{R_O} - \frac{1}{R_W} = \frac{-HLD}{L}$, where $\frac{1}{R_O}$ and $\frac{1}{R_W}$ are oil and water curvatures respectively. L is usually 1.2 to 1.4 longer than the extended chain length, $L_c = 1.5 + 1.265n_c$, where n_c is the number of carbon atoms in the chain. R_O is simply the average radius of the

emulsion drops, while $R_W = \frac{3}{C_S NA}$, where C_S is the surfactant concentration, N is the Avogadro's number, and A is the area per surfactant molecule. Once HLD, L and R_W are known, $1/R_O$ can be estimated to determine the type of emulsion, i.e., OW or WO. Surfactants tend to have a ξ, which means that the average curvature cannot be < $1/\xi$, this prevents an infinite curvature at HLD = 0. The combination of HLD and NAC permit the calculation of fish tail diagrams that allow one to understand the effect of temperature or salinity as a function of surfactant concentration. The fish diagrams show the emulsion type that is present at a given temperature, salt, and surfactant concentration in water which can give a path to induce phase inversion or the formation of a Type III emulsion where coalescence is enhanced.

Fish Tail Diagram Example Based on Model Bilgewater Emulsion Components

The advantage of using the HLD and NAC as the foundation to understand the SOW phase space can be appreciated through a representative fish tail diagram for an emulsion containing several components of the model bilgewater emulsion recipe suggested in the Statement of Need. For this system, the TEP lubricating oil (MIL-PRF-17331K) serves as the oil phase. TEP is based on highly refined mineral oil with hydrocarbon chains ranging from C15 to C50[26], and an estimated EACN of 25 was used in the calculations.[21] The surfactant is a nonionic alcohol ethoxylate (MIL-D-16791G) with an estimated Cc of 0.3, and the water phase contains 3.5 mg of NaCl/100mL.[8] Based on the work by Acosta et al.[27], the estimated surfactant head area (A) is 5.4 nm and chain length (l) is 2.3 nm. At 25 °C the HLD value for this emulsion is -3.5 corresponding to a stable Type I, OW emulsion as required by the MIL-D-16791G specification. Using this information and the tools developed by Prof. Steven Abbott (University of Leeds) and Mr. Seth Lindberg (P&G)[21,28], a temperature as a function of surfactant concentration fish tail diagram was calculated as shown in Figure 11. The diagram shows that at temperatures below 63°C, a Type I OW emulsion is stable at all surfactant concentrations. At temperatures between 63 and 92°C and surfactant concentrations up to 19 wt.%, a Type III emulsion forms while a Type II is present at higher temperatures. A single isotropic micellar solution (Type IV) forms at concentrations > 19 wt.% and at temperatures near 75°C. The diagram shows that it is possible to destabilize a Type I emulsion at concentrations < 19 wt.% by carefully tuning the temperature so the system resides in the Type III emulsion region where the interfacial tension is a minimum and droplet coalescence is enhanced. It is important to note that the suggested bilgewater composition is significantly more complex, containing 5-6 ionic and nonionic surfactants, two

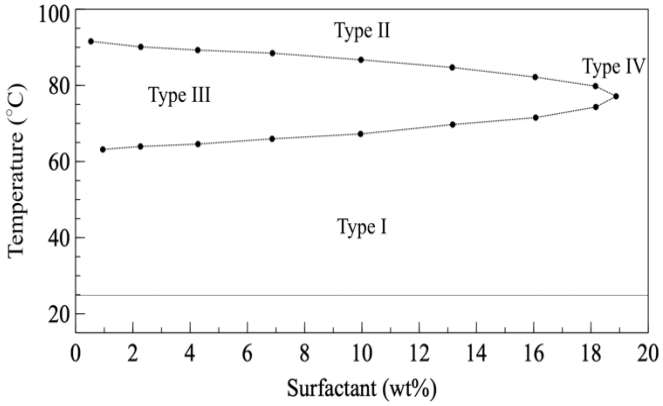

Figure 11: Temperature as a function of ethoxylate surfactant concentration fish diagram. The emulsion system contains TEP lubricating oil and the salinity is 3.5 mg/100 ml. Plot created from data obtained from fish diagram app developed by Prof. Steven Abbott[21,28].

different oils and fuel. However, the power of the HLD and NAC approach becomes evident to obtain a fundamental understanding of the SOW phase space based on the properties of the bilgewater components.[29]

Viscoelastic Characterization of OW Interfaces

The stability of an emulsion is ultimately controlled by the viscoelastic rheological response of the droplet's OW interface, as the early-stage deformations of this two-dimensional interface are what primarily lead to destabilization and droplet coalescence.[15,16,30] The static and dynamic behavior of the OW interface are strongly determined by the nature of adsorbed surfactant and any other material (e.g., particulates and other solid contaminants) that exists at the interface along with the nature of the surrounding media (temperature, pH, salinity).[16] Several studies have indicated that a strong, hydrogen-bonded network is formed by naturally occurring surfactants when these molecules adsorb to OW interfaces.[31–33] A number of interfacial rheometry techniques have been developed to investigate the adsorption and viscoelastic properties of low molecular weight molecules (including surfactants, phospholipids, and proteins) adsorbed to air-water and OW interfaces. The most well-developed of these experimental techniques include: Wilhelmy plate tensiometers,[34] capillary pressure tensiometers,[35,36] spinning droplet tensiometers and straight needle and inverted pendant drop/bubble tensiometers.[15] In this proposed study, spinning droplet and inverted pendant drop tensiometry will be used to measure the adsorption and dilational viscoelastic properties of surfactant-laden OW interfaces; therefore, an overview of this technique is summarized below.

Frequently referred to as "oscillating droplet tensiometry", this technique has been applied to study the conformation of proteins[12,37,38] as well as the viscoelasticity of adsorbed phospholipids,[30] low molecular weight surfactants,[39–41] and mixed surfactant/polymer solutions[14] at OW and air-water interfaces. In this technique, the apparent viscoelasticity of OW interfaces is measured by harmonically oscillating the initial interfacial area (A_0) of a droplet (or bubble) at a small strain and a low frequency (ω) by increasing and decreasing the droplet volume using an in-line mechanical plunger for needle-based techniques (pendant drop) or frequency of revolution for spinning droplet techniques. In order to obtain accurate measurements of the interfacial viscoelasticity, the applied strain and oscillation frequency must be very low, such that the interface is considered to be at mechanical equilibrium.[42] The apparent complex viscoelastic modulus (E*) is determined by measuring the response in interfacial tension variation ($\Delta\gamma$) resulting from the dilational strain ($\Delta A/A_0$), as well as the phase angle (δ) between the periodic interfacial tension and strain curves of an interfacial element[43]:

$$E^*(\omega) = E'(\omega) + iE''(\omega) = |E|\cos\delta + i|E|\sin\delta \quad , \quad \text{where} \quad |E| = \frac{\Delta\gamma}{\Delta A/A_0} \quad .$$

The apparent complex modulus is primarily a measure of the system's response to dilatational deformation (although, there is some evidence to suggest that shear contributions may be present in mm-scale oscillating droplet measurements as well[36,44]) and quantifies the elastic, "storage"

modulus (E') and the viscous, "loss" modulus (E") of the OW interface, both of which depend on the oscillation frequency and the nature of the molecules (surfactant and other) that are adsorbed at the interface.

Prior studies of OW emulsions have indirectly observed and quantified the kinetics of droplet coalescence and other emulsion destabilization mechanisms via dynamic light scattering (DLS) analysis.[15] Until recently, the droplet coalescence phenomenon could only be indirectly measured using characterization techniques including bulk microscopy, dynamic light scattering, oiling-off, and centrifugation methods.[45] However, the development of controlled droplet generation and aging via microfluidic devices coupled with high speed imaging techniques now allows for direct observations of coalescence mechanism between micrometer-scale liquid droplets (Figure 12).

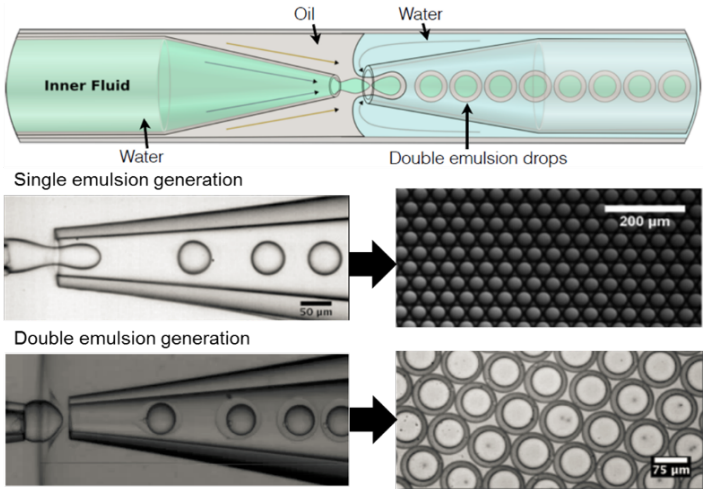

Figure 12: Generation of single and double emulsion droplets using microfluidic devices fabricated by Martinez and coworkers.[175,176]

Materials & Methods

Spontaneous Emulsion Characterization

The aqueous phase was prepared by adding the appropriate amount of NaCl and SLES to deionized water (Barnstead Nanopure Infinity, resistivity ≥ 18 Mohm·cm). The oil phases were prepared by adding the appropriate amount of Span-80 to different types of oil (heptane, decane, dodecane, hexadecane, paraffin oil). To ensure

homogeneity of surfactant in their respective solvents (i.e, water, or oil), the surfactant solutions were mixed overnight with a magnetic stirrer at room temperature.

To prepare the spontaneous emulsion, 1 ml of the aqueous phase was added to a glass cuvette followed by 1 ml of the oil phase by carefully pipetting along the wall of the cuvette onto the surface of the aqueous phase. This step was done to minimize the disturbance at the oil-water interface.

Interfacial Tension

Interfacial tension (IFT) was measured by pendant drop tensiometry with a KRÜSS DSA30 goniometer with inverted needle. Hexadecane with the appropriate amount of Span-80 was used as the drop phase. DI water with the appropriate amount of SLES and NaCl was used as the continuous phase. The IFT value was calculated based on the fitting of the axisymmetric Young-Laplace equation.[46] Each value reported was an average of 3 measurements. The interfacial tension isotherms for Span-80, SLES and their mixture (Span-80:SLES = 5:1, wt./wt.) were collected.

The surfactant ratio was selected based on the HLD_{mix} calculation and spontaneous emulsion behavior. This surfactant composition was found close to the boundary condition where spontaneous emulsification was observed in both oil and aqueous phases. Instead of optimizing the composition to maximize spontaneous emulsification, this study aimed at exploring how the spontaneous emulsion behavior would change with varying HLD_{mix}. At this boundary condition, we can further adjust the salinity and oil type and better determine the spontaneity change through visual observation. Related HLD_{mix} calculation and emulsion characterization will be further discussed in session 3.2.

Emulsion Imaging

The spontaneous emulsification processes were observed by taking a time-lapse using a Nikon camera (D3200). Photographs were taken every 30 seconds for over 48 hours. An LED light source (AL-MX, Aputure) was placed under the sample cuvette and the same lightening condition was used for each sample.

Dynamic Light Scattering

The drop size evolution during spontaneous emulsification was measured in a Malvern Zetasizer Nano ZS. The aqueous phase was added to a glass cuvette and the oil phase was pipetted carefully onto the aqueous phase surface. All measurements were taken at 2 mm away from the oil-water interface by adjusting the volume of water and oil. (Water drop size in the oil phase were measured at 2 mm above the interface. Oil drop size in the aqueous phase were measured at 2 mm below the interface.) For the instrument we used, the measurements were taken at 8 mm from the bottom of the cuvette. When measuring oil drop size evolutions in the aqueous phase, the volume of the aqueous and oil phase was 0.6 ml for each (6 mm + 6 mm in height). Similarly, 1 ml (10 mm in height) aqueous phase and 1 ml oil phase was added when measuring water drop size in the oil phase. Each measurement took approximately 2 minutes. The samples were measured periodically for over 24 hours. Three samples were made for each composition

and each measurement was an average of 11 scans. That is, each drop size distribution reported in this study is an average of 33 scans.

Emulsion Characterization For Dynamic Ageing Tests

To determine the electrostatic stability of emulsions with respect to surfactant chemistry, the zeta potential of emulsion drops was measured (Malvern Zetasizer Nano ZS) with 10 – 2500 ppm SLES or Triton X-100. All emulsions tested contained 0.42 M NaCl. Measurements were made 3 hours after initial emulsification under static storage conditions.

The interfacial tension between surfactant solutions and heavy mineral oil was measured (RameHart Goniometer) via Pendant Drop Method at concentrations of 0.001 – 10 mM of SLES or Triton X-100. Aqueous surfactant solutions contained 0.42 M NaCl and were dispensed through a needle submerged in mineral oil. Drops were equilibrated for at least 60 minutes or until the interfacial tension value (measured every 30 seconds) remained constant over time. The average equilibrium IFT was calculated from three separate drops. The critical micelle concentration (CMC) was determined from the resulting interfacial tension isotherms.

The stability of model bilgewater emulsions was determined by measuring oil drop size at 3 hours, 5, 10, and 20 days after emulsification using laser diffraction (Malvern Mastersizer 3000). Initial oil drop size measurements began at 3 hours to ensure removal of air bubbles generated upon high shear mixing of the emulsions. A drop size distribution was measured using laser diffraction measurements. Laser diffraction calculates a volume average oil drop size distribution and a volume-weighted mean drop diameter, presented as D(4,3).[24] Each size distribution was measured 5 times to produce an average drop size distribution. All emulsion formulations studied were prepared in triplicate, and the reported oil drop size distributions are an average of those three measurements. An aliquot of the emulsions was collected in glass capillaries after gently swirling the bulk emulsion to ensure proper sampling. The prepared glass capillaries were imaged using an Olympus BX41 microscope with the AM Scope software.

Model bilgewater emulsions were prepared in 50 mL centrifuge tubes. Non-ionic surfactant, Triton X-100 (Sigma- Aldrich, Laboratory-grade, M_w = 625 g/mol), or anionic surfactant, sodium lauryl ether sulfate (SLES) (STEOL US-170UB, Stepan Co., M_w = 332.4 g/mol), were used in the preparation of O/W emulsions at concentrations of 10, 100, 500, and 1000 ppm. The continuous phase consists of 0.42 M sodium chloride (Sigma-Aldrich), and the dispersed phase consists of 5000 ppm heavy mineral oil (Sigma-Aldrich) for a total emulsion volume of 15 mL. Consequently, about 70% of air existed within the centrifuge tube. Emulsions in this chapter are referred to emulsions with 70% air. Onboard, it was estimated that oil drops less than 20 μm are difficult to remove after physical separation techniques have been executed.[3, 18] Therefore, before ageing, the emulsions were mixed in a VWR (VDI 25) high shear mixer at 24,000 rpm for 1 minute (energy density of 162 J/mL, see Appendix A for calculation) to form an average oil drop size of 20 μm.

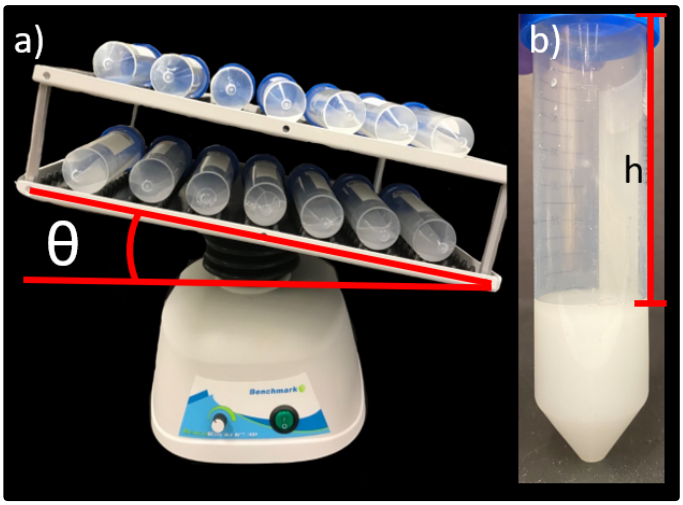

Figure 13: Photograph of a) the Benchmark BenchRocker 3D Nutating Shaker with tilt angle θ, and b) emulsification container with falling height h.

A 3-dimensional rocker (Benchmark BenchRocker 3D Nutating Shaker), shown in Figure 13, was used to emulate ship movement. After 20 days, this provided the emulsions with an additional energy density input of 8.8 J/mL. This value is an upper-end estimate and arises from the balance between a falling object's potential and kinetic energy and can be viewed in the Appendix A. Since the oscillation rate and amplitude of ship rocking depend on maritime conditions, the rocker speed was varied from 12 and 30 rpm to represent low and high oscillation frequencies of ship motion. Prior to ageing, the emulsions were prepared using a rotor-stator mixer to form a target oil drop size of 20 µm.

The most common technique to characterize oil drop size and distribution is through optical microscopy. However, this technique is limited by the resolution of the microscope. For example, drops below 1 µm are not accurately imaged nor measured due to Brownian motion.[22, 23] To overcome this, laser diffraction is employed to effectively measure oil drops ranging from 0.01 to 3000 µm in diameter.[1, 24] During laser diffraction, an aliquot of an emulsion is diluted and exposed to a laser beam to which oil drops scatter the light. The scattering pattern, or the intensity and angle at which a drop scatters light, depends on the drop size.[1, 22, 25] Mie theory is a mathematical model used in instrument software that relates the scattering pattern to the size distribution based on the oil properties. The software produces a plot of oil concentration (volume) as a function of drop diameter based on the best fit distribution between the Mie theory and measured scattering pattern.[1]

Static ageing refers to the storage of emulsions under static conditions. Long-term stability for statically aged O/W emulsions with common anionic and non-ionic surfactants has been established in the literature.[26–29] Under static conditions, oil drops large enough to overcome Brownian motion will experience instability.

Emulsification Process For Accelerated Ageing And High Energy Mixing

An orifice mixer and a rotor-stator were the two selected methods to create model emulsions. First, the orifice mixer is a fluid processing device that mixes and emulsifies multiphase liquids

due to the production of high-energy eddies in highly turbulent regimes for small volumes. The immiscible liquids are pushed towards a mixing chamber, then through the mixing orifice (0.45 mm^2) by actuated positive pumps. The high turbulent jet created at the exit of the mixing orifice is responsible for generating significant external deformation stresses that break highly uniform droplets. [56] Figure 14shows a schematic representation of the orifice mixer device used.

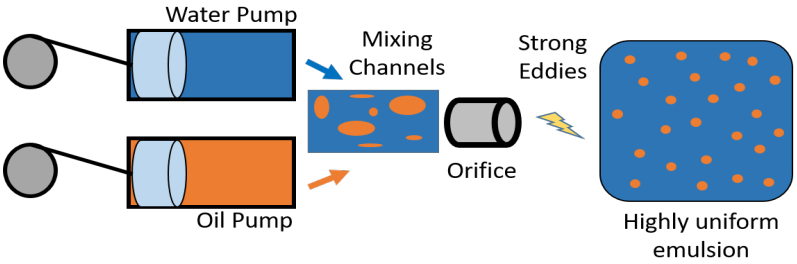

Figure 14: Orifice Mixer Schematics

The rotor-stator mixer is also a ubiquitous fluid processing device. It uses rotation to create high shear regimes to a small volume of liquid. The high shear gap is located between the rotor and stator gap and tightly around the mixing head. [57] The design of the rotor-stator allows for a high local energy dissipation rate. Still, there is a considerable amount of energy that dissipates throughout the whole volume of the tank. [58] Due to the nature of mixing, it is challenging for the entire volume of liquid to experience the same shear that produces the smallest droplet. Figure 15 shows a schematic representation of the rotor-stator used.

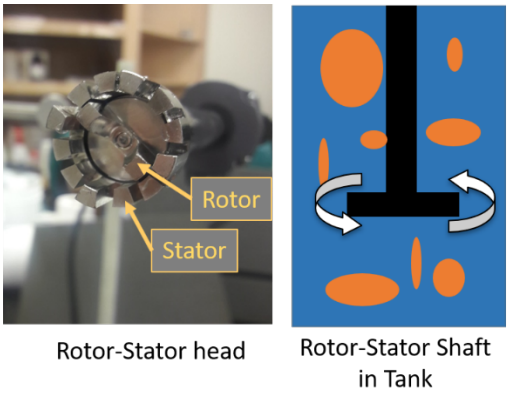

Figure 15. Rotor-Stator schematics

The particular local energy dissipation rate is the main difference between the two emulsification methods used in this experiment. The orifice mixer dissipates its energy in smaller volumes compared to the rotor-stator. Based on these operational assumptions, it is expected that the orifice mixer creates tighter droplet size distributions (DSD) for given power input compared to the rotor-stator.

Accelerated Creaming Tests

The LUMiSizer® analytical centrifuge (LUM GmbH, Germany) was the core equipment used in this project. It uses the space-time resolved extinction profile (STEP) technology [59] to create

light transmission profiles. [60] A light transmission profile represents the time-space resolved concentration of dispersed phase across the whole length of the sample under a centrifugation field. Thanks to the relative variable centrifugation, LUMiSizer® can shorten the time it takes to evaluate creaming/sedimenting behavior. LUMiSizer® can apply up to 2300 times the gravitational acceleration (g) to expedite the movement of droplets. Figure 16 shows the schematics of the LUMiSizer® working principle and the emulsion profile evolution (transmission (%) as a function of position (mm) plot).

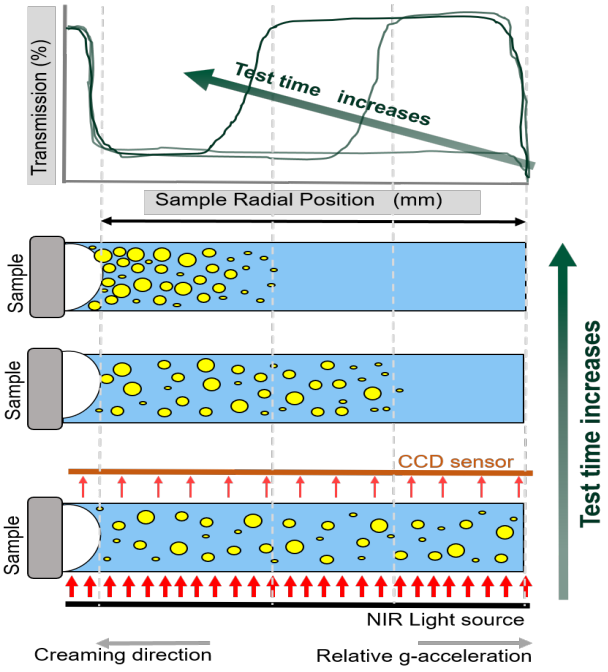

Figure 16: LUMiSizer working principle. The Transmission (%) over Position (mm) fingerprints represent the vial position and concentration of droplets within the bulk of the emulsion under centrifugation. Low transmission values indicate droplet-concentrated areas. High transmission values indicate droplet-depleted areas.

LUMiSizer® measures stability and creaming velocity by tracking the light profile evolution. [61] Also, it can quantify the mean droplet size and droplet size distribution (DSD) by using the Lambert-Beer and Navier-Stokes laws.

Built-in software correlates light transmission to dispersed phase concentration using the Lambert-Beer law (see Equation 1). The Lambert-Beer equation describes the attenuation of incident light caused by the mass of the dispersed phase.

Equation 1 Lambert-Beer's law. I is transmitted intensity, I0 is incident intensity, c is dispersed phase concentration, ε is extinction coefficient, and d is the optical path length.

$$-\ln\frac{I}{I_0} = \varepsilon * c * d$$

Simultaneously, the change in light transmission is used to calculate particle size using the hindered terminal velocity definition of the Navier-Stokes law (see Equation 2).

Equation 2 Navier-Stokes (v_t) and Hindered terminal velocity (v_h). ($\rho_{cp} - \rho_{dp}$) is the density difference between the continuous phase and dispersed phase, RCA is the relative centrifugal acceleration, η_{cp} is the dynamic viscosity of the continuous phase, x is the droplet diameter, C_{dp} is the dispersed phase concentration and $f(H)$ is the Richardson-Zaki hindrance function.

$$\text{Navier} - \text{Stokes} \quad v_t = \frac{(\rho_{cp} - \rho_{dp})x^2}{18\,\eta_{cp}}\text{RCA}$$

$$\text{Hindered} \quad v_h = v_t * f(H); \qquad f(H) = (1 - C_{dp})^{4.65}$$

Terminal velocity of spherical particles (v_t) is given by the equilibrium of viscous drag and relative acceleration due to differences in density between the continuous and dispersed phase and the size of the dispersed phase particles. The equation for the Navier-Stokes terminal velocity describes the movement of monodispersed droplets going through the continuous phase at low Reynolds numbers in a dilute state. However, the free flow is hindered by neighbor particles in a concentrated state. [62] To correct for dispersed phase concentration (C_{dp}) and find the hindered velocity (v_h), it is common to use a hindrance function ($f(H)$) as a factor of multiplication for the Navier-Stokes terminal velocity. The Richardson and Zaki hindrance function with an exponent equal to 4.65 is a common choice for emulsions under low Reynolds number. [63]

Measurement Of Clarification Rate, Instability Index, And Creaming Velocity

Clarification rate, instability index, and creaming velocity are measured parameters used as part of a relative analysis to elucidate creaming behavior. These properties are calculated using the front tracking, integral, and stability modules of SEPView® software. Light profiles were recorded every 4 s for 1.03 h at 265 RCA or every 10 s for 17 h at 70 RCA. Light and temperature normalizations were performed before each test. Figure 17 shows a representation of the calculation process.

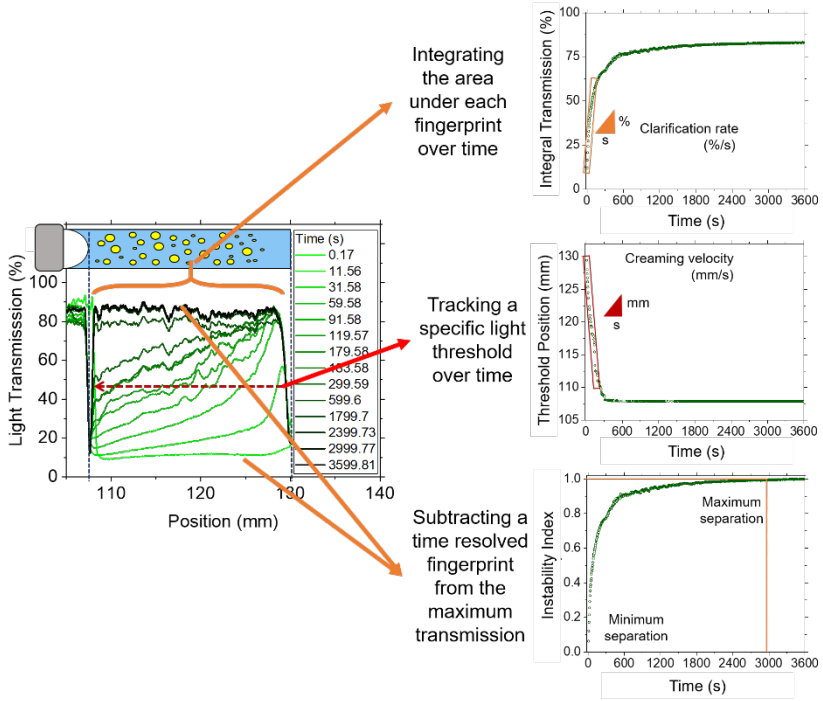

Figure 17: Representation of the clarification rate, instability index, and creaming velocity calculation

The clarification rate measures the mean displacement of droplets within the whole emulsion. [61] It is quantified using the slope of the integrated area under each fingerprint over time (rate in % s^{-1}). This rate represents a time-resolved average change in sample turbidity (from dark to translucent).

The instability index represents the amount of emulsion that phase-separated at a specific time. It can be estimated by subtracting a time-resolved fingerprint from the maximum possible transmission of the emulsion. The instability index is an indirect representation of the mean change in droplet concentration across the sample. This index is a normalized parameter, and it goes from 0 (no separation) to 1 (Maximum separation). [64]

Creaming velocity measures the mean separation rate at which droplets move towards the top of the sample. Creaming velocity is obtained from tracking a specific light threshold position over time. [65] The light threshold is defined in the best attempt to represent most droplet group-sizes. The slope of the linear part of the position over time plot is equal to the creaming velocity. [66]

Measurement Of Droplet Size And Droplet Size Distribution

The LUMisizer® analytical centrifuge and the particle sizing module from SEPView® software were used as the central core of droplet size characterization. Constant position algorithms were used to average five calculations of PSD. The data was presented on a volume basis and fitted to a normal distribution model. Volume-weighted distribution (DSD) uses the calculated volume of each droplet to compute the individual contribution over the whole volume of the dispersed phase.

The centrifugation cycle for DSD measurements is of the step type form. It started at 300 rpm and increased every 40s to a maximum of 4000 rpm. The goal of the relative centrifugal acceleration (RCA) ramp is to sieve the distinct droplet sizes. Thus, accounting for each group can be done more accurately. The physical constants needed for the calculations, such as density, viscosity, and diffraction index, were obtained from the literature. [67] Light transmission normalization was performed with a control sample under the same RCA conditions. The results are expressed as the harmonic mean droplet size (H) and the volume-weighted distribution density.

Measurement Of Remnant Oil

Even after significant aging time, there is a considerable amount of near submicron droplets suspended within the bulk of the emulsion. [68] The volume of droplets that stay behind is of great concern because their total volume of oil could be significant and in majority of cases it is unknown. Therefore, the following experiment was designed to measure the amount of suspended oil after a significant aging time to elucidate the physical and chemical factors associated with this phenomenon.

A UV–vis method to measure the remnant oil concentration in an aged emulsion was developed.

The absorbance at a chosen wavelength is measured to correlate light absorbance to droplet concentration as others have done in similar experiments (Yang and Hogg, 1979). The entire remnant oil measurement protocol comprises emulsion aging, supernatant collection, sample homogenization, the measurement of absorbance, and final contrast of measured absorbance with a calibrated linear fit.

The sample comprises the whole volume of emulsion below the cream layer (supernatant) after the specified aging time has passed. The sample is homogenized to erase the emulsification history of emulsions assuring uniformity in droplet size and size distribution. This uniformity allows reliable and accurate light interactions. Homogenization was carried out using a tip sonicator. Magnetic stirring and a water bath were also implemented to assure homogeneity in droplet concentration and sample temperature.

An UV-VIS spectrometer PerkinElmer Lambda 35 was used to measure the absorbance of calibration and experimental samples. Three profiles of absorbance between 1100 nm and 200 nm were measured. Samples were diluted to adequate concentrations such that absorbance readings stay between 0.05 and 1. The continuous phase of each emulsion was used as the baseline and dilution solution. The calibration curve follows the linear form of the Lambert-beer law in which absorbance is linearly correlated to dispersed phase concentration (see equation 2). The Absorbance values at two 276 nm and 800 nm were used as characteristic wavelengths. The goal of a dual wavelength measurement is to cover a greater range of dispersed phase concentration.

Results and Discussion

Surfactant Composition and Emulsion Stability

The effect of single surfactant concentration on emulsion stability against coalescence was investigated. We looked at the emulsions prepared with either SLES or Triton X-100 at concentrations ranging from 100 to 1000 ppm. As shown in Figure 18, SLES emulsions were not stable and significant coalescence (circled region in Figure 18) could be observed at concentrations below 200 ppm. Similar behavior was observed for Triton X-100 at concentrations below 300 ppm. These unstable emulsions were difficult to measure using the Mastersizer due to rapid coalescence. At concentrations above 200 ppm for SLES and 300 ppm Triton X-100, the emulsions were stable against coalescence, and the distributions were almost identical for surfactant concentrations up to 1000 ppm, as shown in Figure 19. We expect that 200 ~ 300 ppm is the minimum surfactant concentration to ensure the emulsion stability at different surfactant ratios. Increasing surfactant concentration would further improve the emulsion stability against coalescence.

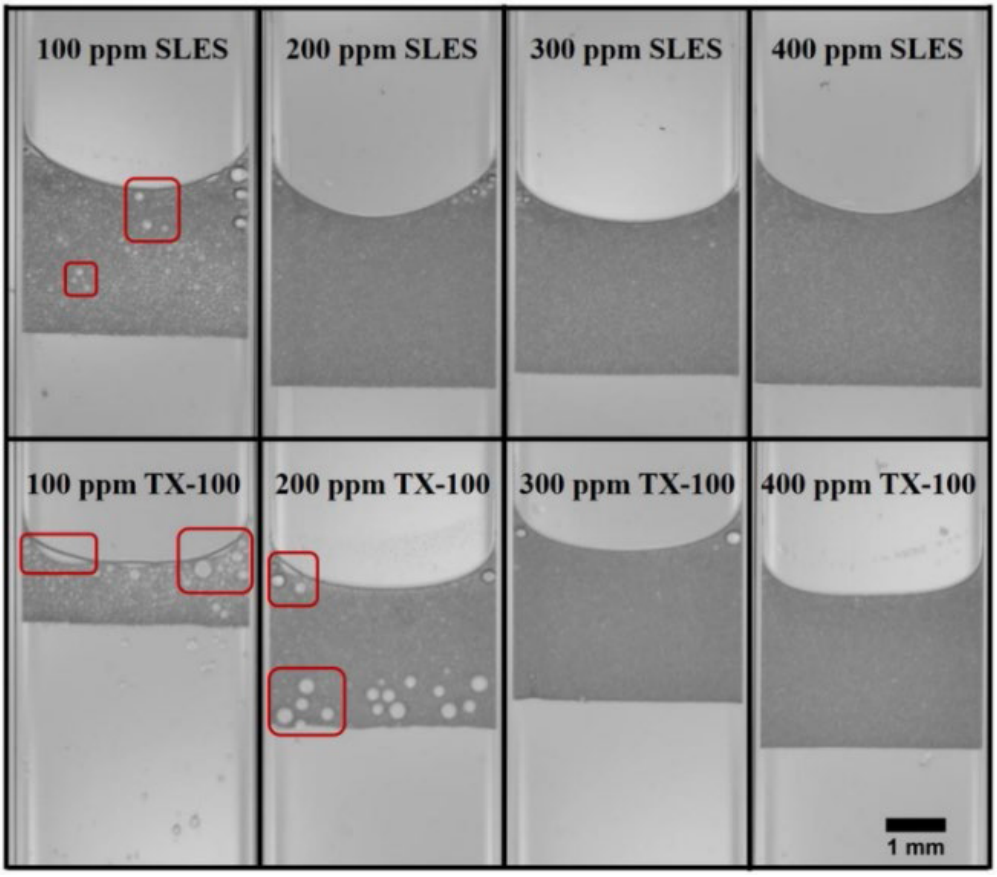

Figure 18. Photographs of the emulsion creaming layer with different surfactant concentrations: 100, 200, 300, 400 ppm SLES or Triton X-100 after 24 hours. The emulsions were collected in sealed capillaries and

stored, photographed vertically. The darker gray regions are the creaming layer, and the lighter region below is the subnatant. The circled

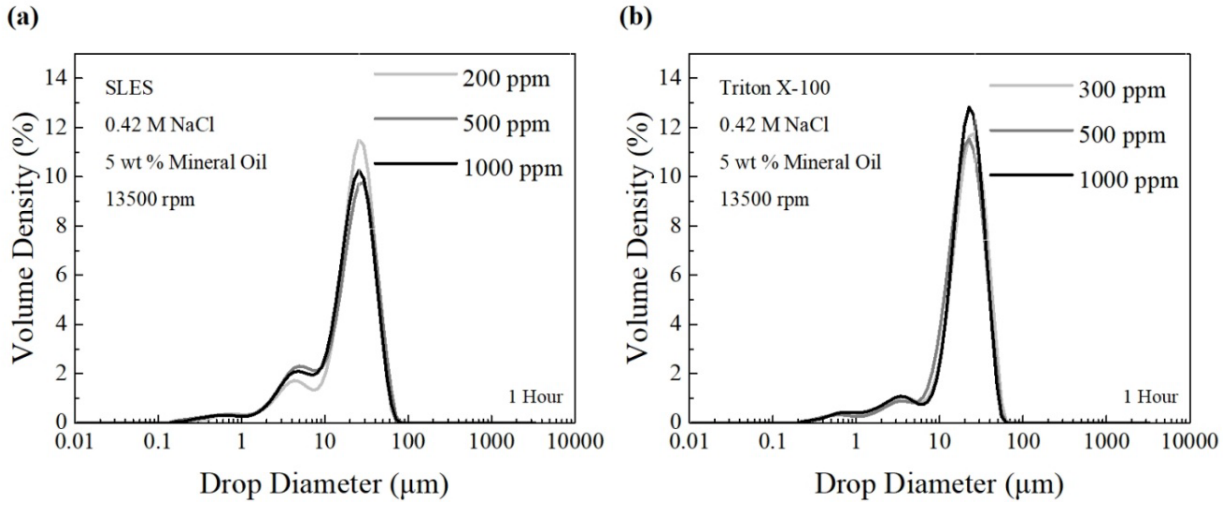

Figure 19. Drop size distribution of emulsions with different surfactant concentrations: (a) 200 ~ 1000 ppm SLES, (b) 300 ~ 1000 ppm Triton X-100. Measurements were taken 1 hour after emulsification.

Both our data and the literature indicate that once a threshold surfactant concentration is reached, there is little difference in the overall emulsion stability. One of the major challenges regarding bilge water treatment is the unknown surfactant concentration. Stable systems with sufficient amount of surfactant would be of great concern due to the difficulty in oil separation. In this work, we used 500 ppm total surfactant concentration to form systems stable against coalescence. The influence of surfactant ratios was then examined. Measuring higher surfactant concentrations is beyond the scope of this work.

Effect of Mixed Surfactant Ratio on Interfacial Surfactant Packing

To investigate the interfacial properties, the equilibrium interfacial tension (IFT) between the aqueous solution and mineral oil was measured for different surfactant ratios (pure SLES, pure Triton X-100, and SLES-Triton X-100 blends) at 500 ppm with 0.42 M NaCl. CMC values were obtained by measuring IFT at lower surfactant concentrations for each surfactant ratio. The results are shown in Figure 20(a), (b).

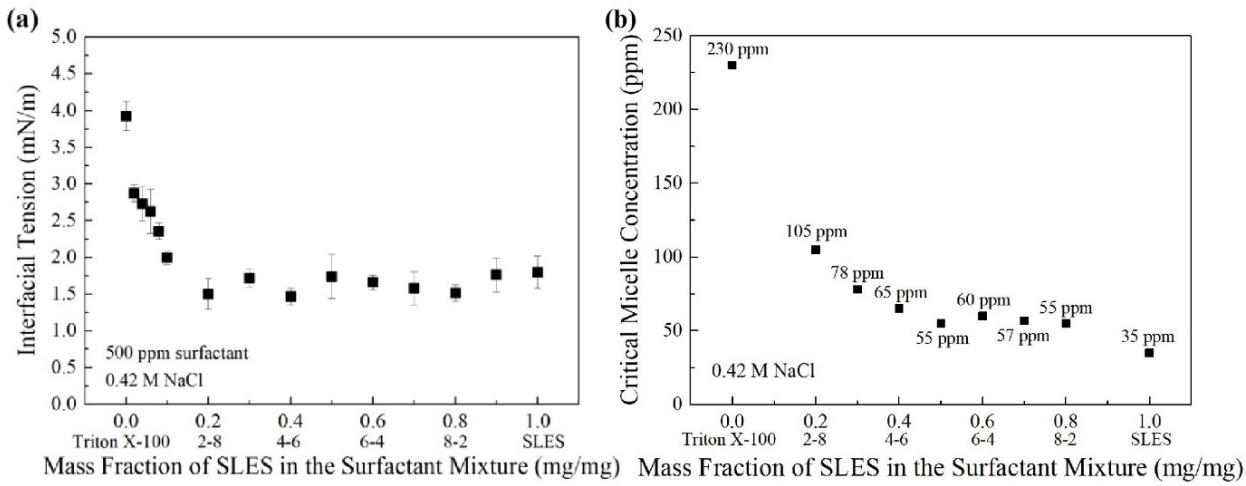

Figure 20: Drop size distribution of emulsions with different surfactant concentrations: (a) 200 ~ 1000 ppm SLES, (b) 300 ~ 1000 ppm Triton X-100. Measurements were taken 1 hour after emulsification.

The surface excess (Γ) were calculated based on Gibbs adsorption isotherm (Eq.2.1) for pure Triton X -100 and pure SLES. The Debye length was estimated based on Eq. 2.2.[69] Here, γ represents the interfacial tension. *C* is the surfactant molar concentration and *R* is the universal gas constant. The interfacial packing density for pure Triton X-100 and SLES were 2.04×10^{-6} mol/m^2 and 5.08×10^{-6} mol/m^2, respectively. The estimated Debye Length was 0.469 nm. It is worth to mention that Eq.2.1 is usually applied to calculate the interfacial packing density of nonionic surfactants. However, the salt molar concentration was more than two orders of magnitude higher than the anionic surfactant molar concentration in the emulsion system we investigated. The strong ionic strength led to electrostatic screening around the head groups of SLES molecules and low Debye Length. The effect of the anionic head group can be neglected and Eq.2.1 was valid for both SLES and Triton X-100 in this case.[70,71]

$$\Gamma = -\frac{1}{RT}\frac{d\gamma}{dlnC} \quad (2.1)$$

$$\frac{1}{\kappa} = \frac{0.304}{\sqrt{[NaCl]}} \quad (2.2)$$

According to the interfacial tension data, the addition of SLES to Triton X-100 can effectively lower the interfacial tension between mineral oil and surfactant solutions in saline environment. The interfacial tension decreased from 3.93 mN/m for 1:0 (100% Triton X-100) to 1.41 mN/m for the 2:8 surfactant ratio (SLES : Triton X-100), then reached a plateau. The average head area is around 32.70 Å for SLES and 81.43 Å for Triton X-100. This is probably due the relatively smaller hydrophilic head group and the straight alkane chain. In comparison, Triton X-100 molecules have larger head group and thicker hydrophobic chains. Considering the high salt concentration (0.42 M), the estimated Debye Length is less than 0.5 nm and the counter ion cloud is suppressed. As a result, SLES can pack in a more compact configuration than Triton X-100 at the interface without electrostatic repulsion.

The CMC data had a similar trend. The CMC measured for pure Triton X-100 is 230 ppm, which is close to the value reported in previous studies.[72,73] At a ratio of 2:8 (SLES : Triton X-100), the CMC value was reduced to 105 ppm. Further increasing the surfactant ratio reduced the CMC but at a lower rate until it reached a value of 35 ppm for 100 % SLES. Previous study shows the CMC of SLES with 0.17 M NaCl is around 100 ppm.[74] It is well known that a shift to a lower CMC is expected for ionic surfactants as the salt concentration is increased. In this work, all the emulsion samples were prepared with 500 ppm of total surfactants and 5 wt.% mineral oil. The surfactant concentration was well above the CMC of either the mixture or the single surfactant. No detrimental effect of combining SLES and Triton X-100 was observed, which agreed with previous study.[75]

Table 5**.** Zeta potential of oil drops with 0.42 M NaCl and 500 ppm surfactant at different ratios.

Surfactant Ratio (SLES : TX-100, mg/mg)	Zeta Potential (mV)
Triton X-100	-3.23
2-8	-11.00
4-6	-16.15
5-5	-21.07
6-4	-26.10
8-2	-38.23
SLES	-46.00

The electrostatic properties of the oil-water interface at different surfactant ratios were characterized by measuring zeta potential of the oil drops. The anionic surfactant can effectively increase the surface charge of the oil drops even with high salt concentration. According to Table 5. Zeta potential of oil drops with 0.42 M NaCl and 500 ppm surfactant at different ratios., the oil drops had negative surface charge at all surfactant ratios. When the oil drops were stabilized by 100 % Triton X-100, the surface charge is slightly negative, which can be attributed to the accumulation of OH^- anions at the oil-water interface.[76–78] The zeta potential increased from -3.23 mV to -46 mV with increasing proportion of SLES in the surfactant mixture. This can be attributed to the anionic nature of SLES molecules. The sodium ion of an SLES molecule will dissociate in the aqueous phase, making the oil drops negatively charged.[74,79]

Effect of Mixed Surfactant Ratio on Emulsion Drop Size Distribution and Stability against Coalescence

Oil drop size distributions were measured for emulsions with different surfactant ratios. Figure 21(a) – (c) shows the drop size distributions after aging for 1 hour, 5 days and 20 days. Figure 21 (b) are photographs of emulsions at 0, 2, 5 and 20 days. To consider the effect of buoyancy, the emulsions were collected in sealed capillaries and stored, photographed vertically. The darker gray regions are the creaming layer, and the lighter region below is the subnatant.

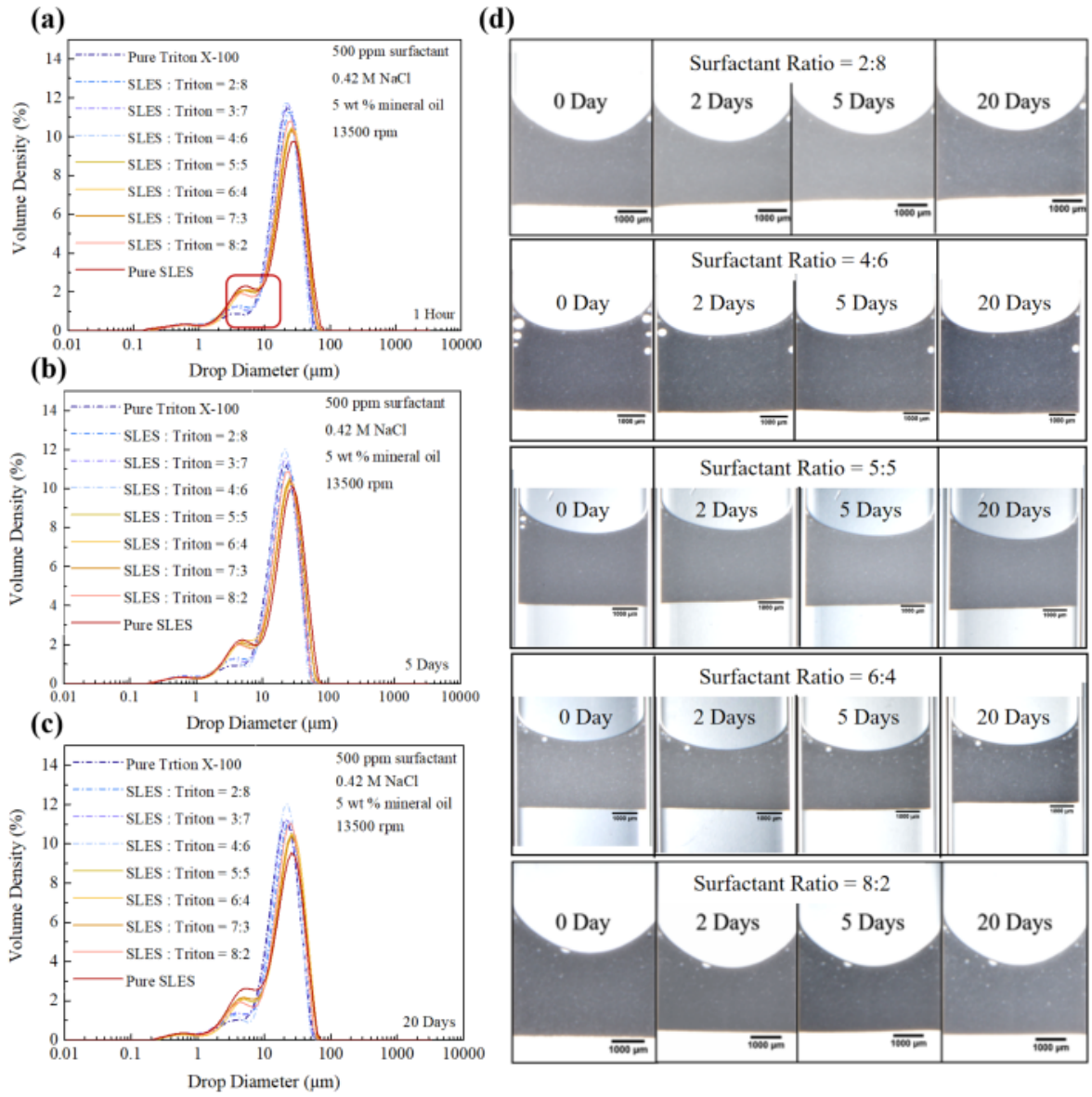

Figure 21: Drop size distribution of emulsions with different surfactant ratios: pure Triton X-100, SLES : Triton X-100 = 2:8, 3:7, 4:6, 5:5, 6:4, 8:2, pure SLES. Measurements were taken (a) 1 hour, (b) 5 days and (c) 20 days after emulsification. (d) Photographs of the emulsion creaming layer with different surfactant ratios: SLES : Triton X-100 = 2:8, 4:6, 5:5, 6:4, 8:2, after 0 day, 2 days, 5 days, and 20 days.

According to Figure 21 (a), the mixed surfactants at different ratios had similar effects on drop size distributions. Each curve had one peak at 20 - 30 μm and the other between 0.2 to 2 μm. A shoulder was present in between (2 μm to 8 μm). The volume density height of the shoulder was different between the emulsions with the highest values corresponding to 100 % SLES emulsion and the lowest to the 100% Triton X-100. Interestingly, there was a gap in this volume density between the 4:6 and 5:5 ratio, suggesting a transition in the emulsification capacity of the SLES-rich surfactant mixtures. There was an opposite trend in the peak at 20 μm (i.e. the highest volume density corresponds to Triton X-100 while the lowest corresponds to SLES).

The emulsion stability against coalescence and coarsening was evaluated by visualization and measuring oil drop size distributions over 20 days. Emulsions containing 500 ppm surfactant and 5 wt. % of mineral oil (surfactant to oil ratio (S/O): 0.01) were stable against coalescence and coarsening in the long term regardless of surfactant ratios. As shown in Fig.2 (a)-(c), The drop size distribution curves did not change significantly, suggesting strong emulsion stability. Macroscale photographs of the creaming layers were taken to ensure there was no large oil drop uncaptured by laser diffraction measurements. In Figure 21 (d), there was no obvious coalescence or formation of large oil drop. We should expect to see some light grayscale regions with growing size over time in the creamed layer if there is significant coalescence. It worth to mention that in some samples (i.e. surfactant ratio = 4:6 and 5:5), there were some air bubbles with diameter larger than 100 μm that disappeared over time.

Overall, these results corroborated that the surfactant mixtures provided strong stability to emulsions regardless of the ratios. However, it does not seem to be a synergy at any surfactant ratio where a lower interfacial tension or enhanced stability was observed. The differences in the volume density height of the shoulder and peak between different surfactant ratios were hard to explain but perhaps were related to the excess surfactant above the CMC available to generate the emulsions. However, it is difficult to prove this with existing data and more experimental results of the interfacial packing is needed.

Effect of Mixed Surfactant Ratio on Emulsion Stability against Flocculation and Creaming Dynamics

Videos and images of the creaming process were taken with the vertical imaging setup. Flocculation occurred in each emulsion sample regardless of surfactant ratio. Figure 22 (a), (c) were taken in the process of creaming, showing the flocs formed in Triton X-100-rich and SLES-rich emulsions, respectively. After 5 hours, SLES-rich emulsions were found with enhanced stability against flocculation and creaming. Figure 22 (b), (d) were typical images of the creamed layer of Triton X-100-rich and SLES-rich emulsions after static aging for 5 days. In the SLES-rich emulsion, there was a dark layer of small oil drops (with diameter below 10 μm) at the bottom of the emulsion, which was not observed in Triton X-100 rich emulsions. The creaming process was visualized and Figure 22 (a), (c) were captured within the first 60 seconds of creaming. Compared SLES-rich (Figure 22 (c)) to Triton X-100-rich emulsion (Figure 22 (a)), more small oil drops or flocs were dispersed instead of being attached to large flocs. These small oil drops or flocs were more stable against flocculation and creamed at a much slower rate, thus accumulating at the bottom of the creamed layer.

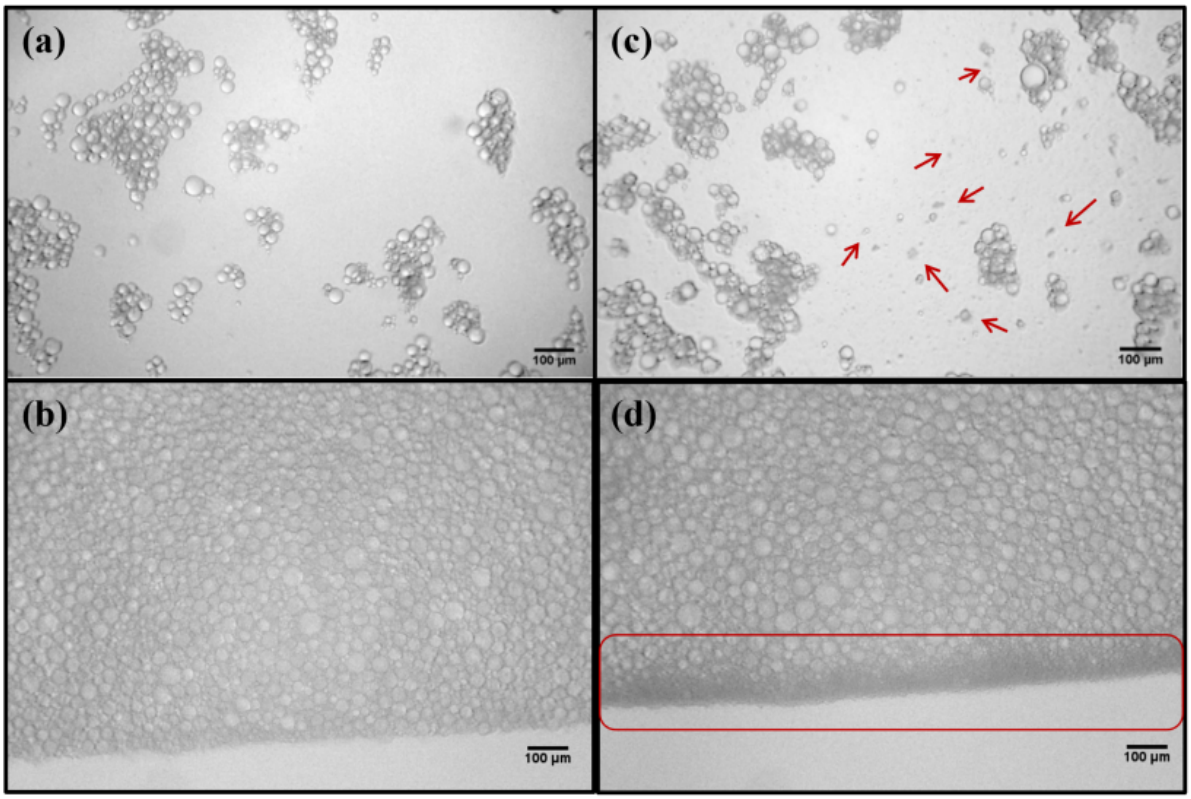

Figure 22. Optical images of (a) emulsion flocculation and creaming in saline environment with 500 ppm mixed surfactant composed of 40 wt. % SLES + 60 wt. % Triton X-100, (c) 50 wt. % SLES + 50 wt. % Triton X-100. (The red arrows are pointing at unflocculated oil drops or small flocs) (b) the bottom of the creamed layer with 500 ppm mixed surfactant composed of 40 wt. % SLES + 60 wt. % Triton X-100, (d) 50 wt. % SLES + 50 wt. % Triton X-100 after aging for 5 days. (The red rectangle is highlighting the layer of small oil drops with diameter less than 10 µm.)

The formation of these layers of small drops in SLES-rich emulsions can be attributed to the higher volume density of small oil drops between 2 to 8 µm, but more importantly, the higher surface charge of the oil drops. As shown in Table 5, the zeta potential of oil drops increases with increasing proportion of SLES. It is widely accepted that higher surface charge will lead to stronger electrostatic repulsion, thus more stable oil drops against flocculation. In the process of creaming, those oil drops were less likely to flocculate or attach to larger flocs. The interaction energy will be further discussed in the next section. The movement of these small oil drops or flocs were influenced by Brownian's motion and any turbulence (i.e. turbulence caused by the movement of larger flocs) to a greater extent. The existence of these oil drops is undesirable for effective physical waste water treatment since they lead to a lower creaming rate, and perhaps an increasing amount of remanent oil in the subnatant.

Effect of mixed surfactant ratio on remnant oil content

Measurement of turbidity has been used to evaluate the stability of emulsions in many studies.[80–84] The turbidity of an emulsion can be determined by measuring the light transmission at relatively high wavelength (> 400 nm). When light passed through the emulsion sample, part of

the light will be diffracted by the oil drops while the other will be transmitted through. There is a small amount of light that will likely be absorbed by the oil phase and can hardly be quantified. To eliminate the absorption, wavelengths higher than 400 nm were selected, assuming there was only diffraction happening.[80,85] Without any absorption, the turbidity of an emulsion is a function of drop size and concentration based on Mie theory.[80,86] Here, all extracted subnatant samples were re-emulsified to obtain a similar size distribution. The purpose of re-emulsification is to reduce the effect of drop size on turbidity thus comparing the oil concentration between samples. The turbidity was measured with a 25 vol% dilution of the sonicated emulsion (1 ml emulsion + 3 ml DI water) to ensure the results lied within the limits of the instrument. As shown in Figure 23, the oil drop size distributions did not change significantly before and after dilution.

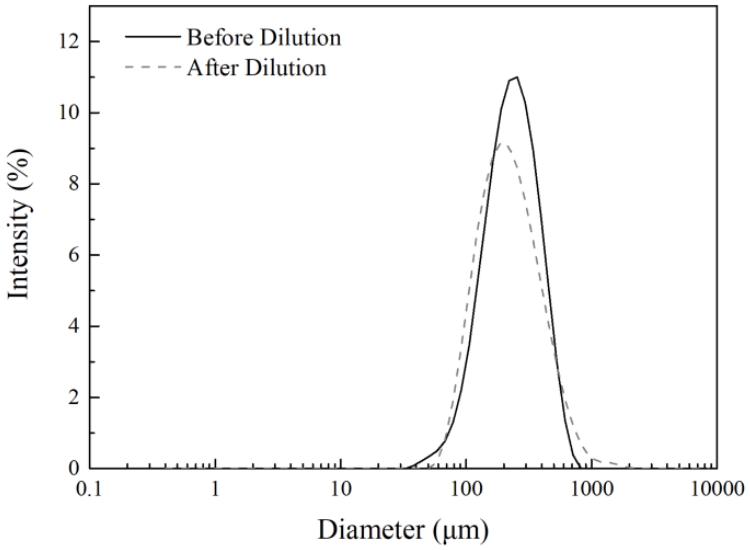

Figure 23: Typical drop size distribution of remanent mineral oil after ultrasonication at 10% power for 20 minutes. The solid line was measured directly after ultrasonication and the dash line was measured with 25 vol% dilution (0.25 ml ultrasonicated emulsion + 0.75 ml DI water)

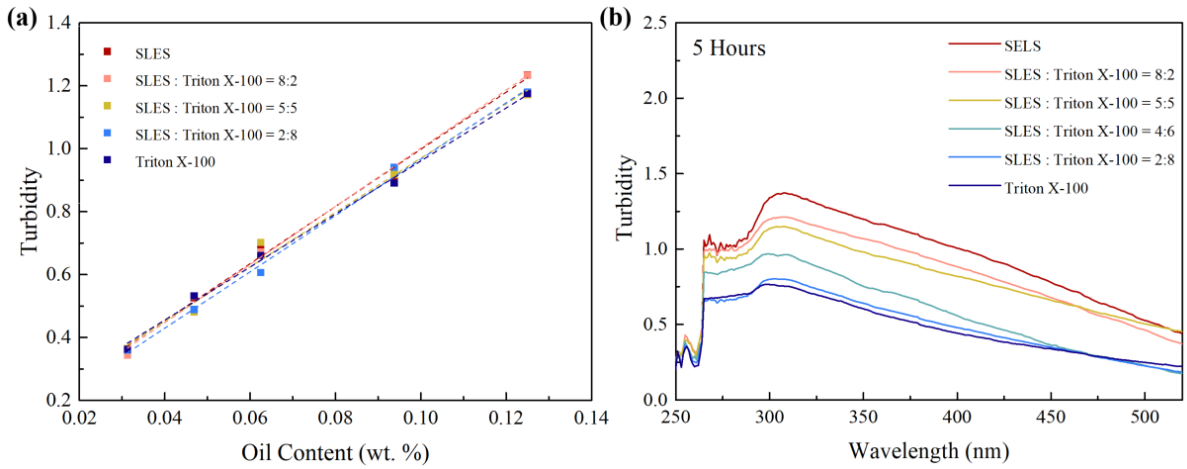

Figure 24.(a) Turbidity of calibration emulsion samples with 0.03125 wt. %, 0.04688 wt. %, 0.0625 wt. %, 0.09375 wt. %, 0.125 wt. % mineral oil and different surfactant ratios (pure SLES, SLES : Triton X-100 = 8:2, 5:5, 2:8, pure Triton X-100). Measurements were conducted at 450 nm wavelength. (b) Turbidity of the bottom layer of aged emulsion samples. Each sample had a volume of 15 ml and was ultrasonicated at 10% power for 20 minutes then diluted with 75 vol% DI water (1 ml ultrasonicated emulsion + 3 ml DI water). The oil concentrations of the calibration samples were calculated after dilution.

The purpose of measuring emulsion turbidity was to compare the residual oil content in the subnatant of aged emulsions with different surfactant ratios. The calibration samples were made with the same ultrasonication, dilution procedure and surfactant, salt concentration but known oil content. For each oil content, emulsions with five different surfactant ratios were prepared and measured. According to the result, different surfactant ratios may influence the turbidity values at a wavelength less than 400 nm. For example, at 300 nm, the turbidity of the emulsion with 0.125 wt. % oil varied from 2.11 to 1.76. However, this effect was reduced at wavelengths greater than 400 nm. At 450 nm, for instance, emulsion turbidity had similar linear relations with the oil content regardless of the surfactant ratios (Figure 24(a)). The turbidity value of the emulsion with SLES and Triton X-100 was mainly determined by the oil content at a high wavelength (> 400 nm).

Based on these results, the remnant oil content in the subnatant of emulsion with different surfactant ratios can be compared by the turbidity values. According to Figure 24 (b), those SLES-rich samples had similar turbidity values between 0.66 and 0.78, while TX-100-rich samples had turbidity values between 0.33 and 0.37 at 450 nm. It can be concluded that TX-100-rich samples had lower remnant oil in the subnatant than SLES-rich samples. All the SLES-rich samples (or TX-100-rich samples) had similar remnant oil content based on the turbidity values. These results agreed with the previous observations and DLVO calculations. When the system had equal to or more than 50 wt. % of SLES in the surfactant mixture, there would be stronger repulsion between the oil drops and the emulsions were more stable against flocculation and creaming. Those unflocculated oil drops or relatively small flocs would be left behind after aging, leading to a higher remnant oil content.

Spontaneous Emulsion

Visual Observations of Spontaneous Emulsification

When toluene was placed in contact with a 500 ppm NPE solution, spontaneous emulsification was observed. Figure 25shows images of toluene in contact with an NPE solution for 0, 30 and 90 minutes as well as the droplet size distribution after 90 minutes of contact. As time progressed, opaque regions could be seen flowing through the aqueous phase, indicated by the white arrow at 30 minutes. At approximately 90 minutes, the bulk toluene was no longer visible on top of the aqueous phase and flow was no longer observed.

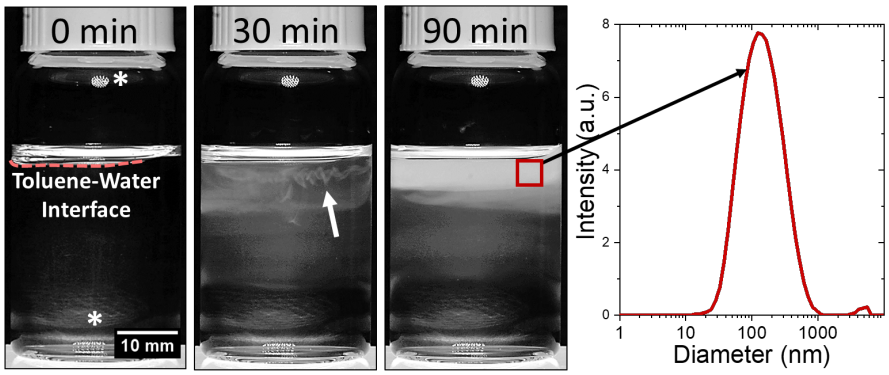

Figure 25: Spontaneous emulsification of 5000 ppm toluene in a 500 ppm NPE solution after 0, 30, and 90 minutes of contact. The toluene-water interface is marked by the red dotted line at 0 minutes. The toluene droplet size distribution at 90 minutes is also reported. Note that toluene was used in such a small quantity that it did not completely cover the air-water interface. The two white asterisks labelled on the far-left image indicate optical artifacts (light reflections) and are not to be mistaken for features of emulsification. These reflections appear in each image.

The observed mixing behavior was caused by convective flows which arise from interfacial tension gradients along the oil-water and air-water interface.[87,88] Initially, regions of high oil concentration have a high interfacial tension with water and demand surfactant. Surfactant flows horizontally along the air-water interface toward the oil (i.e., high to low surfactant concentration) and is caused by the fact that the oil phase did not cover the entire air-water interface. Simultaneously, oil is transported in the vertical direction from the bulk oil droplet to the aqueous phase while consuming surfactant that was once at the oil-water interface. As a result, the oil-water interface is surfactant starved and this perpetuates the horizontal surface flow. These horizontal and vertical flows create a convective flow called a Marangoni roll cell[88,89] and were observed during spontaneous emulsification. Images of the observed roll cells can be seen in Figure 26.

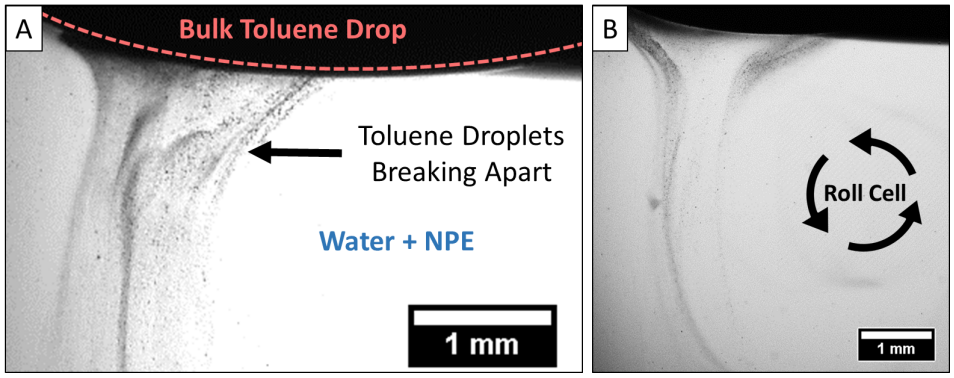

Figure 26: Images depicting (A) convective flow due to interfacial tension gradients along the interface forming streams of toluene droplets from a larger, bulk toluene droplet in an aqueous phase which contained 500 ppm NPE and (B) a roll cell (dark regions surrounding the outside of

the roll cell arrows) formed during spontaneous emulsification of the same toluene droplet located in image A.

Roll cells can be seen on either side of the bulk toluene droplet creating jets of toluene droplets that progress into the aqueous phase and break apart (Figure 26). The direction of the roll cell flow was opposite to those previously observed.[39] The sinusoidal wave indicated by the white arrow in Figure 25 is a relaxation oscillation of Marangoni roll cell.[89,90] Xylenes also showed visible signs of spontaneous emulsification and convective flow. Images showing emulsification after 40 minutes of oil-water contact for all three oils can be seen in Figure 27. Toluene had the most visible mixing and appeared to be more spontaneous than both xylenes and cyclohexane. Cyclohexane did not show any visible signs of spontaneous emulsification.

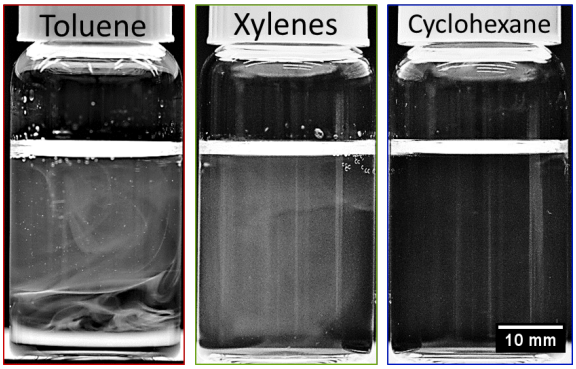

Figure 27: Spontaneous emulsification of 5000-ppm toluene, xylenes, and cyclohexane with a 500-ppm NPE solution after 40 minutes of contact. The scale bar applies to all images.

Emulsion Stability

Although emulsification was spontaneous, this was not the equilibrium state. Figure 28 illustrates the change in emulsion transparency over 30 days for toluene, xylenes, and cyclohexane. After 17 days, toluene emulsions appeared translucent while xylene emulsions were slightly more opaque. After 30 days, all three emulsion compositions were transparent indicating that the emulsions had not yet achieved a thermodynamic equilibrium.

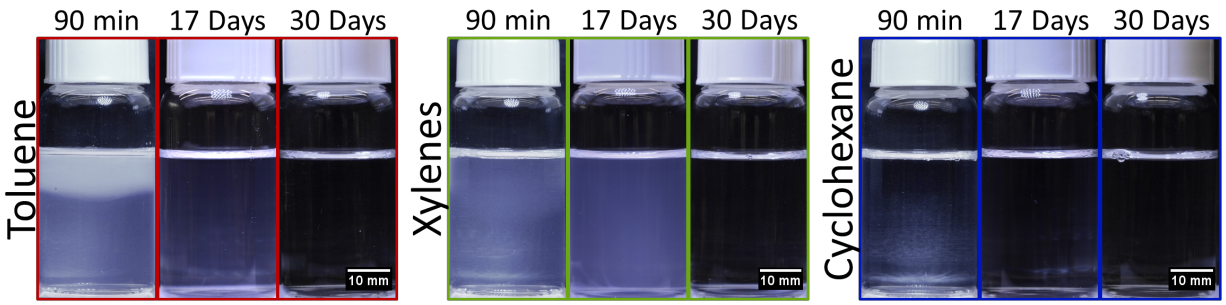

Figure 28: Photographs of toluene, xylene, and cyclohexane emulsions aged for 90 min, 17 days, and 30 days. After 30 days, all emulsions were transparent. The scale bar applies to all images.

To identify if any instability mechanisms were active during the ageing process, DLS was used to record droplet size distributions over 40 days and can be seen in Figure 29**.** For toluene, the droplet size after 90 minutes shows a peak at 176 nm. After 15 days, this peak broadens, and the droplets grow to a larger size of 340 nm. A bimodal distribution can be seen at 30 days with a large peak near the NPE micelle size (14.5 nm) and a second, small peak at 310 nm. After 40 days, only one peak remains that is identical to the NPE micelle size distribution. A similar process occurs during the ageing process of xylenes apart from swollen micelles (21 nm) remaining at 40 days. Note that the use of the term "swollen micelle" here does not indicate formation of a microemulsion but rather is used to describe an oil-filled micelle with a size on the same order of magnitude as an NPE micelle (i.e., less than 100 nm in diameter). Otherwise, the dispersed phase will be referred to as "droplets". Cyclohexane shows a bimodal distribution at 90 minutes; one peak at the NPE micelle size (12.0 nm) and another peak at 285 nm. This indicates that not all the micelles are used to form droplets of cyclohexane, and a large portion of NPE micelles remain. After 15 days, a bimodal distribution remains with a slight peak at 457 nm and a large peak at 13.7 nm, indicating that the NPE micelles have swollen. Between 15 and 30 days, all the droplets return to the NPE micelle size. Swollen micelles have been seen in a similar system but without mention of spontaneous emulsification.[55] Reverse micelle swelling has been seen in a kerosene-Span 80-water system which resulted in a W/O emulsion.[91] Figure 30 shows the trend in the Z-average swollen micelle and droplet diameters from 90 minutes to 40 days for each oil.

From visual observations and data in Figure 29 and Figure 30, three instability mechanisms can be inferred: Ostwald ripening, gravitational separation (creaming), and evaporation. Increases in droplet size between 0 and 15 days are likely due to Ostwald ripening because of the oils' high water solubility and small droplet sizes.[51,54,92] As the micelles grew larger due to Ostwald ripening, they became increasingly unstable to gravitational separation and creamed to the air-water interface.[51] Emulsions containing cyclohexane were the fastest to destabilize and return to the initial micelle size. This is most likely because a relatively small amount of oil was emulsified (indicated by the presence of micelles after emulsification), and droplets likely did not get dispersed far from the air-water interface due to the lack of observed convective flows. This allowed droplets to cream and evaporate at a faster rate.

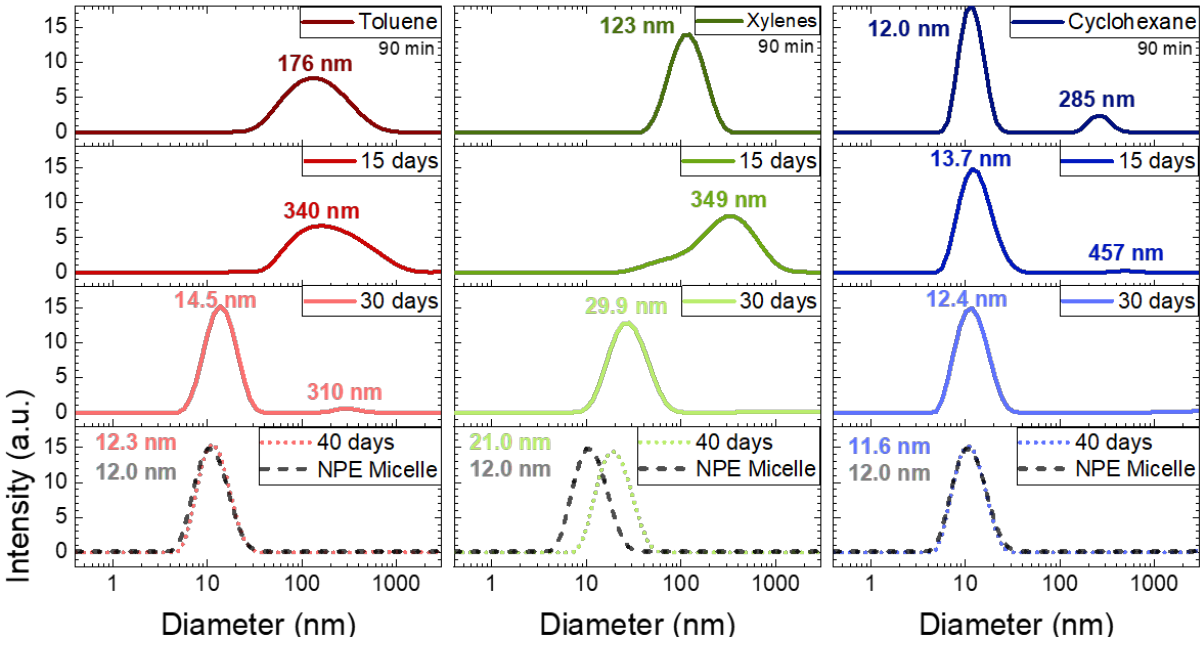

Figure 29: Evolution of swollen micelle and droplet size distributions from 90 minutes to 40 days of ageing for toluene (left), xylenes (middle), and cyclohexane (right). For all 40-day size distributions, the NPE micelle size distribution is overlaid for comparison (dashed line). All peaks are labeled with their corresponding average size ($\boldsymbol{D_{50}}$).

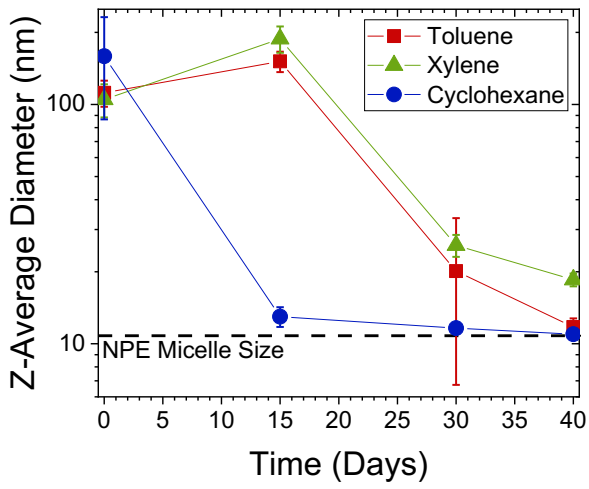

Figure 30: Z-average swollen NPE micelle and droplet diameters for toluene, xylenes, and cyclohexane between 90 minutes and 40 days. Error bars represent one standard deviation. Dotted line represents the NPE micelle diameter. The y-axis is plotted on a logarithmic scale.

A calculation using the Stokes' velocity and accounting for Brownian motion predicts that a 500 nm diameter oil droplet would take less than 19 days to cream from the bottom of the vial to the air-water interface (3 cm). Size distributions in Figure 29 show that droplets larger than 500 nm are present and therefore, are capable of creaming at a faster rate (e.g., a 1000 nm droplet would take 4.5 days to reach the air-water interface). Another consideration is that not all the droplets reside at the bottom of the vial and do not have to travel as far to reach the air-water interface (see the high concentration of droplets at 90 minutes near the air-water interface in Figure 28). Although creaming was observed before 40 days, a creamed layer did not remain at 40 days. Because of this observation, it is believed that the oils evaporated into the vial headspace after creaming to the air-water interface. This is also suggested by the aroma of each oil present when the samples were opened for size measurements. Before each size measurement, the emulsion was gently mixed by swirling the vial just enough to evenly disperse the concentrated emulsion layer that can be seen at the top of the aqueous phase in Figure 25 and Figure 28 at 90 minutes. This was only performed for systems that were not already uniformly dispersed to obtain representative and uniform samples. The low energy input of swirling was not expected to have an impact on droplet size.

Since only NPE micelles or slightly swollen NPE micelles remained after 40 days, it can be concluded that the oil was no longer in solution due to evaporation. To confirm this, an emulsion was made with excess toluene on top of the aqueous phase to ensure total coverage of the air-water interface with an oil-water interface. Excess toluene (10 mL of toluene on top of 10 mL of an aqueous phase containing 500 ppm NPE) replaced the entire air-water interface and created an oil-water interface unlike the last experiments in which the oil did not cover the air-water interface. Therefore, once creaming occurs, the toluene will no longer evaporate and leave the system. If the toluene-filled micelles coalesce or undergo disproportionation into the bulk toluene phase, there will be excess toluene in contact with the aqueous phase to replenish any lost toluene. Because of this replenishing, an equilibrium state could be obtained that was not previously observed. Figure 31 shows the Z-Average swollen micelle and droplet diameters from 90 minutes to 40 days and images of the emulsion at 0, 2, 11, and 32 days.

Excess toluene resulted in slower micelle swelling when compared to emulsions with 5000 ppm toluene. After 90 minutes, NPE micelles grew to 17.6 nm in the presence of excess toluene whereas 5000 ppm toluene caused NPE micelles to grow to approximately 112 nm. This occurred due to the lack of convective flows from interfacial tension gradients along the interface when toluene covered the entire interface. Excess toluene also prevented evaporation of toluene in the water phase. Once formed, the droplets did not significantly reduce in size over 40 days as was seen with emulsions containing 5000 ppm toluene (see Figure 30). Spontaneous emulsification in the absence of any observable Marangoni flows suggests that interfacial turbulence although expedited the process, is not needed for spontaneous emulsification and that another mechanism is active.

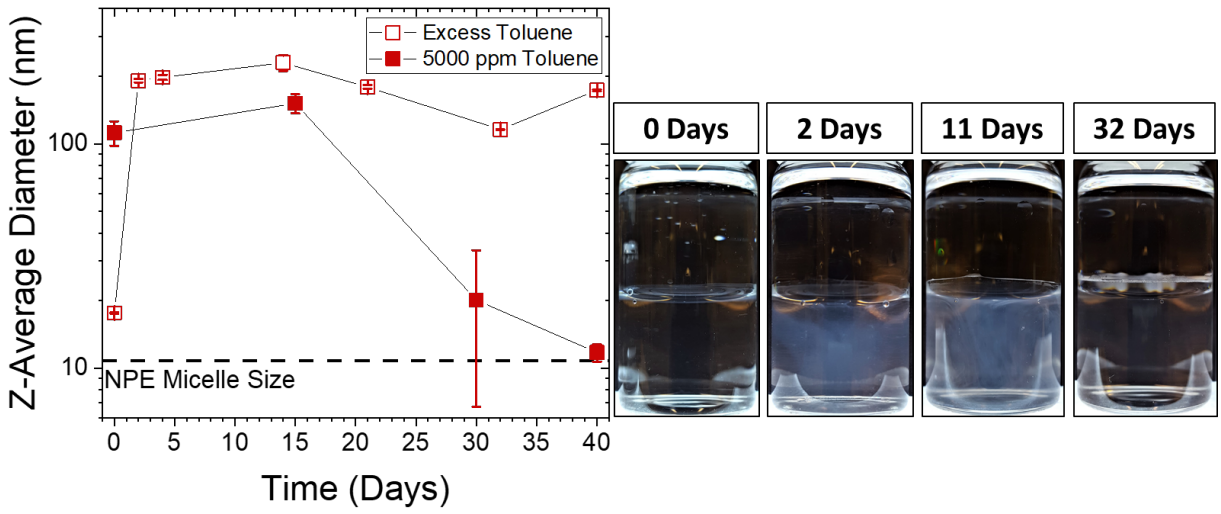

Figure 31**:** Z-Average swollen NPE micelle and droplet diameters for an emulsion containing 5000 ppm toluene (solid symbols) and excess toluene (open symbols) between 90 minutes to 40 days. Error bars represent one standard deviation. The y-axis is plotted on a logarithmic scale. To the right of the plot are images of the spontaneous emulsion with excess toluene at 0, 2, 11, and 32 days. Light reflections can be seen in the bottom corners of each vial and should not be mistaken for features of emulsification.

Spontaneity via Micelle Swelling

Previously, emulsion sizes were measured after emulsification occurred. To further investigate the spontaneity and mechanisms of emulsification, DLS was performed during emulsification. To do this, 0.8 mL of a 500 ppm NPE surfactant solution was placed into a DLS measurement cell. After measuring the initial micelle size, 0.2 mL of oil (~ 173,400 ppm) was placed on top of the aqueous phase. These experiments were attempted at an oil concentration of 5000 ppm but the oil did not cover the entire air-water interface and as a result, Marangoni flows were present. This increased the rate of spontaneous emulsification to the point where micelle swelling could not be captured. Unlike the previous experiments, the oil phase covered the entire surface of the aqueous phase and convective flows were not observed.

Figure 32 shows NPE micelle size distributions before and after exposure to toluene. NPE micelles were measured to be 10.6 ± 0.1 nm in diameter. Once toluene was placed on the surface of the surfactant solution, NPE micelles began to swell over time. After 30 and 60 minutes of exposure to toluene, the micelles grew to 17.9 ± 0.6 and 26.6 ± 1.6 nm, respectively. As time increased, the micelle size distribution broadened and the PDI increased; for 0, 30, and 60 minutes, the PDI was 0.12 ± 0.01, 0.14 ± 0.01, 0.18 ± 0.02, respectively. This indicates that not all the micelles were swelling at the same time but instead, it is likely that micelles closer to the oil-water interface began swelling before micelles located farther from the oil-water interface.

Micelle swelling was measured periodically over 60 minutes for toluene, xylenes, and cyclohexane; these results can be found in Figure 33**A**. Two distinct regions can be seen for each oil. Here, region one will be referred to as the "diffusion region" where the micelle size is

somewhat constant and similar to the initial NPE micelle size (d_0). An inflection in micelle size occurs at t_0 the time at which the micelle size begins to linearly increase. This inflection point marks the onset of region two which is the "swelling region". A third, equilibrium region can be seen for cyclohexane and occurs at approximately 46 minutes. At this point, swelling stops and the micelle size remains constant. This region is not observed for toluene or xylenes because the spontaneous mixing of larger oil droplets (as seen in Figure 25 and Figure 27) increased the count rate past the range that could be used to reliably collect data using DLS. In other words, larger oil droplets obstructed the DLS laser, preventing accurate measurements of the swelling micelles.

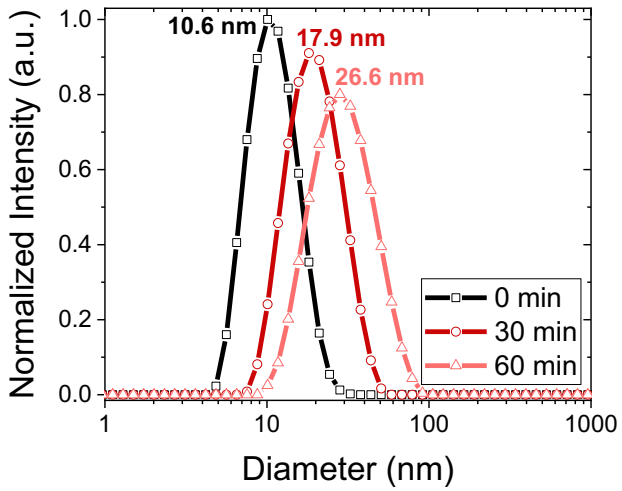

Figure 32: Swollen NPE micelle size distribution before (0 min) and after contact with toluene for 30 and 60 minutes. Intensity was normalized to the size distribution at 0 min. Z-average diameters are reported above each size distribution.

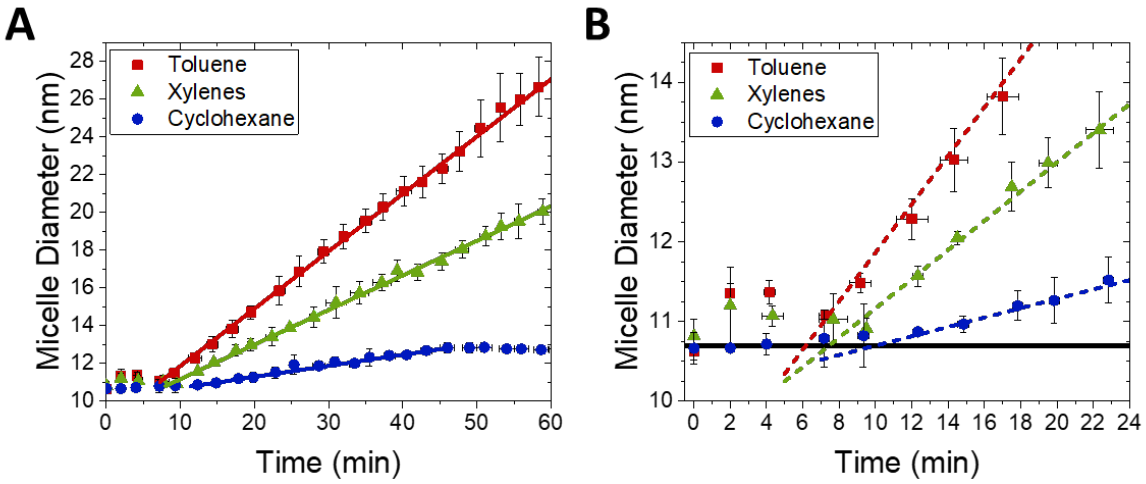

Figure 33: NPE micelle swelling response in the presence of excess oil for (A) 60 minutes and (B) magnification of data in the early stages of swelling. Plot B illustrates the intersection of each data series with the initial micelle size (d_0 horizontal line) to determine approximate values of t_0 (reported in Table 5). Error bars represent one standard deviation in both micelle diameter and time.

Figure 33**B** shows the transition between the diffusion and swelling regions in more detail. Toluene and xylenes show a slight increase in diameter (less than 1 nm) followed by an immediate decrease back towards the initial micelle size before time t_0. This is likely due to experimental error during the placement of oil on top of the aqueous solution causing some initial micelle swelling to occur. Each oil displayed a different t_0, calculated from the intersection between the initial micelle size (solid black line) and the linear swelling region (dotted lines) in Figure 33**B**. Values for t_0 are reported in Figure 25. A delay in swelling response can be attributed to the time it takes for the oil molecules to diffuse from the oil-water interface, through the water, and into the micelles at the point where the measurement is being taken (see Figure 36). Because of this, the absolute value of t_0 is arbitrary as it can change by altering the distance from the oil-water interface to the measurement location. However, the same distance of 0.225 cm was used for each experiment, giving the relative values of t_0 significance for comparing the spontaneity of different oils.

From the calculated t_0 values, it appears that toluene reached the NPE micelles first, followed by xylenes, and cyclohexane. This implies that toluene is the "most spontaneous" of the three oils tested. Micelle growth rates (k_m), calculated as the slope of the swelling region from t_0 to 60 minutes (t_{60}; 46 minutes for cyclohexane), also suggest that toluene is the most spontaneous of the three oils and are reported in Table 6.

Similar to values of t_0, only the relative values of k_m are meaningful due to the experimental setup. Toluene resulted in the fastest growth of NPE micelles at almost twice the rate of xylenes and 5.5 times the rate of cyclohexane. This demonstrates that toluene is capable of emulsifying with NPE faster than xylenes and cyclohexane and thus, is more spontaneous. As a result of this spontaneity, toluene-filled micelles grew to the largest size after 60 minutes of swelling (d_{60}).

A positive correlation was found between an oil's spontaneity and its solubility in water; that is, oils with a larger solubility (e.g., toluene, see Table 6) were more spontaneous. To further demonstrate this, mineral oil was used to represent an insoluble oil (S_o ~ 0 ppm). After 24 hours, there were no visible signs of spontaneous emulsification and the NPE micelles did not swell when in contact with mineral oil (from 10.7 to 10.2 nm after 24 hours). If mineral oil did contain water-soluble components, they were not at a significant concentration to cause micelle swelling. And even if the oil molecules are water soluble, the surfactant micelles must also have the capability of solubilizing those molecules.

Table 6: Initial micelle diameter (d_0), swelling start time (t_0), micelle growth rate (k_m), micelle diameter at 60 minutes (d_{60}), and solubility in water at 25 °C (S_o) for toluene, xylenes, cyclohexane, and mineral oil. Errors represent one standard deviation.

Oil	**d_0 (nm)**	**t_0 (min)**	**k_m (nm/min)**	**d_{60} (nm)**	**S_o (ppm)**
Toluene	10.7 ± 0.2	6.18 ± 0.67	0.315 ± 0.03	26.6 ± 1.6	515 [93]
Xylenes	10.7 ± 0.2	7.49 ± 1.2	0.176 ± 0.01	20.0 ± 0.7	177 [a 94,95]
Cyclohexane	10.7 ± 0.2	10.1 ± 3.6	0.057 ± 0.01	12.7 ± 0.2	55 [93]
Mineral Oil	10.7 ± 0.2	∞	0	10.3 ± 0.03	0 [b 95]

[a] Average solubility of o-xylene, m-xylene, and p-xylene.

[b] Solubility of decane ($C_{10}H_{22}$) in water. Mineral oil contains a mixture of alkanes greater than decane.

Values of t_0 can be normalized by the distance over which the molecules traveled to reach the measurement location (0.225 cm), giving a diffusion coefficient for each oil in the NPE solution ($D_{oil\text{-}NPE}$). **Equation 3** shows how the diffusion coefficients were calculated where $\langle x^2 \rangle$ is the mean square displacement.

$$D_{oil-NPE} = \frac{\langle x^2 \rangle}{2t_0}$$

(3)

Table 7 reports the calculated values of $D_{oil\text{-}NPE}$ as well as the diffusion coefficient from literature for each oil in water ($D_{oil\text{-}water}$). It is important to note that $D_{oil\text{-}NPE}$ does not represent diffusion strictly due to Brownian motion but is a combination of Brownian, molecular, and turbulent diffusion as well as micelle solubilization.

Table 7: Calculated diffusion coefficient for each oil in a 500 ppm NPE solution ($D_{oil\text{-}NPE}$), diffusion coefficient for each oil in water ($D_{oil\text{-}water}$), and the ratio of $D_{oil\text{-}NPE}$ to $D_{oil\text{-}water}$.

Oil	**$D_{oil\text{-}NPE}$ (*10^{-6} cm^2/s)**	**$D_{oil\text{-}water}$ (*10^{-6} cm^2/s)**	**$D_{oil\text{-}NPE}$ / $D_{oil\text{-}water}$**
Toluene	68 ± 7	8.5 [96]	8.0
Xylenes	56 ± 9	8.5 [97]	6.6
Cyclohexane	42 ± 10	8.4 [96]	5.0

Diffusion coefficients of all oils in water increase when NPE is added to the aqueous phase. An increase in the diffusion coefficient could be due to Marangoni flow. However, this flow was less prominent when the oil covered the entire surface of the water as it did in micelle swelling experiments. When the oil resided as a small droplet on the surface, as in Figure 26, a larger interfacial tension gradient at the air-water-oil interface existed and resulted in stronger convective flows. In micelle swelling experiments, the oil covered the entire surface of the water which resulted in a more uniform interfacial tension across the interface and thus, dampened or inhibited the flow. Diffusion coefficients may have increased simply due to the presence of NPE micelles and the non-zero solubility of oil inside the micelles. To investigate this, micelle sizes were measured as a function of oil concentration and compared with predicted micelle sizes.

Impact of Oil Concentration on Micelle Size

Figure 34 shows the measured and predicted equilibrium swollen micelle size at different concentrations of toluene. Equilibrium was obtained after at least 90 minutes or when all the oil was consumed by the micelle solution and was no longer visible on the surface. Predicted micelle diameters were calculated under the following assumptions: The NPE micelle aggregation number (n) was 172 (average from 3 literature values[98–100]). The aggregation number and number of micelles in solution (N_m) were constant during swelling. The total number of surfactant molecules (N_s) at a concentration of 500 ppm was calculated using an average molecular weight of 702 g/mol.[98] All toluene added was distributed equally into each micelle and none was left dispersed in the water. The swollen micelle diameter (d_s) was taken as the initial micelle diameter (d_0) plus the diameter of a sphere of toluene (d_t) containing the same volume as the number of toluene molecules in each micelle (N_t). The number of toluene molecules per micelle was taken as the total amount of toluene molecules at a given concentration (n_t) divided by N_m. A molar volume of 1.06x10^{-4} m^3/mol was used for toluene (V_{mol}).[93] Predicted swollen micelle diameters were calculated using **Equation 4, 5,** and **6**, where N_A is Avogadro's number.

$$d_s = d_0 + d_t$$
(4)

$$d_t = 2\left(\frac{3N_t * V_{mol}}{4\pi N_A}\right)^{\frac{1}{3}} = 2\left(\frac{3n_t * V_{mol} * n}{4\pi N_s * N_A}\right)^{\frac{1}{3}}$$
(5)

$$N_m = \frac{N_s}{n}$$
(6)

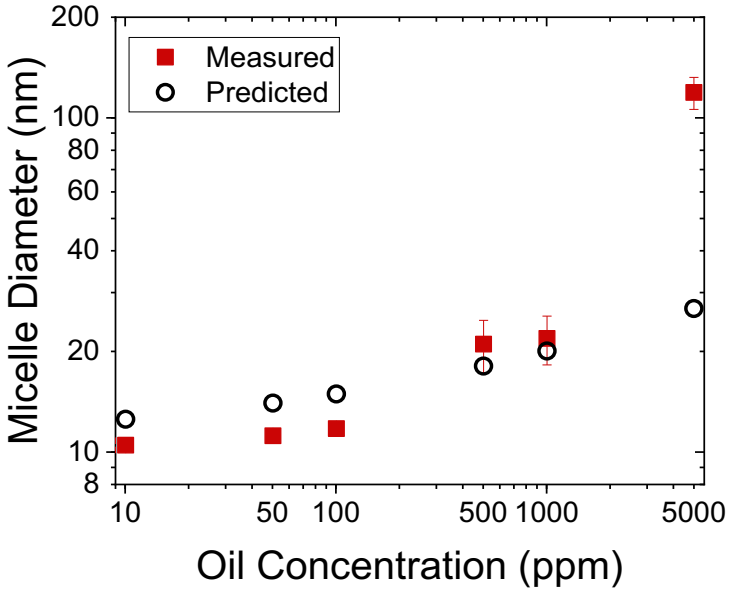

Figure 34: Measured (red squares) and predicted (open circles) equilibrium NPE micelle diameter for different concentrations of toluene. Error bars represent one standard deviation.

Predicted micelle diameters agree well with the measurements but overestimate the diameters at low concentrations (< 500 ppm). At concentrations of 500 and 1000 ppm, the predicted value is within one standard deviation from the measured value. When the concentration of toluene was 5000 ppm, the predicted diameter was 92 nm smaller than the measured diameter.

An overestimation of the swollen micelle diameters could be caused by underestimating the number of micelles in solution (e.g., if there are more micelles then the magnitude of swelling would decrease) or the assumption that all the oil was distributed into the micelles and none was dissolved in water. Since these predictions are accurate within one standard deviation at concentrations of 500 and 1000 ppm, it is more likely that the former is true; the number of micelles at low concentrations were underestimated. At concentrations near the solubility of toluene in water (515 ppm), the assumption that all the toluene was distributed equally into each micelle and none was left dispersed in water appears to match the data. This suggests that toluene prefers to be inside the NPE micelles and is only in the water as it transports from the oil

phase to the micelles. The preference for toluene to be inside NPE micelles instead of water supports the claim that diffusion coefficients increased in the presence of NPE micelles due to the oil's increased solubility inside micelles compared to pure water.

An underestimation of the micelle size at 5000 ppm is most likely due to the false assumption that the aggregation number and number of micelles are constant. Instead, as the oil emulsifies, larger micelles grow, forming droplets and consuming surfactant from smaller micelles. This means that the number of micelles decreased, and the aggregation number increased.

Dynamic Interfacial Tension

Dynamic interfacial tension measurements for toluene, xylenes, cyclohexane, and mineral oil in contact with an aqueous solution containing 500 ppm NPE can be found in Figure 35. Equilibrium interfacial tension measurements were not accessible due to spontaneous emulsification of the oil into the aqueous phase and the transfer of surfactant from the aqueous phase to the oil phase. Spontaneous emulsification was observed inside of the water droplet and as a result, the density of the aqueous phase decreased to unknown values over time which caused an increase in the interfacial tension. Transport of surfactant from the interface into the bulk oil was also likely as NPE is miscible with xylene.[101] Additionally, systems that did not display significant or any spontaneous emulsification (cyclohexane and mineral oil) also exhibited an increase in interfacial tension over time. This suggests that initially, surfactant adsorbed to the interface followed by desorption into the oil phase which reduced the amount of surfactant at the interface (i.e., increased the interfacial tension). Since the equilibrium interfacial tension could not be obtained, the initial interfacial tension was used as a comparison between oils.[102]

These relatively high interfacial tensions suggest that the mechanism of ultralow or negative interfacial tension was not responsible for the observed spontaneous emulsification and is in agreement with other work.[91,103–106] Systems that were more spontaneous also had larger interfacial tensions (toluene and xylenes) in comparison to systems that showed little to no spontaneous emulsification (cyclohexane and mineral oil). Indeed, the correlation between interfacial tension and spontaneity was opposite of what one would expect if interfacial tension had a significant role in the spontaneous emulsification of these systems.

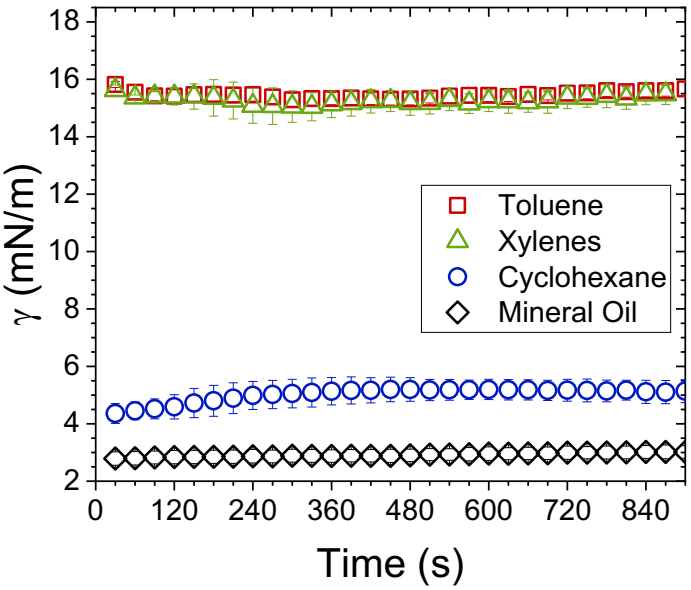

Figure 35: Dynamic interfacial tension of toluene, xylenes, cyclohexane, and mineral oil with an aqueous solution containing 500 ppm NPE. In these experiments, the pendant drop contained the aqueous phase and was surrounded by a continuous phase of oil.

Mechanism of Spontaneous Emulsification

The previous results give insight into how spontaneous emulsification occurred for these systems. Convective flow caused by the Marangoni effect visibly contributed to emulsification when oil did not cover the entire surface of the aqueous phase. However, when oil covered the surface of the aqueous phase, Marangoni flows were not observed but spontaneous emulsification still occurred (Figure 31). This suggests that diffusion was the dominating mechanism and Marangoni flows can contribute to but are not primarily responsible for spontaneous emulsification of these systems. Additionally, these convective flows were driven in part by the diffusion of oil into the aqueous phase as Marangoni flows were not observed for oils with little to no solubility (cyclohexane and mineral oil).

Figure 36 shows a diagram of the proposed governing mechanism for spontaneous emulsification during DLS experiments. At some time less than t_0, oil molecules begin to diffuse through the water. At t_0, the oil molecules reach the fixed measurement location, enter surfactant micelles in that vicinity, and swelling is detected. Between time t_0 and 60 minutes (t_{60}), the micelles at the measurement location grow linearly with time (see Figure 33).

The proposed mechanism of spontaneous emulsification requires the oil to be soluble in water and the surfactant micelles, if only slightly (see S_o in Table 7). Insoluble oils (mineral oil) could not diffuse through the water and into micelles while toluene, xylenes, and cyclohexane were shown to be soluble in both water and the NPE micelles. This mechanism also requires the presence of surfactant micelles (i.e., the surfactant concentration must be above the CMC) which

has been seen previously.[91] To confirm this, toluene was placed on top of an NPE solution below the CMC (10 ppm) and spontaneous emulsification was not observed .

Experiments with varying oil concentration confirm that oil molecules favor being inside micelles as opposed to dispersed in water (Figure 34). At some critical concentration of oil, micelles grow rapidly and consume surfactant from the smaller, surrounding micelles. After approximately 90 minutes, the oil was spontaneously emulsified and reached an equilibrium for these timescales (hours). However, this is a metastable state because the emulsions are not stable at larger timescales (several weeks, see Figure 28, Figure 29, and Figure 30).

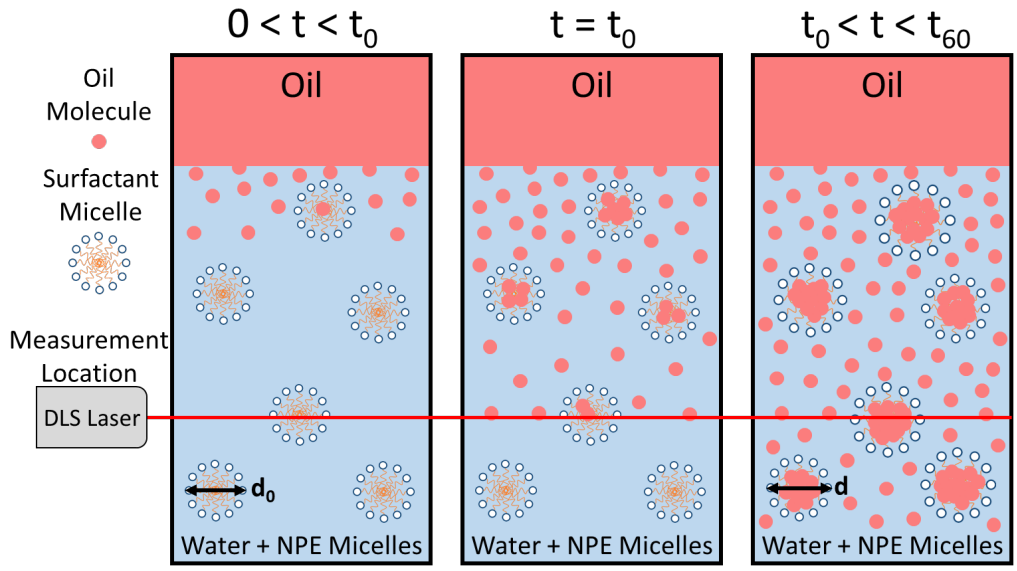

Figure 36: Diagram displaying the governing mechanism for spontaneous emulsification of toluene, xylenes, and cyclohexane in an NPE surfactant solution during DLS experiments. The initial micelle size (d_0) is smaller than the micelle size after swelling with oil (d). Image not to scale. Times *t* correspond to relevant times in micelle swelling experiments (Error! Reference source not found. and Table 7).

Predicting Spontaneous Emulsification using HLD Model

Gibbs adsorption isotherms were measured to understand the surface adsorption and micellar properties of NPE, SDBS, and NPE-SDBS mixed surfactant systems and how salt impacts these properties. Figure 37 shows the Gibbs adsorption isotherms for all three surfactant systems in NaCl solutions ranging from 0 to 0.42 M. SDBS solutions began salting out (phase separating) at concentrations between 0.27 and 0.31 M NaCl and therefore were not tested above 0.21 M NaCl. From these adsorption isotherms, surfactant and micellar properties were calculated and are reported in Table 8.

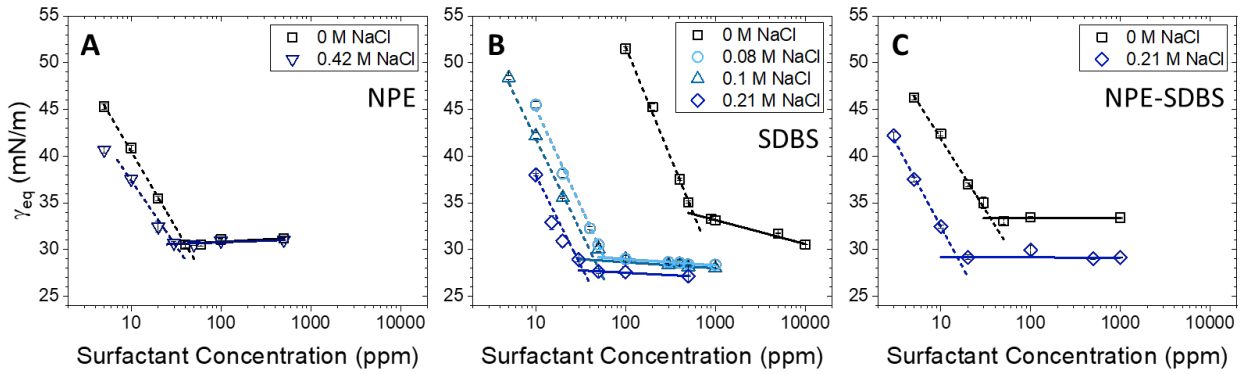

Figure 37: Gibbs adsorption isotherms for (A) NPE, (B) SDBS, and (C) an equal molar NPE-SDBS mixture at different concentrations of NaCl. Dotted and solid lines represent a best curve fit before and after the CMC, respectively. Error bars represent one standard deviation from the mean of three equilibrium surface tension measurements.

Table 8: Surface excess concentration (Γ), surfactant head group area (A_0), critical micelle concentration (CMC), packing parameter (P), and the mole fraction of surfactant in the mixed micelle (x) for NPE, SDBS, and an equal molar NPE-SDBS mixture at different salt concentrations. Errors represent the propagated standard error of the fitted curve(s) from which the calculation originated.

Surfactant	**NPE**		**SDBS**				**NPE-SDBS**	
[NaCl] (M)	**0**	**0.42**	**0**	**0.08**	**0.10**	**0.21**	**0**	**0.21**
Γ / 10^{-6} (mol/m^2)	2.88 ± 0.32	2.47 ± 0.46	2.07 ± 0.052	3.68 ± 0.32	3.47 ± 0.74	3.38 ± 0.48	-	-
A_0 ($Å^2$)	57.6 ± 6.4	67.3 ± 13	80.1 ± 2.0	45.2 ± 3.9	47.8 ± 10	49.1 ± 7.0	-	-
CMC (ppm)	39.9 ± 9.0	30.4 ± 11	573 ± 150	57.9 ± 13	45.2 ± 21	33.8 ± 9.4	35.7 ± 9.8	15.2 ± 3.3
CMC (mM)	0.060 ± 0.014	0.046 ± 0.017	1.64 ± 0.43	0.166 ± 0.037	0.129 ± 0.060	0.097 ± 0.027	0.071 ± 0.019	0.030 ± 0.0065
P	0.46	0.39	0.32	0.57	0.53	0.52	-	-
x	-	-	-	-	-	-	0.76 for NPE	0.55 for NPE

Nonionic surfactants like NPE are relatively insensitive to changes in salt concentration[107,108] as seen here. As the NaCl concentration increased from 0 to 0.42 M, the head group area increased by approximately 10 $Å^2$. However, this increase is within the propagated standard error of the

measurement and a t-test concluded that the difference between the two values was not statistically significant (p-value = 0.53, all t-tests are conducted using a two-tailed hypothesis unless otherwise stated). The same holds true for the slight decrease observed in the CMC.

Contrarily, anionic surfactants like SDBS are sensitive to salt. For example, an increase in NaCl from 0 to 0.08 M resulted in a decrease in head group area by approximately 35 $Å^2$ and a decrease in the CMC by an order of magnitude; both decreases were statistically significant with p-values of 0.0005 and 0.006, respectively. A reduction in the head group area was due to the shielding of the anionic SDBS head group by the sodium cations which compressed the Debye length. The approximated Debye length for the salt-free system was 9.9 nm (i.e., 0.95 mM of Na^+ ions using an ionization of 66% for SDBS)[109] and decreased to 1.1, 0.96, and 0.66 nm when 0.08, 0.10, and 0.21 M NaCl was added, respectively.[110] This shielding effect along with the reduced solvent quality contributed to the reduction in the CMC.

For the equal molar NPE-SDBS mixed surfactant system, the CMC at 0 M NaCl was like that of pure NPE. However, due to the presence of SDBS, this mixed system was also sensitive to salt indicated by the reduction of the CMC by approximately 20 ppm to 15.2 ppm from the addition of 0.21 M NaCl and was found to be statistically significant with 95% confidence (p-value was 0.035, using one-tailed hypothesis). This CMC was the lowest value measured across all systems which suggests that the NPE and SDBS interact synergistically. This synergistic effect has been observed previously between Triton X-100 (similar in chemistry to NPE) and SDBS.[108]

From the calculated head group area, the packing parameter (P) was also calculated to determine the micelle structure under different salt concentrations. From these calculations, NPE is predicted to form oblong-spherical to cylindrical micelles independent of salt concentration.[111] SDBS is predicted to form spherical micelles in salt-free (i.e., no additional salt added) environments and cylindrical micelles at salt concentrations between 0.08 and 0.21 M NaCl.[109,112,113]

For equal molar NPE-SDBS mixed surfactant systems, the concentration of adsorbed surfactant at the interface or aggregated in the micelle may not be equal to the bulk surfactant concentration. Therefore, the nonideal mixed micelle model was used to calculate the mole fraction of each surfactant at an interface or in a mixed micelle (x). At 0 M NaCl, x for NPE was 0.76 (0.24 for SDBS), meaning 76% of the molecules at the interface or in the mixed micelle were NPE and 24% were SDBS. NPE and SDBS have different surface coverage areas (i.e., head group areas), making it important to also consider their respective area fractions at the interface. For NPE, the area fraction of the total surfactant coverage was reduced to 0.69 (0.31 for SDBS) due to the larger head group area of SDBS. In saltwater (0.21 M NaCl), the molar adsorption is more balanced with 55% of the molecules being NPE and 45% being SDBS. However, the area fraction still favors NPE at 0.61 due to the reduction in SDBS head group area with salt. It should be noted that x at 0.21 M NaCl was calculated using the average CMC of NPE at 0 and 0.42 M NaCl and is justified by the statistically insignificant change in CMC over that salt concentration.

Spontaneous Emulsification in NPE-Saltwater Environments

It has been demonstrated previously that NPE can spontaneously emulsify with oils, including toluene, in salt-free systems.[114] However, the impact of salt on spontaneous emulsification with NPE has not been investigated. Figure 38 shows images of toluene on the surface of an aqueous

solution of NPE after four hours of contact in salt-free (top row) and 0.42 M NaCl (bottom row) environments. It should be noted that the entire aqueous surface was covered by toluene, eliminating interfacial turbulence and thus, reducing the rate of emulsification.[114] A minimum surfactant concentration above the CMC was needed for spontaneous emulsification to occur[114] and is shown here to be between 50 and 100 ppm of NPE. As salt increased from 0 to 0.42 M NaCl, there was a small increase in emulsification observed at 100 and 500 ppm of NPE indicated by the cloudy, translucent regions. Samples containing 50 ppm NPE did not show visible spontaneous emulsification.

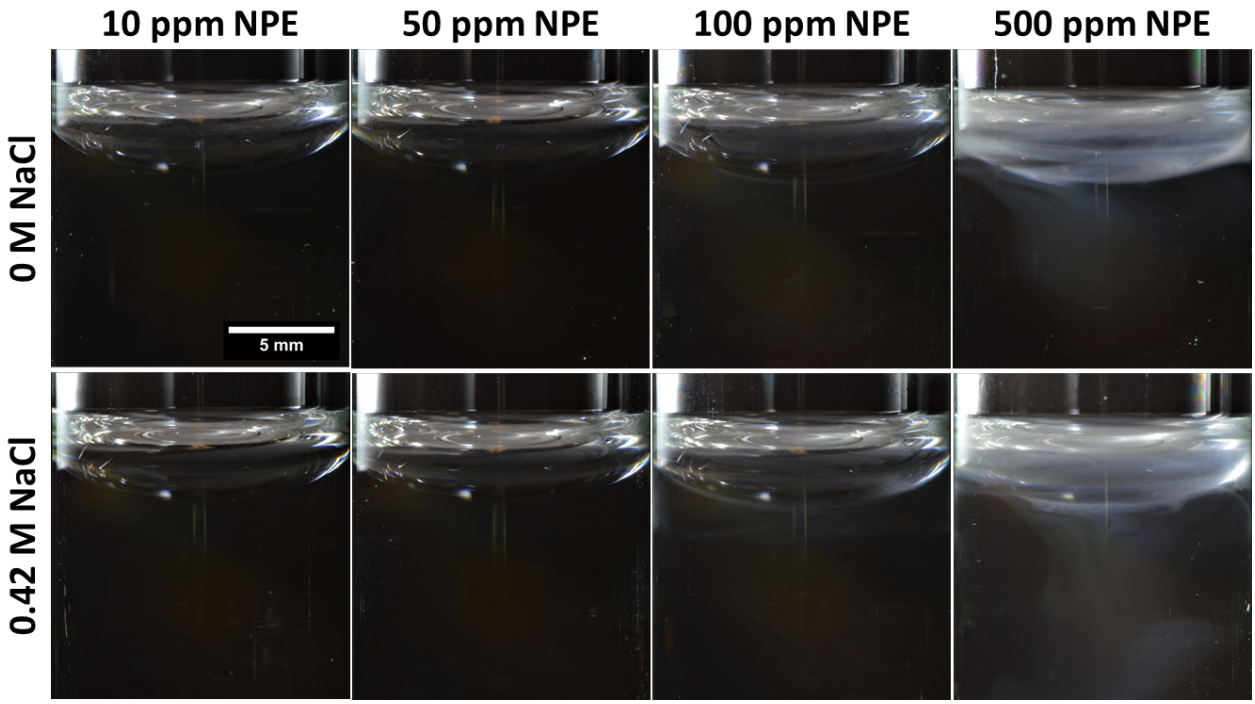

Figure 38: Images of spontaneous emulsification for toluene with NPE aqueous solutions containing (top row) 0 M NaCl and (bottom row) 0.42 M NaCl using 10, 50, 100, and 500 ppm of NPE. The top layer of the vial is toluene, and the bottom layer is the aqueous solution. Each image was taken four hours after toluene was pipetted onto the surface of the aqueous solution. The scale bar is 5 mm and applies to all images.

To quantify the impact that salt had on the spontaneity of emulsification in NPE solutions, micelle swelling experiments were performed at 0, 0.21, and 0.42 M NaCl and are presented in Figure 39. Time zero represents the initial micelle size of each solution and this increased with salt concentration. At some time after toluene contacted the surface of the aqueous solution, the micelle size increased (i.e., swelling began) linearly over time. Before linear swelling, there was an initial increase and subsequent decrease in micelle size within the first ten minutes. This increase is explained by the placement of oil onto the surface that created interfacial turbulence and mixing resulting in the rapid swelling of few micelles. As these swollen micelles were dispersed into solution, the average size decreased back towards the original micelle size. This phenomena was observed previously for micelle swelling experiments.[114] The slopes of the micelle swelling curves indicated by the solid lines in Figure 39 give the micelle swelling rate (nm/min) and can be compared between samples to quantify their spontaneity. Error! Reference s ource not found. shows the micelle swelling rate for each salt concentration. There was no

statistical evidence that concluded a significant difference between the 0 M and 0.21 M micelle swelling rates (p-value = 0.29). However, there was a statistically significant difference in the micelle swelling rates when comparing 0 M to 0.42 M (p-value <0.00001) and 0.21 M to 0.42 M (p-value = 0.00002). This result and statistical analysis show quantitatively that salt increased the spontaneity of NPE-toluene systems.

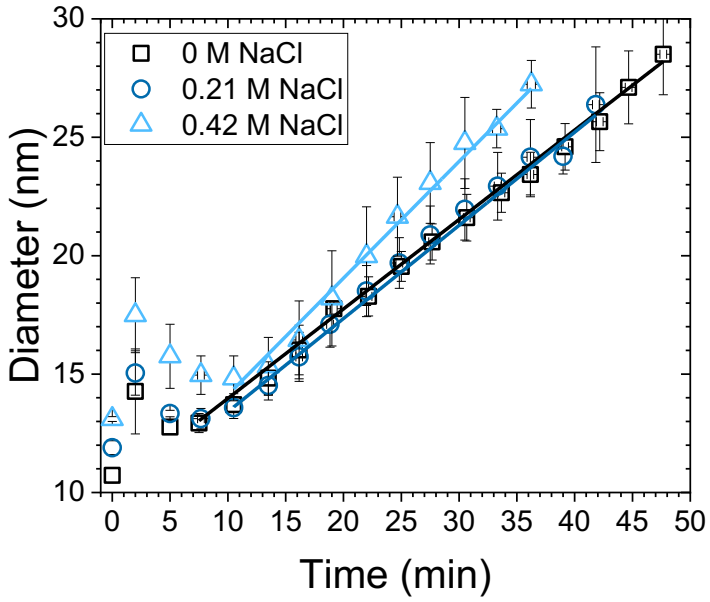

Figure 39: Spontaneity measurements via dynamic light scattering over time for 500 ppm NPE solutions containing 0, 0.21, and 0.42 M NaCl. Solid lines represent the fitted curves for the swelling region of each system. Error bars represent one standard deviation from the mean of three measurements.

Table 9: NPE micelle swelling rates at 0, 0.21, and 0.42 M NaCl calculated from the slope of the micelle size over time. Error represents the standard error from the corresponding fitted curve.

[NaCl] (M)	**Micelle Swelling Rate (nm/min)**
0	0.377 ± 0.010
0.21	0.393 ± 0.011
0.42	0.493 ± 0.014

Spontaneous Emulsification in SDBS-Saltwater Environments

Solutions containing 5000 ppm SDBS were tested in different salt concentrations to see if spontaneous emulsification with toluene would occur; images of this can be seen in Figure 40. Unlike NPE, SDBS did not spontaneously emulsify with toluene in salt-free systems, and this was confirmed using DLS. Salt concentrations above 0.06 M were needed to see emulsification

after four hours of contact with toluene. As the salt concentration increased, the solutions became cloudier indicating an increase in emulsification. Increases in spontaneity and emulsification with increasing salt were more apparent for SDBS than NPE.

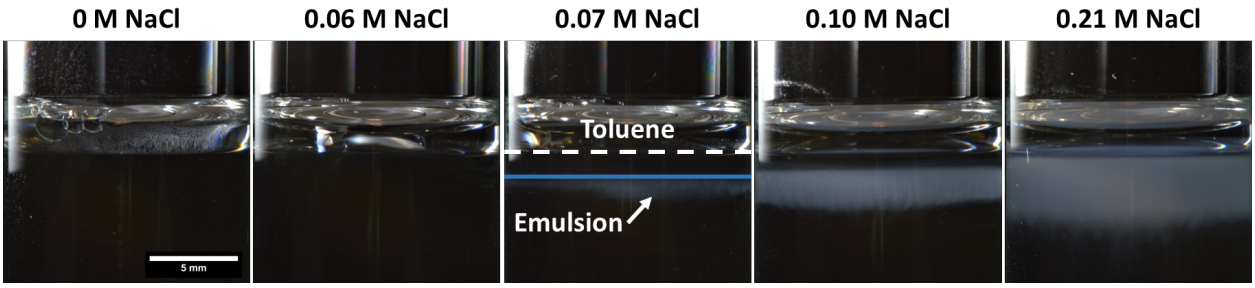

Figure 40: Images of spontaneous emulsification for toluene with 5000 ppm SDBS aqueous solutions containing 0, 0.06, 0.07, 0.10, and 0.21 M NaCl. The top layer of the vial is toluene, and the bottom layer is the aqueous solution. The dotted white line in the 0.07 M NaCl image represents the oil-water interface and the solid blue line represents the top of the emulsified oil layer in the aqueous phase. Each image was taken four hours after toluene was pipetted onto the surface of the aqueous solution. The scale bar is 5 mm and applies to all images.

Figure 41 shows how salt impacted the minimum concentration of SDBS that was needed for spontaneous emulsification to occur. As the concentration of salt increased, the surfactant concentration needed for spontaneous emulsification decreased. For example, at 300 ppm SDBS, emulsification was not observed at 0.08 M NaCl but was observed at 0.10 and 0.21 M NaCl. This is likely due to the reduction in the CMC and surface tension of SDBS as the salt concentration increased. To quantify the spontaneity of this system with salt, dynamic light scattering measurements were made over time.

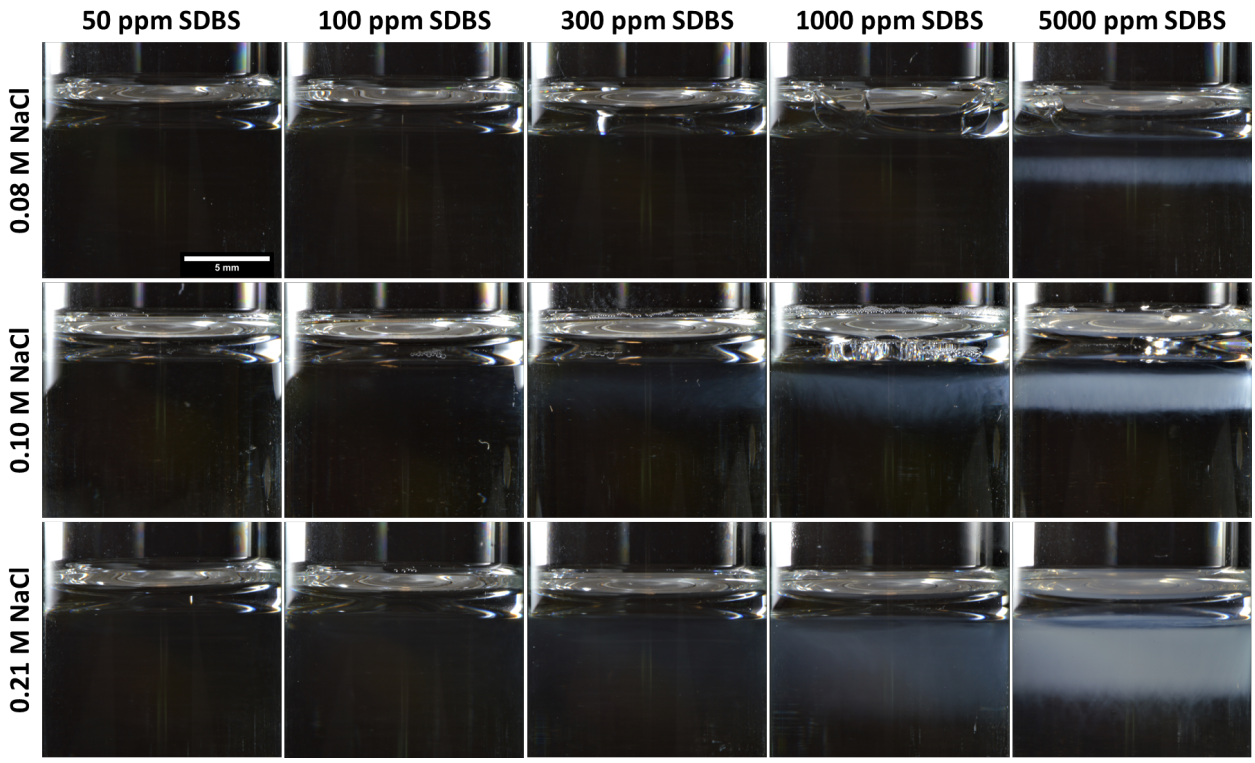

Figure 41: Images of spontaneous emulsification for toluene with SDBS aqueous solutions containing (first row) 0.08 M NaCl, (second row) 0.10 M NaCl, and (third row) 0.21 M NaCl using 50, 100, 300, 1000, and 5000 ppm of SDBS. The top layer of the vial is toluene, and the bottom layer is the aqueous solution. Each image was taken four hours after toluene was pipetted onto the surface of the aqueous solution. The scale bar is 5 mm and applies to all images.

Figure 42 shows spontaneity measurements for a 5000 ppm SDBS system with 0.10, 0.15, and 0.21 M NaCl at various times after toluene was placed on the surface of the aqueous solution. As the droplet size distributions change from light to dark, the time after contact with toluene increases. The light grey curves in each plot are similar in value to the initial micelle size distributions. This means that after 63, 40, and 17 minutes of contact with toluene, the micelle size did not change for 0.10, 0.15, and 0.21 M NaCl, respectively. In the very next measurement (two to three minutes was the time resolution for these experiments), the intensity of the micelle size distribution decreased and droplets approximately an order of magnitude larger than the micelles (140 to 280 nm) appeared. Over time, the micelle size distributions were diminished, and droplets continued to grow. At approximately 80 minutes, droplets with an average diameter between 630 and 780 nm were formed and the droplet size decreased with increasing salinity.[115]

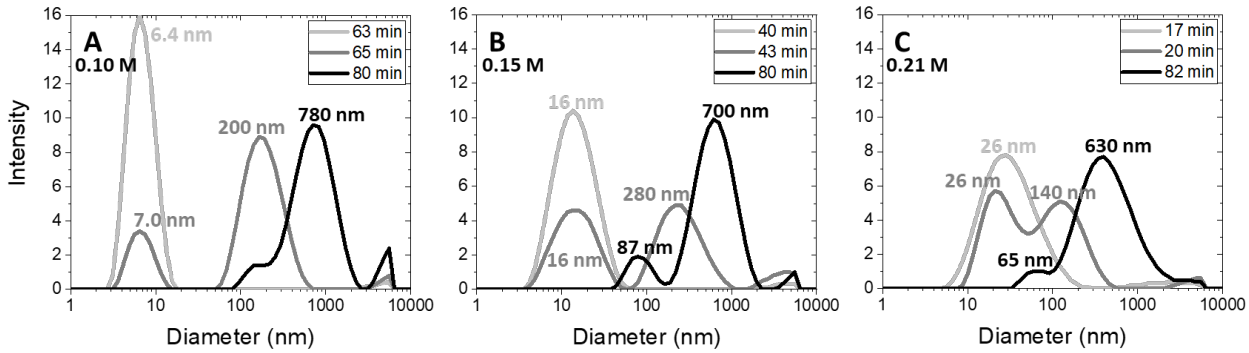

Figure 42: Spontaneity measurements via dynamic light scattering for aqueous solutions containing 5000 ppm SDBS with (A) 0.10, (B) 0.15, and (C) 0.21 M NaCl. The time label for each curve represents the elapsed time after toluene was pipetted onto the surface of the aqueous solution. The first curve (light grey) in each plot is similar to the initial micelle size. The next two curves (medium grey and black) represent the first detection of droplets and droplet growth, respectively. Labels for each peak represent the mean droplet diameter of that peak.

The evolution of the size distributions in Figure 42 were not gradual and continuous like those observed for NPE systems which displayed micelle swelling. Instead, the appearance of droplets within two to three minutes indicated that a different mechanism was responsible for spontaneous emulsification. This mechanism was likely diffusion and stranding[116] due to the sudden appearance of droplets which is expected after nucleation and growth.[114,117–119] Images in Figure 40 and Figure 41 also support this mechanism because a gap can be observed between the oil-water interface and the layer of emulsified oil. This gap has been seen previously[120] and represents the diffusion region below which supersaturation occurred, promoting nucleation and growth.

Although micelle swelling rates could not be calculated to quantify the spontaneity between these systems, the time until nucleation was used instead. As salt concentration increased from 0.10 to 0.15 and 0.21 M NaCl, the time until nucleation occurred was an average of 58 ± 6, 39 ± 4, and 22 ± 6 minutes, respectively. This shows that salt increased the spontaneity of these systems.

Spontaneous Emulsification in Mixed NPE-SDBS Systems

Equal molar NPE-SDBS solutions containing 5000 ppm of total surfactant were tested to identify the salt concentration needed for spontaneous emulsification to occur. Figure 43 shows images after four hours of toluene on the surface of an aqueous NPE-SDBS solution at salt concentrations between 0 and 0.21 M NaCl. After 4 hours, spontaneous emulsification was only seen at salt concentrations above 0.01 M NaCl. This was less salt needed than for pure SDBS systems which required more than 0.06 M NaCl. Like pure SDBS systems, as the salt concentration increased, more emulsification was observed.

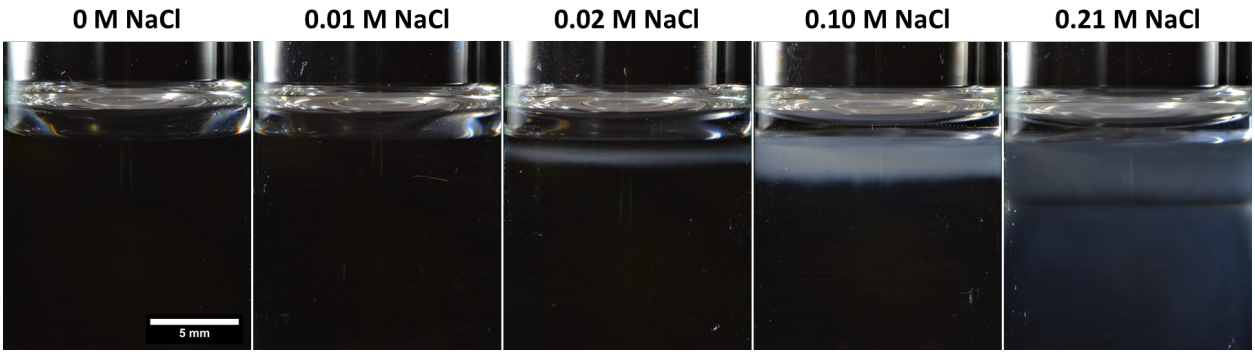

Figure 43: Images of spontaneous emulsification for toluene with a 5000 ppm, equal molar NPE-SDBS solution containing 0, 0.01, 0.02, 0.10, and 0.21 M NaCl. The top layer of the vial is toluene, and the bottom layer is the aqueous solution. Each image was taken four hours after toluene was pipetted onto the surface of the aqueous solution. The scale bar is 5 mm and applies to all images.

It is important to note that the 0 and 0.01 M NaCl systems did show signs of emulsification after six days of contact with toluene (see Figure 44). However, this was not considered to be a spontaneous system. First, the droplets in these samples were significantly larger than the spontaneous emulsions with some reaching between 100 and 500 µm in diameter. Because of their relatively large size, the droplets creamed to the surface quickly after being disturbed and were not dispersed throughout the aqueous phase like the spontaneous systems seen in Figure 43. These droplets likely formed due to the transportation of samples between laboratories which supplied an external energy input. This would be considered a self-emulsifying system and not a truly spontaneous system because small amounts of energy were needed to form droplets.[118,120]

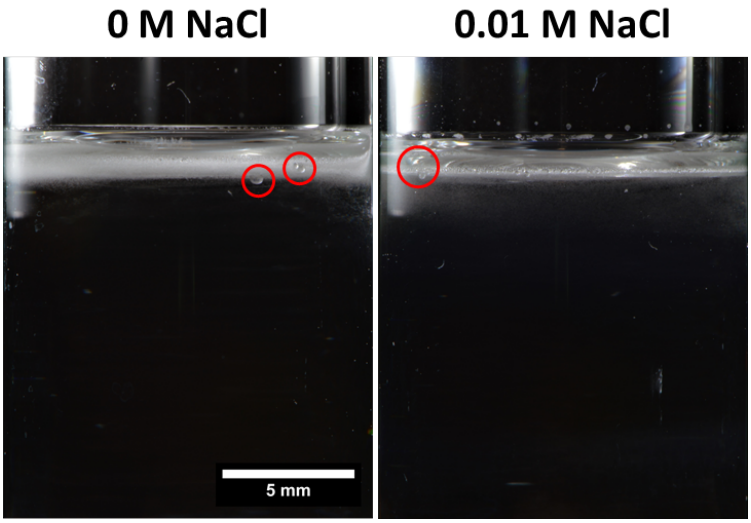

Figure 44: Images of toluene on top of a 5000 ppm, equal molar NPE-SDBS solution containing 0 and 0.01 M NaCl. These images were taken six days after toluene was pipetted onto the surface of the aqueous solution. Red circles locate larger droplets that can be seen at the surface of the aqueous solution. The scale bar represents 5 mm and applies to both images.

DLS experiments were conducted to quantify the spontaneity of the 5000 ppm, equal molar NPE-SDBS mixed surfactant system. Figure 45 shows the micelle swelling curve for 0.10 M NaCl. Time zero represents the initial micelle size which was 19.5 ± 0.1 nm. After toluene was placed on the surface, the micelle size increased slightly followed by a subsequent decrease as seen previously for pure NPE systems. At approximately 10 minutes, the micelles began swelling linearly with time. The slope of the fitted curve in the swelling region (solid black line) resulted in a micelle swelling rate of 0.296 ± 0.0042 nm/min. This swelling rate was smaller than the rate calculated for all pure NPE systems and was found to be statistically significant (p-value < 0.00001 when compared to salt-free NPE). Like pure NPE, the NPE-SDBS system at 0.10 M NaCl spontaneously emulsified via micelle swelling. However, the addition of SDBS reduced the rate of swelling.

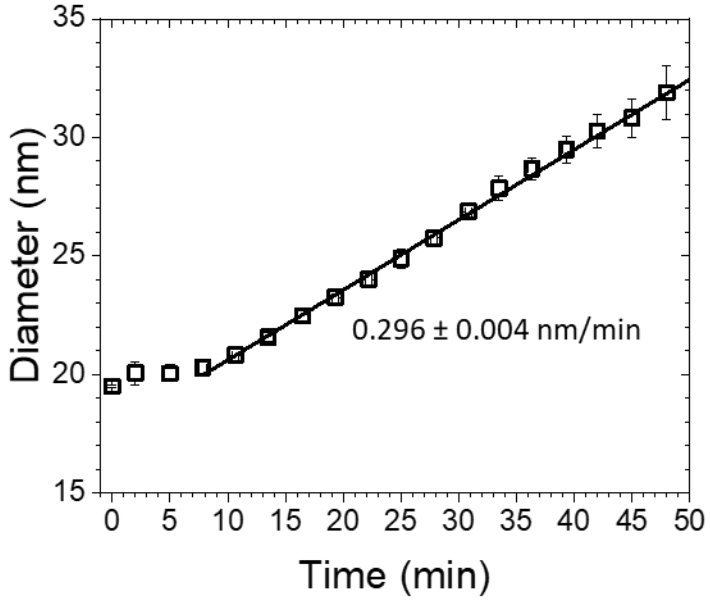

Figure 45: Spontaneity measurements via dynamic light scattering over time for 5000 ppm, equal molar NPE-SDBS solutions containing 0.10 M NaCl. The solid line represents the fitted curve for the swelling region. Error bars represent one standard deviation from the mean of three measurements. The micelle swelling rate (i.e., the slope of the fitted curve) was 0.296 ± 0.004 nm/min.

At higher concentrations of NaCl, micelle swelling was initially observed followed by a rapid droplet growth that resembled nucleation and growth (i.e., diffusion and stranding). Figure 46 shows the micelle and droplet size distributions over time for systems containing (A) 0.15 and (B) 0.21 M NaCl. Initial micelle size distributions (0 minutes) are represented by the dashed light grey lines. Micelles began swelling until the size distribution suddenly split into a bimodal distribution (dark grey dotted line) that represented droplets and micelles. Over time, the droplets grew (between 250 and 350 nm) while micelles remained in solution. As salt increased from 0.15

to 0.21 M NaCl, the time to see rapid droplet growth decreased from approximately 37 to 17 minutes indicating that salt increased spontaneity.

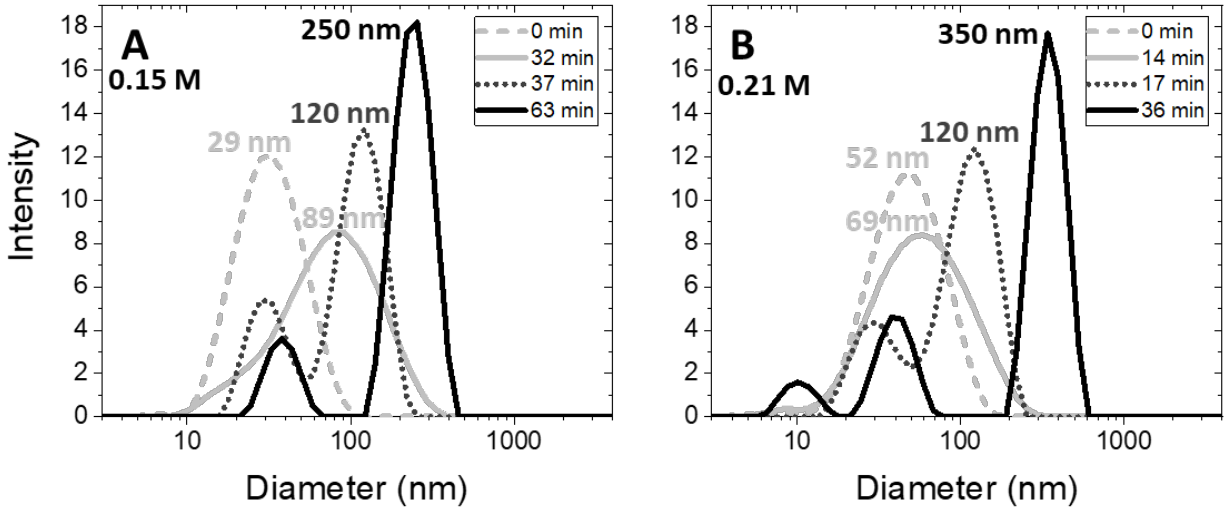

Figure 46: Spontaneity measurements via DLS for aqueous solutions containing 5000 ppm, equal molar NPE-SDBS with (A) 0.15 and (B) 0.21 M NaCl. The time label for each curve represents the elapsed time after toluene was pipetted onto the surface of the aqueous solution. Labels for each major peak represent the mean droplet diameter of that peak.

HLD Analysis of Spontaneous Emulsification

To better understand the results for spontaneous emulsification, HLD calculations were made for each system as well as for systems studied previously by Davis, *et al.*[114] Figure 47 shows the calculated HLD values as a function of salt concentration for different surfactant-oil systems. Green symbols represent samples that spontaneously emulsified while red symbols represent samples that did not spontaneously emulsify. All samples above the green reference line at an HLD of -2.05 were spontaneous and all samples below the red reference line at an HLD of -2.4 were not spontaneous. In the region between an HLD of -2.4 and -2.05, samples transitioned from non-spontaneous to spontaneous.

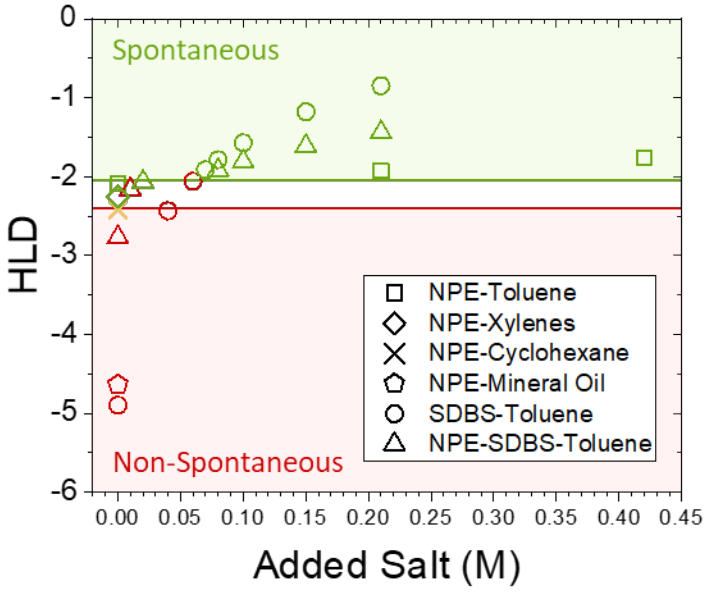

Figure 47: Calculated HLD values as a function of salt (NaCl) concentration for different surfactant-oil systems. Green symbols represent samples that showed spontaneous emulsification while red symbols represent samples that were not spontaneous. The symbol for cyclohexane is yellow because there was very little emulsification that could only be detected via DLS. Xylenes, cyclohexane, and mineral oil systems were observed in a previous study.[114]

Figure 47 demonstrates the relationship between HLD and spontaneous emulsification: as the HLD of a system approaches zero, it is more likely to spontaneously emulsify. However, this relationship only shows whether emulsification occurred and does provide information on spontaneity or the extent of emulsification. Therefore, turbidity measurements were made to quantify the relative spontaneity between systems that emulsified.

Figure 48 shows the turbidity of spontaneous emulsions after two days of contact with toluene as a function of the calculated HLD value. As the HLD value approached zero (salt concentration increased), turbidity (the amount of emulsified toluene) also increased. Turbidity measurements confirmed the visual observations shown previously but were used here to quantify spontaneity. HLD not only models when spontaneous emulsification will occur but also the relative spontaneity within a given system. This model can then be used to better prevent or promote spontaneous emulsion systems. For example, if a system contains SDBS, toluene, and NaCl, Figure 47 and Figure 48 can aid in determining the amount of salt need to promote emulsification or the amount of dilution needed to prevent emulsification.

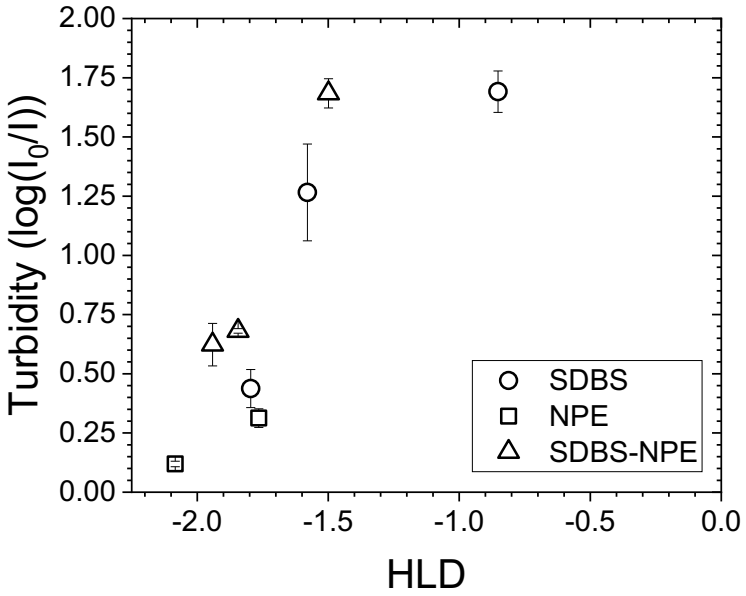

Figure 48: Calculated HLD values for samples with different turbidities (i.e., total emulsified toluene). Turbidity was taken as the absorbance at 400 nm and was measured after two days of contact with toluene. Error bars represent one standard deviation from the mean of three measurements.

Although the HLD model can be useful for understanding spontaneous emulsion systems, it is not without limitations and these limitations are important to consider when modeling spontaneous emulsions. As seen previously[114], spontaneous emulsification is dependent on surfactant concentration which is not accounted for in the current HLD model. This model assumes enough surfactant is present to spontaneously emulsify. The current model also does not account for the phase separation or "salting out" of surfactant which occurred at approximately 0.29 M NaCl for SDBS. Co-surfactants like alcohols are not easily modeled using HLD[21] and are often used to promote spontaneous emulsification.[120] Mixed surfactant systems can be modeled using HLD, as shown here, but not without additional measurements to obtain the CMC and C_c values. The HLD model is not well defined for mixed oil systems which can also spontaneously emulsify. Additionally, the HLD model is only predictive within a given system and not across systems. For example, if one surfactant system spontaneously emulsifies at an HLD of -2, that does not mean a different surfactant chemistry will also spontaneously emulsify at that same HLD value. This model is empirical and has not been proven to predict the emulsification of samples that have not been tested. However, the testing of more surfactant and oil chemistries could provide a more predictive model. The goal of this research is not to predict emulsification for all systems but to show the correlation between HLD and spontaneous emulsification that, to the authors' knowledge, has not been adequately discussed.

Influence of Surfactant Ratio on Spontaneous Emulsification

For systems with mixed surfactants, HLD_{mix} depends on the surfactant ratio. Changing the surfactant concentration in either the oil or aqueous phase could result in different surfactant packing at the oil-water interface, changing the effective C_c, and thus, changing the HLD_{mix}. Here, the HLD_{mix} was calculated using a simplified rule of mixtures approach. This calculation is only an approximation and does not correctly account for the surfactant interactions and molar ratios at the interface. However, this simplified model showed trends of how HLD_{mix} changes when the surfactant ratios changed. In our systems, an increasing proportion of Span-80 (or decreasing proportion of SLES) would result in higher (more positive) HLD_{mix} due to its positive C_c. In this set of experiments, the sample salinity was fixed at 0.1 M NaCl to allow the most change in HLD_{mix} away from 0.

To visualize the spontaneous emulsification, 1 ml of each the oil (upper) and aqueous (lower) phases were added to a cuvette. In Figure 49, the same aqueous phase composition was used (100 ppm SLES with 0.1 M NaCl) and the oil phases were hexadecane with increasing Span-80 concentration (from left to right). Similarly, Figure 50 shows samples with the same oil phase (hexadecane with 500 ppm Span-80) but decreasing SLES concentration (from left to right) in the aqueous phase. The opaque regions were emulsified oil or water. In Figure 49, no emulsification was visualized with $HLD_{mix} \leq -2.80$. This result was confirmed by DLS measurements. The spontaneity in the aqueous phase increased as HLD_{mix} increased from -1.09 to -0.47. A small amount of emulsified oil was observed in the circled region in Figure 49 (24 h: 300 ppm Span-80, 100ppm SLES, 0.1 M NaCl). Further increasing HLD_{mix} led to the formation of w/o emulsion in the oil phase. When the HLD_{mix} reached 0.7, spontaneous emulsification could only be observed in the oil phase. Similarly in Figure 50, spontaneous emulsification in the aqueous phase was only observed when HLD_{mix} was between -0.95 and 0.12. The spontaneity in the oil phase increased when HLD_{mix} increased from -0.47 to 0.12. For example, the sample with 50 ppm SLES ($HLD_{mix} = 0.12$) showed emulsification in the oil phase 20 minutes after the two phases were put into contact, while the samples with 100 ppm SLES ($HLD_{mix} = -0.47$) showed slower emulsification rate and less turbidity in the oil phase.

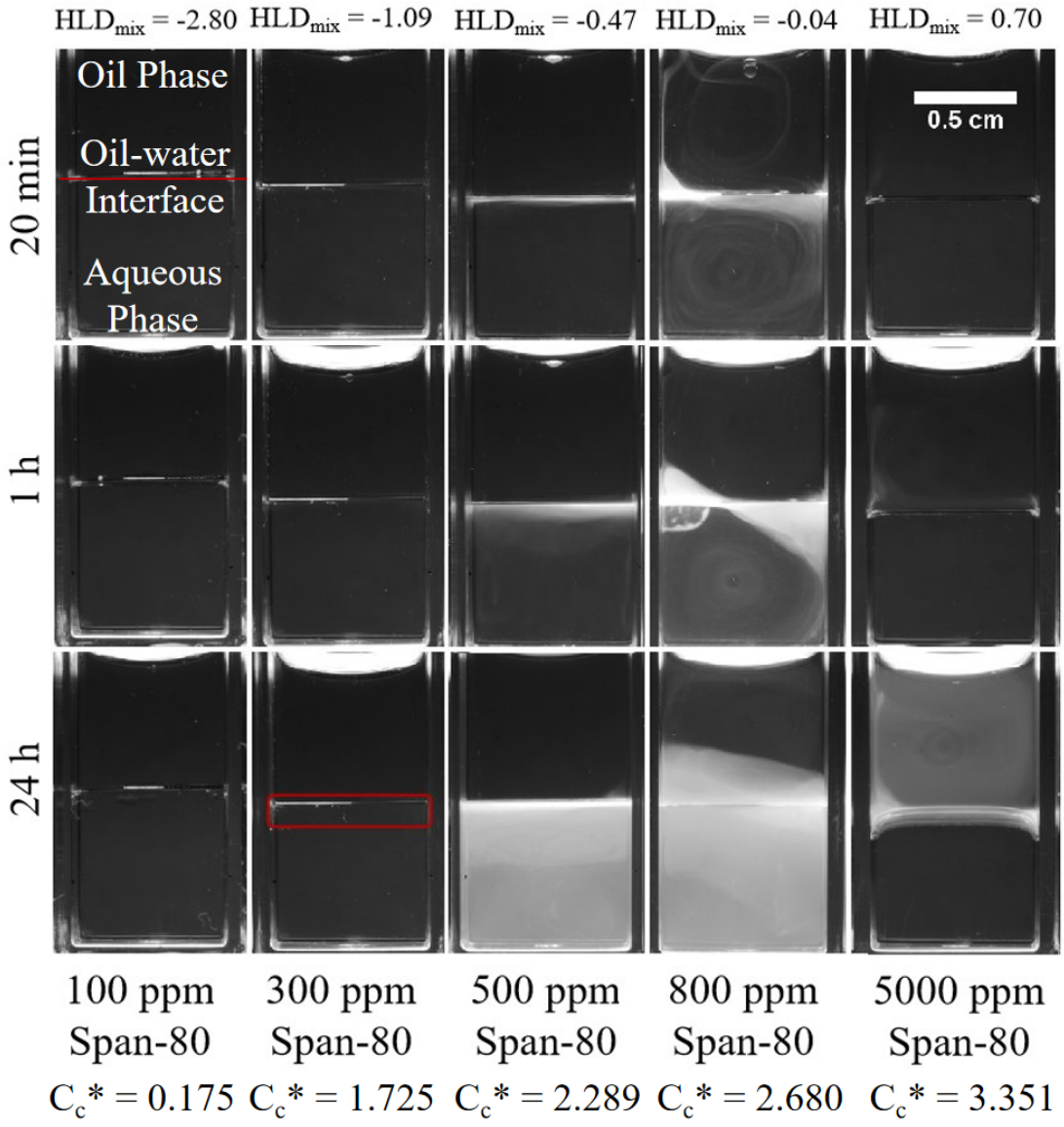

Figure 49. Photographs of spontaneous emulsification at 20 minutes, 1 hour and 24 hours. The oil phase (upper phase) is hexadecane with 100, 300, 500, 800, 5000 ppm Span-80 (from left to right). The aqueous phase (bottom phase) is DI water with 100 ppm SLES and 0.1 M NaCl. The C_c* values were estimated based on molar mixing rule.

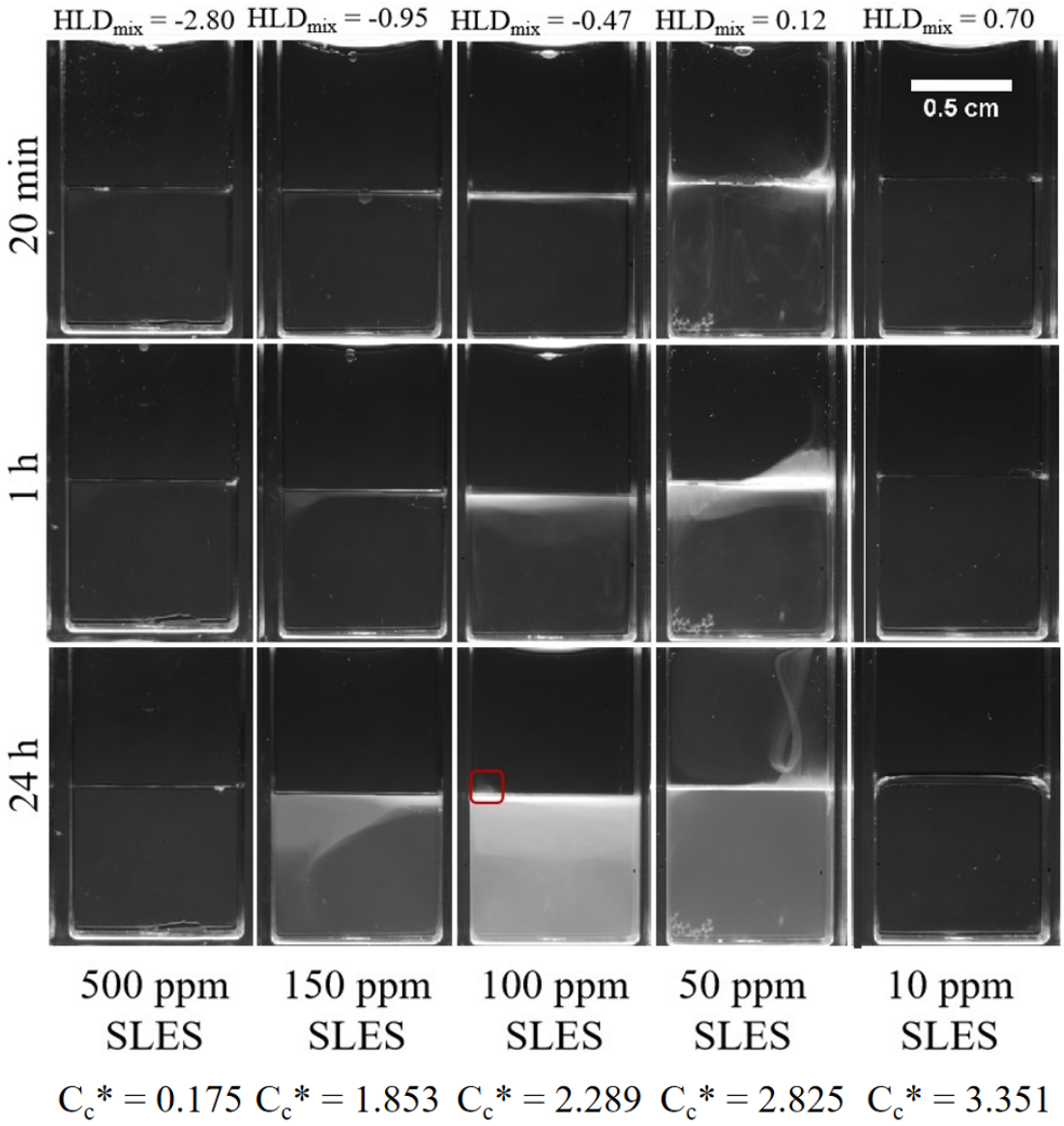

Figure 50. Photographs of spontaneous emulsification at 20 minutes, 1 hour and 24 hours. The oil phase (upper phase) is hexadecane with 500 ppm Span-80. The aqueous phase (bottom phase) is DI water with 10, 50, 100, 150, 500 ppm SLES (from left to right) and 0.1 M NaCl. The C_c* values were estimated based on molar mixing rule.

Overall, an o/w emulsion was more likely to form with a negative HLD_{mix}, while a w/o emulsion was more likely to form with a positive HLD_{mix}, When the systems were close to the transition point ($HLD_{mix} \sim 0$), spontaneous emulsification could be observed in both phases within a shorter time, indicating higher spontaneity. Since the calculated HLD_{mix} values are approximated, the transition does not occur at an HLD of exactly 0, but there is a region of HLD_{mix} where the transition occurs. With all the systems we tested, HLD_{mix} = -0.47 (500 ppm SLES, 100 ppm SLES, 0.1 M NaCl) was the lower limit, and HLD_{mix} = 0.12 was the upper limit where spontaneous emulsion could be formed in both oil and aqueous phases.

3.1 Influence of Salt Concentration on Spontaneous Emulsification

Besides surfactant ratio, HLD_{mix} also depends on the salinity of the system. In this set of experiments, the salt concentration in the aqueous phase was changed from 0 M to 0.42 M. The salinity of seawater was selected as the upper limit considering its connection to bilge water. The surfactant ratio was fixed at 5:1 (500 ppm Span-80 and 100 ppm SLES). This is the ratio we found in the previous session for the system to start spontaneously emulsifying in both oil and aqueous phases. With this surfactant composition, we can better determine whether the spontaneity was increased or decreased with changing salinity through visual observation. Instead of optimizing the surfactant composition to allow the most spontaneous emulsification, we are exploring how the emulsion behavior change when HLD_{mix} moves away from (or closer to) 0.

The HLD_{mix} values estimated for each system were -1.02, -0.47, -0.27, -0.14 and -0.02 (from left to right, as noted in Figure 51). An increased spontaneity was observed with increasing salinity. According to Figure 51, all four systems started to emulsify within 20 minutes (first row). The highest emulsification rate was observed in the samples with 0.2 ~ 0.42 M salt. Relatively large opaque regions were observed in both oil and aqueous phases between 20 minutes and 1 hour for salt concentrations of 0.2, 0.3 and 0.42 M NaCl. In the salt-free sample, very little spontaneous emulsification could be observed. The circled region (in Figure 51: No Salt, 24 h) corresponding to the w/o emulsion formed in the upper phase. The sample with 0.1 M salt exhibited a similar behavior in the oil phase, but more oil was emulsified in the aqueous phase. From 1 to 24 hours (Figure 51, 0.1 M NaCl), the oil drops were continuously formed and diffused away from the interface. A larger opaque region was formed in the aqueous phase compared to the salt-free sample.

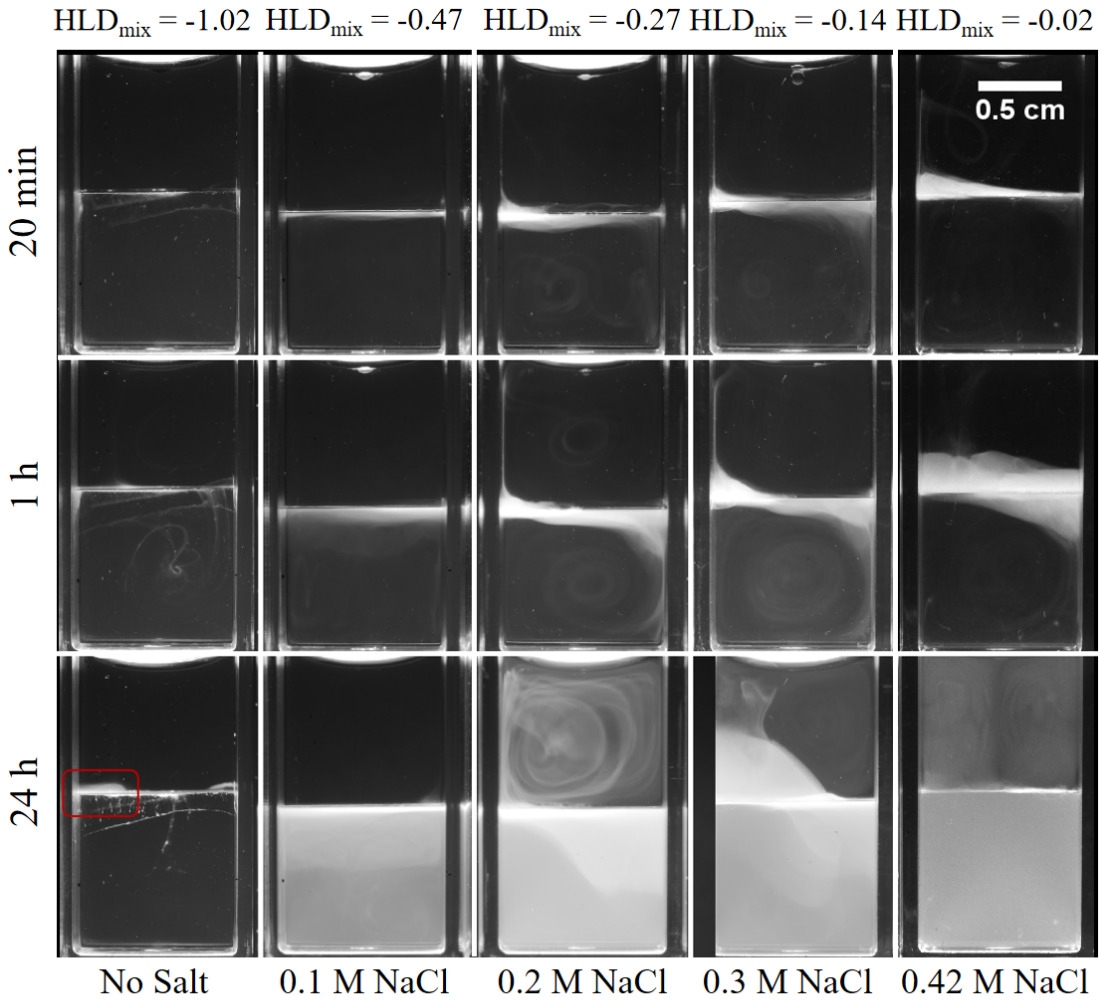

Figure 51. Photographs of spontaneous emulsification at 20 minutes, 1 hour and 24 hours. The oil phase (upper phase) was hexadecane with 500 ppm Span-80. The aqueous phase (bottom phase) was DI water with 100 ppm SLES and 0, 0.1, 0.2, 0.3, 0.42 M NaCl (from left to right).

To better compare the spontaneity of the systems, the drop size distributions were measured periodically in both the oil and aqueous phases. Results from DLS measurements agreed with the visual observation. Increasing salt concentration led to a higher emulsification rate in both oil and aqueous phases.

Figure 52 shows the oil drop size evolutions in the aqueous phase with 0-0.3 M NaCl. The results measured for sample with 0.42 M NaCl was similar to the 0.3 M sample. The major peaks were labeled with their corresponding mean diameter (D_{50}). In the sample with salt (Figure 52 (b)-(d)), SLES concentration was beyond CMC and micelle sizes (centered between 7 to 10 nm) were measured. The micelle size was confirmed by measuring SLES and NaCl solutions without an oil phase on the top. In the sample without salt (Figure 52 (a)), the first signal occurred 2 hours after the oil and aqueous phase placed in contact, indicating the onset of the spontaneous emulsification. Increasing salinity shortens the time when oil drops can be detected. In the samples with 0.1 M NaCl (Figure 52 (b)), only SLES micelles were measured at 20 minutes and the drops were detected after 30 minutes. When the salt concentration was beyond 0.2 M (Figure

52 (c), (d)), the bimodal distributions occurred almost instantaneously (within the 2-minute time resolution of the measurement technique). The bimodal distributions evolved into single peak distributions overtime and the size distributions were stable up to 24 hours. These results suggest a higher emulsification rate and stronger flow with increasing salinity, and thus a HLD_{mix} closer to 0.

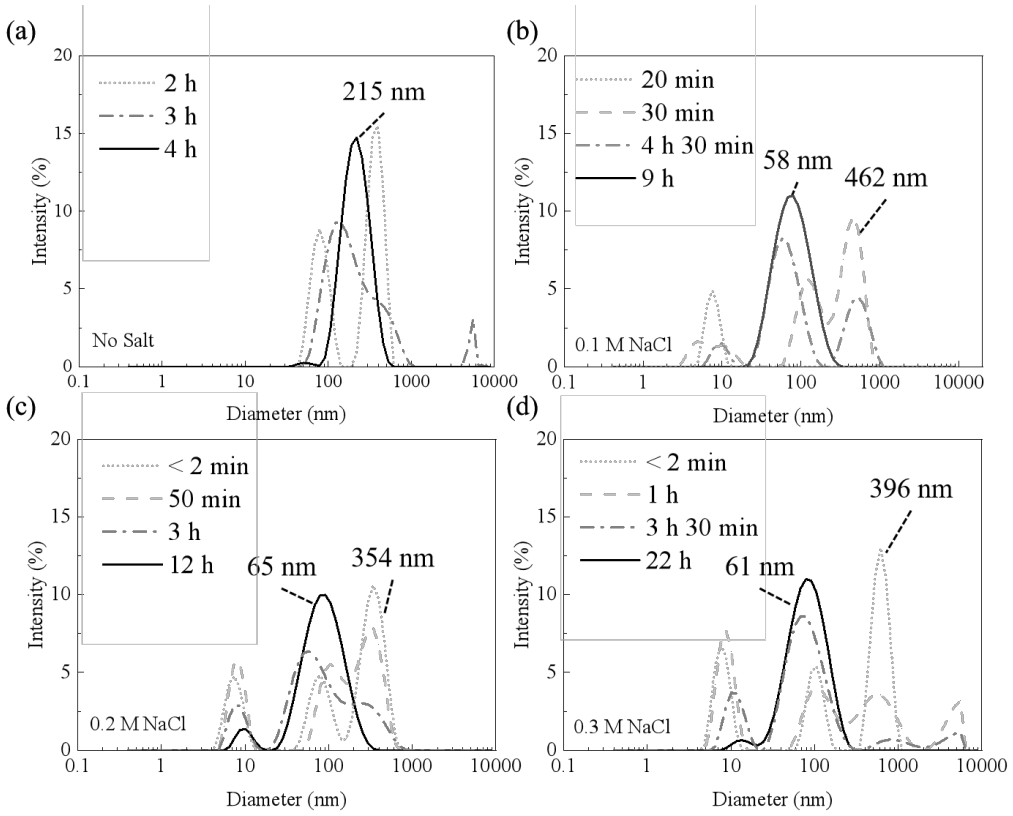

Figure 52. Oil drop size evolution in the aqueous phase with (a) 0 M, (b) 0.1 M, (c) 0.2 M, (d) 0.3 M NaCl. The measurements were made at 2 mm below the oil-water interface. The mean drop diameter (D_{50}) at equilibrium were noted in each figure.

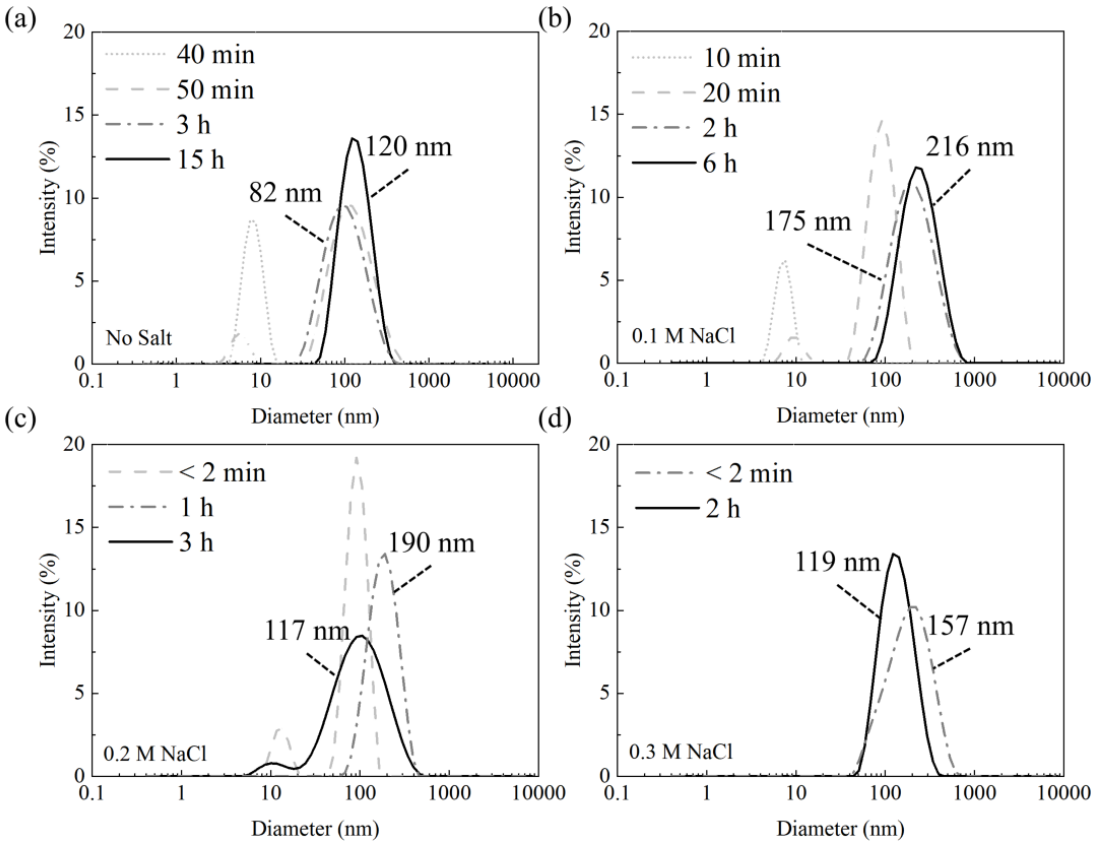

Figure 53: Water drop size evolution in the oil phase with (a) 0 M, (b) 0.1 M, (c) 0.2 M, (d) 0.3 M NaCl. The measurements were made at 2 mm above the oil-water interface. The mean drop diameter (D_{50}) of the peaks were noted in each figure.

Similarly, the water drop size distributions in the oil phase were also measured for 24 hours (Figure 53). Span-80 micelles were captured in the systems with 0, 0.1 and 0.2 M NaCl. The micelle size was between 3 to 11 nm, which is close to what previously reported for Span-80 micelle size in heptane (3 to 8 nm).[121] The micelles were not captured in the system with 0.3 M NaCl and this could result from a fast spontaneous emulsification. In the samples with 0, 0.1 M NaCl, the water drops were detected 50 and 20 minutes, respectively, after placing oil and aqueous phase in contact. In the samples with higher salinity, this time was reduced to less than 2 minutes. Both the time where water drops were detected, and micelles disappeared decreased with increasing salinity, indicating an increasing emulsification rate.

Besides emulsification rate, salt concentration also influenced the water drop size evolution. In systems with 0 and 0.1 M NaCl, the water drop size tended to grow over time (3 – 15 h for 0 M NaCl sample, 2 – 6 h for 0.1 M NaCl sample). This continuous size growth was likely due to Span-80 micelle swelling, which has been observed in previous studies.[91,121,122] This size growth was not observed at higher salt concentrations. Silva, Pedro S., et al.[91] found that Span-80 micelle swelling was eliminated with increasing salt concentration. In the Span-80-SLES system, the spontaneous emulsification in the oil phase could have resulted from a combined effect of micelle swelling, ultra-low IFT and diffusion and stranding. The mechanisms of spontaneous emulsification will be discussed in detail in session 3.4.

3.2 Influence of Oil Type on Spontaneous Emulsification

Oils with different EACN values were used to investigate their impact on spontaneous emulsion behavior. The same surfactant and salt concentration were used in each sample (500 ppm Span-80 in the oil phase, 100 ppm SLES with 0.1 M NaCl in the aqueous phase). The EACN values of the oil ranged from 18 to 7 (from left to right) and the corresponding HLD_{mix} ranged from -0.83 to 1.07. According to the 1-hour images in Figure 54 (second row), only w/o emulsion was formed in heptane (EACN =7) when the HLD_{mix} = 1.07. Similarly, a negative HLD_{mix} resulted in greater spontaneity in the aqueous phase than in the oil phase, as shown in the hexadecane (EACN = 16) and paraffin oil (EACN = 18) samples. The strongest spontaneity in both oil and aqueous phases was observed when HLD_{mix} was close to 0 (HLD_{mix} = 0.21~0.55, decane, EACN = 10 and dodecane, EACN = 12 samples).

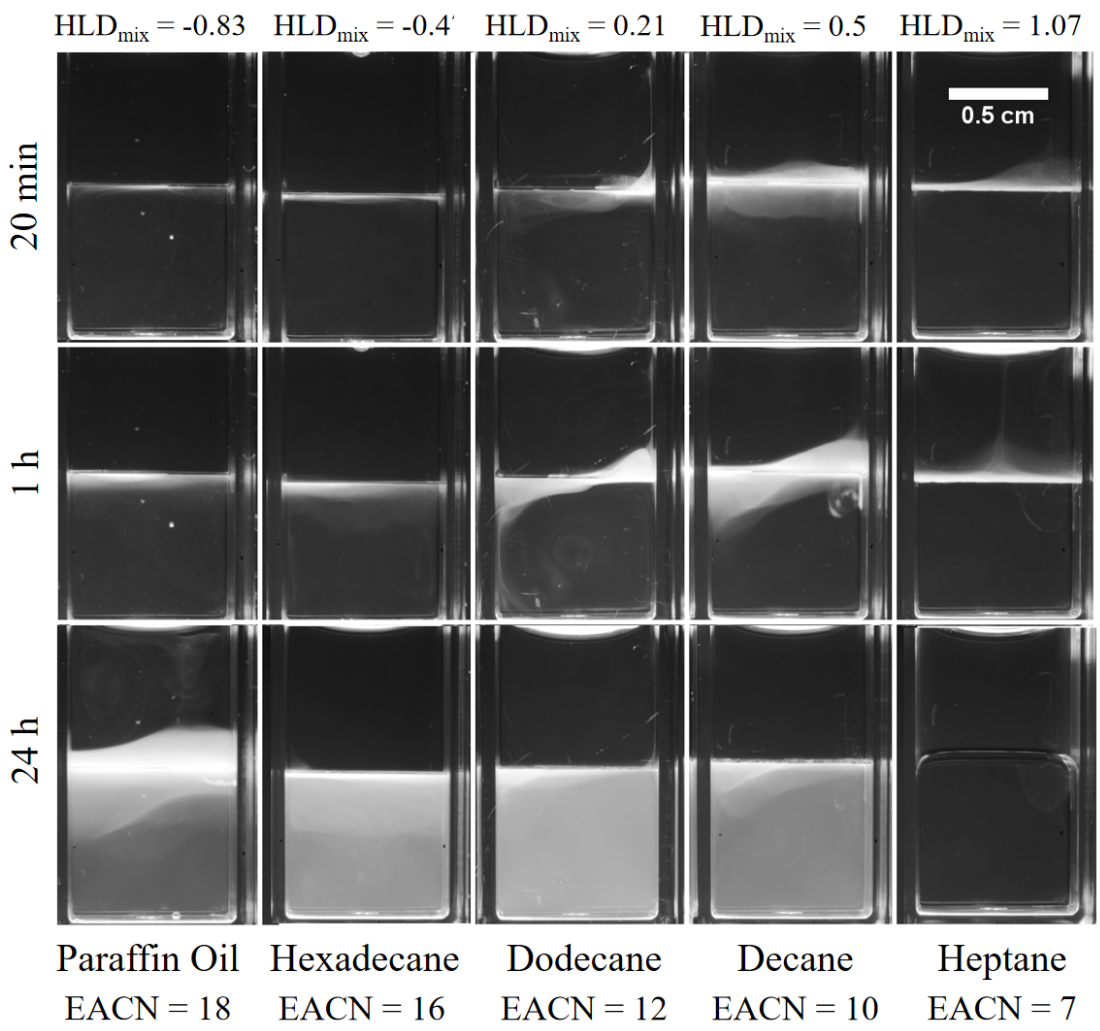

Figure 54. Photographs of spontaneous emulsification at 20 minutes, 1 hour and 24 hours with different oils. The oil phase (upper phase) was paraffin oil, hexadecane, dodecane, decane and heptane (from left to right) with 500 ppm Span-80. The EACN values were noted below the figure.[123] The aqueous phase (bottom phase) was DI water with 100 ppm SLES and 0.1 M NaCl.

Images taken after 24 hours (row three) could be misleading. The w/o emulsions formed with heptane, decane and dodecane exhibited relatively short-term kinetic stability. The w/o emulsion destabilized after 24 hours, and no water drops was detected in DLS. This result highlights a limitation of the HLD model which cannot predict emulsion stability. The conditions to form stable spontaneous emulsions vary depending on the components in that system and the environmental conditions it is aged in. Previous studies found the spontaneous emulsion stability could be influenced by the interfacial rheology, polarity and viscosity of the oil phase, emulsifier concentration, temperature, etc.[124–127] More experimental data is needed to explain the destabilization process of these systems and is beyond the scope of the current study.

Overall, the HLD model could serve as a guide to indicate the spontaneity and spontaneous emulsification behavior with different oils, which is valuable in bilge water emulsion prevention and treatment processes. For instance, Table 10 shows the estimated HLD_{mix} values with the Span-80-SLES system and some common oils. The salinity of seawater was used due to its connection with bilge water. According to the calculation, those oils leading to an HLD_{mix} close to 0 (EACN = 12~16) could be the most problematic in bilge water with the surfactant composition we investigated. The other oils with lower EACN values would most likely lead to the formation of w/o emulsions, which would be less concerning for bilge water. However, HLD_{mix} would decrease with decreasing salinity. In that case, those oils with EACN values under 12 could be problematic. This model could potentially suggest oils that are creating conditions favorable to produce nanometer-sized spontaneous emulsion. The bilge water collecting process could also be optimized to avoid the formation of nano-sized drops.

Table 10. Estimated HLD values with different oils. The same surfactant composition (Span-80:SLES = 5:1, wt./wt.) and the salinity of seawater (0.42 M NaCl) was used.

EACN	Oil	HLD_{mix}
7~10	Heptane, Octane, Ethyl oleate	1~1.48
10~12	Decane	0.66~1
12~16	Dodecane, Isohexadecane, Sunflower Oil	-0.02~0.66
16~20	Corn Oil, Hexadecane, Paraffin Oil, Canola, Soy, etc.	-0.66~-0.02

3.4 Spontaneous Emulsification Mechanisms and HLD model

In the Span-80-SLES systems, we found that the HLD model could be used to predict the spontaneity and spontaneous emulsion phase behavior with different surfactant ratio (effective C_c), salinity (S), or oil type (EACN). To have a better understanding of the spontaneous emulsification mechanism, the interfacial tension (IFT) was measured for Span-80, SLES and the

5:1 mixture. With the 5:1 mixture, the IFT was close to 1 mN/m at 360 ppm total surfactant concentration. The IFT reached 1 mN/m at 60 ppm total surfactant concentration when 0.3 M NaCl was added. Further increasing the surfactant concentration reduced the IFT to lower values. At the total surfactant concentration used in this study (600 ppm), the IFT would be under 1 mN/m, which is considered as an ultra-low value.[128,129]

The ultra-low interfacial tension theory could explain the spontaneous emulsification and the HLD modeling in this study. When the HLD_{mix} approaches 0, a bicontinuous phase is predicted to formed at the oil-water interface. Due to the ultra-low IFT, the bicontinuous phase breaks up over time, forming water (or oil) drops near the interface. A system with a positive HLD_{mix} is more likely to form a w/o emulsion, while an o/w emulsion is more likely to form with a negative HLD_{mix}.

Dynamic Aging and Low Energy Emulsification

The impact of ship motion on the stability of model bilgewater emulsions with anionic and non-ionic surfactants has not been studied in the literature. Any process during storage, such as sloshing of liquids that produces sub-micron drops, is unfavorable to bilgewater filtration. In this work, model emulsions were dynamically aged to mimic the storage of bilgewater on a ship at sea. Model emulsions were composed of anionic or non-ionic surfactant concentrations between 10 and 1000 ppm with fixed concentrations of 0.42 M sodium chloride to resemble the concentration of seawater[5], and a fixed concentration of 5000 ppm mineral oil to represent engine lubricants. The liquids were emulsified in a centrifuge tube and stored under static and dynamic conditions for 20 days. Static ageing provides a baseline for the minimum surfactant concentration required to form stable emulsions. This condition would also mimic the behavior of a ship at port. The behavior of a ship exposed to ocean waves was modeled by placing the emulsions on a three-dimensional rocker at two different speeds. Mineral oil drop size measurements were conducted via laser diffraction and optical microscopy after 0, 5, 10, and 20 days to determine emulsion stability. The evolution of oil drop size distributions during dynamic ageing was compared to the drop size distributions during static ageing to investigate the effects of ship rocking on the generation of sub-micron oil drops. Understanding the chemical and physical behaviors of the emulsions found in bilgewater is relevant to reducing ocean pollution and potentially reducing the cost of current filtration systems by preventing the formation of stable emulsions. These results will expand on existing knowledge of bilgewater and potentially lead to strategies for cleaning bilgewater that reduce ocean pollution.

Anionic and non-ionic surfactants can stabilize oil in water emulsions at different concentrations due to the electrostatic charge at the oil-water-surfactant interface. The magnitude of the charge at the oil/water interface depends on the type of the surfactant[15–17, 37, 38] and impacts the distance at which oil drops can approach each other. The zeta potential of emulsions made with 5000 ppm mineral oil and 0.42 M NaCl was measured over a range of surfactant concentrations (10 ppm – 2500 ppm). These experiments establish a baseline for the stability of the emulsions based on surfactant type and concentration under static conditions. Figure 55 shows the zeta potential for SLES and Triton X-100 emulsions after 3 hours of statically ageing. An electrostatic double-layer exists around the drops that consist of counterions in solution and provides a screening effect. The double-layer shrinks as the salt concentration increases and drops interact at shorter

distances before experiencing electrostatic repulsion.[15, 16] For example, at a salt concentration of 0.42 M NaCl, the Debye length, or the distance at which the electrostatic effects are prevalent, is approximately 0.47 nm. This distance can be compared to the Bjerrum length, or the distance at which the electrostatic interaction between two charged drops is comparable to thermal energy, which is 0.71 nm in room temperature deionized water.[39]

It is known that without the addition of surfactants and salt, the charge at the oil-water interface is negative due to the adsorption of hydroxide ions that exist in water.[40] The results in Figure 55 show that for the non-ionic surfactant, 100 ppm of Triton X-100 reduced the zeta potential. This is due to limited adsorption of hydroxide ions onto the O/W interface due to the energetically favorable adsorption of the neutral surfactant onto the oil drops.[37] Figure 56 shows optical microscopy images of emulsions with 500 ppm Triton X-100 and 0.42 M NaCl that were statically aged for 3 hours. Figure 55 shows that oil drops around 200 μm were flocculated, resulting from zeta potential values close to zero. The addition of salt greater than 0.1 M produced signs of instability such as flocculation and coalescence for non-ionic surfactant emulsions.[38]

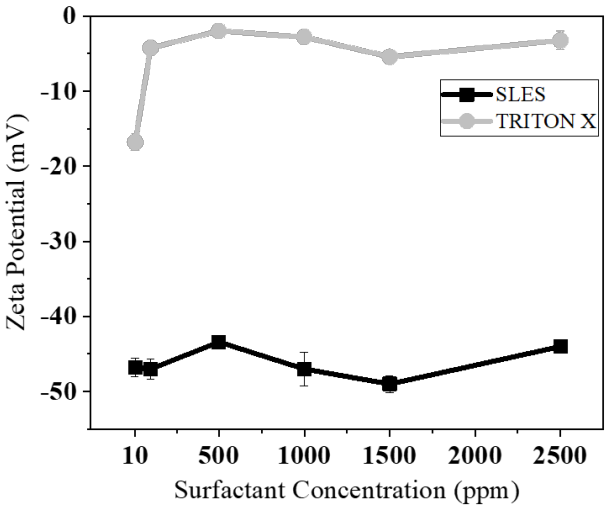

Figure 55**:** Zeta potential of emulsions with 5000 ppm mineral oil, 0.42 M NaCl, and 10 ppm - 2500 ppm SLES (black) and Triton X-100 (gray) after 3 hours of static ageing.

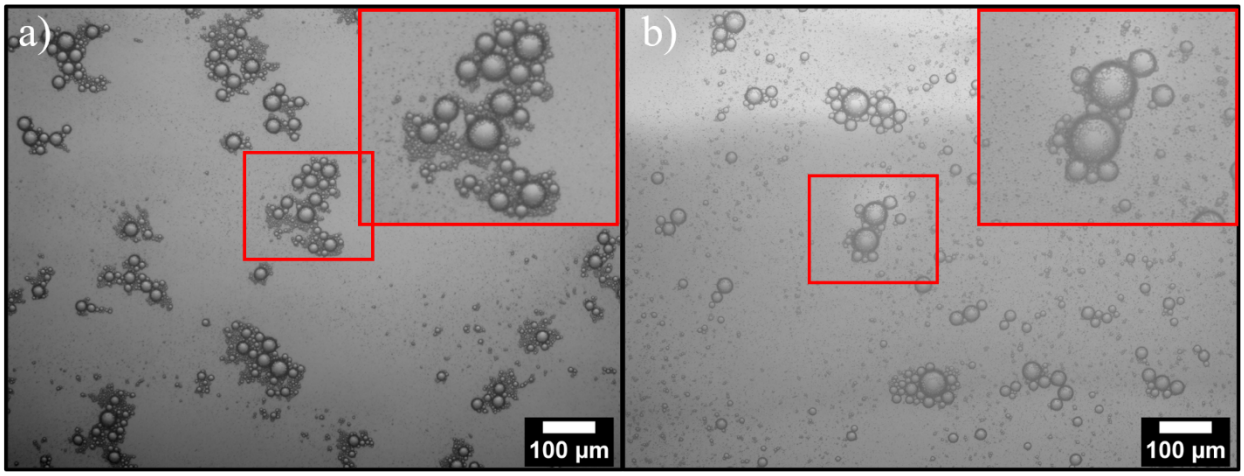

Figure 56: Optical microscopy of emulsions made with 5000 ppm Mineral Oil, 0.42 M NaCl, and 500 ppm of a) Triton X-100 and b) SLES after 3 hours of static ageing.

Emulsions prepared with SLES showed a greater magnitude of zeta potential compared to emulsions with Triton X-100. As anionic surfactants adsorb to oil drops, the zeta potential becomes more negative and increases in magnitude compared to surfactant-free oil drops in water.[15] As the anionic surfactant-covered oil drops approach each other, the repulsion between the drops is greater than oil drops with non-ionic surfactants due to the charged head group on the surfactant.[16] As a result, the degree of flocculation due to van der Waals forces for emulsions with anionic surfactant is less than that of emulsions with a non-ionic surfactant. The optical image in Figure 56**b** shows that with 500 ppm SLES (concentration above the CMC), many of the smallest visible oil drops remain singularly dispersed, and there is less oil in large flocs than the drops in Figure 56**a**. The implications of these results are discussed in the proceeding sections.

Effect of interfacial tension on O/W emulsion stability

The addition of surfactants to an oil-in-water emulsion reduces the interfacial tension (IFT) between the two phases and lowers the energy needed for emulsification.[41] Obtaining the IFT with respect to surfactant concentration aids in the determination of the critical micelle concentration (CMC), the surface concentration (Γ_s), and the surfactant head group area (Å). The CMC is the concentration at which surfactants can align into a configuration with the lowest surface energy. Below this concentration, there is not enough surfactant to effectively cover the oil/water interface and therefore, the emulsion is unstable due to coalescence.[42] The surface concentration (Γ_s), is the concentration of surfactant that forms a monolayer around an oil drop and is inversely proportional to the surfactant head area. Therefore, as the surfactant head group area is reduced, the surface concentration increases due to efficient surfactant packing at the interface, and the IFT is reduced.[43] The resulting oil drop size is not only dependent on the total surfactant concentration but also the surfactant-to-oil ratio (S/O).[17, 31, 44] For example, oil in water emulsions did not form if the S/O is below a critical threshold of 0.1.[17] However, this threshold is not universal and depends on salt concentration, energy added during emulsion generation, and surfactant type.

Figure 57 displays the equilibrium IFT, γ, between mineral oil and SLES, and mineral oil and Triton X-100, both in aqueous 0.42 M NaCl. Two regimes were present within the IFT isotherms: where the IFT is dependent on surfactant concentration and a regime where the IFT is constant with surfactant concentration. After performing a linear regression on the two regimes, the CMC was calculated from the intersection of the two fitted lines. The slope of the data points within the first regime was steeper for SLES than Triton X-100. The value of each slope was used in Equation 7[30, 46] to determine the concentration of surfactant per area at the surface (Γ_s). The value of n depends on the number of adsorbed species (surfactants and/or counterions) onto the interface.[30, 47, 48] For the system with a non-ionic surfactant or anionic surfactant in the presence of salt, the value of n is 1.[49, 50] An additional estimation of the amount of each surfactant (C_a) needed to form monodisperse drops (d) at a given oil volume fraction (Φ) was calculated using Equation 8.[1] Table 11 summarizes the calculated surfactant characteristics based on the IFT measurements; SLES has a greater surface concentration and smaller head group area, which can pack more densely at the oil-water interface than with Triton X-100.

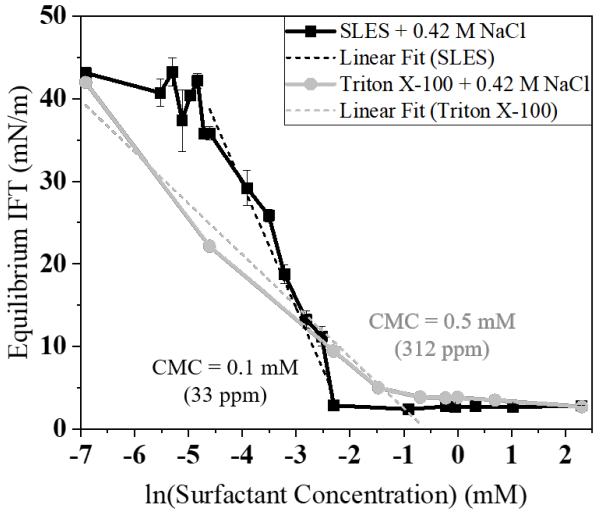

Figure 57**:**Equilibrium interfacial tension of SLES + 0.42 M NaCl (black) and Triton X-100 + 0.42 M NaCl (gray) in mineral oil as a function of surfactant concentration. Equilibrium IFT was obtained via the Pendant Drop Method.

$$\Gamma_s = \frac{-1}{nRT} * \frac{\partial \gamma}{\partial \ln(C_a)} \quad (7)$$

$$C_a = \frac{6\Gamma_s \phi}{d} \quad (8)$$

Table 11**:**Values of CMC, surface excess concentration, and surfactant head group area for SLES and Triton X-100 in the presence of salt.

Surfactant Type	**CMC with 0.42M NaCl [ppm]**	**Surface Concentration, Γ_s $[10^{-6}\ mol/m^2]$**	**C_a Needed to form 1 µm monodisperse drops [ppm]**	**Surfactant Head Area, A $[Å^2/molecule]$**
SLES	33	6.05	70	27.4
Triton X-100	312	2.51	55	66.2

In a salt-free environment, previous studies found the CMC and surface excess concentration were 324 ppm and 2.43 × 10^{-6} mol/m^2, respectively for Triton X-100[30], and agrees with the data in Table 11. In other published experiments, the CMC for salt-free emulsions with SLES was between 233 ppm[51] and 288 ppm.[52] Therefore, we can expect the CMC to be less than 233 ppm in the presence of salt, which agrees with the data in Table 11. Previously established by Kedar and Bhagwat, the addition of 0.17 M NaCl reduced the IFT of SLES and crude oil to 3 mN/m. The surface concentration calculated was approximately 2 × 10^{-6} mol/m^2. [48] Thus, we can expect an increase in the surface concentration for SLES with increasing salt concentration, as more anionic surfactant molecules can pack at the oil/water interface. This assumption is verified by the data in Table 11, which shows that the surface concentration for SLES is 6.05 × 10^{-6} mol/m^2 with the addition of 0.42 M NaCl. The following sections discuss the stability against coalescence of mineral oil-in-water emulsions concerning the effects of electrostatic charge and interfacial tension.

Oil drop size after static ageing in salt

Emulsions aged under static conditions were used as a control for the stability of model bilgewater emulsions. Surfactant type and concentration were varied to explore the range of surfactant chemistries and concentrations present in bilgewater. Figure 58**a** and Figure 58**b** present the average oil drop size distributions of statically aged emulsions with 10 to 1000 ppm of SLES and Triton X-100, respectively, and were measured at 0 days (3 hours), 5, 10, and 20 days. In Figure 58**a**, emulsions with < 10 ppm SLES were unstable, shown by a shift in the drop size distribution at 0-days. For example, within 10 days, the initial peak at 5-6 µm shifted towards 40 µm, and a new peak at 2 mm was formed. This behavior contributed to an overall increase in D(4,3) over time. At 10 ppm SLES, a concentration below the CMC (~ 30 ppm), there was not enough surfactant to form stable emulsions, and coalescence occurred. As the concentration of SLES increased to 100 ppm, the distribution did not change between 5 and 20 days and was

stable against coalescence. According to Table 11, about 30 ppm SLES is needed to form 1 µm monodisperse oil drops, so it can be expected that 100 ppm SLES is sufficient to produce an emulsion stable to coalescence. Between 0 and 5 days for 100 ppm SLES, there was an increase in volume % of 20 µm oil drops and a decrease in volume % for 2 µm oil drops due to coalescence of the smaller oil drops as the emulsion attempts to reach equilibrium. There is significant excess surfactant for concentrations ≥ 500 ppm SLES, and the emulsion remained stable over time.

The CMC is larger in emulsions with Triton X-100, meaning more surfactant is required to stabilize Triton X-100 emulsions. Figure 58**b** shows that emulsions prepared with ≤ ~300 ppm Triton X-100 exhibited a shift in the distribution similar to emulsions with 10 ppm SLES (Figure 58**a**) and indicate that coalescence has occurred. Emulsions with ≥ 500 ppm Triton X-100 were stable against coalescence between 0 and 20 days, as there was more than enough surfactant to stabilize the drops.

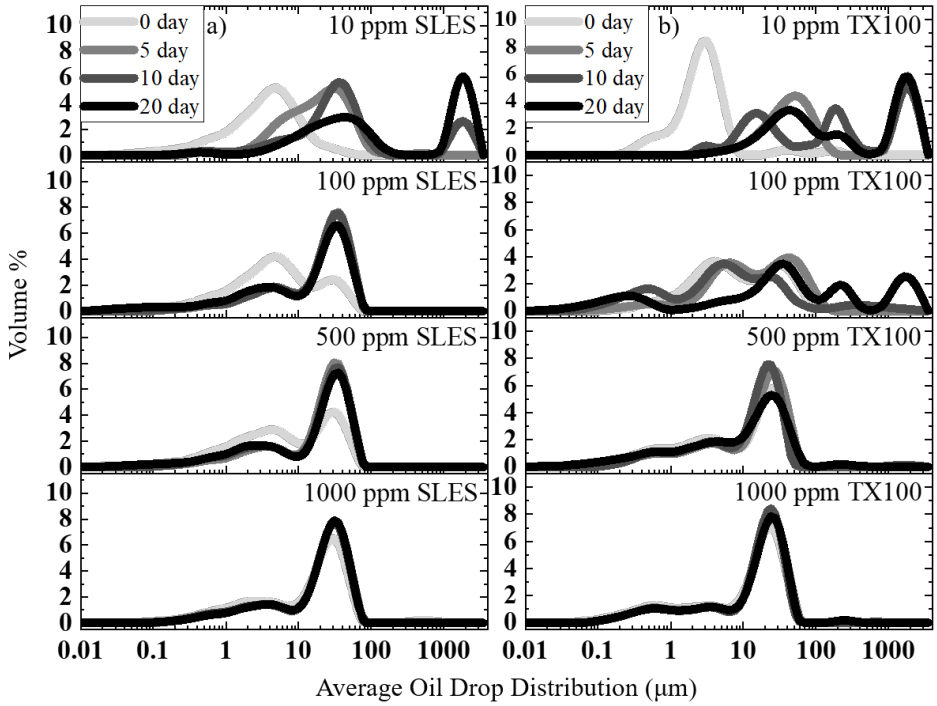

Figure 58:The evolution of average oil drop size distribution over 20 days for statically aged emulsions with a) SLES and b) Triton X-100 from 10 to 1000 ppm surfactant. The darkening of the distribution curves is proportional to time.

Figure 59 summarizes the results presented in Figure 58 by plotting the D(4,3) over 20 days for all SLES and Triton X-100 concentrations. Three hours after emulsification (0 days on the chart), the average oil drop sizes for all surfactant concentrations and chemistries were between 5 µm and 30 µm in diameter. For SLES emulsions, the D(4,3) increased over time for concentrations ≤ 10 ppm due to coalescence but did not change significantly for concentrations ≥ 100 ppm. The

average oil drop diameter after 20 days with 1000 ppm SLES was 25 µm. For Triton X-100 emulsions, the D(4,3) increased within 20 days for concentrations ≤ 100 ppm due to coalescence but was constant for concentrations ≥ 500 ppm. The oil drop diameter after 20 days for 1000 ppm Triton X-100 was 22 µm. During static ageing, the minimum surfactant concentration to form stable emulsions is 100 ppm, or 0.30 mM SLES and 500 ppm, or 0.80 mM Triton X-100 for emulsions made with 5000 ppm mineral oil. In this case, it takes less SLES to form stable emulsions during static ageing.

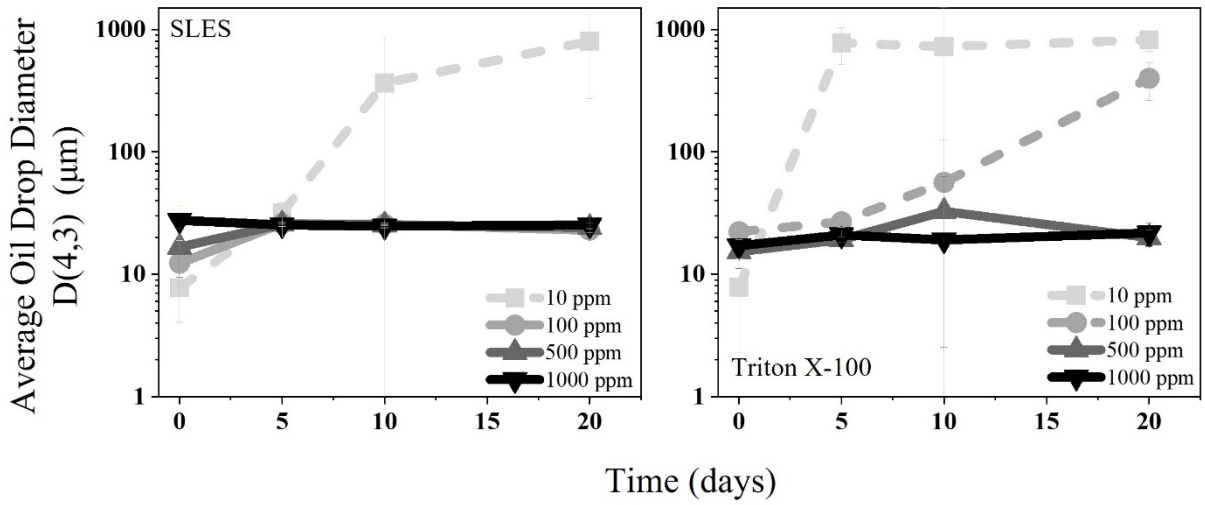

Figure 59**:**Average oil drop diameter, D(4,3) during static ageing with increasing concentrations of SLES (left) and Triton X-100 (right). Lines were added between data points as visual guides. Dashed lines represent unstable emulsions that result from increased over time. Error bars represent the standard deviation.

Visual observations verified the coalescence of oil drops in emulsions made with 10 ppm – 100 ppm of surfactant. Figure 60 shows optical images of the surface of an emulsion with 10 ppm Triton X-100 aged statically for 20 days. Millimeter-sized oil drops that were not present after the initial emulsification were formed due to coalescence and creaming. Coalescence was not observed in emulsions with ≥ 500 ppm of either surfactant. Figure 61 presents optical micrographs of an emulsion with 500 ppm SLES after 20 days of static ageing. The vials were gently swirled before sampling to ensure the optical micrographs represented the bulk emulsion. Drops approximately 50 µm in diameter were not included in the initial drop size distribution but existed at the surface of the emulsion as a result of creaming; however, these emulsions were considered stable because they did not undergo coalescence to cause an increase in overall D(4,3).

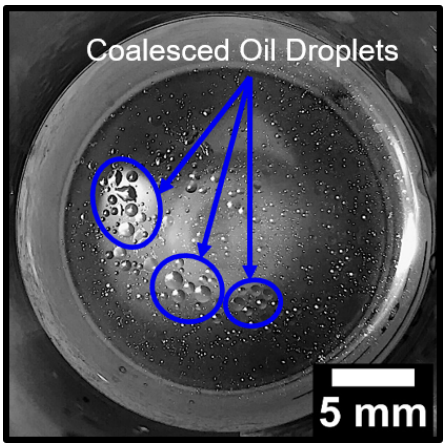

Figure 60**:** Photograph of the top view of a statically aged emulsion (20 days) with 0.42M NaCl, 10 ppm Triton X-100, and 5000 ppm mineral oil in a 50 mL centrifuge tube.

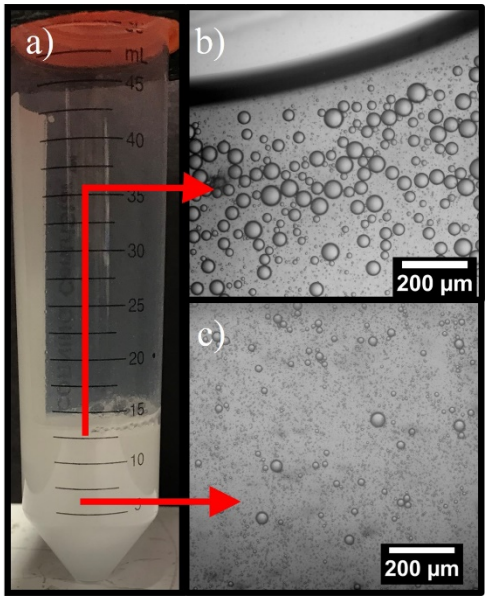

Figure 61**:**Photographs of (a) 500 ppm SLES, 0.42 M sodium chloride, and 5000 ppm mineral oil in a 50 mL centrifuge tube. The figure shows brightfield optical images of 500 ppm SLES, 0.42 M sodium chloride, and 5000 ppm mineral oil 20 days after emulsification.

According to the oil drop size distributions and D(4,3) plots in Figure 58 and Figure 59, the minimum concentration is required to form an emulsion with little change in oil drop size distribution over time is greater for Triton X-100 than SLES. This is because SLES had a greater magnitude of zeta potential than Triton X-100 in the presence of salt. The adsorption of charged molecules onto an oil/water interface increased as NaCl was added and, in turn, increased the magnitude of the zeta potential.[15] Oil in water emulsions stabilized by anionic surfactants obtained zeta potential values as low as -60 mV in the presence of NaCl,[17] which coincide with the zeta potential values for SLES in Figure 55. The stability of the oil drops was due to the adsorption of charged surfactants and subsequent repulsion between oil drops. From visual observations in Figure 56, oil drops covered in SLES experienced more repulsion than oil drops covered in Triton X-100. Larger zeta potential values lead to repulsion that decreased the

coalescence rate of oil drops at high surfactant concentration and constant ionic strength (0.01 M NaCl).[53]

During emulsification, the initial oil drop sizes are dependent on the amount of energy used to make the emulsion, the surfactant concentration and type[45] , the interfacial tension[41], and the surfactant-to-oil ratio.[17] Assuming the high-energy input for this system remains constant at 24,000 rpm for 1 minute, and the oil volume fraction was constant at 0.0058, the oil drop distribution is contingent on the properties provided by the surfactant. After emulsifying oil and water at high input energy, small oil drops are formed, which causes an increase in the total interfacial area.[17] If the surfactant concentration is low enough, the oil drops coalesce until the surfactant can efficiently cover the oil drops.[30, 54] As a result, the interfacial tension decreases as the surfactant concentration increases up to the CMC.[43, 52, 55] Beyond this concentration, an excess amount of surfactant provides sufficient coverage of oil drops and stabilizes them against coalescence.[45, 56] The resulting average oil drop size depends on surfactant type. For example, previous work showed that without salt, anionic surfactants formed smaller oil drops than non-ionic surfactants when the S/O was greater than 0.03.[57] Therefore, at any surfactant above its CMC, it is expected to see the average oil drop size reach a value independent of surfactant concentration.

For each surfactant tested, the surfactant concentration threshold to form stable emulsions is also dependent on the surface concentration. For example, SLES had a greater surface concentration than Triton X-100, meaning more SLES was at the oil/water interface than Triton X-100. The results from static ageing indicate stable emulsions were present at a S/O of 0.02 for SLES. Stable emulsions with Triton X-100 existed at a S/O of 0.1. Therefore, at a constant oil volume fraction, less SLES is required for stable emulsions. The general trend is vital in bilgewater applications because the surfactant concentration can vary significantly.[30, 32]

As mentioned previously, the estimated Peclet diameter for mineral oil drops is about 2.8 μm. The oil drop size distributions in Figure 58 show that most of the distributions are composed of drops with diameters larger than 2.8 μm and will cream due to gravity. Therefore, static ageing conditions. However, ships at sea are not static, and ship motion can easily redisperse creamed oil drops. Therefore, it is necessary to investigate how the stability threshold changes when emulsions are subjected to movement during ageing.

Oil drop size after dynamic ageing at 12 rpm

The previous section established a foundation for the effect of surfactant concentration and type on the stability of statically aged emulsions. In addition, a threshold for the minimum concentration of each surfactant needed to form stable emulsions was determined. The purpose of observing O/W emulsions under dynamic storage conditions is to provide insight into the effects of ship movement or other low-energy events on the stability of model bilgewater emulsions. After initial emulsification, the samples were stored on a three-dimensional gyrating rocker at 12 and 30 rpm to mimic shipboard movement, and contained 70% air within the ageing vials.

Figure 62 shows the oil drop size distributions for dynamically aged emulsions at 12 rpm for up to 20 days with 70% air. Emulsions made with 10 ppm of either surfactant exhibit similar behavior to emulsions of the same composition in Figure 58 that were aged statically. As the concentration of SLES increased to 100 ppm, two additional peaks appeared in the distribution at 2 mm and 0.5 μm. The peak at 2 mm for 100 ppm is lower than the peak at 2 mm formed at 10 ppm SLES; however, the peak at 0.5 μm indicates that small drops are formed due to the energy provided by rocking at 12 rpm. The formation of small drops can be explained by the effective change in the capillary number, which is a ratio of fluid velocity and interfacial tension, where large capillary numbers indicate a dominant inertial force.[43] Compared to static ageing, dynamic ageing at 12 rpm introduced a greater fluid velocity, which indicates an increased capillary number. For systems with large capillary numbers, oil drop diameters decreased due to the deformation and breakup of oil.[58] This process is likely a combination of rapid drop breakup and relatively slower coalescence of the subsequent small drops. At 500 ppm SLES, the initial peak at 40 μm decreased, and an additional peak at 0.5 μm formed within 5 days of ageing due to the breakup of drops. However, after 10 days of ageing, the peak at 0.5 μm decreased, and the peak at 40 μm increased, suggesting that subsequent coalescence has occurred. Although this emulsion did not produce oil drops 2 mm in diameter, the distribution at 20 days resulted from coalescence and drop breakup. Finally, at 1000 ppm SLES, drop breakup is dominant within the first 5 days of ageing as the initial peak around 30 μm shifts toward 2 μm. By 10 days, a peak around 40 μm formed, indicating coalescence. After 20 days, this peak shifted toward 50 μm and the peak at 2 μm continued to shift towards 0.5 μm. An optical micrograph of this emulsion is presented in Figure 63, where drops ≤ 50 μm exist. When an emulsion is mixed in a high shear mixer, the oil drop size is produced due to the competition between coalescence and oil drop breakup. Even though dynamic ageing at 12 rpm provides minimal energy compared to high shear mixing, the evolution of emulsion drop size also competes between coalescence and drop breakup.

The behavior for Triton X-100 emulsions is similar to that of SLES emulsions. At 10 ppm, there is a clear indicator for coalescence as the 0-day peak at 1.5 μm shifts to 20 μm, and a second peak at 2 mm was formed. As mentioned earlier, at this concentration of Triton X-100, there is not enough surfactant to effectively cover the interface of oil drops and prevent coalescence. At 100 and 500 ppm Triton X-100, there are indications for both coalescence and drop breakup. The results of static ageing determined that 100 ppm was not enough to stabilize oil drops, so coalescence is expected. As shown in Table 11, 55 ppm of Triton X-100 was needed to form 1 μm monodisperse drops, so the small peak at 0.5 μm is expected due to the energy provided rocker. At 500 ppm Triton X-100, signs of coalescence did not occur until after 10 days as the 2 mm peak was not present at 0 or 5 days of dynamic ageing. Because 500 ppm Triton X-100 is above the CMC and the energy input was > 0 for dynamic ageing, a peak at 0.5 μm appeared at 5 days, indicating drop breakup. However, the height of the peak decreased after 20 days of ageing, which denotes coalescence. As with SLES, there is a competition between drop breakup and coalescence during dynamic ageing at 12 rpm. At 1000 ppm Triton X-100 there is more than enough surfactant to stabilize the emulsion. Drop breakup is evident as the initial peak at 20 μm shifts to 0.4 μm after 20 days. The shift in distribution toward smaller oil drop sizes provides evidence of further emulsification.

Overall, at a surfactant concentration of ≥ 100 ppm for either surfactant, rocking at 12 rpm produced more oil drops ≤ 1 μm in diameter than after initial emulsification. These oil drops are smaller than the Peclet diameter and are disadvantageous to oil separation in bilgewater, as they are dominated by Brownian motion rather than gravity.

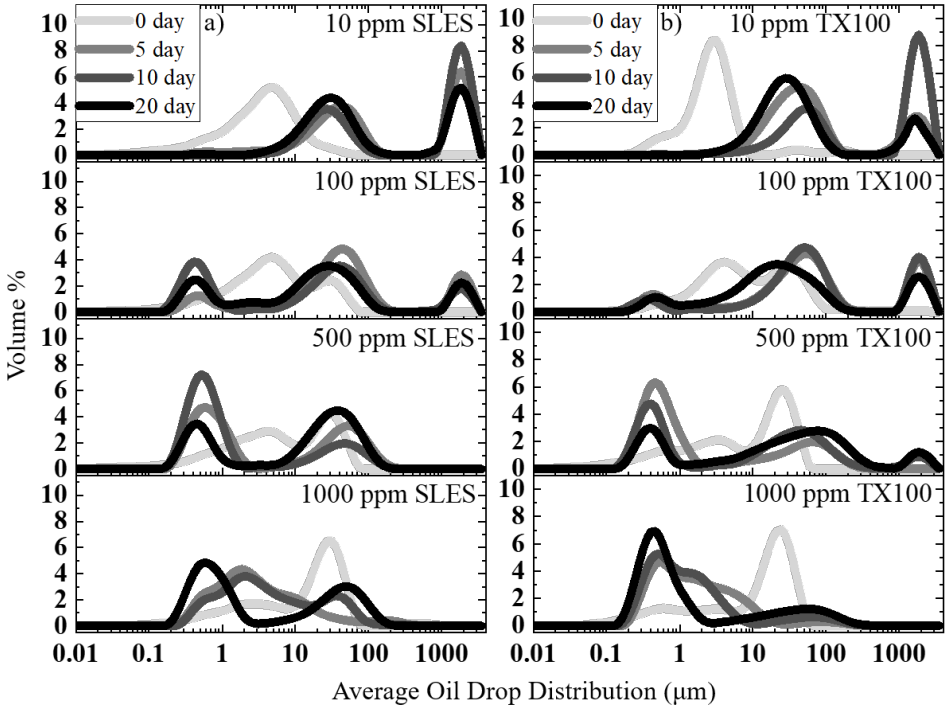

Figure 62**:**The evolution of average oil drop size distribution over 20 days for dynamically aged emulsions with 70% air at 12 rpm with a) SLES and b) Triton X-100 from 10 to 1000 ppm surfactant. The darkening of the distribution curves is proportional to time.

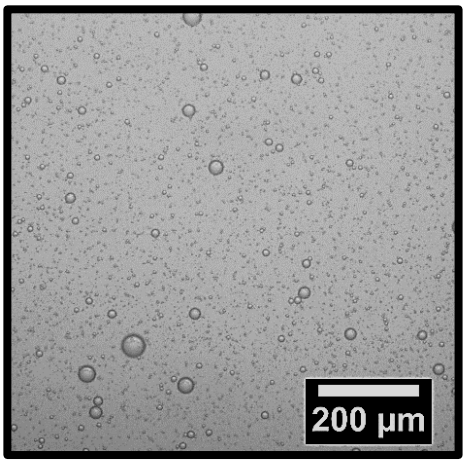

Figure 63**:**Brightfield optical image of 1000 ppm SLES aged for 20 days at 12 rpm.

A summary of the average oil drop diameters during dynamic ageing at 12 rpm is shown in Figure 62. Figure 62**a** displays an increase in D(4,3) for emulsions with 10 and 100 ppm SLES between 0 and 5 days. Figure 62**b** shows that the D(4,3) increases within 5 days for emulsions with 10, 100, and 500 ppm of Triton X-100 due to coalescence. However, both drop breakup and coalescence occurred for ≤ 100 ppm SLES and ≤ 500 ppm Triton X-100, coalescence was dominant and produced an overall increase in D(4,3) within 5 days. This threshold differs from static ageing due to the energy imparted by the rocker.

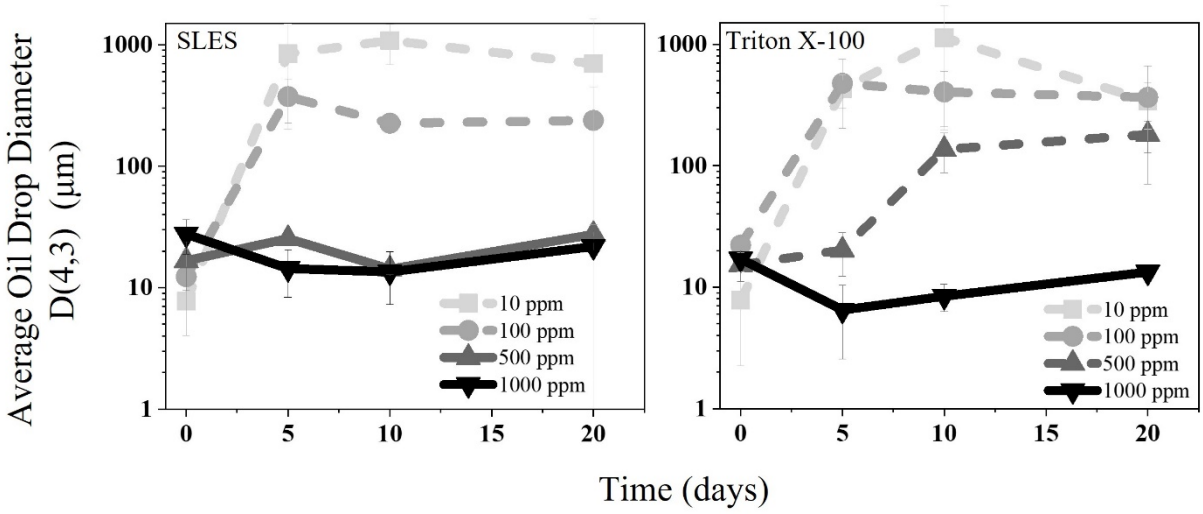

Figure 64**:** Average oil drop diameter, D(4,3) during dynamic ageing at 12rpm with 70% air and increasing surfactant concentration for SLES (left) and Triton X-100 (right). Dashed lines represent unstable emulsions that result from increased oil drop size over time. The darkening of the distribution curve is proportional to time.

According to these results, the threshold of emulsion stability against coalescence was increased compared to static ageing. The S/O ratio required to form stable emulsions during dynamic ageing at 12 rpm is 0.1 for SLES and 0.2 for Triton X-100. The electrostatic repulsion between oil drops with Triton X-100 was less than the repulsion between oil drops with SLES and existed in a more flocculated state, as seen in Figure 58. However, these flocs were easily broken up if disturbed. During dynamic ageing, the emulsion is in motion, and the flocs are broken, but the electrostatic charge on the oil drops should not change. Drops covered in non-ionic surfactants exist closer than oil drops covered in anionic surfactants due to their increased steric repulsion brought on by anionic surfactants.[16, 17] Therefore, oil drops with Triton X-100 have a greater probability of colliding and coalescing than oil drops with SLES. This explains the increase in the stability threshold between the different surfactant types.

The increase in stability threshold between surfactant concentrations can be explained through the available interfacial area for surfactant adsorption. Below the stability threshold, dynamic ageing at 12 rpm causes oil drops to coalesce and influence a larger average drop size. At a larger average drop size, there is less interfacial area for SLES or Triton X-100 to adsorb to the oil/water interface. Therefore, fewer smaller drops were produced, and there was not enough

surfactant to efficiently cover the surface of oil drops, and instability to coalescence was observed.[30, 54]

Oil spill remediation attempts to add dispersants to the ocean's surface to lower the interfacial tension between the floating oil and water to form dispersed oil drops.[31, 44] This process reduces the amount of oil at the ocean's surface due to oil spills and benefits animals and other marine life that frequent the ocean surface. The effectiveness of the dispersants was studied by Li et al., who utilized a wave tank simulator to replicate the motion of waves at sea: crashing waves and calm, non-crashing waves. It was found that the dispersion effectiveness depends on how much energy was produced by the wave. For the case of calm waves, little energy was provided, and large oil drops greater than 200 μm in diameter were produced without the presence of surfactants, and smaller drops were present at greater depths with surfactants.[31] Similarly, at a S/O ratio of 0.04, sub-micron drops existed in the presence of turbulent motion.[44] This information supports the results in this paper by proving that the energy provided by waves is enough to generate emulsions.

The usage of the rocker at 12 rpm was intended to mimic normal sea conditions. The amount of energy provided at 12 rpm was enough energy to break large oil drops and induce coalescence. A ship at sea is subjected to not only calm waters but also storms, larger waves, or other sources of increased mechanical energy. In the following section, the maximum speed of the rocker, 30 rpm, was utilized to simulate the motion of bilgewater under more aggressive mixing conditions.

Oil drop size after dynamic ageing at 30 rpm

Dynamic ageing was increased to 30 rpm, and the tilt angle was increased to increase the energy input into the system. The amount of air within the ageing vial remained constant at 70%. The corresponding oil drop size distributions are shown in Figure 65. For 10 and 100 ppm of both SLES and Triton X-100, the same trends found in dynamic ageing at 12 rpm apply. That is, there are three peaks at 0.5 μm, 50 μm, and 2 mm, indicating drop breakup and coalescence. However, at 100 ppm SLES, the coalescence of drops 50 μm and 2 mm in diameter was not sufficient to cause an overall increase in D(4,3). At 500 ppm SLES, peaks at 50 μm or 2 mm do not exist, and a transition to smaller oil drop sizes over the 20 days. At 1000 ppm of SLES, a wider distribution between 0.2 – 20 μm appears after 5 days and does not change with time. Figure 66 shows an optical image of 1000 ppm SLES after 20 days of ageing at 30 rpm and includes oil drops sizes well below 50 μm. It is noticeable that stability against coalescence is achieved at SLES concentrations ≥ 100 ppm.

At 500 ppm Triton X-100, there were no 2 mm oil drops present. In turn, the distribution shifts toward 0.2 and 9 μm within 5 days. Between 10 and 20 days, a small peak formed at 50 μm, which demonstrates the coalescence of oil drops; however, there was not enough coalescence to increase the D(4,3) over time. At 1000 ppm, a peak formed between 0.2 – 9 μm within 5 days and did not change much over time. For Triton X-100, stability against coalescence was found at concentrations ≥ 500 ppm. These results indicate that at 30 rpms, the O/W emulsions can form oil drops far below 1 μm and lead to stabilization of oil drops against coalescence.

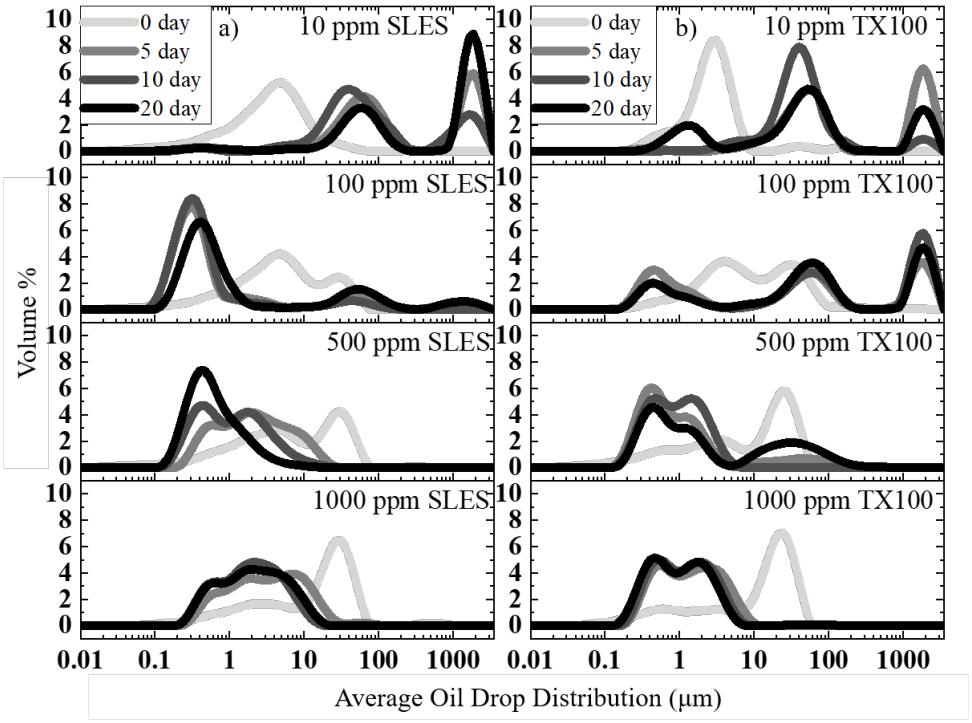

Figure 65**:**The evolution of average oil drop size distribution over 20 days for dynamically aged emulsions with 70% air at 30 rpm with a) SLES and b) Triton X-100 from 100 to 1000 ppm surfactant. The darkening of the distribution curves is proportional to time.

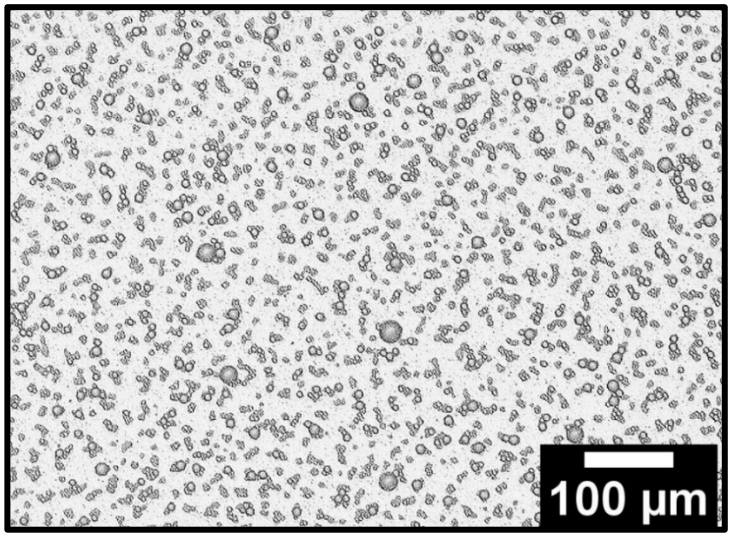

Figure 66**:** Brightfield optical image of an emulsion (0.42M NaCl, 1000ppm SLES, 5000ppm mineral oil) dynamically aged at 30rpm for 20 days and with 70% air within the ageing vial.

Figure 67 shows that dynamically ageing emulsions at 30 rpm caused an overall decrease in oil drop size over 10 days for 100 – 1000 ppm SLES and 500 – 1000 ppm Triton X-100, which indicates the formation of small oil drops within the emulsion. For 10 ppm SLES and 10 – 100 ppm Triton X-100, the D(4,3) increased over 20 days, suggesting coalescence. The minimum surfactant concentration required to form stable emulsions for dynamic ageing at 30 rpm is similar to static ageing. However, the oil drop size distributions in Figure 65 revealed that dynamic ageing at 30 rpms produced smaller drops at surfactant concentrations above the stability threshold within 5 days.

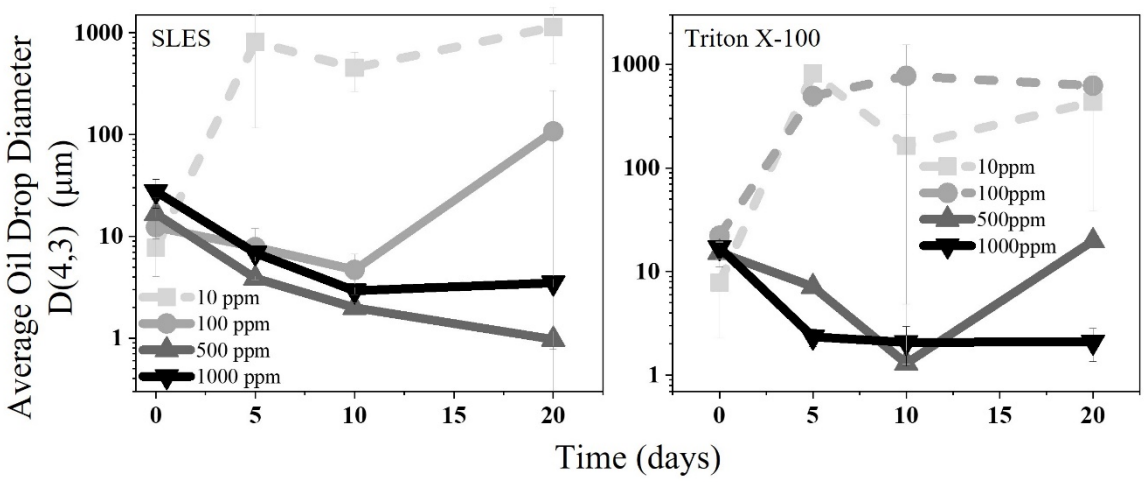

Figure 67**:** Average oil drop diameter, D(4,3) during dynamic ageing with 70% air at 30 rpm and increasing surfactant concentration for SLES (left) and Triton X-100 (right). Dashed lines represent unstable emulsions that result from increased oil drop size over time. The darkening of the lines is proportional to increased surfactant concentration.

The surfactant concentration required to prevent oil drop coalescence was 100 ppm SLES and 500 ppm Triton X-100. The amount of SLES needed to stabilize the emulsions is still less than that of Triton X-100 due to the difference in zeta potential between the surfactant chemistries. Although oil drops stabilized by Triton X-100 have less electrostatic repulsion and can approach each other more closely than SLES-stabilized oil drops, the speed of the 3D rocker was sufficient enough to break larger oil drops and reduce the probability of coalescing oil drops.

The CMCs for SLES and Triton X-100 listed in Table 11 correlate to the stability thresholds during dynamic ageing at 30 rpm and static ageing. For static ageing, emulsions made with a surfactant concentration above the stability threshold, the oil drop size distribution does not change with time. Dynamic ageing at 30 rpm promoted oil drop breakup, which increased the number of small drops or the interfacial area.[55] Many small oil drops were stabilized upon increasing surfactant concentration because there was enough surfactant to cover the interfacial area.[30] Dynamically aged emulsions (30 rpm) made with a S/O $\geq$ 0.02 for SLES or $\geq$ 0.1 for Triton X-100 are still considered stable because the average oil drop size after 20 days was less than 1 μm.

The mechanisms of drop coalescence and drop formation can be explained by the amount of energy the rocker provides for the system. Utilizing the rocker at low speeds or at low energy input increases the drop-drop collision frequency to promote coalescence. Previous work showed how stirred tanks[35, 26] and swirled flasks[59] were used to observe oil drop breakup and coalescence, which depends on the effectiveness of surfactants. For example, Fingas et al. showed that drop breakup was achieved by swirling O/W emulsions in a flask above 150 rpm.[59] In contrast, stirred tanks that utilize an impeller to mix emulsions found that at low surfactant concentration, the coalescence rate of oil increased at a stir speed of 460 rpm. However, fine oil drop sizes were achieved at higher concentrations of surfactant.[35] Self-emulsification, or emulsification due to little energy input, has also been studied for drug delivery in pharmaceutical industries.[60] Self-emulsifying systems form emulsions under gentle agitation. Self-emulsifying emulsions with a low concentration of non-ionic surfactants produced an oil drop size distribution with high polydispersity (Polydispersity Index = 7) and contained sub-micron and 100 μm diameter drops.[60] This behavior is similar to model bilgewater emulsions studied here.

Many other studies have investigated coalescence and drop breakup of emulsions in turbulent shear flows.[19, 32, 43] These studies provide examples of other "dynamically" aged emulsions. For example, for the application of oil spill remediation, it was found that over time, large crashing waves dispersed oil slicks to greater depths and produced oil drops 50 μm in diameter in the presence of surfactants.[31] Other studies[26, 31, 34, 35, 59, 60] provide insight into the mechanisms observed, such as drop breakage during dynamic ageing; however, they do not fully model the experimental setup and physical system presented in this paper. Therefore, an estimation of energy density input is required to quantify the behavior of dynamic ageing.

Emulsions made with a surfactant concentration that produced the most changes in oil drop size distributions after 20 days between static ageing and dynamic ageing were chosen to summarize the stability behavior of the emulsions. Figure 68 summarizes the oil drop size distributions that result from emulsions with 100 ppm SLES and 500 ppm Triton X-100 that were statically aged, dynamically aged at low speeds, and dynamically aged at high speeds. The light gray curves represent statically aged emulsions, the dark gray curves show dynamically aged emulsions at 12 rpm, and the black curves represent dynamically aged emulsions at 30 rpm. For both surfactants, drop coalescence and drop formation was observed for dynamic aged emulsions at 12 rpm. It can also be seen that for 100 ppm SLES, dynamic ageing at high energy produced more sub-micron drops than when statically aged or dynamically aged at low energy. These results are similar for 500 ppm Triton X-100. Therefore, the inclusion of motion during ageing is unfavorable for destabilizing emulsions to coalescence due to the formation of sub-micron drops.

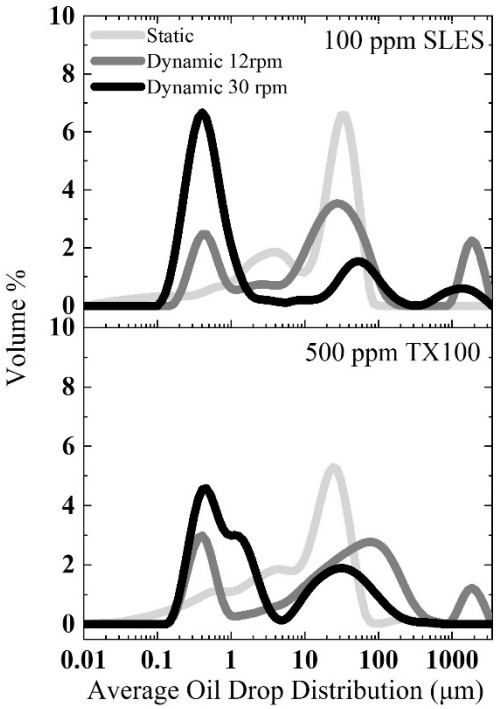

Figure 68**:** Average oil drop size distribution after 20 days for 100 ppm SLES and 500 ppm Triton X-100 aged statically, dynamically at 12 rpm, and dynamically at 30 rpm.

Two conditions were tested in which air was expelled from the syringe so that there was either 50% of air inside the tube or 0% air inside the tube. In the latter condition, the emulsion occupied 100% of the volume. Surfactant foam and bubbles produced from emulsification destabilized within 3 hours, to which all the air was successfully expelled from the syringe. Throughout this document, these samples will be referred to as emulsions with 50% air and 0% air. Figure 69 shows photographs of the emulsification chamber for 70%, 50% and 0% air emulsions.

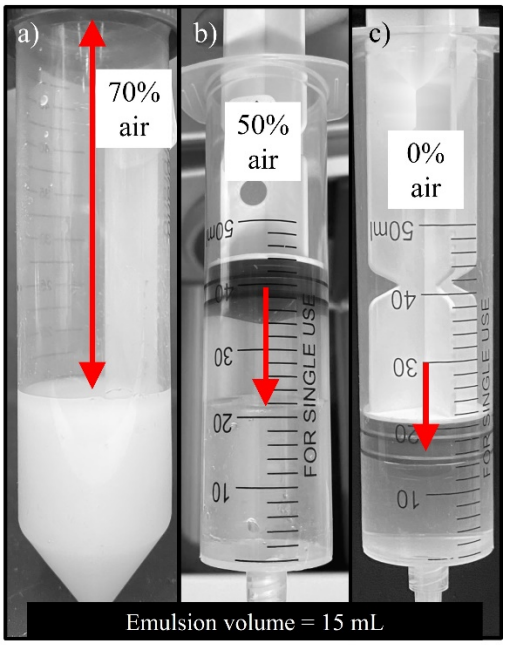

Figure 69**:** Photographs of a 15 mL emulsion inside a) a 50 mL centrifuge tube with 70% air, b) a syringe with 50% air and c) a syringe with all air removed (0% air).

Emulsion ageing conditions and characterization

Ship rocking due to sea waves was replicated via dynamic ageing. A three-dimensional rocker (Benchmark BenchRocker 3D Nutating Shaker) was used and set at 30 rpm and a tilt angle of 24 degrees. The air-capped emulsions were placed on the 3D rocker at 30 rpm for 5, 10, and 20 days. This set of experiments will be compared to emulsions with 70% air that were statically and dynamically aged.

The oil drop distribution was measured via laser diffraction (Malvern Mastersizer 3000) after 5, 10, and 20 days for the air-capped emulsions. Optical microscopy was used with an Olympus BX41 Microscope and AM Scope software to visualize the distribution of oil drops for some emulsions.

Energy density for dynamic ageing

This estimation for the energy density input for dynamic ageing was based on the balance between the potential and kinetic energy of a falling object. This approach found that for 20 days of ageing, 8.83 J/mL was provided by the rocker for emulsions with 70% air. It is predicted that emulsions with 0% air will experience 0 J/mL of energy during dynamic ageing, to which the oil

drop distribution does not change over time. However, this prediction is questionable since oil drops can move throughout the aqueous phase due to density differences between mineral oil and saltwater.

Effect of dynamic ageing with 50% and 0% air inside the ageing vial

After initial emulsification in the high shear mixer, emulsions were placed in a syringe 50% of the air was expelled to reduce the amount of splashing during dynamic ageing. Figure 69**a** and Figure 69**b** shows the oil drop size distributions over 20 days for emulsions with 10 – 1000 ppm SLES and Triton X-100, respectively, that have been dynamically aged at 30 rpm with 50% air inside the ageing vial. For emulsions with 10 ppm SLES, the distribution indicates that after 20 days, the emulsions were unstable due to coalescence. For 100 – 500 ppm SLES, the curves at 0 days consist of two peaks at 20 μm and 5 μm. After 5 days, the distributions shift to a single peak centered at 0.5 μm and remains stable throughout the 20 days. This indicates that once the 0.5 μm oil drops are formed, they are stabilized by SLES.

For Triton X-100 emulsions, the behavior of the evolution of the oil drop distribution for 10 ppm is similar to 10 ppm SLES in that the oil drops coalesce over time due to insufficient surfactant concentration. For 100 ppm Triton X-100, the distribution at 0 days consists of two peaks at 20 and 5 μm. After 5 days, the distribution shifts to form three peaks at 0.5 μm, 200 μm and 2mm. After 10 days, the heigh of the peak at 0.5 μm drops increases as the peaks at 200 μm and 2mm no longer exist. However, after 20 days, the peak at 200 μm reappears and the height of the peak at 0.5 μm drops decreases. For 500 – 1000 ppm Triton X-100, the bimodal peaks at 0 days shifts to a singular peak at 0.5 μm after 10 days. After 20 days, the height of the peak at 0.5 μm decreases and a peak at 200 μm appears.

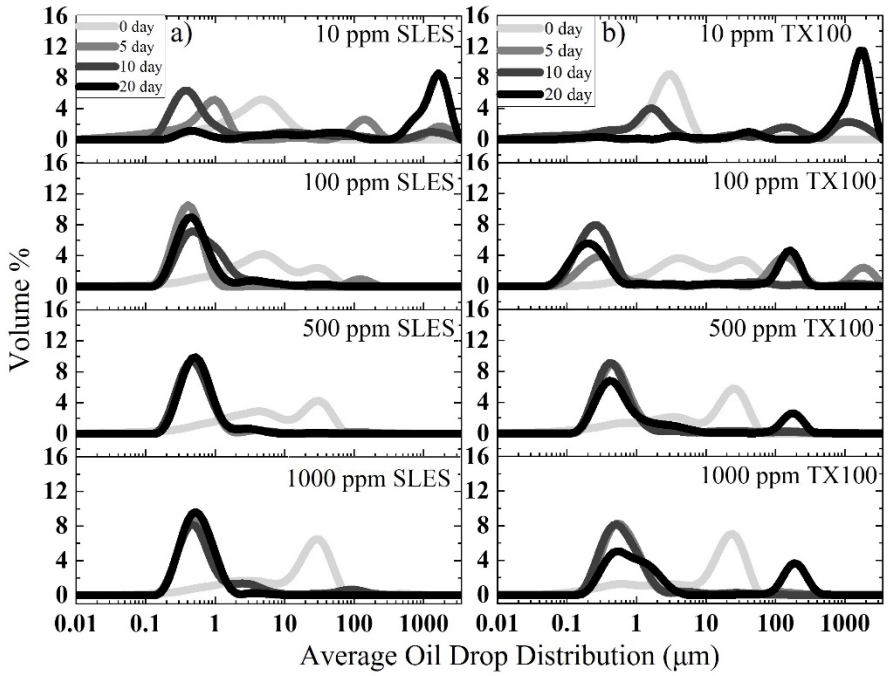

Figure 70**:** The evolution of average oil drop distribution over 20 days for dynamically aged emulsions with 50% air and concentrations from 10 – 1000 ppm of SLES. The darkening of the distribution curves is proportional to time.

Because there was less air in the ageing vial for emulsions with 50% air than emulsions with 70% air, it was expected that the generation of sub-micron oil drops would occur more slowly over time. For example, Figure 62**a** shows that for 500 ppm SLES with 70% air, the distribution gradually shifts from 20 μm at 0 days to 0.5 μm at 20 days. Therefore, it was expected that for emulsions with 50% air, there would be less sloshing that occurred, and the opportunity for oil drops to break up into sub-micron sizes would be reduced. However, Figure 70**a** indicates that for 500 ppm SLES, sub-micron drops were generated after 5 days. Overall, the oil drop sizes that were present after 20 days for emulsions with 100 – 1000 ppm SLES and 50% air are similar to the sizes present after 20 days for the same emulsions with 70% air. For Triton X-100 emulsions with 50% air, the appearance of a peak at 200 μm after 20 days indicates that when air is removed from the ageing vial, larger drops are formed due to coalescence. This may be explained by the fact that Triton X-100 is ineffective in stabilizing the sub-micron drops over time as SLES.

Overall, it was expected that sloshing would be reduced upon reducing the amount of air within the ageing vial, which would reduce the velocity at which oil drops collide. Therefore, it would take longer for oil drops to break up into sub-micron sizes. However, this was not the case, as sub-micron drops were formed after 5 days and remained throughout the duration of ageing.

In a second condition, all the air was expelled to eliminate any splashing during dynamic ageing. As stated in Chapter 2, mineral oil drops larger than 2.8 μm are desired as they are large enough to cream to the surface and remove. All emulsions aged with 0% air inside the ageing vial experienced creaming. Figure 71 shows a creamed layer in an emulsion made with 100 ppm SLES.

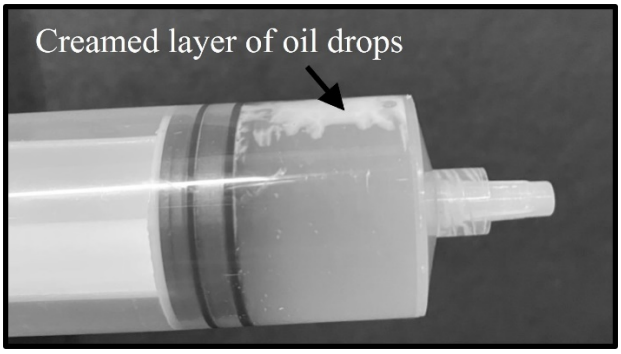

Figure 71: Photograph of an emulsion dynamically aged for 5 days with 100 ppm SLES, 0.42 M sodium chloride, 5000 ppm mineral oil, and 0% air.

Figure 70**a** and Figure 70**b** show the oil drop distributions over 20 days for SLES and Triton X-100, respectively. For 10 ppm Triton X-100, the average size of the oil drops was too large to be measured via laser diffraction after 5 days. This was the result of coalescence during ageing. For emulsions with 10 ppm SLES, the distribution varied over time and resulted in three separate peaks (at 0.5 μm, 10.5 μm, and 2 mm) after 20 days. The accuracy of the curves for 10 ppm SLES is unreliable for similar reasons to emulsions with 10 ppm Triton X-100. Coalescence was observed for 10 ppm SLES and is shown in Figure 71. For 100 ppm SLES, the curve at 0 days consisted of a major peak at 9 μm and a secondary peak at 12 μm. Within 5 days, the peak at 12 μm disappeared, and the peak at 9 μm remained. After 10 days, the peak shifted towards 2 μm, and two new peaks were measured at 0.5 μm and 100 μm. After 20 days, the height of the peak at 0.5 μm and 100 μm decreased while the height of the peak at 2 μm increased. A small peak at 200 μm also existed after 20 days. At 500 ppm SLES, the oil drop distribution at 0 days and 5 days was nearly identical. After 10 and 20 days of ageing, the distribution shifted to a peak ranging from 0.2 – 10 μm and a small peak at 200 μm. At 1000 ppm SLES, there is an exchange in the volume % of oil drops that were 20 μm at 0 days to oil drops between 0.2 – 10 μm at 20 days. However, a small peak at 200 μm was measured after 20 days. The change in the oil drop size over time shows that although there was no sloshing inside the syringe, coalescence and drop generation occurred. Figure 74 shows optical images of emulsions at each concentration of SLES after 20 days to support the measured oil drop distributions in Figure 72**a**.

The evolution of oil drop distributions over 20 days for emulsions with 0 % air and Triton X-100 is shown in Figure 72**b**. Again, the evolution of oil drop size distribution was not measured for 10 ppm Triton X-100. For 100 ppm Triton X-100, the distribution at 0 days consists of one peak at 40 μm and one at 4 μm. After 5 days, the distribution shifted to consist of a major peak centered at 8 μm and a minor peak around 0.6 μm. After 10 days, the peak at 0.6 μm remained, and the

major peak at 8 μm now shifted to 6 μm, indicating drop breakup. After 20 days, the peak at 6 μm shifted in the opposite direction toward 25 μm, and a new peak at 2 mm was measured. The peak at 0.6 μm remained. For concentrations ≥ 500 ppm Triton X-100, the distributions evolved similarly to that of 1000 ppm SLES. For example, there was an exchange in the volume % of 20 μm oil drops at 0 days to 0.3 – 8 μm oil drops at 20 days. A small peak at 200 μm existed after 20 days for 500 ppm and 1000 ppm Triton X-100.

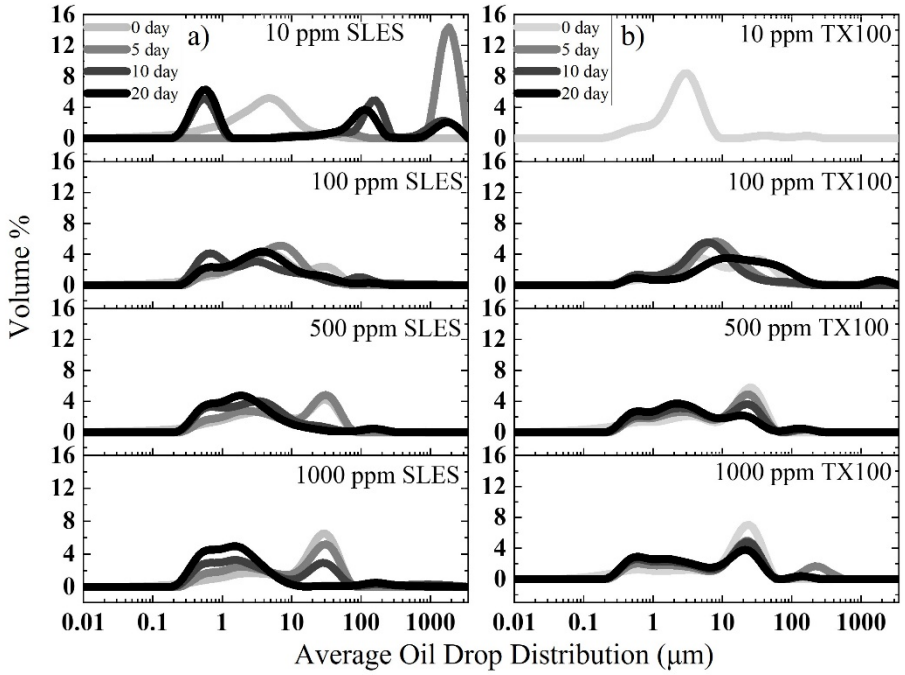

Figure 72**:** The evolution of average oil drop distribution over 20 days for dynamically aged emulsions with 0% air and concentrations from 10 – 1000 ppm of SLES. The darkening of the distribution curves is proportional to time.

Figure 73**:**Top view photograph of coalesced mineral oil drops in an emulsion with 10 ppm SLES, 0.42 M sodium chloride, and 5000 ppm mineral oil after 20 days of ageing with 0% air inside the syringe.

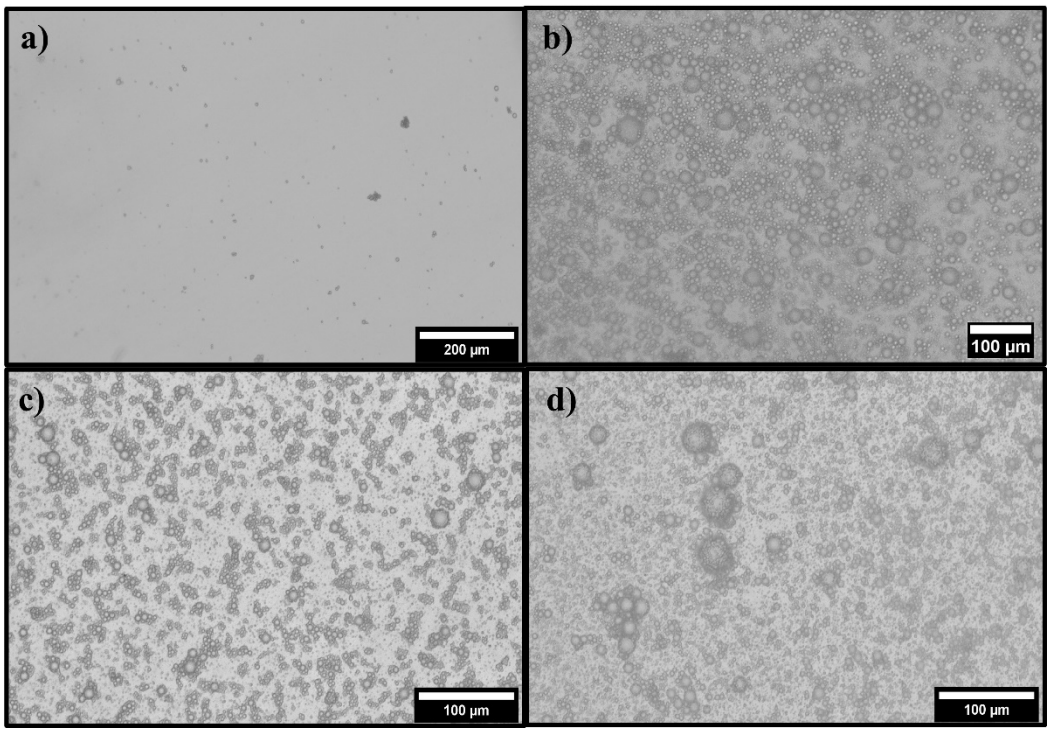

Figure 74: Brightfield optical images of a) 10 ppm b) 100 ppm c) 500 ppm and d) 1000 ppm SLES after 20 days of dynamic ageing with 0% air inside the syringe.

Earlier, it was predicted that dynamic ageing of emulsions with 0 % air imparts 0 J/mL. If this were true, the evolution of oil drop size distributions would look identical to the distributions statically aged emulsions in Chapter 2, section 3.3. Instead, the oil drop size distribution shifted toward smaller sizes for emulsions with ≥ 500 ppm SLES or Triton X-100.

One explanation for the breakup of oil drops in air-capped emulsions during dynamic ageing arises from the difference in density between oil and water. As established earlier, removing the free space within the emulsification chamber successfully eliminated any splashing during dynamic ageing. However, the density of mineral oil (0.86 g/mL) is less than that of saltwater with 0.42 M NaCl (1.023 g/mL). Therefore, mineral oil drops shear against the aqueous phase during dynamic ageing even when there is no air inside the ageing vial. The speed at which the oil drops move depends on their size. Over time, the oil drops collide with one another and either break up into smaller oil drops or coalesce, which can be seen by the shift in oil drop size distribution toward smaller and larger sizes, shown in Figure 72. The extent to which oil drop breakup occurs depends on surfactant concentration. At a surfactant concentration ≥ 100 ppm SLES or ≥ 500 ppm Triton X-100, the interfacial tension between mineral oil and the surfactant and salt solutions decreases to 2.7 mN/m and 3.5 mN/m, respectively (Chapter 2). Here, the energy required to break up oil drops is less than that for emulsions with < 100 ppm SLES or < 500 ppm Triton X-100. Therefore, at concentrations ≥ 100 ppm SLES or ≥ 500 ppm Triton X-100, drops are broken into a given size, to which there is enough surfactant to cover the interfacial area.

For all dynamically aged air-capped emulsions, creaming was experienced, and the average oil drop size was above 2.8 μm in diameter, regardless of surfactant concentration. However, sub-micron drops were formed in emulsions with a S/O greater than 0.01 for either surfactant during dynamic ageing. A greater number of sub-micron oil drops were formed for dynamically aged emulsions with 70 % air inside the ageing vial (Chapter 2). No matter the extent, the generation of sub-micron oil drops is unfavorable for bilgewater emulsions. Ship rocking is unavoidable and causes bilgewater to further emulsify due to the sloshing of the liquids. Mitigating the sloshing by removing air from the ageing vial does not entirely prevent the formation of sub-micron oil drops due to the difference in density between oil and water.

Effect of dynamic ageing on the dispersion of oil into surfactant and salt solutions

Prior to this section, the liquids were pre-mixed to represent bilgewater that has been pumped through pipes and tanks before entering the bilge tank. In this section, emulsions were dynamically aged without being pre-emulsified in the high-shear mixer to represent a situation in which a volume of oil is dispensed on the surface of bilgewater and is subjected to ship rocking over time. Figure 75 shows a bulk volume of oil that was placed on the surface of a solution with SLES and salt. It is important to note that the mineral oil volume fraction of the emulsions was only 0.0058 (5000 ppm). These preliminary results will provide some evidence for the effect of ultra-low energy input via dynamic ageing on the emulsification of model bilgewater liquids. The energy provided during dynamic ageing is significantly less than the energy added during initial emulsification via high shear mixing. For example, after 10 days of dynamic ageing, it was estimated that 4.4 J/mL of energy is added to an emulsion with 70% air inside the ageing vial.

This is compared to 162 J/mL added during high shear mixing. The following section provides preliminary results from dynamic ageing without pre-emulsifying the liquids under the two previously established scenarios: dynamic ageing with 0% and 70% air inside the ageing vial. Scenario 1 consists of emulsions with 10 – 1000 ppm SLES were subjected to dynamic ageing with 0% air. Scenario 2 consists of emulsions with 10 – 1000 ppm SLES or Triton X-100 that were subjected to dynamic ageing with 70% air. The oil drop sizes were analyzed for each scenario after 10 days.

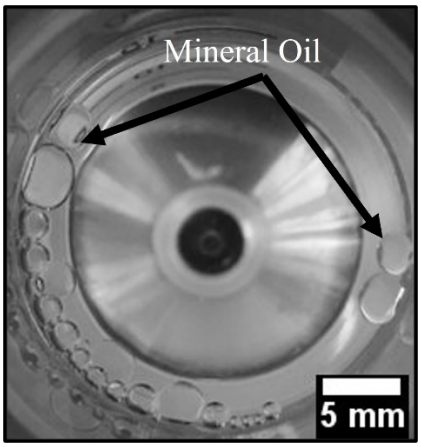

Figure 75**:** Photograph of the top view of a SLES and salt solution with 5000 ppm mineral oil added to the surface (0 days aged).

Scenario 1: Dynamically ageing non-pre-mixed emulsions with 0% air

In the first scenario, 5000 ppm mineral oil, 0.42 M NaCl, and various surfactant concentrations were placed into a syringe to which all the air was expelled before dynamic ageing at 30 rpm for 10 days. Again, the oil was not pre-emulsified. All emulsions were transparent after 10 days of ageing and the oil drop size was too large to measure via laser diffraction. Figure 76**a** and Figure 76**b** show photographs of the surface of emulsions with 10 ppm and 1000 ppm SLES that were aged for 10 days with 0% air.

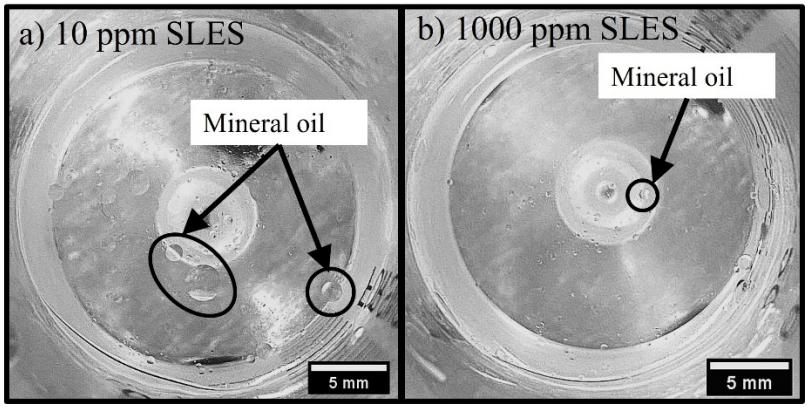

Figure 76: Photographs of the top view of emulsions with a) 10 ppm SLES and b) 1000 ppm SLES, 0.42 M sodium chloride, and 5000 ppm mineral oil that were not pre-emulsified and dynamically aged with 0% air for 10 days.

The average oil drop size was larger for 10 ppm SLES than for 1000 ppm SLES. This trend is expected, as there is enough surfactant to cover the oil-water interface for 1000 ppm SLES. Nevertheless, dynamically ageing the non-pre-mixed and air-capped emulsions showed signs of reduction in initial oil drop size over time due to the difference in density between mineral oil and salt water. Since all emulsions that were dynamically aged with 0% air were transparent after 10 days, it can be assumed that a great number of sub-micron drops were non-existent; however, the oil drop size within the subnatant was not measured. Regardless of surfactant concentration, the oil drops formed were large enough to cream to the surface. The implications of these results indicate that the formation of sub-micron droplets can be prevented if the amount of free space in the bilge tank is reduced and if the bilgewater initially contained only millimeter-sized oil drops. However, the latter condition is difficult to achieve as micron-sized oil drops are likely present in bilge water after being pumped through a series of pipes and tanks prior to filtration.

These results indicate that the energy produced by the oil shear against the tube walls is not enough to generate sub-micron drops. Consequently, if sloshing during dynamic ageing is not significant, there is not enough energy to promote drop breakup. Therefore, a more complex process must be driving the changes in drop size distributions for emulsions that were pre-mixed and dynamically aged with 0% air inside the ageing vial.

Scenario 2: Dynamically ageing non-pre-mixed emulsions with 70% air

Figure 77 shows the oil drop size distributions after 10 days of dynamic ageing with 70% air for SLES and Triton X-100. These samples were not pre emulsified and 5000 ppm mineral oil was dispensed on top of the surfactant solution prior to ageing. Therefore, the oil drop size distribution at zero days for both surfactants is not included in Figure 77**,** as the oil drop sizes were too large to measure via laser diffraction. Recall that Figure 75 shows an image that represents the oil drop sizes at zero days for all emulsions. For either surfactant, there is a reduction in oil drop size from 0 to 10 days of dynamic ageing. For 10 ppm SLES, part of the bulk oil was emulsified into droplets around 0.5 μm, 2 μm, 100 μm, and 2 mm as indicated by the four peaks. For 100 ppm SLES, the bulk oil was emulsified into droplets around 0.5 μm and 10 μm in diameter after 10 days. At 500 ppm SLES, one major peak existed at 100 μm and two minor peaks existed at 20 μm and 2 mm. Lastly for 1000 ppm SLES, a unimodal distribution was measured and centered at about 100 μm. Figure 78 verifies the oil drop size distributions for 10 ppm and 1000 ppm SLES and Figure 79 shows images of the evolution of oil drop size for 1000 ppm SLES over 2 days.

Similar behavior for Triton X-100 is presented in Figure 77**b**. At 10 ppm Triton X-100, one major peak was measured at 50 μm. As the concentration of Triton X-100 increased to 100 ppm, a peak at 0.5 μm was measured. For both 500 ppm and 1000 ppm Triton X-100, two peaks existed at 40 μm and 2 mm.

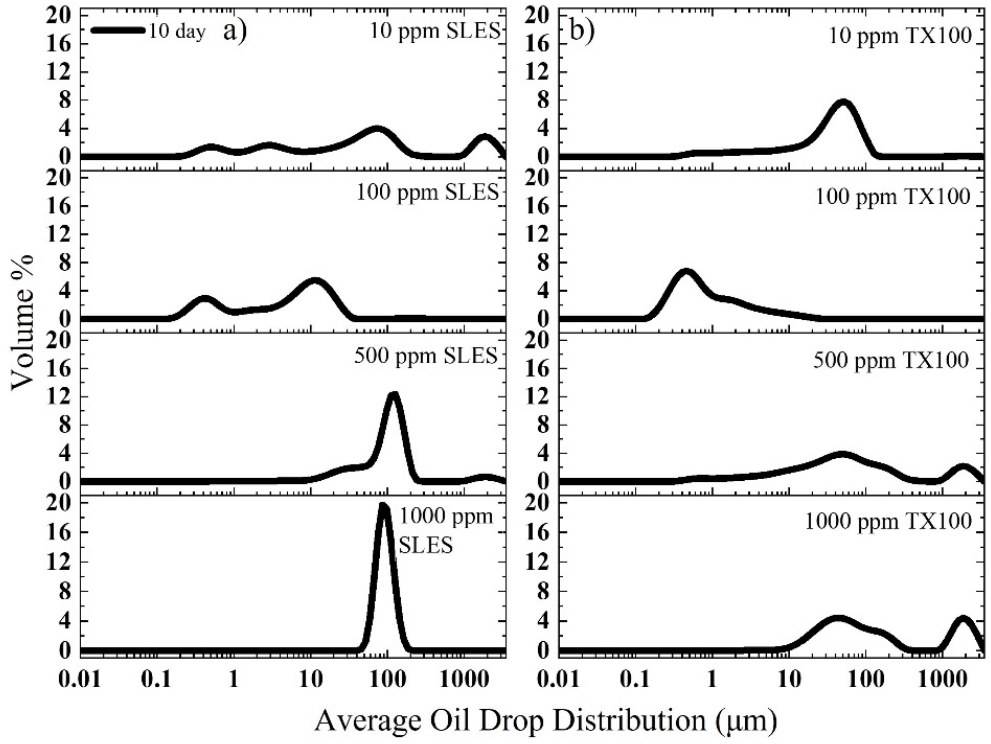

Figure 77**:**The average oil drop distribution for 10 – 1000 ppm of a) SLES and b) Triton X-100 after 10 days of dynamic ageing with 70% air. Mineral oil (5000 ppm) was dispensed, and the liquids were not pre-emulsified prior to ageing.

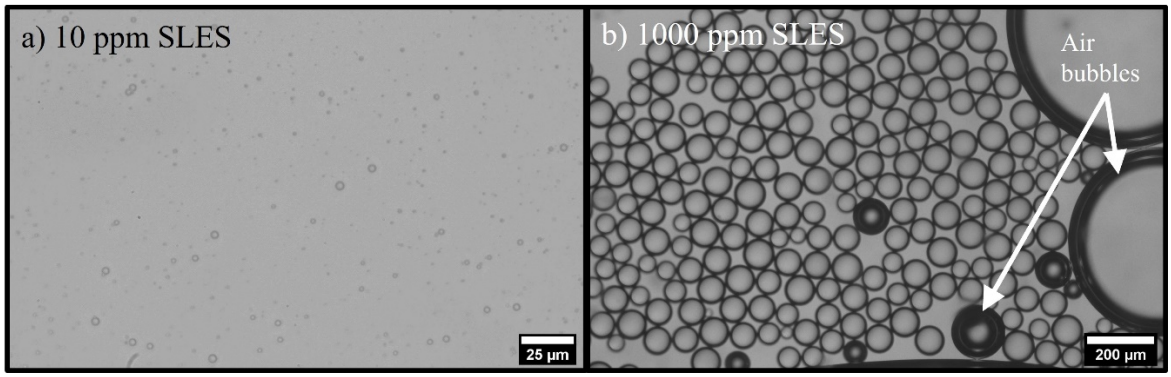

Figure 78**:** Brightfield optical images of a) 10 ppm and b) 1000 ppm SLES, 0.42 M sodium chloride, and 5000 ppm mineral oil after 10 days of dynamic ageing with 70% air and no pre-mixing.

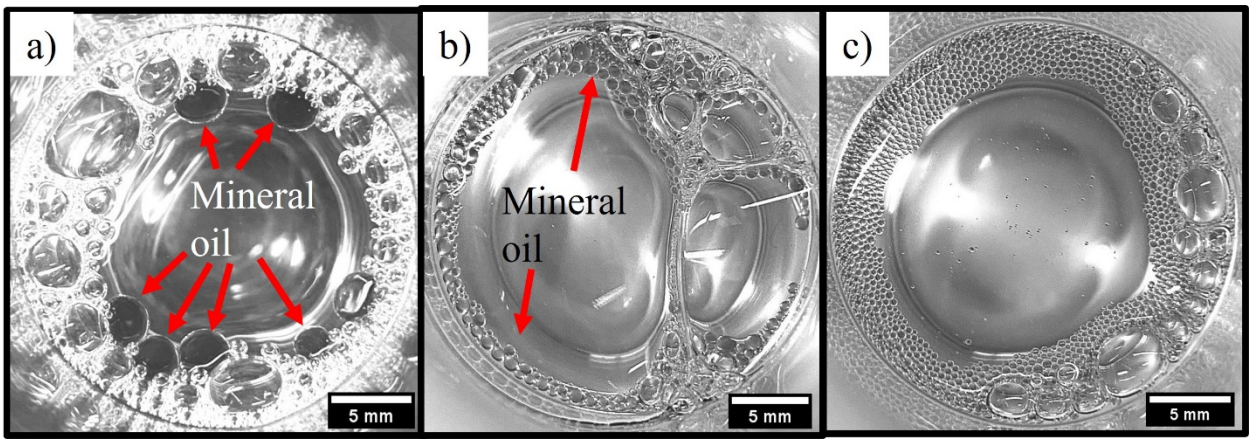

Figure 79**:**Top view photographs of an emulsion with 1000 ppm SLES, 0.42 M sodium chloride, 5000 ppm Mineral oil after a) 0 days, b) 5 hours, and c) 2 days of dynamic ageing with 70% air and no pre-mixing.

After 10 days of dynamic ageing with 70% air, both 10 ppm and 100 ppm SLES emulsions were optically opaque, indicating that sub-micron drops exist. This is verified through the oil drop size distributions for 10 ppm and 100 ppm SLES shown in Figure 77. Figure 80 shows an optical image of an emulsion with 100 ppm SLES that appears cloudy, however there was bulk oil that remained at the surface of the emulsion was not emulsified during dynamic ageing. Since the emulsions were not pre-mixed, the oil initially existed as one large drop at the surface of the surfactant solution. As dynamic ageing begun, the oil drop was stretched and broken into smaller drops. After 10 days, an opaque emulsion was formed after stretching and pinching of the oil which generated micron-sized oil drops that were stabilized by surfactant. However, a large oil drop existed on the surface of the emulsions after ageing.

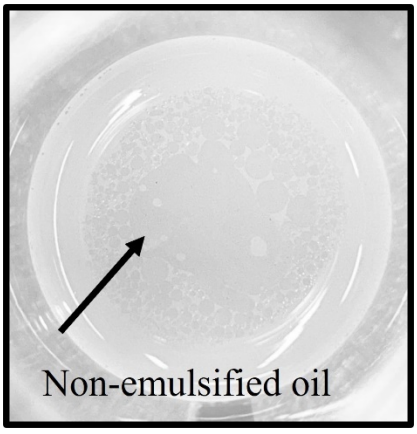

Figure 80**:** Photograph of the top view of an emulsion with 100 ppm SLES, 0.42 M sodium chloride, and 5000 ppm mineral oil after 10 days of dynamic ageing with 70% air and no pre-mixing.

To understand these results, we must first consider the effect of wave motion on oil droplet formation. Several published experiments have attempted to understand the formation of oil droplets due to crashing waves.[31, 44, 63–66] The application for this investigation arises from oil spill remediation. When a large volume of oil is spilled out into the ocean, surfactants are added to the surface of the ocean where the oil was spilled to disperse the oil throughout the ocean. The energy provided by waves breakup the oil slick into droplets whose size depends on the energy of the wave, the type and concentration of surfactant used[31, 44], and the interfacial tension between the oil and water.[63] Using a wave-tank apparatus, the work by Li et. Al established that the energy provided by a crashing wave was large enough to form sub-micron oil droplets at a S/O of 0.04.[31, 44] The sub-micron droplets existed at greater depths than that of the larger drops. The sub-micron droplets are well dispersed by ocean currents and dominated by Brownian motion so that they may never reach the surface. The larger drops were dominated by a buoyancy force that caused them to coalesce and cream to the surface where they are influenced by surface and wind currents.[65] This causes the bulk oil to stretch in a non-uniform manner caused by a reduction in interfacial tension between oil and water in the presence of surfactants.[63] This behavior was seen in for 10 and 100 ppm SLES.

As the concentration of SLES or Triton X-100 was increased to 500 ppm and 1000 ppm, the emulsified droplets were larger than that of 10 ppm or 100 ppm SLES or Triton X-100. It is well known that the oil droplet size decreases with surfactant concentration, however, this is not the case for these emulsions. A justification to these results is explained by depletion flocculation from the formation of surfactant micelles. It has been estimated that the critical micelle concentration (CMC), or the concentration at which micelles form was around 30 ppm SLES and 300 ppm Triton X-100 for this system (Table 12). Therefore, emulsions with 500 ppm and 1000 ppm SLES or Triton X-100 will form micelles within the solution. The amount of surfactant that does not contribute to the formation of a micelle is available to adsorb to the oil-water interface. Consequently, the concentration of surfactant at the oil-water interface is less than that of the amount of surfactant initially added to the emulsion due to the formation of micelles. Therefore, the size of the oil drops is limited by the energy provided by dynamic ageing (4.4 J/mL after 10 days).

A limitation of the experiments in Scenario 1 and Scenario 2Scenario 2: Dynamically ageing non-pre-mixed emulsions with 70% air exists due to the fact that it is unlikely for bilgewater not to be emulsified after collection and treatment. However, the results from Scenario 2 were intriguing in that a narrow drop size distribution with an average size of 100 μm was produced after 10 days for an emulsion with an S/O of 0.2 SLES (1000 ppm SLES, 5000 ppm mineral oil). Therefore, this technique could be advantageous to industries that aim to fabricate large quantities of monodisperse particles. In the following section, emulsions with various surfactant-to-oil ratios were dynamically aged to produce a narrow drop size distribution.

Surfactant-to-oil ratios that produce narrow drop size distributions

In Scenario 2, a narrow drop distribution was formed after 10 days for a dynamically aged emulsion with 1000 ppm SLES, 0.42 M NaCl, 5000 ppm mineral oil, and 70% air within the ageing vial. This section presents preliminary data that aims to investigate different emulsion

compositions that produce a unimodal drop size distribution under the same ageing conditions and viscosity's impact on dynamically aged emulsions. The emulsions in this section were not pre-emulsified prior to ageing. Table 12 lists the emulsion compositions and corresponding S/O's used for the following experiments, and Table 13 lists the density and viscosity of heavy and light mineral oil.

Table 12**:** Emulsion compositions used to investigate unimodal drop distributions after dynamic ageing.

Emulsion	SLES concentration (ppm)	Mineral Oil Type	Oil Concentration (ppm)	S/O	NaCl Concentration (M)
1	1000	Heavy	5000	0.2	0.42
2	1000	Heavy	15,000	0.07	0.42
3	1000	Heavy	10,000	0.1	0.42
4	3000	Heavy	15,000	0.2	0.42
5	1000	Light	15,000	0.07	0.42
6	1000	Light	10,000	0.1	0.42
7	3000	Light	15,000	0.2	0.42

Table 13**:** Light and heavy mineral oil density and viscosity at 40°C

Mineral Oil Type (Sigma Aldrich)	Density (g/mL)	Viscosity at 40°C (10^{-3} Pa*s)
Heavy	0.862	57.8
Light	0.846	13.2

Recall that Figure 78**b** shows an optical image of Emulsion 1. Figure 81 shows optical images of emulsions 2 – 4 that were dynamically aged for 10 days with heavy mineral oil. The oil drops appear to be less uniform in diameter in Figure 81**a** and Figure 81**b** than in Figure 81**c**. Figure 82 shows optical images of emulsions 5 – 7 that were dynamically aged for 10 days with light mineral oil. Here, the uniformity of drop diameter increases with S/O similar to the emulsions in Figure 81; however, the drops in Figure 81**c** appear more uniform in diameter than Figure 82**c**. Therefore, at a constant S/O, the viscosity of the oil impacts how uniform the drops are in diameter. For example, since light mineral oil has a lower viscosity than heavy mineral oil, it is more susceptible to perturbations during dynamic ageing. To confirm that hypothesis, the interfacial tension between light mineral oil and SLES must be measured and analyzed.

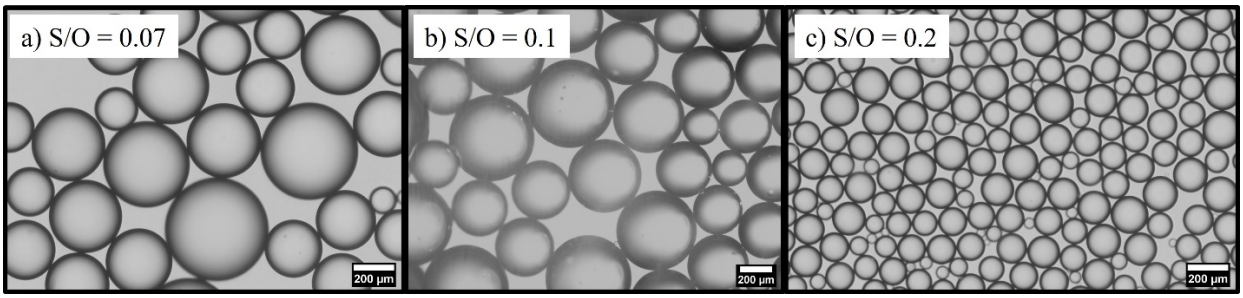

Figure 81**:** Optical Images of emulsions a) 2, b) 3, and c) 4 that were dynamically aged for 10 days at 30 rpm with 70% air within the ageing vial. The emulsions were made with heavy mineral oil and were not pre-mixed prior to ageing.

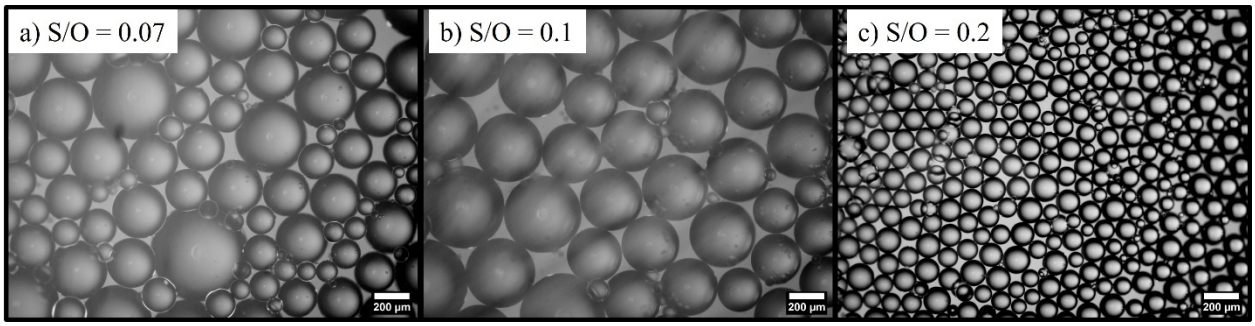

Figure 82**:**Optical Images of emulsions a) 5, b) 6, and c) 7 dynamically aged for 10 days at 30 rpm with 70% air within the ageing vial. The emulsions were made with light mineral oil and were not pre-mixed prior to ageing.

While the oil drops in Figure 82**c** are not perfectly monodisperse, they appear to have a narrow distribution in size, which may be favorable for foods, cosmetics, and other industries that need to produce large quantities of drops of similar sizes. This technique of dynamic ageing without prior mixing provides a way to fabricate similar-sized oil drops that is easy and cost-effective.

Impact of processing routes on droplet size

Droplet Size as a function of Energy Density

The emulsification of two immiscible liquids often requires the application of external energy. The applied energy is proportional to the amount of the newly created interface on the dispersed phase. In turn, the newly created interface is a factor that helps to define the minimum achievable droplet size of the dispersed phase. [51] Figure 83 shows the behavior of the resulting droplet size with increasing energy density for mineral oil and water emulsions stabilized with SLE_1S. This emulsion was mixed using the orifice mixer.

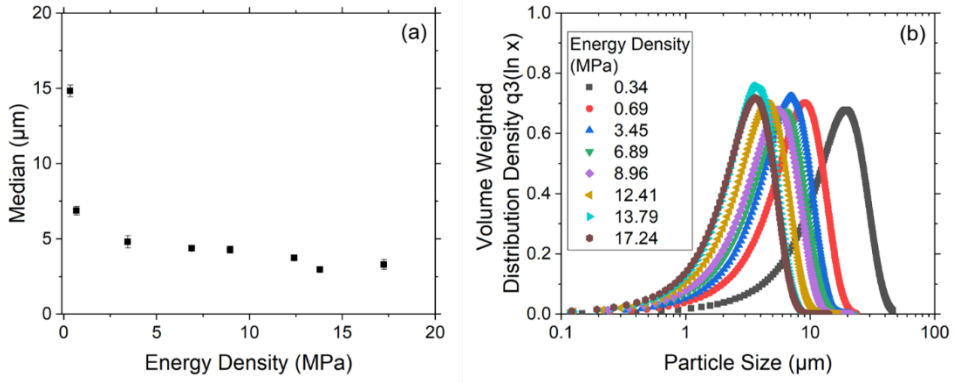

Figure 83 Droplet size and size distribution of mineral oil (5 wt%), SLE_1S (1 wt%) in water emulsions fabricated with variable energy density. (a) Median droplet size as a function of energy density. (b) Volume distribution density as a function of droplet size

It can be observed in Figure 83a that the median droplet size decreases in a power law form respect to increasing energy density. The most significant reduction occurred for mixing energy densities between 0.34 to 3.45 MPa. Within this range, median droplet size decreases up to 10 µm. Further increase in energy density did not produce a significant change in droplet size. Hence, it is assumed that the efficiency of the system stalls after 3.45 MPa.

The formation of droplets of smaller diameter above the 3.45 MPa for the given formula-mixer pair is less probable. [166] The maximum efficiency in droplet size reduction depends on the battle between droplet breakup and droplet coalescence of the formula-mixer pair. [167] Pass the 3.45 MPa mark, the mixer is able to produce levels of surface area that cannot be stabilized given the type or concentration of surfactant. [56]

Yet, surfactant concentration may be just enough to stabilize a greater amount of interface. It is observed in Figure 83b that increasing energy density shifts the entire DSD toward smaller sizes. DSD at higher emulsification energies show a greater density of near submicron droplets (droplet size <1 µm) and a depopulation of very large droplets (> 10 µm). Hence, there is enough surfactant to stabilize a greater amount of newly created interface.

Small amphiphilic molecules can provide stabilization to droplets even during mixing. However, their ability to do so is associated to the surfactant absorption velocity and concentration in the initial formula. In Figure 83b, it is observed that larger droplets still are transformed into the smallest possible droplet for the given formula-mixer pair at increasing energy density. Consequently, the limitation of 3.45MPa shown in Figure 5a may be correlated to absorption velocity rather than concentration of surfactant. That is, the time-scales of the orifice mixer at higher energy densities than 3.45 MPa may be faster than diffusional properties of SLE_1S molecules.

Droplet size as a function of the emulsification process

The droplet size and size distribution is tied to the application of a specific level of energy density. However, it was demonstrated that the duration of turbulent regime is very important to maximize droplet stabilization given a specific surfactant chemistry and concentration. Yet, the

turbulent regime depends not only on the level of energy but on the form of application and dissipation of such energy.

Figure 84 shows the differences in mean droplet size and droplet size distribution (DSD) as a function of two different emulsification processes. Mineral oil-water emulsions stabilized with SLE_1S are mixed using the orifice mixer and the rotor-stator. Figure 84a shows how the orifice mixer acquires a similar droplet size using a lower energy density compared to the rotor-stator (almost two orders of magnitude). Furthermore, Figure 84b exhibits a tighter droplet size distribution (DSD) weighted in smaller sizes for the orifice mixer.

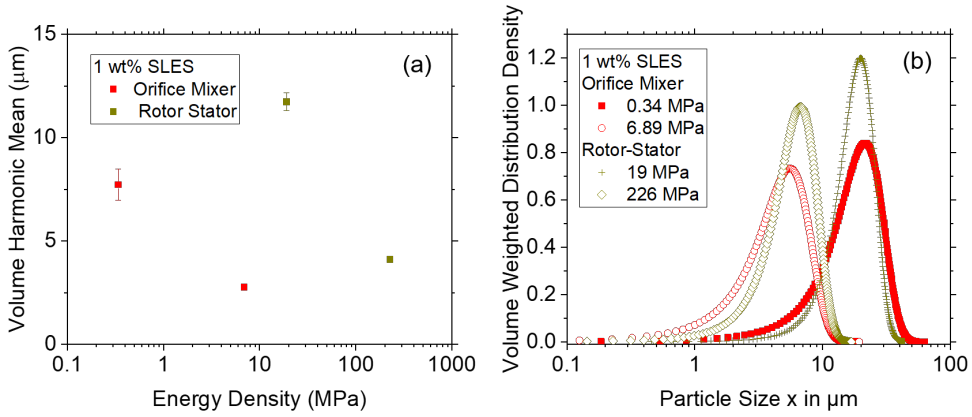

Figure 84 Mean droplet size as a function of the emulsification process and energy density. Mineral oil-waterer emulsions stabilized with SLE_1S and mixed with orifice mixer and rotor-stator. (a) Volume harmonic mean (b) Droplet size distribution

This behavior is attributed to the differences in the local energy dissipation of the two emulsification methods. As a rule of thumb, emulsification efficiency is more significant for the orifice mixer than the rotor-stator. [167] The orifice mixer continuously drives the liquid through a small opening (0.0045 cm^2), creating a highly turbulent regime which duration is proportional to the applied energy density. (represented in Figure 85a). The small dimensions of the mixing chamber assure a uniform distribution of turbulence across the volume, creating an initial allocation of very consistent-in-size small droplets and enough time before the liquid reach a laminar regime for surfactant to diffuse to the interface.

Conversely, the rotor-stator delivers non-uniform turbulence. The applied energy dissipates radially from the center of the rotor to the vessel wall, as represented in Figure 85b. The applied energy is diluted by a large pool of non-dispersing zones because the maximum turbulence is only delivered on a small volume of liquid near the rotor. Even though the fluid circulates in and out of the rotor-stator creating a turbulent regime, the duration of the turbulent regime is always interrupted by long times of possible laminar regime. Consequently, the whole mass of liquid experience uneven shear conditions. This results in lower probability to obtain the smallest droplet size but also high probability to achieve broad size distributions. [167]. Finally, it is expected that an orifice mixer develops a smaller droplet size and more uniform DSD than rotor-stator at similar energy densities.

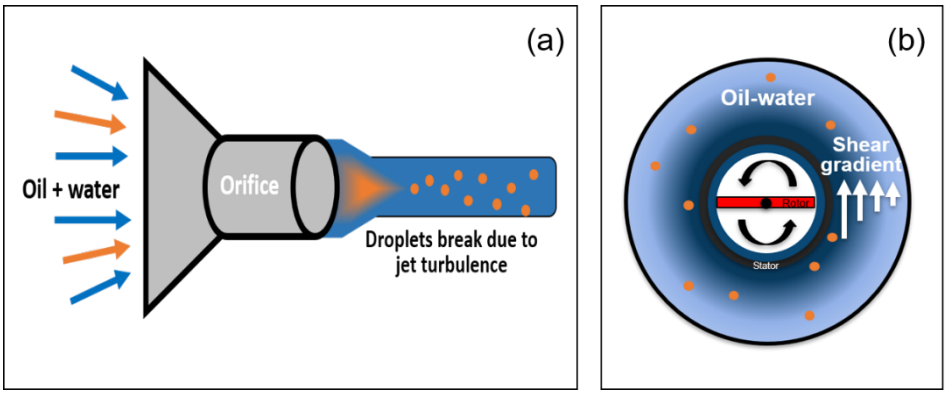

Figure 85 (a) Representation of the reduction in channel size of the orifice mixer. (b) Representation of the energy dissipation in the radial direction of the rotor-stator mixer

Droplet size as a function of oil concentration

The behavior shown in Figure 83 suggest that pass the 3.45 MPa there are other factors different than energy application that dominate the resulting droplet size and size distribution. For instance, Figure 86 shows the resulting droplet size and droplet size distribution (DSD) as a function of increasing mineral oil concentration (0.5 wt% to 20 wt%) for emulsions mixed in the orifice mixer with constant energy density (3.45 MPa) and stabilized with 1 wt% SLE_1S.

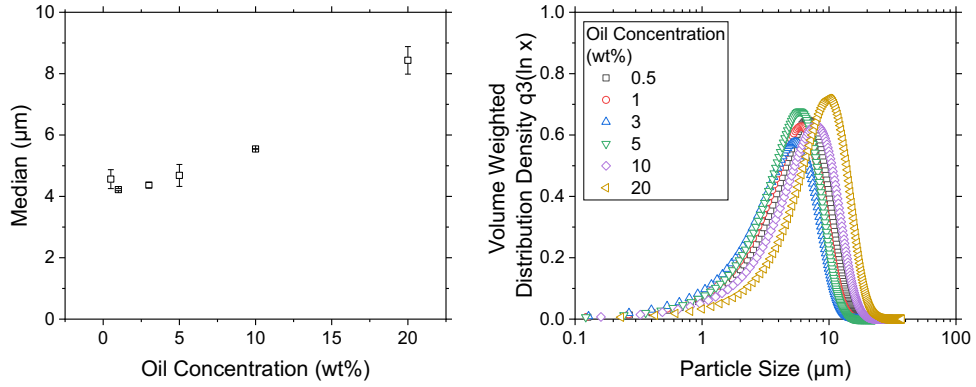

Figure 86 Droplet size and size distribution of emulsions with variable oil concentration. Emulsions: mineral oil ranging between 0.5 wt% to 20 wt%, SLE_1S at 1 wt%, and energy density of 3.45 MPa. (a) Median droplet size as a function of mineral oil concentratio. (b) Volume distribution density as a function of droplet size

Figure 86 shows that emulsions mixed at the limit of efficiency (3.45 MPa) with an increasing oil concentration resulted in a non-monotonous behavior of the mean droplet size. Figure 8a depicts a constant median droplet size for emulsions that contains up to 5 wt% oil. Yet, an oil concentration beyond 5 wt% produced a slight increase in median size proportional to the oil concentration increment. These observations are also reflected in the DSD behavior. Figure 86b shows very similar DSD for all emulsions containing up to 5wt% but emulsions containing 10

wt% and most notable on emulsions containing 20 wt% oil are shifted toward populations of greater sizes.

The behavior observed in Figure 8 just reflects the limit for a formula containing 1 wt% SLE_1S mixed at 3.45 MPa. 5 wt% oil is the limit. Beyond this point, the surfactant coverage will be poor on any interface and the probability for droplet coalescence is greatly increased.

The surfactant to oil concentration ratio was set to avoid excessive synergic effects. On the contrary, the following experiment, schematically shown in Figure 9, uses variable surfactant concentrations (1 ppm or 0.0001 wt%, and 10 ppm or 0.001 wt%) and variable mineral oil concentration (0.1 vol% to 20 vol%) to study creaming behavior. The mineral oil-water- SLE_1S emulsions were mixed using the rotor-stator mixer at an energy density of 195 MPa.

Figure 87 shows a summary of the light transmission profiles for emulsions stabilized with 1 ppm and 10 ppm SLE_1S and mineral oil at 1, 10, and 20 vol%. the ligth transmission profiles represent the spacial change in droplet concetration as a fucntion of centrifugation time.

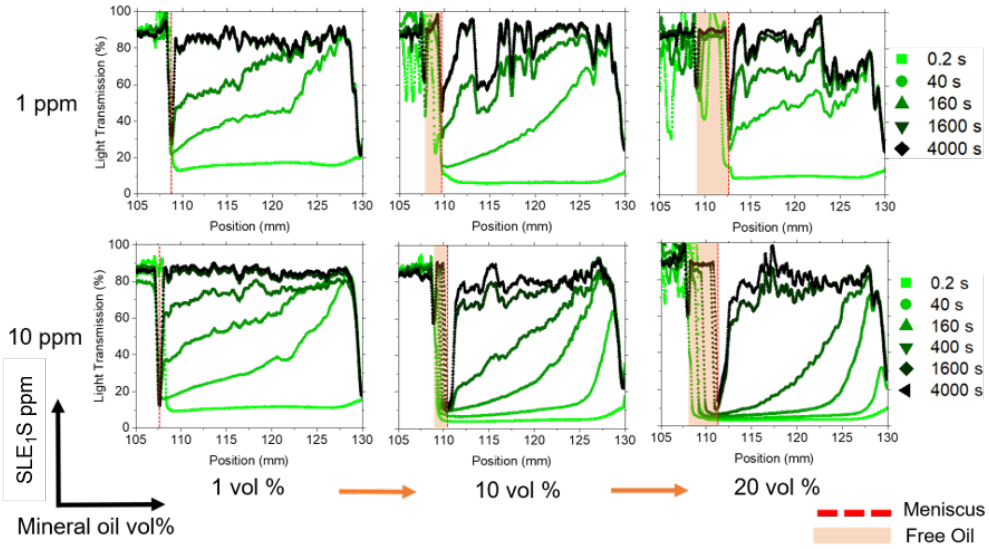

Figure 87 Light transmission profiles of emulsions stabilized with 1 and 10 ppm SLE_1S. Mineral oil concentration 1, 10 and 20 vol%

Figure 87 shows a faster rate for profile evolution in emulsions stabilized with 1 ppm compared to emulsions stabilized with 10 ppm SLE_1S. The rate of change of light transmission as a function of centrifugation time is independent of oil concetration for emulsions stabilized with 1 ppm SLE_1S. Conversely, emulsions stabilized with 10 ppm showed a slower evolution as oil concentration increases. An interesting observation is the creation of a double meniscus area (between 107 to 113 mm position) for emulsions with high mineral oil concentration. This area (orange shadow) is observed to be proportional to oil concentration, and it is believed to be a layer of free oil. The free oil layer develops slowly over time for emulsions with 10 ppm SLE_1S, but for emulsions stabilized with 1 ppm SLE_1S immediately develops after the test starts.

Figure 88 also shows evidence of a free-oil layer. Figure 88shows a photograph of the LUMiSizer® cells (type-2 cell) after the centrifugation cycle used for this study. In can be seen that 1 ppm and 10 ppm SLE_1S concentrations are not enough to stabilize the full range of formulated oil. Hence, a layer of free-oil became significant at oil concentrations higher than 1 vol%.

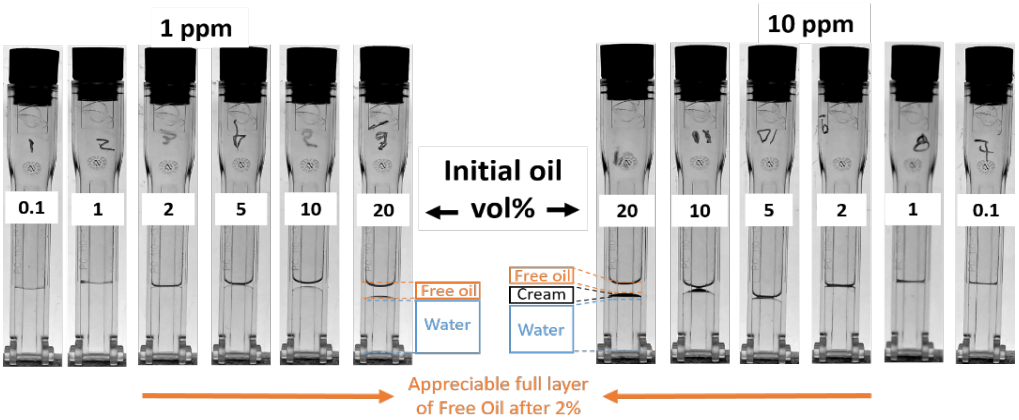

Figure 88 Mineral oil-water-SLE_1S emulsions at variable surfactant/oil concentrations. The picture was taken after the centrifugation cycle in LUMiSizer® (time=1.03 h. Centrifugation at RCA= 265 g)

Variable oil to surfactant ratio primary affected the droplet size and size distribution. With less surfactant available, the stabilization of newly created interface is diminished. Figure 89 shows the droplet size characterization for all emulsions. Despite a couple of rogue points, the harmonic mean droplet size (Figure 89a) stays consistent for each surfactant concentration. The harmonic mean droplet size increased with increasing oil concentration for emulsions with 1 ppm SLE_1S. Meanwhile, emulsions with 10 ppm SLE_1S showed a constant harmonic mean droplet size with increasing oil concentration. On the other hand, Figure 16b shows how the DSD for emulsions with 1ppm SLE_1S progressively merge towards the larger droplet size range at increasing oil concentrations. On the other hand, Figure 11c illustrates how the DSD for emulsions with 10 ppm SLE_1S consistently scattered around the average mean value with no clear trend but identical submicron droplet density.

The specific availability of SLE_1S surfactant molecules to saturate and stabilize the created interfaces during emulsification explains the results in Figure 11. Surfactant concentration (1 ppm or 10 ppm) dictates the maximum amount of stable interface. [168] As a result, the ration between oil concentration and surfactant concentration directly determines the resulting mean droplet size and DSD. [67] For instance, the increasing mean droplet size with increasing oil concentration for emulsions with 1ppm SLE_1S can be attributed to an insufficient surfactant concentration that caused quick coagulation and coalescence of unstable droplets during and after mixing. [169] Conversely, the stable mean droplet size depicted in emulsions stabilized with 10 ppm SLE_1S can be attributed to a partial stabilization effect. A 10 ppm SLE_1S concentration was not enough to completely stabilize the newly created interface but enough to maintain stable a more significant amount of interface than 1 ppm SLE_1S. Therefore, coalescence only occurred until the resulting interface was kinetically stable. [169]

The statements above are supported by the existence of stable droplets coagulated in the cream layer after centrifugation (See Figure 88) on emulsions stabilized with 10 ppm SLE_1S only. Figure 88 is the existence of a visible cream layer (dark shadow bellow second meniscus) for samples stabilized only with 10 ppm SLE_1S. The dark shadow that represented the cream layer was absent or non-visible for the samples stabilized with 1 ppm SLE_1S.

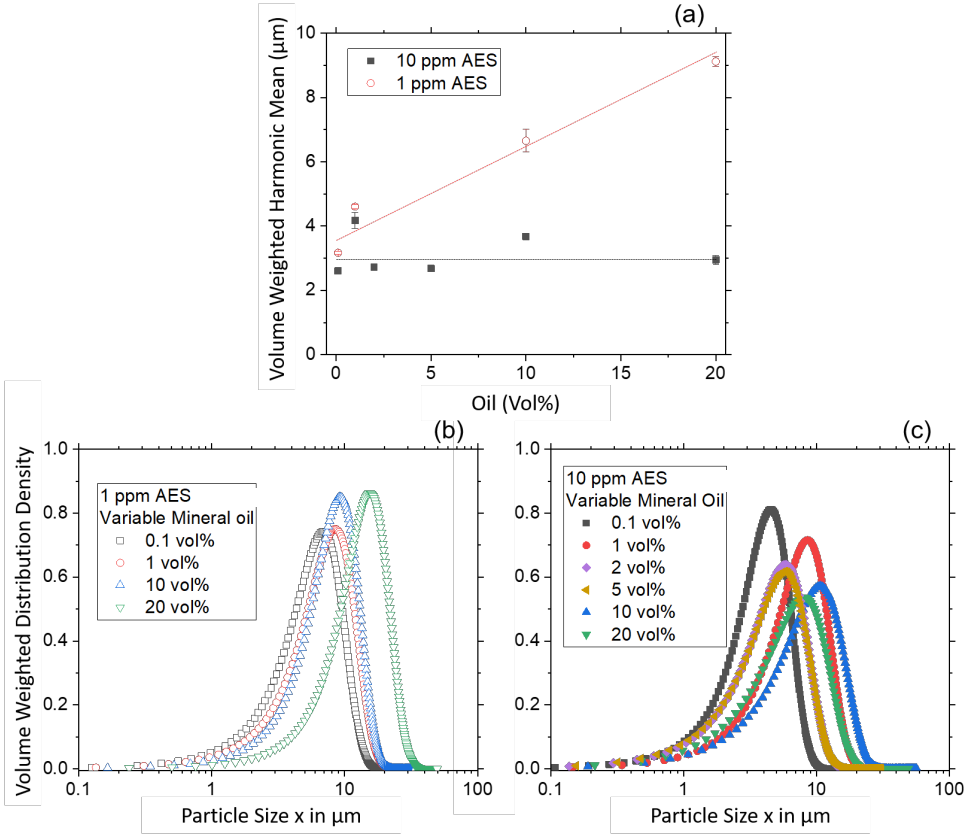

Figure 89. Droplet size characterization of mineral oil-water emulsions stabilized with SLE_1S. (a) Harmonic mean droplet size (b) DSD for emulsions with 1 ppm SLE_1S (c) DSD for emulsions with 10 ppm SLE_1S

Droplet size as a function of surfactant chemistry

Other factors that can contribute to the resulting droplet size on a given formula-mixer pair is surfactant chemistry. The molecular chemistry of surfactants can define the affinity for the oil as well as the absorption capabilities. Yet, it is important to clarify that surfactant coverage and absorption is linked not only to the ability of surfactant molecules to diffuse but also to the duration of turbulent regime. The last, is linked directly to the specific mixer used.

For instance, Figure 90 and Table 14 show the resulting droplet size of two emulsions mixed in an orifice mixer and stabilized with SLE_1S or Surfonic.

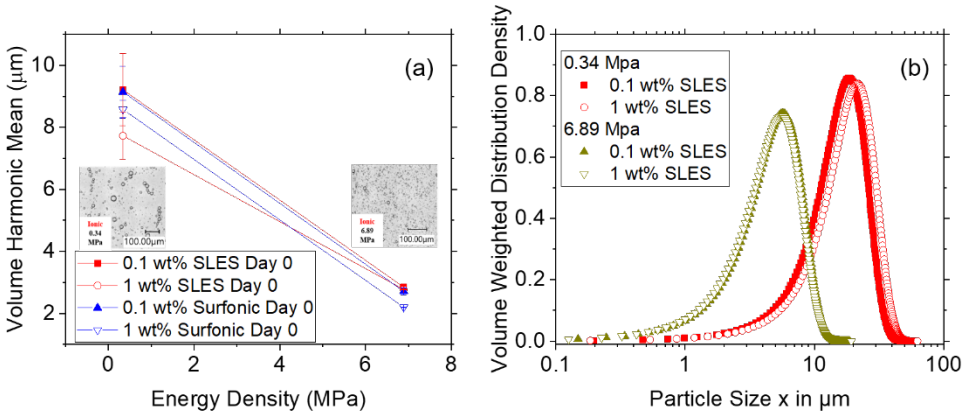

Figure 90. Mean droplet size as a function of energy density using the orifice mixer. Mineral oil–water emulsions fabricated with orifice mixer (a) Volume harmonic mean of emulsions stabilized with SLE_1S and Surfonic. (b) DSD for emulsions stabilized with SLE_1S at two different concentrations

Table 14. Summary of the harmonic mean droplet size for emulsions in Figure 53

Surfactant	0.1 wt% Surfactant		1 wt% Surfactant		Energy Density (MPa)
	Volume Harmonic Mean (µm)	Standard error	Volume Harmonic Mean (µm)	Standard error	
SLES (Ionic)	9.21	1.16	7.72	0.76	0.34
	2.84	0.049	2.77	0.02	6.89
Surfonic (non-ionic)	9.14	0.83	8.59	0.29	0.34
	2.71	0.11	2.20	0.01	6.89

Figure 90 and Table 14 show that the resulting droplet size of emulsions mixed with orifice mixer is independent of surfactant chemistry (SLE_1S or Surfonicic) or surfactant concentration (0.1 wt% or 1 wt%). These results suggest that the form of application of energy dominates over the different chemistries used to stabilize emulsions. That is, the duration of the turbulent regime in the orifice mixer is longer than the time that SLE_1S or Surfonic requires to fully populate the created interface. [56] Furthermore, these emulsions are in a rich-surfactant regime. In other words, the surfactant concentration is several orders of magnitude above their respective CMCs and all newly created surfaces are fully protected. [166]

Conversely, Figure *91* presents the resulting droplet size distribution of two emulsions mixed in a rotor-stator and stabilized with 1wt% SLE_1S or Surfonic.

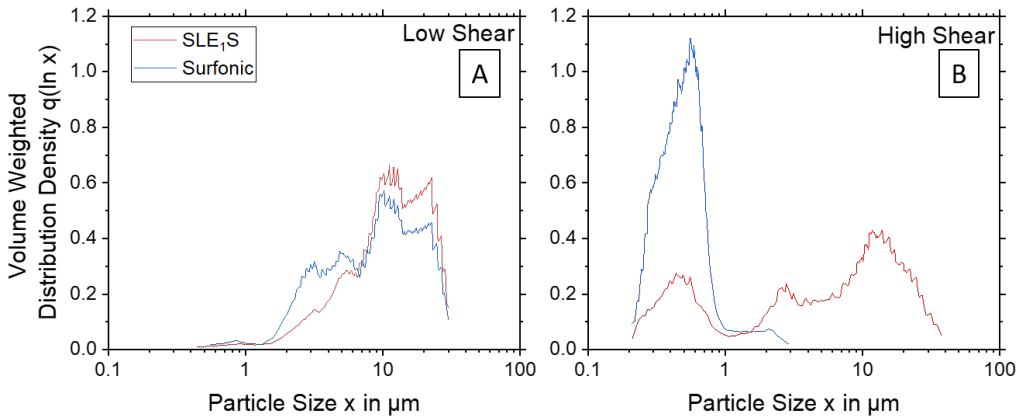

Figure 91. Size distribution as a function of two levels of energy density using a rotor stator. Mineral oil (5wt%) emulsions stabilized with 1 wt% SLE_1S or Surfonic (a) Rotor-stator at low shear (9500 rpm 1 min) (b) Rotor-stator at high shear (13500 rpm 5 min)

Figure *91* showed that the resulting droplet size behavior using a rotor-stator is dependent of the level of applied energy and surfactant chemistry. It is observed that emulsions stabilized with SLE_1S and Surfonic showed a relative similar behavior when mixing occurred at low energy densities. However, Surfonic oveperformed SLE_1S at high energy densities. Compared to SLE_1S, Surfonic was able to significantly reduce the droplet size when energy level rose.

Let us remember that an emulsion mixed with a rotor-stator experienced a repetitive series of turbulent and laminar regimes as the mix enter and leaves the mixing head. Also, the duration and continuity of the turbulent regime in a rotor-stator may be shorter than in an orifice mixer [56]. Hence, in this experiment, results show that surfactant chemistry dominates over the application of energy. In this specific case, the conditions of mixing favor molecules with larger polar heads such Surfonic (9 Ethoxylate groups) to diffuse generally faster to newly created interfaces.

Nevertheless, the level of the applied energy is not always dominant over chemistry behavior. Figure *92* shows the resulting droplet size distribution of two emulsions mixed in a rotor-stator and stabilized with 1wt% Sugante or Surfonic. The results presented in Figure *92* suggest that natural surfactant chemistries have similar behavior at high energy densities. That is, their absorption capabilities equal once shear conditions are increased. Yet, at low energy densities, Sugamulse tend to stabilize smaller droplets.

Let us remember that these are glucose-based surfactants. Their affinity for oil is based on the carbon chain length and water affinity is based on the nature of their amphiphilic group but also on the amount of hydroxyl groups (-OH) attached to the whole length of their backbone. Sugamulse is a non-ionic crosspolymer surfactant and Suganate is an anionic surfactant with a sulfonate group.

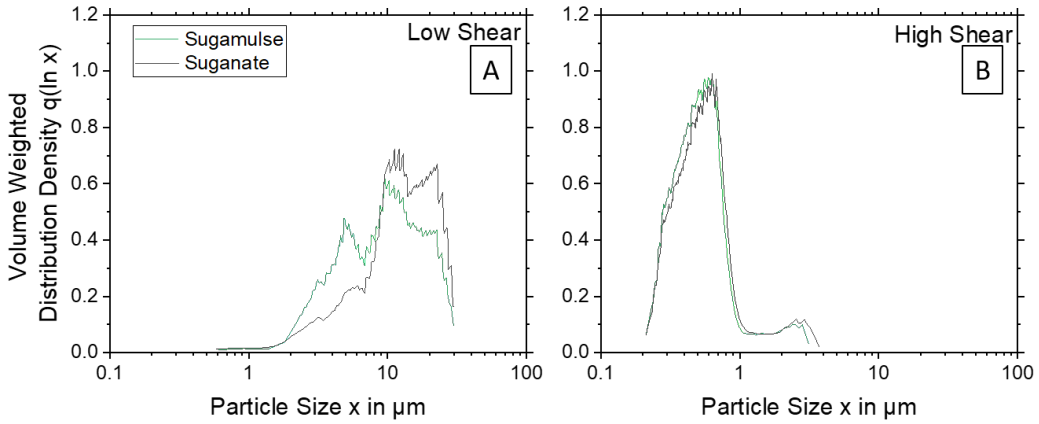

Figure 92 Size distribution as a function of two levels of energy density using a rotor stator. Mineral oil (5wt%) emulsions stabilized with 1 wt% Sugamulse or Suganate (a) Rotor-stator at low shear (9500 rpm 1 min) (b) Rotor-stator at high shear (13500 rpm 5 min)

Droplet Size as a Function of Ageing Time

Aging of emulsions was not a primary goal for this study. Yet, the following experiment show a brief learning exercise embedded within the larger experimental body. Figure *93* shows the resulting droplet size behavior to increasing mineral oil concentration (0.5 wt% to 20 wt%) for model emulsions mixed with constant energy density (3.45 MPa) and stabilized with SLE_1S 1 wt%.

Figure *93*a shows a constant median droplet size (day 0) for all emulsions that contains up to 5 wt% mineral oil. Further increase in oil concentration produced a proportional increase in droplet size. These insights are also reflected in their respective size distribution (day 0) which is shown in Figure 84b. Only the size distributions of emulsions containing 10 wt% and 20 wt% oil are shifted toward populations of greater sizes.

As expected, emulsion aging resulted in the grow of droplets which turned to be proportional to initial oil concentration. It is observed in Figure *93*a that median size is increased after 90 days of aging. The median droplet increased evenly around 3 µm on emulsions with oil concentrations up to 5 wt%. Emulsion with 10 wt% and 20 wt% oil showed a more significant increase with 11 µm and 13 µm respectively. The increase in median droplet size is better observed in Figure *93*c. Depopulation of near submicron droplets and an increase in population of droplets above 10 µm is more significant for emulsions with 10 wt% and 20 wt%.

These results are just expected. It is true that two immiscible liquids can coexist in the form of stable emulsions. However, droplets within the emulsion are kinetically trapped but still are thermodynamically unstable. It is a matter of appropriate timescales for emulsions to become two fully separated phases again. In this case, it takes long times (90 days) and high oil concentrations (10 to 20 wt%) to show significant change in droplet size. The high surfactant to oil ratio can lead to higher repulsions due to the creation of self-organized surfactant structures

between droplets. [170] once this ratio is reduced, the shielding action of SLE_1S (electrostatic) is not enough to overcome the desire of mineral oil droplets to reach each other.

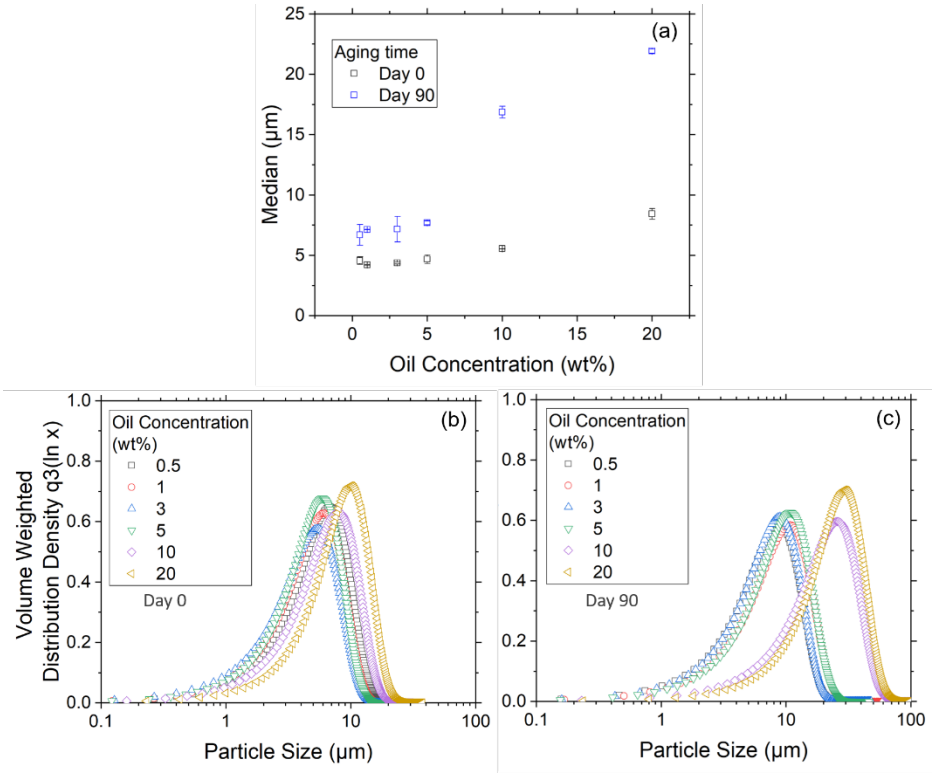

Figure 93 Droplet size and size distribution of model emulsions with variable dispersed phase concentration at 0 and 90 days of aging. Model emulsions: mineral oil ranging between 0.5 wt% to 20 wt%, SLE_1S at 1 wt%, and energy density of 3.45 MPa. (a) Median droplet size as a function of mineral oil concentration at 0 and 90 days. (b) Volume distribution density as a function of droplet size for day 0. (c) Volume distribution density as a function of droplet size for day 90.

Impact of processing routes on creaming dynamics

Creaming behavior was evaluated using the clarification rate, creaming velocity, or instability index. Either of these parameters represent a change in droplet concentration as a function of centrifugation time. These parameters are proportional to the mean displacement of droplets, which in turn is proportional to diameter of the individual oil droplets (Equation 2) and the droplet concentration. As a result, the creaming behavior can be inferred from the droplet size distribution and an integral analysis of number of droplets based on oil concentration.

Creaming as a function of droplet size distribution

For this experiment, Canola oil (5 wt%) and water emulsions stabilized with SLE_1S or Surfonic (1 wt%) were fabricated. The emulsions were mixed using the rotor-stator at 19 MPa or 226 MPa. Figure *94*a shows the droplet size and DSD, and Figure *94*b shows their respective

accelerated creaming results. The result in Figure *94*b can be analyzed using the slope of integral transmission% over time plot which is called the clarification rate.

Figure *94*a shows that emulsions mixed at low energy densities (19 MPa) have similar harmonic mean droplet size (H) and similar DSD with a high concentration of droplets above 10 µm. Conversely, at high energy density (226 MPa), the resulting droplet size and DSD is dissimilar and as expected the population of droplets shifted toward the near submicron range.

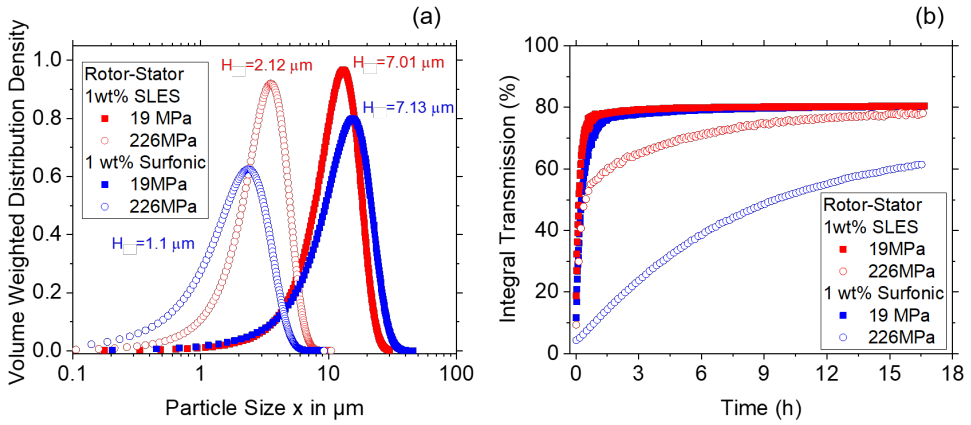

Figure 94 Canola oil - water emulsion stabilized with SLE_1S or Surfonic at 1wt%. Rotor-stator at 19 and 226 MPa. (a) Resulting harmonic mean droplet size and DSD (b) Clarification rate (slope of the initial linear part of curve)

Hence, the observed clarification rate in Figure *94*b can be attributed to the droplet size behavior. First, the increasing clarification rate as energy density decreases is solely due to differences in the resulting mean droplet size. The explanation is simplified if we consider dilute-emulsions with considerably different droplet dimensions (H). Since the square of the droplet size dictates the velocity at which droplets move (Equation 2), a 7 µm droplet could cream 45 times faster than a 2 µm droplet.

However, the justification for the clarification rate must include an analysis of the whole DSD. Concentrated emulsions have a high probability for droplet – droplet collision, which reduces the free movement of droplets. [61] As a result, the reduction of motion is proportional to dispersed phase concentration and droplet concentration (number of droplets). [68]

Furthermore, the clarification of polydispersed emulsions is the result of the convoluted interaction of all different size-groups. [85] An individual size-group with a predominant concentration will carry the weight of the clarification rate of an emulsion. For instance, Surfonic and SLE_1S stabilized emulsions with similar DSD at 19 MPa. Consequently, their clarification rate is almost identical because the concentration of the specific size-groups is equivalent. On the other side, emulsions mixed at 226 MPa, which depicted considerable differences in DSD, showed very different clarification rates. Besides the apparent difference in harmonic mean size, emulsions stabilized with Surfonic showed a higher concentration of submicron droplets and a lower concentration of larger droplets. The high concentration of tiny droplets produces a dual

effect: slow terminal velocities due to size and high probability of collision due to high droplet number.

Creaming behavior as a function of oil and surfactant concentration

Figure *95* shows the creaming behavior for emulsions stabilized with 1 ppm and 10 ppm SLE_1S and variable oil concentration. The creaming behavior is characterized using the instability index and creaming velocity. The instability index represents the level of phase separation as a function of centrifugation time. This index is a normalized index, then 0 represent the original state of the emulsion and 1 represent the maximum phase separation. Similarly, the creaming velocity represent the average displacement of droplets. It is a quantification of creaming.

Figure *95*a and Figure *95*b (1 ppm SLE_1S emulsions) show the same instability index and creaming velocity independently of oil concentration. On the other hand, Figure *95*c and Figure *95*d (10 ppm SLE_1S emulsions) depict an instability index and a creaming velocity that reduces with increasing oil concentration. If only instability index and measured creaming velocity are analyzed, one may conclude that increasing oil concentration sustain or diminish the phase separation behavior.

It was demonstrated that emulsions with initial oil concentrations higher than 1 vol% developed a top layer of free-oil, which was proportional to the initial oil concentration. AS a result, the calculation of instability index and creaming velocity does not consider the separation of this oil, which is translucent to the light sensor for being free oil. Therefore, the measured instability index did not correlate the ability of these emulsions to keep the full amount of initial oil stabilized. Instead, the measured instability index may represent the number of scattering surfaces or stable droplets that move within the bulk of the emulsion during testing. Such volume of droplets is lower than original volume of oil.

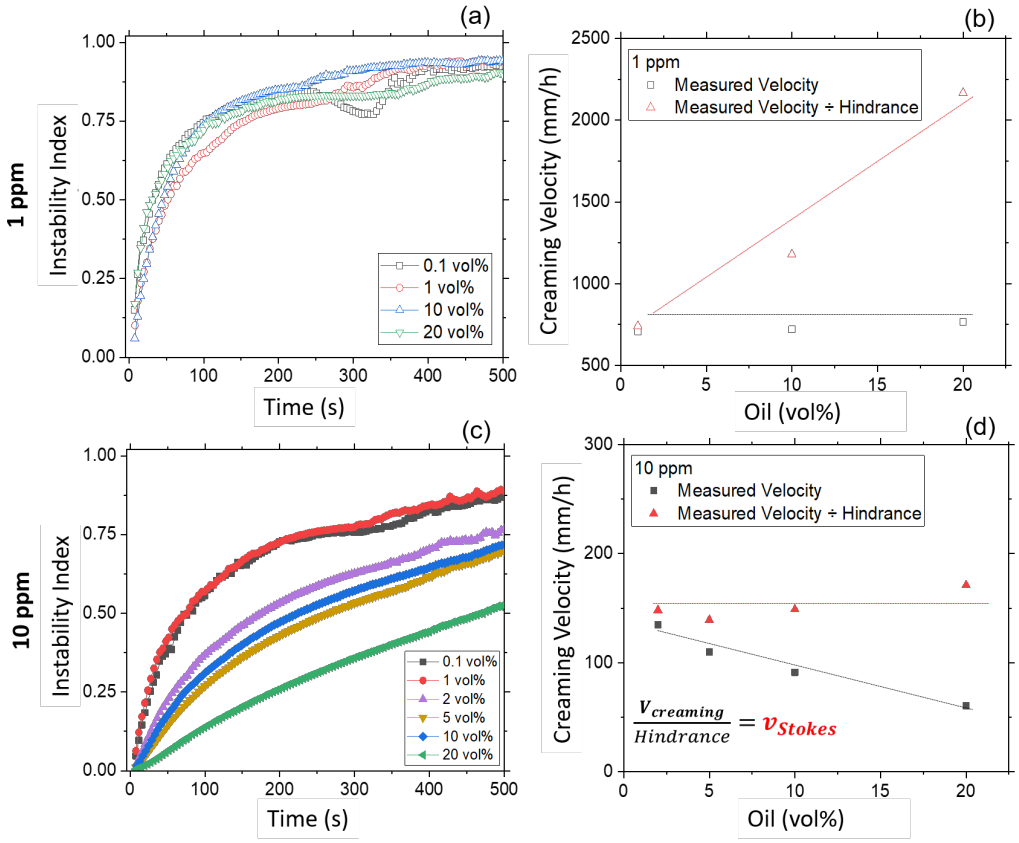

Figure 95: Creaming dynamics characterization of Mineral oil - water emulsions stabilized with SLE_1S (a) Instability index of emulsions with 1 ppm SLE_1S (b) Creaming velocity of emulsions with 1 ppm SLE_1S (c) Instability index of emulsions with 10 ppm SLE_1S (d) Creaming velocity of emulsions with 10 ppm SLE_1S

Yet, the results in Figure *95*b and Figure *95*d can be useful. All droplets are produced proportionally in density and number with increasing oil concentration during mixing. However, big-size droplets cream and coalesce faster than small droplets under centrifugation. [60] The above makes big-size droplets very prone to form super-droplets (free-oil) with deficient scattering properties. [85] Consequently, the analysis of the creaming velocity can be weighted on the contribution of the small droplets and their synergy with free-oil.

Submicron droplets constrains to a higher degree the individual flow of free-oil. [169]. Then, accounting for oil concentration hindrance can yield a more useful set of results. For instance, the red curve in Figure *95*b and Figure *95*d represents the stokes terminal velocity calculation using the Richardson-Zaki hindrance function. [62] The correction for dispersed phase concentration yielded very consistent results that agreed precisely to the expected behavior of the harmonic mean droplet size. The Navier-Stokes terminal velocity for emulsions with 1 ppm SLE_1S increased with increasing oil concentration. Meanwhile, constant Navier-Stokes terminal velocity was observed with increasing oil concentration for emulsions with 10 ppm SLE_1S.

Remnant Oil measurement

To measure the mass of oil that do not make it to the cream layer, an UV-VIS protocol was developed. An UV-VIS spectrometer measures the intensity of the transmitted light compared to the incident light (Transmittance relative to Absorbance) when monochromatic light travels through a sample in a wide range of wavelengths. This principle can be used to measure droplet concentration by using a linear fit such as the one observed in the Lambert-Beer law described in Equation 2. [171]

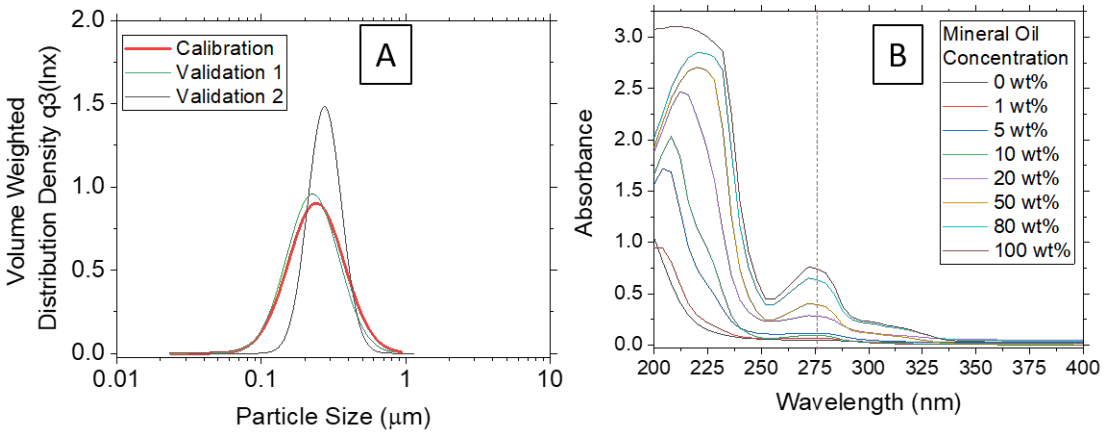

Figure 96 Calibration curve data. (a) droplet size distribution after homogenization. (b) characteristic peak for mineral oil solutions in isooctane. O% represent pure isooctane and 100% represents pure mineral oil.

Two important steps on the development of a successful linear fit are achieving a homogeneous sample and the identification of the characteristic wave lengths to measure. First, Figure *96*a shows the respective DSD for the calibration curve after the homogenization protocol. The homogenization protocol should be design so that all samples including the calibration emulsion have very similar DSD. This step assures that light interaction can be accurately correlated to number of droplets in a repetitive manner. Second, Figure *96*b shows one of two points used to measure. The peak at 276nm of the mineral oil solutions was identified as a characteristic peak to measure. The second characteristic peak selected was 800 nm as previously recommended by different literature references.

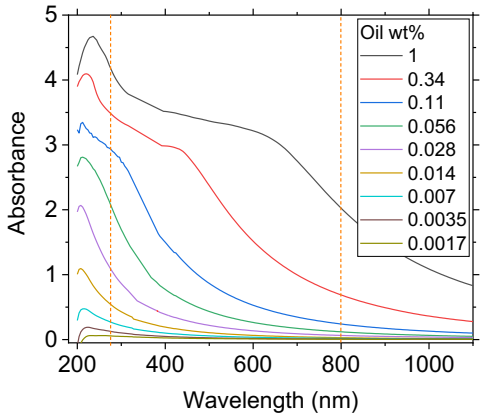

Figure 97*:* Absorbance of calibration emulsions

The construction of the calibration fit starts with the measurement of absorbance in samples with calibrated oil-concentration. Figure 97 shows the absorbance signal of each calibrated emulsion as a function of wavelength and oil or droplet concentration. As expected, droplet concentration played a significant role on the absorbance readings. Yet, only values of absorbance between 0.05 and 1 were used to create two linear fits: $A_{276} = 32.28 \pm 0.5 * C$; where A_{276} is measured absorbance at 276 nm and C is mineral oil concentration in wt% and $A_{800} = 2.02 \pm 0.01 * C$. Both fittings are linear models with fixed intercept equal to zero and adjusted R-square parameters above 0.99. The calibration fits above were validated by measuring validation emulsion with known oil concentration. This validation yielded reading with errors within an acceptable 10% deviation.

Once the calibration curve is ready, measurement of samples can start. Figure 98a shows the remnant oil results for emulsions mixed with variable energy density and constant oil concentration (5 wt% oil - 1 wt% SLE_1S). Figure 98 shows the remnant oil results for emulsions with variable oil concentration mixed under a constant energy density (3.45 MPa – 1 wt% SLE_1S).

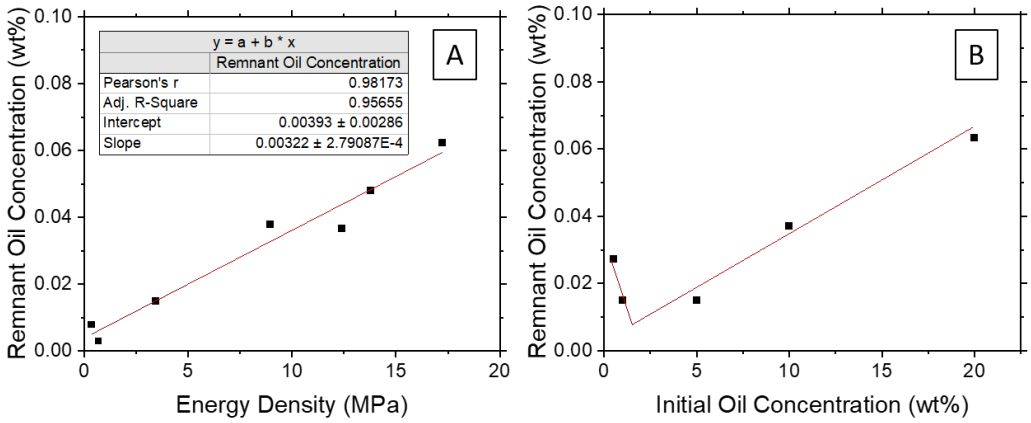

Figure 98. Remnant oil of aged emulsions mixed with an orifice mixer. (a) emulsions mixed with variable energy density and constant oil concentration (5 wt% oil - 1 wt% SLE1S) (b) emulsions with variable oil concentration mixed under a constant energy density (3.45 MPa – 1 wt% SLE1S)

It is observed in Figure 98 that measured remnant oil increases linearly with increasing energy density. The linear fit between these two parameters shows an adjusted R square value greater than 0.95. On the other hand, Figure 98b exhibit a non-monotonic relationship between the initial oil concentration and the remnant oil. The spline lines in Figure 98b suggest the possible existence of a lowest point for remnant oil concentration about 1 wt% to 2 wt% initial oil concentration. After this point, the remnant oil increases linearly with increasing initial oil concentration.

The remnant oil behavior in Figure 98 can be attributed and correlated to the resulting droplet size distributions. Near submicron droplet are most likely to fluctuate without a real displacement because they are affected by thermal fluctuations. Thus, the remnant oil concentration is proportional to the number of droplets under Brownian motion.

The idea above is supported by the results shown in the creaming dynamic section. All emulsion with a high concentration of near submicron droplets depicted a slow creaming behavior. Yet, the results in Figure 98 are contrasting. A minimum value of remnant oil found to be between 1 wt% and 2 wt% initial oil concentration contradict the initial assumption. It has been previously discussed that the concentration of near submicron droplets are drivers of slow creaming behavior due to size, but also due to hindrance effects. In this case, the behavior shown in Figure 98b is affected the most by hindrance. At very low levels of oil concentration, the number of droplets is low and hence their interaction is near non-existing. So, it would be expected that remanat oil would be minimal which I clearly not the case in Figure 98. Still, the reasons for this behavior are unknown and requires further research.

Conclusions and Implications for Future Research

The core of this report focused in crating correlations between emulsion processing routes, chemistry of surfactants, droplet size characterization and creaming behavior.

The following main points can be drawn related to energy input on emulsion stability:

- Increasing energy density results in the formation of smaller droplets. Yet, this relationship is not linear. A power law was found using the orifice mixer set up.
- The droplet size distribution is dependent not only on the energy density but also on the method of emulsification and surfactant concentration.
- The resulting droplet size and droplet size distribution is direct responsible of the creaming behavior of the studied emulsions. Near submicron droplets are drivers of slower creaming. This statement is supported by creaming studies and remnant oil measurements.
- The concentration of submicron droplets is not only attached to energy density, but also to the initial oil and surfactant concentration used in the formulation of emulsions.
- Big droplets in the form of free oil accelerates creaming behavior. Since creaming velocity is proportional to diameter square, big droplets cream at high velocities.
- 0.1 wt% and 1 wt% surfactant concentrations are relative good at keep stable up to 5 wt% oil. Further oil concentrations lead to coalescence and faster creaming.
- Droplet size for rich-surfactant emulsions is linked to energy density. Droplet size for poor surfactant emulsions is linked to surfactant availability.
- Submicron size droplet are the main cause of worry from the environmental point of view. They move slow, isolate themselves due to thermal effects and are difficult to capture. These are the source of increasing the operational cost necessary for complete oil removal. Coalescence may be the right way to approach this situation

The work presented in this document shows that once a minimum surfactant concentration is reached, *emulsification due to dynamic ageing is inevitable*. Therefore, the most practical way to support oil removal of bilgewater is to lower the total surfactant concentration.

Emulsion stability against coalescence for model bilgewater systems depends on the surfactant type, surfactant concentration, and ageing conditions. For both static and dynamic ageing conditions, SLES stabilized oil drops at a lower concentration than Triton X-100. This behavior is due to a higher surface concentration for SLES and 0.42 M NaCl, to which more surfactant molecules can pack at the oil-water interface to prevent coalescence. However, if the Triton X-100 concentration was large enough, coalescence was hindered just as effectively as SLES and salt. For statically aged emulsions, coalescence was observed for surfactant concentrations < 10 ppm SLES and < 100 ppm Triton X-100 . Dynamic ageing encouraged coalescence at surfactant concentrations ≤ 100 ppm and drop break up at ≥ 500 ppm for both SLES and Triton X-100. Thus, the energy added due to ship rocking alters the minimum amount of surfactant required to

make a thermodynamically stable emulsion. These results show that the movement of bilgewater during storage affects the stability of O/W emulsions and can aid or convolute oil filtration.

A solution to prevent emulsion formation during ship rocking includes the possible redesign of the bilge tank by investigating the behavior of O/W emulsions when the amount of air within the emulsification chamber is reduced during dynamic ageing. At 70% air inside the ageing vial, sloshing is responsible for drop formation and coalescence. Therefore, reducing the amount of air within the emulsification chamber will limit the sloshing and inhibit further emulsion formation and possible coalescence.

This work additionally provides a fundamental understanding of the mechanisms governing spontaneous emulsification, knowledge of which is valuable for optimizing nanoemulsion fabrication as well as controlling or preventing spontaneously formed emulsions in oily wastewater. The components studied here are found in many wastewater systems and could lead to the formation of nanoemulsions that may be difficult to detect and remove during water treatment operations. And although the emulsions displayed limited stability under static laboratory conditions, it is rarely the case that wastewater is stationary for extended amounts of time. Thus, spontaneously formed oil droplets could be dispersed indefinitely in wastewater depending on environmental and processing conditions (e.g., mixing, presence of salts, additional surfactants).

Spontaneous emulsification was observed in different SOW systems. The influence of surfactant ratio, salinity and oil type were investigated and the corresponding HLD_{mix} values were calculated. The conclusions were as follows:

- HLD_{mix} was changed by adjusting surfactant ratio, salinity, and oil type. Overall, increasing salinity, increasing the proportion of Span-80 (or decreasing proportion of SLES), and reducing the EACN led to a higher HLD_{mix}. Spontaneous emulsification was only observed when the HLD_{mix} was between -1.1 to 0.7 in the systems studied. The spontaneity increased in both oil and aqueous phases when the HLD_{mix} approached 0. With a negative HLD_{mix}, the spontaneity in the aqueous phase (forming o/w emulsion) was always greater than that in the oil phase (forming w/o emulsion), and vice versa. When the HLD_{mix} was in the transition range (-0.27 to 0.12 in our systems), significant spontaneous emulsification could be observed within 20 minutes in both oil and aqueous phases and these systems displayed the largest spontaneity.
- Spontaneous emulsification was observed in many different oils, even the non-aromatic one (e.g., paraffin oil). This result indicates many oils collected in bilge water could spontaneously emulsify when an appropriate HLD_{mix} was reached.
- *HLD_{mix} is a good model to use in predicting spontaneous emulsions and can be used by DoD to select preferred cleaning agents to be more compatible with preventing spontaneous emulsions within bilgewater*

Spontaneous emulsification is a complex phenomenon governed by many different mechanisms and involving several variables. The chemical compositions and conditions used to produce spontaneous emulsions have been largely trial and error until recently.[1] This work provides further development of the HLD model as a practical way to guide what salinity, surfactant composition, and oil type creates the conditions favorable (unfavorable) to promote (prevent) spontaneous emulsification. HLD_{mix} calculations agreed well with the experimental results in this study. This

model also has limitations. This simplified method predicted emulsion phase transitions reasonably well considering the significant simplification in using the rule of mixtures instead of the more complicated and time-consuming mixed micelle model.[1] Further characterization of the interfacial surfactant packing, and more experimental data of different systems would be helpful to consolidate this empirical model.

Literature Cited

1. Davis CR, Martinez CJ, Howarter JA, Erk KA. Predicting Spontaneous Emulsification in Saltwater Environments Using the HLD Model. *Lanmguir*. 2021;37(29):8866-8875. doi:10.1021/acs.langmuir.1c01277
2. Zheng Y, Caicedo-Casso EA, Davis CR, Howarter JA, Erk KA, Martinez CJ. Impact of mixed surfactant composition on emulsion stability in saline environment: anionic and nonionic surfactants. *J Dispers Sci Technol*. 2021. doi:10.1080/01932691.2021.1999255/SUPPL_FILE/LDIS_A_1999255_SM3836.JPG
3. Sabatello RG. IMPACT OF DYNAMIC AGEING ON THE FORMATION AND STABILITY OF MODEL BILGE WATER OIL-IN-WATER EMULSIONS. December 2021. doi:10.25394/PGS.17147681.V1
4. Davis CR, Martinez CJ, Howarter JA, Erk KA. Diffusion-Controlled Spontaneous Emulsification of Water-Soluble Oils via Micelle Swelling. *Langmuir*. 2020;36(26):7517-7527. doi:10.1021/ACS.LANGMUIR.0C01121
5. Zheng Y, Davis CR, Howarter JA, Erk KA, Martinez CJ. Spontaneous Emulsions: Adjusting Spontaneity and Phase Behavior by Hydrophilic-Lipophilic Difference-Guided Surfactant, Salt, and Oil Selection. *Langmuir*. 2022;38(14):4276-4286. doi:10.1021/ACS.LANGMUIR.1C03444/SUPPL_FILE/LA1C03444_SI_017.MP4
6. Davis CR, Martinez CJ, Howarter JA, Erk KA. Impact of saltwater environments on the coalescence of oil-in-water emulsions stabilized by an anionic surfactant. *ACS ES&T Water*. 2021;1(8):1702-1713. doi:10.1021/acsestwater.1c00066
7. Tomaszewska M, Orecki A, Karakulski K. Treatment of bilge water using a combination of ultrafiltration and reverse osmosis. *Desalination*. 2005;185(1-3):203-212. doi:10.1016/j.desal.2005.03.078
8. Nordvik AB, Simmons JL, Bitting KR, Lewis A, Strøm-Kristiansen T. Oil and water separation in marine oil spill clean-up operations. *Spill Sci Technol Bull*. 1996;3(3):107-122. doi:10.1016/S1353-2561(96)00021-7
9. Mclaughlin C, Falatko D, Danesi R, Albert R. Characterizing shipboard bilgewater effluent before and after treatment. *Environ Sci Pollut Res*. 2014;21(8):5637-5652. doi:10.1007/s11356-013-2443-x
10. Ghidossi R, Veyret D, Scotto JL, Jalabert T, Moulin P. Ferry oily wastewater treatment. 2009;64:296-303. doi:10.1016/j.seppur.2008.10.013
11. Körbahti BK, Artut K. Electrochemical oil/water demulsification and purification of bilge water using Pt/Ir electrodes. *Desalination*. 2010;258(1-3):219-228. doi:10.1016/j.desal.2010.03.008
12. Wang JM, Xia N, Yang XQ, et al. Adsorption and dilatational rheology of heat-treated soy protein at the oil-water interface: Relationship to structural properties. *J Agric Food Chem*. 2012;60(12):3302-3310. doi:10.1021/jf205128v
13. Howarter J a, Youngblood JP. Amphiphile grafted membranes for the separation of oil-in-water dispersions. *J Colloid Interface Sci*. 2009;329(1):127-132. doi:10.1016/j.jcis.2008.09.068
14. Sharipova A, Aidarova S, Mucic N, Miller R. Dilational rheology of polymer/surfactant mixtures at water/hexane interface. *Colloids Surfaces A Physicochem Eng Asp*.

2011;391(1-3):130-134. doi:10.1016/j.colsurfa.2011.04.035
15. Nash JJ, Erk KA. Stability and Interfacial Viscoelasticity of Oil-Water Nanoemulsions Stabilized by Soy Lecithin and Tween 20 for the Encapsulation of Bioactive Carvacrol. *Colloids Surfaces A Physicochem Eng Asp*. 2016:(Accepted/in press) doi: 10.1016/j.colsurfa.2016.1. doi:doi: 10.1016/j.colsurfa.2016.12.056
16. Georgieva D, Schmitt V, Leal-Calderon F, Langevin D. On the possible role of surface elasticity in emulsion stability. *Langmuir*. 2009;25(10):5565-5573. doi:10.1021/la804240e
17. Bécu L, Manneville S, Colin A. Yielding and Flow in Adhesive and Nonadhesive Concentrated Emulsions. *Phys Rev Lett*. 2006;96(13):138302. doi:10.1103/PhysRevLett.96.138302
18. Yuan S, Tong M, Wu G. Destabilization of emulsions by natural minerals. *J Hazard Mater*. 2011;192(3):1882-1885. doi:10.1016/j.jhazmat.2011.06.047
19. Hanafy M, Nabih HI. Environmental Effects Treatment of Oily Wastewater Using Dissolved Air Flotation Technique Treatment of Oily Wastewater Using Dissolved Air. 2016;7036(December). doi:10.1080/009083190948711
20. Boyd J, Parkinson C, Sherman P. Factors affecting emulsion stability, and the HLB concept. *J Colloid Interface Sci*. 1972;41:359-370.
21. Abbott PS. Surfactant Science : Principles and Practice. 2015.
22. Acosta EJ, Kiran SK, Hammond CE. The HLD-NAC model for extended surfactant microemulsions. *J Surfactants Deterg*. 2012;15(4):495-504. doi:10.1007/s11743-012-1343-2
23. Salager JL, Forgiarini A, Marquez L, et al. Using emulsion inversion in industrial processes. *Adv Colloid Interface Sci*. 2004;108-109:259-272. doi:10.1016/j.cis.2003.10.008
24. Zarate-Munoz S, Texeira De Vasconcelos F, Myint-Myat K, Minchom J, Acosta E. A Simplified Methodology to Measure the Characteristic Curvature (Cc) of Alkyl Ethoxylate Nonionic Surfactants. *J Surfactants Deterg*. 2016;19(2):249-263. doi:10.1007/s11743-016-1787-x
25. Edgar Acosta †, Erika Szekeres †, David A. Sabatini *,‡ and, Jeffrey H. Harwell† §. Net-Average Curvature Model for Solubilization and Supersolubilization in Surfactant Microemulsions. 2002. doi:10.1021/LA026168A
26. Chevron. TEP Turbine Oil. MSDS No. 4764. http://qclubricants.com/msds/CHEVRON_turbine_2190_TEP_msds.pdf. Published 2015. Accessed February 27, 2017.
27. Acosta EJ. The HLD-NAC equation of state for microemulsions formulated with nonionic alcohol ethoxylate and alkylphenol ethoxylate surfactants. *Colloids Surfaces A Physicochem Eng Asp*. 2008;320(1-3):193-204. doi:10.1016/j.colsurfa.2008.01.049
28. Abbott SB. fishtail.php.stevenabbott.co.uk. https://www.stevenabbott.co.uk/practical-surfactants/fishtail.php. Accessed February 20, 2017.
29. Jin L, Jamili A, Li Z, et al. Physics based HLD–NAC phase behavior model for surfactant/crude oil/brine systems. *J Pet Sci Eng*. 2015;136:68-77. doi:10.1016/j.petrol.2015.10.039
30. Li JB, Kretzschmar G, Miller R, Möhwald H. Viscoelasticity of phospholipid layers at different fluid interfaces. *Colloids Surfaces A Physicochem Eng Asp*. 1999;149(1-3):491-497. doi:10.1016/S0927-7757(98)00729-8
31. Shchipunov Y a, Schmiedel P. Phase behavior of lecithin at the oil/water interface. *Langmuir*. 1996;7463(13):6443-6445. doi:10.1021/la960082y

32. Shchipunov Y a. Lecithin organogel: A micellar system with unique properties. *Colloids Surfaces A Physicochem Eng Asp*. 2001;183-185:541-554. doi:10.1016/S0927-7757(01)00511-8
33. Kumar R, Katare OP. Lecithin organogels as a potential phospholipid-structured system for topical drug delivery: a review. *AAPS PharmSciTech*. 2005;6(2):E298-E310. doi:10.1208/pt060240
34. Cicuta P, Terentjev EM. Viscoelasticity of a protein monolayer from anisotropic surface pressure measurements. *Eur Phys J E*. 2005;16(2):147-158. doi:10.1140/epje/e2005-00016-y
35. Russev SC, Alexandrov N, Marinova KG, et al. Instrument and methods for surface dilatational rheology measurements. *Rev Sci Instrum*. 2008;79(10):1-10. doi:10.1063/1.3000569
36. Kotula AP, Anna SL. Regular perturbation analysis of small amplitude oscillatory dilatation of an interface in a capillary pressure tensiometer. *J Rheol (N Y N Y)*. 2015;59(1):85-117. doi:10.1122/1.4902546
37. Wan Z-L, Wang L-Y, Wang J-M, Yuan Y, Yang X-Q. Synergistic Foaming and Surface Properties of a Weakly Interacting Mixture of Soy Glycinin and Biosurfactant Stevioside. *J Agric Food Chem*. 2014;62:6834-6843.
38. Cascão Pereira LG, Théodoly O, Blanch HW, Radke CJ. Dilatational Rheology of BSA Conformers at the Air/Water Interface. *Langmuir*. 2003;19(6):2349-2356. doi:10.1021/la020720e
39. Ravera F, Ferrari M, Santini E, Liggieri L. Influence of surface processes on the dilational visco-elasticity of surfactant solutions. *Adv Colloid Interface Sci*. 2005;117(1-3):75-100. doi:10.1016/j.cis.2005.06.002
40. Ravera F, Loglio G, Kovalchuk VI. Interfacial dilational rheology by oscillating bubble/drop methods. *Curr Opin Colloid Interface Sci*. 2010;15(4):217-228. doi:10.1016/j.cocis.2010.04.001
41. Dicharry C, Arla D, Sinquin A, Graciaa A, Bouriat P. Stability of water/crude oil emulsions based on interfacial dilatational rheology. *J Colloid Interface Sci*. 2006;297(2):785-791. doi:10.1016/j.jcis.2005.10.069
42. Leser ME, Acquistapace S, Cagna A, Makievski A V., Miller R. Limits of oscillation frequencies in drop and bubble shape tensiometry. *Colloids Surfaces A Physicochem Eng Asp*. 2005;261(1-3):25-28. doi:10.1016/j.colsurfa.2004.11.043
43. Derkach SR, Krägel J, Miller R. Methods of measuring rheological properties of interfacial layers (Experimental methods of 2D rheology). *Colloid J*. 2009;71(1):1-17. doi:10.1134/S1061933X09010013
44. Yeung A, Dabros T, Masliyah J. Dissipative interfaces and departures from the Young-Laplace equation. *Langmuir*. 1997;13(13):6597-6606. doi:10.1021/la9706835
45. McClements DJ. *Food Emulsions Principles, Practices, and Techniques*. CRC Press; 2005. doi:10.1093/acprof:oso/9780195383607.003.0002
46. Berry JD, Neeson MJ, Dagastine RR, Chan DYC, Tabor RF. Measurement of surface and interfacial tension using pendant drop tensiometry. *J Colloid Interface Sci*. 2015;454:226-237. doi:10.1016/j.jcis.2015.05.012
47. Malvern Panalytical. Basic principles of particle size analysis. Technical report [Application Note]. 2013.
48. Caplan J, Newton C, Kelemen D. Tech-Report-Novel-OilWater-Separator.pdf. 2000:111-

115.
49. Hunter JR. *Introduction to Modern Colloid Science*. Oxford, UK; 1993. doi:10.1524/zpch.1995.189.part_2.277a
50. McClements DJ. *Principles, Practicies, and Techniques*. Vol 2.; 2005.
51. McClements DJ. Critical review of techniques and methodologies for characterization of emulsion stability. *Crit Rev Food Sci Nutr*. 2007;47(7):611-649. doi:10.1080/10408390701289292
52. Hunter JR. *Foundations of Colloid Science*. Vol 1. Oxford, UK; 1986. doi:10.1016/s0927-7757(02)00170-x
53. Narayan S, Metaxas AE, Bachnak R, Neumiller T, Dutcher CS. Zooming in on the role of surfactants in droplet coalescence at the macroscale and microscale. *Curr Opin Colloid Interface Sci*. 2020;50:101385. doi:10.1016/j.cocis.2020.08.010
54. Egger H, McGrath KM. Aging of oil-in-water emulsions: The role of the oil. *J Colloid Interface Sci*. 2006;299(2):890-899. doi:10.1016/j.jcis.2006.03.022
55. Malassagne-Bulgarelli N, McGrath KM. Emulsion ageing: Effect on the dynamics of oil exchange in oil-in-water emulsions. *Soft Matter*. 2013;9(1):48-59. doi:10.1039/c2sm26229k
56. Schultz S, Wagner G, Urban K, Ulrich J. High-Pressure Homogenization as a Process for Emulsion Formation. *Chem Eng Technol*. 2004;27(4):361-368. doi:10.1002/ceat.200406111
57. John TP, Panesar JS, Kowalski A, Rodgers TL, P. Fonte C. Linking power and flow in rotor-stator mixers. *Chem Eng Sci*. 2019;207:504-515. doi:10.1016/j.ces.2019.06.039
58. Özcan-Taşkın G, Kubicki D, Padron G. Power and flow characteristics of three rotor-stator heads. *Can J Chem Eng*. 2011;89(5):1005-1017. doi:10.1002/cjce.20553
59. Sobisch T, Lerche D. Thickener performance traced by multisample analytical centrifugation. *Physicochem Eng Asp*. 2008;331:114-118. doi:10.1016/j.colsurfa.2008.05.040
60. Chiu HT, Chang CY, Chiang TY, Kuo MT, Wang YH. Using analytical centrifugation to characterize the dispersibility and particle size distributions of organic/inorganic composite coatings. *J Polym Res*. 2011;18(6):1587-1596. doi:10.1007/s10965-011-9563-0
61. Lerche D. Dispersion Stability and Particle Characterization by Sedimentation Kinetics in a Centrifugal Field. *J Dispers Sci Technol*. 2002;23(5):699-709. doi:10.1081/DIS-120015373
62. Kumar S, Pirog TW, Ramkrishna D. A new method for estimating hindered creaming/settling velocity of particles in Polydisperse Systems. *Chem Eng Sci*. 2000;55(10):1893-1904. doi:10.1016/S0009-2509(99)00457-1
63. Salinas-Salas G, Espinosa-Fuentes F, Babick F, Stintz M. Determinación del exponente de la función de obstrucción para partículas sub-micrométricas no coloidales. *Inf Tecnol*. 2009;20(2):19-27. doi:10.1612/inf.tecnol.4042it.08
64. Xu D, Aihemaiti Z, Cao Y, Teng C, Li X. Physicochemical stability, microrheological properties and microstructure of lutein emulsions stabilized by multilayer membranes consisting of whey protein isolate, flaxseed gum and chitosan. 2016. doi:10.1016/j.foodchem.2016.01.052
65. Sobisch T, Lerche D. Separation behaviour of particles in biopolymer solutions in dependence on centrifugal acceleration: Investigation of slow structuring processes in formulations. *Colloids Surfaces A Physicochem Enig Asp*. 2018;536:74-81.

doi:10.1016/j.colsurfa.2017.07.038
66. Tehrani-Bagha AR. Cationic gemini surfactant with cleavable spacer: Emulsion stability. *Colloids Surfaces A Physicochem Eng Asp*. 2016;508:79-84. doi:10.1016/j.colsurfa.2016.08.020
67. Komaiko J, McClements DJ. Low-energy formation of edible nanoemulsions by spontaneous emulsification: Factors influencing particle size. *J Food Eng*. 2015;146:122-128. doi:10.1016/j.jfoodeng.2014.09.003
68. Ghanbari M, Esmaeilzadeh F, Binazadeh M. An experimental investigation of creaming phenomenon using a novel optical method: A case study of mineral oil-in-water emulsion. *J Dispers Sci Technol*. 2018;39(5):634-643. doi:10.1080/01932691.2017.1379019
69. Jacob N. Israelachvili. *Intermolecular and Surface Forces*.; 1991.
70. Tajima K. Radiotracer Studies on Adsorption of Surface Active Substance at Aqueous Surface. II. The Effect of Excess Salt on the Adsorption of Sodium Dodecylsulfate. *Bull Chem Soc Jpn*. 1970;43(10):3063-3066. doi:10.1246/bcsj.43.3063
71. Martínez-Balbuena L, Arteaga-Jiménez A, Hernández-Zapata E, Márquez-Beltrán C. Applicability of the Gibbs Adsorption Isotherm to the analysis of experimental surface-tension data for ionic and nonionic surfactants. *Adv Colloid Interface Sci*. 2017;247:178-184. doi:10.1016/j.cis.2017.07.018
72. Yekeen N, Manan MA, Idris AK, Samin AM. Influence of surfactant and electrolyte concentrations on surfactant Adsorption and foaming characteristics. *J Pet Sci Eng*. 2017;149:612-622. doi:10.1016/j.petrol.2016.11.018
73. Muherei MA, Junin R. Investigating Synergism in Critical Micelle Concentration of Anionic-Nonionic Surfactant Mixtures before and after Equilibration with Shale. *J Appl Sci Res*. 2009;5(2):181-189.
74. Kedar V, Bhagwat SS. Effect of salinity on the IFT between aqueous surfactant solution and crude oil. *Pet Sci Technol*. 2018;36(12):835-842. doi:10.1080/10916466.2018.1447953
75. Aoudia M, Al-Maamari T, Al-Salmi F. Intramolecular and intermolecular ion-dipole interactions in sodium lauryl ether sulfates (SLES) self-aggregation and mixed micellization with Triton X-100. *Colloids Surfaces A Physicochem Eng Asp*. 2009;335(1-3):55-61. doi:10.1016/j.colsurfa.2008.10.026
76. Franks G V., Djerdjev AM, Beattie JK. Absence of specific cation or anion effects at low salt concentrations on the charge at the oil/water interface. *Langmuir*. 2005;21(19):8670-8674. doi:10.1021/la051379b
77. Thakkar K, Bharatiya B, Shah DO, Ray D, Aswal VK, Bahadur P. Interaction of ionic liquid type cationic surfactants with triton X-100 nonionic micelles. *Colloids Surfaces A Physicochem Eng Asp*. 2015;484:547-557. doi:10.1016/j.colsurfa.2015.08.039
78. Beattie JK, Djerdjev AM. The Pristine Oil/Water Interface: Surfactant-Free Hydroxide-Charged Emulsions. *Angew Chemie Int Ed*. 2004;43(27):3568-3571. doi:10.1002/anie.200453916
79. Zdrali E, Okur HI, Roke S. Specific Ion Effects at the Interface of Nanometer-Sized Droplets in Water: Structure and Stability. *J Phys Chem C*. 2019;123(27):16621-16630. doi:10.1021/acs.jpcc.9b01001
80. Rudel H, Seitz W. Corrosion inhibiting lubricating composition. September 1957.
81. Wasilewski T, Sulek MW. Paraffin oil solutions of the mixture of sorbitan monolaurate-ethoxylated sorbitan monolaurate as lubricants. *Wear*. 2006;261(2):230-234.

doi:10.1016/j.wear.2005.10.005
82. Fan J, Zhu H, Li R, Chen N. Montmorillonite Modified by Cationic and Nonionic Surfactants as High-Performance Fluid-Loss-Control Additive in Oil-Based Drilling Fluids. *J Dispers Sci Technol*. 2015;36(4):569-576. doi:10.1080/01932691.2014.917052
83. Huang Z, Xu Z, Quan Y, et al. Research on a New Oil Based Drilling Fluid System. *IOP Conf Ser Earth Environ Sci*. 2018;170:22044. doi:10.1088/1755-1315/170/2/022044
84. Donald C, Van S. Solvent soaps and methods employing same. August 1994.
85. Reddy SR, Fogler HS. Emulsion stability: Determination from turbidity. *J Colloid Interface Sci*. 1981;79(1):101-104. doi:10.1016/0021-9797(81)90052-7
86. Lee M, Kang H, Do W. Application of nonionic surfactant-enhanced in situ flushing to a diesel contaminated site. *Water Res*. 2005;39(1):139-146. doi:10.1016/j.watres.2004.09.012
87. Kim H, Muller K, Shardt O, Afkhami S, Stone HA. Solutal Marangoni flows of miscible liquids drive transport without surface contamination. *Nat Phys*. 2017;13(11):1105-1110. doi:10.1038/nphys4214
88. Sterling C V., Scriven LE. Interfacial turbulence: Hydrodynamic instability and the marangoni effect. *AIChE J*. 1959;5(4):514-523. doi:10.1002/aic.690050421
89. Schwarzenberger K, Köllner T, Linde H, Boeck T, Odenbach S, Eckert K. Pattern formation and mass transfer under stationary solutal Marangoni instability. *Adv Colloid Interface Sci*. 2014;206:344-371. doi:10.1016/j.cis.2013.10.003
90. Köllner T, Schwarzenberger K, Eckert K, Boeck T. Multiscale structures in solutal Marangoni convection: Three-dimensional simulations and supporting experiments. *Phys Fluids*. 2013;25(9). doi:10.1063/1.4821536
91. Silva PS, Zhdanov S, Starov VM, Holdich RG. Spontaneous emulsification of water in oil at appreciable interfacial tensions. *Colloids Surfaces A Physicochem Eng Asp*. 2017;521:141-146. doi:10.1016/j.colsurfa.2016.05.041
92. Gupta A, Eral HB, Hatton TA, Doyle PS. Nanoemulsions: formation, properties and applications. *Soft Matter*. 2016;12:2826-2841. doi:10.1039/c5sm02958a
93. McAuliffe C. Solubility in Water of Paraffin, Cycloparaffin, Olefin, Acetylene, Cycloolefin, and Aromatic Hydrocarbons. *J Phys Chem*. 1966;70(4):1267-1275. doi:10.1021/j100876a049
94. Polak J, Lu BC-Y. Mutual solubilities of hydrocarbons and water at 0 and 25 C. *Can J Chem*. 1973;51(24):4018-4023. doi:10.1139/v73-599
95. Yang M. *Produced Water*. 2nd ed. Springer; 2011. doi:10.1007/978-1-4614-0046-2
96. Bonoli L, Witherspoon PA. Diffusion of aromatic and cycloparaffin hydrocarbons in water from 2 to 60.deg. *J Phys Chem*. 2005;72(7):2532-2534. doi:10.1021/j100853a045
97. Yaws CL. *Transport Properties of Chemicals and Hydrocarbons*. William Andrew Inc.; 2009.
98. Birdi KS. Determination of size and shape of micelles by gel filtration chromatography. *Colloid Polym Sci*. 1974;252:551-554.
99. Schick MJ, Atlas SM, Eirich FR. Micellar Structure of Non-Ionic Detergents. *J Phys Chem*. 1962;66(7):1326-1333. doi:10.1021/j100813a027
100. Becher P. Nonionic surface-active compounds IV. Micelle formation by polyoxyethylene alkanols and alkyl phenols in aqueous solution. *J Colloid Sci*. 1961;16(1):49-56. doi:10.1016/0095-8522(61)90061-7
101. Schott H, Royce AE. Effect of Inorganic Additives on Solutions of Nonionic Surfactants

V : Emulsion Stability. *J Pharm Sci*. 1983;72:1427-1435.
102. Shahidzadeh N, Bonn D, Meunier J, Nabavi M, Airiau M, Morvan M. Dynamics of spontaneous emulsification for fabrication of oil in water emulsions. *Langmuir*. 2000;16(25):9703-9708. doi:10.1021/la000493l
103. Bochner De Araujo S, Merola M, Vlassopoulos D, Fuller GG. Droplet Coalescence and Spontaneous Emulsification in the Presence of Asphaltene Adsorption. *Langmuir*. 2017;33(40):10501-10510. doi:10.1021/acs.langmuir.7b02638
104. Reiss H. Entropy-Induced Dispersion of Bulk Liquids. *J Colloid Interface Sci*. 1975;53(I):61-70.
105. Ruschak KJ, Miller CA. Spontaneous Emulsification in Ternary Systems with Mass Transfer. *Ind Eng Chem Fundam*. 1972;11(4):534-540. doi:10.1021/i160044a017
106. El-Aasser MS, Lack CD, Vanderhoff JW. The Miniemulsification Process - Different Form of Spontaneous Emulsification. *Colloids and Surfaces*. 1988;29:103-118.
107. Santos FKG, Neto ELB, Moura MCPA, Dantas TNC, Neto AAD. Molecular behavior of ionic and nonionic surfactants in saline medium. *Colloids Surfaces A Physicochem Eng Asp*. 2009;333(1-3):156-162. doi:10.1016/j.colsurfa.2008.09.040
108. Li Y, He X, Cao X, Zhao G, Tian X, Cui X. Molecular behavior and synergistic effects between sodium dodecylbenzene sulfonate and Triton X-100 at oil/water interface. *J Colloid Interface Sci*. 2007;307(1):215-220. doi:10.1016/j.jcis.2006.11.026
109. Banipal TS, Kaur H, Banipal PK, Sood AK. Effect of head groups, temperature, and polymer concentration on surfactant - Polymer interactions. *J Surfactants Deterg*. 2014;17(6):1181-1191. doi:10.1007/s11743-014-1633-y
110. Israelachvili J. *Intermolecular and Surface Forces*. 2nd ed. Elsevier; 1991.
111. Calvo E, Bravo R, Amigo A, Gracia-Fadrique J. Dynamic surface tension, critical micelle concentration, and activity coefficients of aqueous solutions of nonyl phenol ethoxylates. *Fluid Phase Equilib*. 2009;282(1):14-19. doi:10.1016/j.fluid.2009.04.016
112. Cheng DCH, Gulari E. Micellization and intermicellar interactions in aqueous sodium dodecyl benzene sulfonate solutions. *J Colloid Interface Sci*. 1982;90(2):410-423. doi:10.1016/0021-9797(82)90308-3
113. Sood AK, Aggarwal M. Evaluation of micellar properties of sodium dodecylbenzene sulphonate in the presence of some salts. *J Chem Sci*. 2018;130(4):1-7. doi:10.1007/s12039-018-1446-z
114. Davis CR, Martinez CJ, Howarter JA, Erk KA. Diffusion-Controlled Spontaneous Emulsification of Water-Soluble Oils via Micelle Swelling. *Langmuir*. 2020;36(26):7517-7527. doi:10.1021/acs.langmuir.0c01121
115. Zabar MK, Nguyen C V., Phan CM. Quantifying the influence of salinity on spontaneous emulsification of hydrocarbons. *Colloids Surfaces A Physicochem Eng Asp*. 2020;588(December 2019):1-5. doi:10.1016/j.colsurfa.2019.124376
116. Davies JT, Rideal EK. *Interfacial Phenomena*. 2nd ed. New York: Academic Press; 1963.
117. Solans C, Morales D, Homs M. Spontaneous emulsification. *Curr Opin Colloid Interface Sci*. 2016;22:88-93. doi:10.1016/j.cocis.2016.03.002
118. Miller CA. *Spontaneous Emulsification: Recent Developments with Emphasis on Self-Emulsification*. Vol 132. (Sjoblom J, ed.). Taylor & Francis; 2006.
119. Miller CA. Spontaneous Emulsification Produced by Diffusion - A Review. *Colloids and Surfaces*. 1988;29(1):89-102. doi:10.1016/0166-6622(88)80173-2
120. Lopez-Montilla JC, Herrera-Morales PE, Pandey S, Shah DO. Spontaneous

emulsification: Mechanisms, physicochemical aspects, modeling, and applications. *J Dispers Sci Technol*. 2002;23(1-3):219-268. doi:10.1081/DIS-120003317
121. P B, SH H. Spontaneous Formation of Double Emulsions at Particle-Laden Interfaces. *J Colloid Interface Sci*. 2021;587:510-521. doi:10.1016/J.JCIS.2020.10.064
122. Santana-Solano J, Quezada CM, Ozuna-Chacón S, Arauz-Lara JL. Spontaneous emulsification at the water/oil interface. *Colloids Surfaces A Physicochem Eng Asp*. 2012;399:78-82. doi:10.1016/J.COLSURFA.2012.02.032
123. Abbott S. *Surfactant Science: Principles and Practice*.; 2016.
124. Ariyaprakai S, Hu X, Tran MT. Spontaneous Formation of Flavor Oil Emulsions by Using Sucrose Esters and Emulsion Stability Study. *Food Biophys 2018 141*. 2018;14(1):41-48. doi:10.1007/S11483-018-9555-2
125. Mehrnia MA, Jafari SM, Makhmal-Zadeh BS, Maghsoudlou Y. Crocin loaded nano-emulsions: Factors affecting emulsion properties in spontaneous emulsification. *Int J Biol Macromol*. 2016;84:261-267. doi:10.1016/J.IJBIOMAC.2015.12.029
126. Wasan DT, Shah SM, Chan M, Sampath K, Shah R. SPONTANEOUS EMULSIFICATION AND THE EFFECT OF INTERFACIAL FLUID PROPERTIES ON COALESCENCE AND EMULSION STABILITY IN CAUSTIC FLOODING. *ACS Symp Ser*. 1979;(91):115-140. doi:10.1021/BK-1979-0091.CH007
127. Feng H, Kang W, Wu H, et al. Study on the relationship between emulsion stability and droplet dynamics of a spontaneous emulsion for chemical enhanced oil recovery. *https://doi.org/101080/01932691201713916999*. 2017;39(8):1214-1222. doi:10.1080/01932691.2017.1391699
128. Shahidzadeh N, Bonn D, O Aguerre-Chariol. Spontaneous emulsification: relation to microemulsion phase behaviour. *Elsevier*. 1999.
129. Miller CA, Hwan RN, Benton WJ, Fort T. Ultralow interfacial tensions and their relation to phase separation in micellar solutions. *J Colloid Interface Sci*. 1977;61(3):554-568. doi:10.1016/0021-9797(77)90473-8
130. Boehmer-Christiansen S. *Estimates of Oil Entering the Marine Environment from Sea-Based Activities, Reports and Studies No. 75*. Vol 19.; 2008. doi:10.1260/095830508784815955
131. Marinova KG, Alargova RG, Denkov ND, et al. Charging of oil-water interfaces due to spontaneous adsorption of hydroxyl ions. *Langmuir*. 1996;12(8):2045-2051. doi:10.1021/la950928i
132. Velev OD, Gurkov TD, Chakarova SK, Dimitrova BI, Ivanov IB, Borwankar RP. Experimental investigations on model emulsion systems stabilized with non-ionic surfactant blends. *Colloids Surfaces A Physicochem Eng Asp*. 1994;83(1):43-55. doi:10.1016/0927-7757(93)02639-V
133. Ghosh P, Banik M. Effects of Salts Containing Mono-, Di-, and Trivalent Ions on Electrical and Rheological Properties of Oil-Water Interface in Presence of Cationic Surfactant: Importance in the Stability of Oil-in-Water Emulsions. *J Dispers Sci Technol*. 2014;35(4):471-481. doi:10.1080/01932691.2013.791990
134. Gurkov TD, Dimitrova DT, Marinova KG, Bilke-Crause C, Gerber C, Ivanov IB. Ionic surfactants on fluid interfaces: Determination of the adsorption; Role of the salt and the type of the hydrophobic phase. *Colloids Surfaces A Physicochem Eng Asp*. 2005;261(1-3):29-38. doi:10.1016/j.colsurfa.2004.11.040
135. Kundu P, Agrawal A, Mateen H, Mishra IM. Stability of oil-in-water macro-emulsion

with anionic surfactant: Effect of electrolytes and temperature. *Chem Eng Sci*. 2013;102:176-185. doi:10.1016/j.ces.2013.07.050
136. Netz RR. Water and ions at interfaces. *Curr Opin Colloid Interface Sci*. 2004;9(1-2):192-197. doi:10.1016/j.cocis.2004.06.007
137. Jungwirth P. Spiers Memorial Lecture: Ions at aqueous interfaces. *Faraday Discuss*. 2008;141:9-30. doi:10.1039/b816684f
138. Walstra P. Principles of emulsion formation. *Chem Eng Sci*. 1993;48(2):333-349. doi:10.1016/0009-2509(93)80021-H
139. Narsimhan G, Goel P. Drop coalescence during emulsion formation in a high-pressure homogenizer for tetradecane-in-water emulsion stabilized by sodium dodecyl sulfate. *J Colloid Interface Sci*. 2001;238(2):420-432. doi:10.1006/jcis.2001.7548
140. Li Z, Lee K, King T, Boufadel MC, Venosa AD. Assessment of chemical dispersant effectiveness in a wave tank under regular non-breaking and breaking wave conditions. *Mar Pollut Bull*. 2008;56(5):903-912. doi:10.1016/j.marpolbul.2008.01.031
141. Li C, Miller J, Wang J, Koley SS, Katz J. Size distribution and dispersion of droplets generated by impingement of breaking waves on oil slicks. *J Geophys Res Ocean*. 2017;122:7938-7957. doi:10.1038/175238c0
142. He Y, Yazhgur P, Salonen A, Langevin D. Adsorption-desorption kinetics of surfactants at liquid surfaces. *Adv Colloid Interface Sci*. 2015;222:377-384. doi:10.1016/j.cis.2014.09.002
143. Church J, Willner MR, Renfro BR, et al. Impact of Interfacial Tension and Critical Micelle Concentration on Bilgewater Oil Separation. *J Water Process Eng*. 2021;39(October 2020):101684. doi:10.1016/j.jwpe.2020.101684
144. Rosen MJ, Kunjappu JT. *Surfactants and Interfacial Phenomena: Fourth Edition*.; 2012. doi:10.1002/9781118228920
145. Eastoe J, Nave S, Downer A, et al. Adsorption of ionic surfactants at the air-solution interface. *Langmuir*. 2000;16(10):4511-4518. doi:10.1021/la991564n
146. Kirby SM, Anna SL, Walker LM. Sequential adsorption of an irreversibly adsorbed nonionic surfactant and an anionic surfactant at an oil/aqueous interface. *Langmuir*. 2015;31(14):4063-4071. doi:10.1021/la504969v
147. Tzocheva SS, Kralchevsky PA, Danov KD, Georgieva GS, Post AJ, Ananthapadmanabhan KP. Solubility limits and phase diagrams for fatty acids in anionic (SLES) and zwitterionic (CAPB) micellar surfactant solutions. *J Colloid Interface Sci*. 2012;369(1):274-286. doi:10.1016/j.jcis.2011.12.036
148. Khosharay S, Rahmanzadeh M, ZareNezhad B. Surface Behavior of Aqueous Solutions of Sodium Lauryl Ether Sulfate, Additives and Their Mixtures: Experimental and Modeling Study. *Int J Thermophys*. 2020;41(12):1-17. doi:10.1007/s10765-020-02738-0
149. Mohan S, Narsimhan G. Coalescence of protein-stabilized emulsions in a high-pressure homogenizer. *J Colloid Interface Sci*. 1997;192(1):1-15. doi:10.1006/jcis.1997.5012
150. Tcholakova S, Denkov ND, Banner T. Role of surfactant type and concentration for the mean drop size during emulsification in turbulent flow. *Langmuir*. 2004;20(18):7444-7458. doi:10.1021/la049335a
151. Mittal KL, Vold RD. Effect of the initial concentration of emulsifying agents on the ultracentrifugal stability of oil-in-water emulsions. *J Am Oil Chem Soc*. 1972;49(9):527-532. doi:10.1007/BF02628897
152. Llamas S, Santini E, Liggieri L, et al. Adsorption of Sodium Dodecyl Sulfate at Water-

Dodecane Interface in Relation to the Oil in Water Emulsion Properties. *Langmuir*. 2018;34(21):5978-5989. doi:10.1021/acs.langmuir.8b00358
153. Taisne L, Walstra P, Cabane B. Transfer of oil between emulsion droplets. *J Colloid Interface Sci*. 1996;184(2):378-390. doi:10.1006/jcis.1996.0632
154. Djaković L, Dokić P, Radivojević P, Šefer I, Sovilj V. Action of emulsifiers during homogenization of o/w emulsions. *Colloid Polym Sci*. 1987;265(11):993-1000. doi:10.1007/BF01412403
155. Church J, Lundin JG, Diaz D, et al. Identification and characterization of bilgewater emulsions. *Sci Total Environ*. 2019;691:981-995. doi:10.1016/j.scitotenv.2019.06.510
156. Amstad E, Datta SS, Weitz DA. The microfluidic post-array device: High throughput production of single emulsion drops. *Lab Chip*. 2014;14(4):705-709. doi:10.1039/c3lc51213d
157. Bak A, Podgórska W. Investigation of drop breakage and coalescence in the liquid-liquid system with nonionic surfactants Tween 20 and Tween 80. *Chem Eng Sci*. 2012;74:181-191. doi:10.1016/j.ces.2012.02.021
158. Fingas MF, Huang E, Fieldhouse B, Wang L, Mullin J V. The effect of energy, settling time and shaking time on the swirling flask dispersant apparatus. *Spill Sci Technol Bull*. 1996;3(4):193-194. doi:10.1016/S1353-2561(97)00010-8
159. Pouton CW. Self-emulsifying drug delivery systems: assessment of the efficiency of emulsification. *Int J Pharm*. 1985;27(2-3):335-348. doi:10.1016/0378-5173(85)90081-X
160. Madden AJ, Damerell GL. Coalescence frequencies in agitated liquid-liquid systems. *AIChE J*. 1962;8(2):233-239. doi:10.1002/aic.690080221
161. Nandi A, Khakhar D V., Mehra A. Coalescence in surfactant-stabilized emulsions subjected to shear flow. *Langmuir*. 2001;17(9):2647-2655. doi:10.1021/la001473m
162. Shaw JM. A microscopic view of oil slick break-up and emulsion formation in breaking waves. *Spill Sci Technol Bull*. 2003;8(5-6):491-501. doi:10.1016/S1353-2561(03)00061-6
163. Nissanka ID, Yapa PD. Oil slicks on water surface: Breakup, coalescence, and droplet formation under breaking waves. *Mar Pollut Bull*. 2017;114(1):480-493. doi:10.1016/j.marpolbul.2016.10.006
164. Li M, Garrett C. The relationship between oil droplet size and upper ocean turbulence. *Mar Pollut Bull*. 1998;36(12):961-970. doi:10.1016/S0025-326X(98)00096-4
165. Chen Z, Zhan CS, Lee K. Formation and vertical mixing of oil droplets resulting from oil slick under breaking waves-A modeling study. *Environ Forensics*. 2009;10(4):347-353. doi:10.1080/15275920903347438
166. Tcholakova S, Denkov ND, Danner T. Role of Surfactant Type and Concentration for the Mean Drop Size during Emulsification in Turbulent Flow. 2004. doi:10.1021/la049335a
167. Stang M, Schuchmann H, Schubert H. Emulsification in High-Pressure Homogenizers. *Eng life Sci*. 2001;1(4):151-157. doi:10.1002/1618-2863(200110)1:4<151::AID-ELSC151>3.0.CO;2-D
168. McClements DJ. Edible nanoemulsions: Fabrication, properties, and functional performance. *Soft Matter*. 2011;7(6):2297-2316. doi:10.1039/c0sm00549e
169. Lobo L, Svereika A. Coalescence during emulsification 2. Role of small molecule surfactants. *J Colloid Interface Sci*. 2003;261:498-507. doi:10.1016/S0021-9797(03)00069-9
170. Krebs T, Schroën K, Boom R. Coalescence dynamics of surfactant-stabilized emulsions studied with microfluidics. *Soft Matter*. 2012;8(41):10650-10657.

doi:10.1039/c2sm26122g
171. Burgess C. Chapter 1 The basics of spectrophotometric measurement. In: *UV-Visible Spectrophotometry of Water and Wastewater*. Vol 27. ; 2007:1-19. doi:10.1016/S0167-9244(07)80003-5
172. Myers KJ, Reeder MF, Ryan D. Power draw of a high-shear homogenizer. *Can J Chem Eng*. 2001;79(1):94-99. doi:10.1002/cjce.5450790114
173. Kowalski AJ. An expression for the power consumption of in-line rotor-stator devices. *Chem Eng Process Process Intensif*. 2009;48(1):581-585. doi:10.1016/j.cep.2008.04.002
174. Zhang J, Xu S, Li W. High shear mixers: A review of typical applications and studies on power draw, flow pattern, energy dissipation and transfer properties. *Chem Eng Process Process Intensif*. 2012;57-58(October 2017):25-41. doi:10.1016/j.cep.2012.04.004
175. Martinez CJ. Drop Generation in Microfluidic Devices. 2016:MSE 597 Soft Materials Course Notes.
176. Shah RK, Shum HC, Rowat AC, et al. Designer emulsions using microfluidics. *Mater Today*. 2008;11(4):18-27. doi:10.1016/S1369-7021(08)70053-1

Appendices

Energy Density of Emulsions Prepared via High Shear Mixing

The energy density provided by high shear mixing is described by the following equation.

$$E_D = \frac{P_o \rho N^3 D^5 t}{V} \quad \text{(A1)}$$

This energy depends on the power number (P_o)[1–3], density of the fluid (ρ), rotation speed (N), diameter of the mixer (D), emulsification time (t), and emulsion volume (V).

Derivation of Energy Density for Dynamic Aging

An energy balance between potential energy and kinetic energy can be derived for a falling object as:

$$mghsin\theta = {}^1/_2\, mv^2 \quad \text{(A2)}$$

Where θ is the tilt angle, and h is the height, or the distance in which that object falls. Solve for the velocity to find:

$$v_{final} = \sqrt{2ghsin\theta} \quad \text{(A3)}$$

Where the kinetic energy is:

$$KE_{final} = {}^1/_2\, m(v_{final})^2 \quad \text{(A4)}$$

An equation for energy density is related to the kinetic energy of the emulsion, the RPM of the rocker, the ageing time, and the volume of the emulsion.

$$E_D = \frac{KE_{final} * RPM * t}{30 * V_E} = \frac{m(v_{final})^2 * RPM * t}{30 * V_E} \quad \text{(A5)}$$

Substitute mass and volume terms for the density of the emulsion:

$$\frac{m}{V_E} = \rho_E = (\phi_{oil} * \rho_{oil}) + (1 - \phi_{oil})\rho_{water} \quad \text{(A6)}$$

Where ϕ_{oil} is the dispersed phase volume fraction. The energy density for dynamic ageing can be calculated by knowing the density of the emulsion, the falling height of the emulsion, the tilt angle and speed of the rocker, and the ageing time:

$$E_D = \frac{\rho_E * (ghsin\theta) * RPM * t}{30}$$

1. Visual Bibliography

<table>
<tr>
<td>[1] Davis, C. R.; Martinez, C. J.; Howarter, J. A.; Erk, K. A. Predicting Spontaneous Emulsification in Saltwater Environments Using the HLD Model. Langmuir 2021, 37 (29), 8866–8875. https://pubs.acs.org/doi/full/10.1021/acs.langmuir.1c01277</td>
<td> 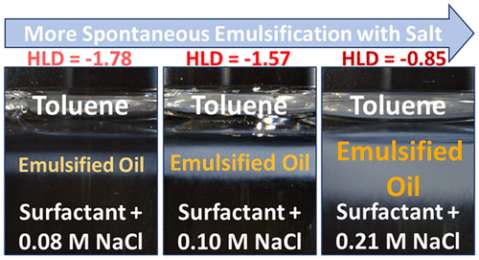
</td>
</tr>
<tr>
<td>[2] Zheng, Y.; Caicedo-Casso, E. A.; Davis, C. R.; Howarter, J. A.; Erk, K. A.; Martinez, C. J. Impact of Mixed Surfactant Composition on Emulsion Stability in Saline Environment: Anionic and Nonionic Surfactants. J. Dispers. Sci. Technol. 2021. https://www.tandfonline.com/doi/full/10.1080/01932691.2021.1999255</td>
<td> 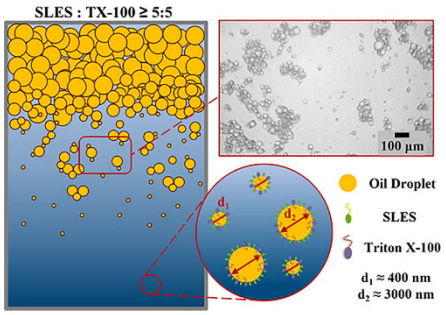
</td>
</tr>
<tr>
<td>[3] Sabatello, R. G. Impact of Dynamic Ageing on the Formation and Stability of Model Bilge Water Oil-in-Water Emulsions. 2021. MS Thesis, Purdue University https://doi.org/10.25394/PGS.17147681.V1</td>
<td> 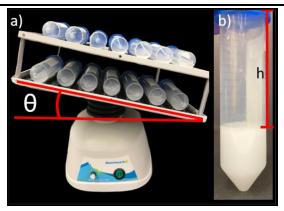
</td>
</tr>
</table>

[4] Davis, C. R.; Martinez, C. J.; Howarter, J. A.; Erk, K. A. Diffusion-Controlled Spontaneous Emulsification of Water-Soluble Oils via Micelle Swelling. *Langmuir* **2020**, 36 (26), 7517–7527. https://pubs.acs.org/doi/full/10.1021/acs.langmuir.0c01121	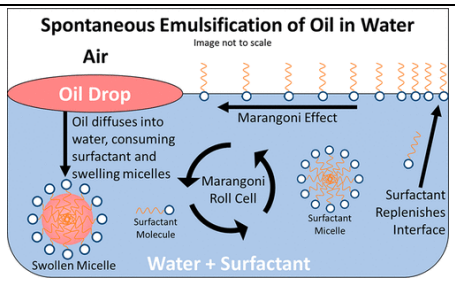
[5] Zheng, Y.; Davis, C. R.; Howarter, J. A.; Erk, K. A.; Martinez, C. J. Spontaneous Emulsions: Adjusting Spontaneity and Phase Behavior by Hydrophilic-Lipophilic Difference-Guided Surfactant, Salt, and Oil Selection. *Langmuir* **2022**, 38 (14), 4276–4286. https://pubs.acs.org/doi/full/10.1021/acs.langmuir.1c03444	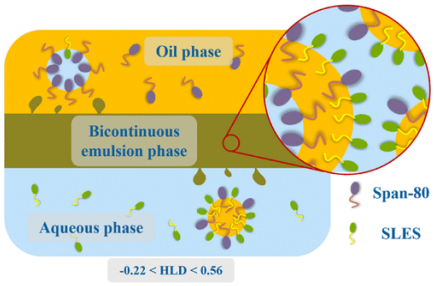
[6] Davis, C. R.; Martinez, C. J.; Howarter, J. A.; Erk, K. A. Impact of Saltwater Environments on the Coalescence of Oil-in-Water Emulsions Stabilized by an Anionic Surfactant. *ACS ES&T Water* **2021**, 1 (8), 1702–1713. https://pubs.acs.org/doi/full/10.1021/acsestwater.1c00066